MEDIA ARRANGEMENT AND AEROSOL LOADING CHARACTERISTICS OF PANEL FILTERS

BY

ROBERT OWEN

A DOCTORAL THESIS
SUBMITTED IN PARTIAL FULFILMENT OF THE REQUIREMENTS
FOR THE AWARD OF
DOCTOR OF PHILOSOPHY
FROM LOUGHBOROUGH UNIVERSITY OF TECHNOLOGY

MAY 1987

ACKNOWLEDGEMENTS

The work reported in the following pages could not have been carried out successfully without the help and cooperation of many people to whom I am indebited and wish to thank.

1. Dr. Ian Stenhouse for his continuous help, support and enthusiasm throughout his supervision of my work.

2. Professor D.C. Freshwater for his support as Director of Research.

3. The United Kingdom Atomic Energy Authority, Harwell, for their guidance and financial support. In particular I would like to thank Ron Pratt, Betty Green and Jim Cunningham.

4. Yasmin for all the typing over the past 3 years.

5. The particle sizing laboratory staff for their help with analysis especially Ruth and Anjna.

6. The workshop staff for construction of the experimental rig...

7. Geoff Boyden for all his efforts with the photography.

CONTENTS

Chapter 2

ABSTRACT

The effect of media arrangement within fibrous filter units on
aerosol and dust loading characteristics has been studied. The
behaviour of the media alone was measured. This was then compared
with the performance of two units in which the media geometrical
arrangement differed substantially. The effects which can be
attributed specifically to media arrangement were thus isolated. An
"ideal" model of a pleat type filter unit in which the dust
distribution is uniform is proposed.

The model gives a reasonable description of the behaviour of a
typical deep pleat type of design although ancillary mechanisms of
enhanced deposition at the channel entrance and on horizontal spacers
were identified experimentally. Theoretical analysis confirmed
inertial migration and gravity sedimentation as reponsible for this.

The ideal model is significantly in error when applied to the
mini pleat type of design. The system was studied experimentally and
theoretically and the relevant ancillary mechanisms isolated. It is
postulated that inertial migration determines the deposition pattern
within the channels. Additionally, as loading proceeds, considerable
deposition is seen on the panel surface and the upstream channel
expands at the expense of that downstream. These effects have been
incorporated into a more general model which describes the
characteristics of the mini pleat type of design. Further
developments are proposed which will enable these models to be used
in optimising media arrangement within HEPA filter units.

NOMENCLATURE

The following table describes the symbols used in the text. Dimensions are given for all but constants specifically defined within the text. The symbols used are:

L – length
T – time
M – mass
K – temperature
C – charge
  – number only (no dimensions)
* – refer to text for specific definition

Symbol	Description	Dimensions
A	(1) Defined constant	
	(2) Area of filter media	L^2
A_f	Face area of a filer unit	L^2
A_{avail}	Filter media area available for filtration	L^2
A_x	Cross-sectional area of a channel	L^2
A_H	Hamakers constant	$M\,L^2T^{-2}$
B	Defined constant	
B'	Darcy's permeability constant	L^{-2}
C	(1) Defined constant	
	(2) Particle concentration	L^{-3} or ML^{-3}
C'	Initial particle concentration	L^{-3} or ML^{-3}

C_i — Initial particle concentraton into a channel L^{-3} or ML^{-3}
section

C_o — Particle concentration leaving a channel section L^{-3} or ML^{-3}

C_{av} — Average particle concentration in a channel L^{-3} or ML^{-3}
section

C_f — Concentration of particles lost from filtration L^{-3} or ML^{-3}

C_s — Concentration of particles lost by sedimentation L^{-3} or ML^{-3}

C_I — Concentration of particles lost from the L^{-3} or ML^{-3}
interaction of filtration and sedimentation

C_D — Drag coefficient

C_{Do} — Drag coefficient at the original fibre diameter

C_{Dm} — Drag coefficient with increasing load

$C_{D\alpha}$ — Drag coefficient at fibre packing α

C_p — Pressure coefficent

C_m — Accommodation coefficient

D — (1) Defined constant

(2) Depth of a filter unit   L

E_f — Overall filter efficiency

Overall fibrous filter efficiency (in
combination)

E_g — Overall granular bed efficiency (in combination)

E_L — Overall efficiency, loaded filter

E_o — Coulombic force due to an external field

F — Height dust settles in time t   L

F_D — Drag force $M L T^{-2}$

Ga — Gallileos number

H — Channel height/total height of channels in a L
filter unit

H_f — Total free space height of a filter panel

H_s	Height available for dust settling	L
I	Inertial factor	
J	Defined constant	
K	Hydrodynamic factor	
K'	Defined constant	
K''	Geometrical factor in Kozeny-Carman equation	
$K_{1,2,3,4}$	Regression coefficients	
K_I	Characterisation parameter, inertia	
K_D	Characterisation parameter, diffusion	
K_R	Characterisation parameter, interception	
K_ϵ	Correction factor	
Kg'	Hydrodynamic factor, sphere	
Kg	Secondary hydrodynamic correction factor, sphere	
K_f	Hydrodynamic factor, fan model	
K'_f	Secondary hydrodynamic correction factor, fan model	
K_L	Hydrodynamic factor, cell model	
Kn	Knudsen number	
Kn_f	Fibre Knudsen number	
L	(1) Depth of filter media/bed	L
	(2) Channel/duct length	L
L_s	Filter service life	T
M	Molecular weight	
N	Ratio of cell to cylinder radius	
N_P	Number charged particles per unit volume	L^{-3}
N_{Qq}	Charge parameter	
N_{Pl}	Number of pleats	
N_S	Number of seams	
N_c	Number of channels	

P	Pressure	$M L^{-1} T^{-2}$
P*	Penetration	
P_o*	Initial penetration	
Pe	Peclet number	
ΔP	Pressure drop	$M L^{-1} T^{-2}$
ΔPexpt	Experimentally measured pressure drop	$M L^{-1} T^{-2}$
ΔP_{ch}	Pressure drop along a channel	$M L^{-1} T^{-2}$
ΔPmd	Pressure drop through a media/dust layer	$M L^{-1} T^{-2}$
ΔP_J	Pressure drop from channel entrance effects	$M L^{-1} T^{-2}$
ΔP_T	Total pressure drop of a filter unit	$M L^{-1} T^{-2}$
ΔP_m	Maximum acceptable pressure drop of a filter unit	$M L^{-1} T^{-2}$
ΔP_o	Pressure drop of a clean European minipleat filter	$M L^{-1} T^{-2}$
Q	(1) Total gas flow rate	$L^3 T^{-1}$
	(2) Fibre charge/unit length in an electrostatic field	$C L^{-1}$
R	(1) Interception parameter	
	(2) Radius of neutral collector in an elec. field	L
R'	Resistance	$L T^2 M^{-1}$
R'_o	Initial resistance	$L T^2 M^{-1}$
Re	Reynolds number	
Re_f	Fibre Reynolds number	
Re_p	Particle Reynolds number	
St	Stokes number	
T	Absolute temperature	K
U	Velocity (general)	$L T^{-1}$
U_o	Filter face velocity	$L T^{-1}$
U_{oa}	Average filter face velocity	$L T^{-1}$
$U_{1, 2}$	Filter face velocities as defined	$L T^{-1}$

$U_{r,o}$	Polar coordinates of a defined velocity	$L\,T^{-1}$
$U_{x,y}$	Cartesian coordinates of a defined velocity	$L\,T^{-1}$
U_c	Gas velocity round a cylinder - 1st component	$L\,T^{-1}$
U_f	Gas velocity to a porous cylinder - 1st component	$L\,T^{-1}$
U_s	Particle settling velocity	$L\,T^{-1}$
U_g	Gas velocity	$L\,T^{-1}$
U_p	Particle velocity	$L\,T^{-1}$
V	Gas velocity through a channel/parallel plates	$L\,T^{-1}$
V_{av}	Average gas velocity through a channel	$L\,T^{-1}$
V_i	Channel entrance velocity	$L\,T^{-1}$
V_o	Channel outlet velocity	$L\,T^{-1}$
V_∞	Gas velocity approaching a filter unit	$L\,T^{-1}$
$V_{x,y}$	Cartesian coordinates of a defined velocity	$L\,T^{-1}$
V_r	Radial component of a velocity	$L\,T^{-1}$
V_t	Transverse component of a velocity	$L\,T^{-1}$
V_{rel}	Relative velocity gas to particle	$L\,T^{-1}$
V_c	Velocity round a cylinder - 2nd component	$L\,T^{-1}$
V_f	Velocity to a porous cylinder - 2nd component	$L\,T^{-1}$
V'	Gas velocity (resolved) towards a porous cylinder	$L\,T^{-1}$
V^*	Capture limit velocity	$L\,T^{-1}$
W	Total width of channels	L
Z_s	Half separation distance between minipleat panels	L
a	Acceleration force	$L\,T^{-2}$
a'	Effective area of unit deposit	L^2
b	Length of a side of an equalateral triangle	L
c	Channel pitch	L
$\bar{c}$	r.m.s. gas molecule velocity	$L\,T^{-1}$
$C_{1,2}$	Defined constants	
d_f	Fibre diameter	L

d_g	Granule diameter	L
d_p	Particle diameter	L
d_{fe}	Effective fibre diameter	L
d_{fs}	Fibre surface average diameter	L
D_{fm}	Fibre diameter with increasing deposit	L
e	coefficient of resitution	
F	Adhesion factor	
F_f	Friction factor	
g	Acceleration due to gravity	$L T^{-2}$
$g(\epsilon)$	Influence function (granular bed theory)	
h	Channel height	L
h'	Effective channel height with inreasing load	L
i,j	Defined number (in summation etc.)	
k	(1) Boltzmann constant	$M L^2 T^{-2} K^{-1}$
	(2) Defined constant	
k_o	Defined constant	
m	Defined constant	
m_p	Particle mass	M
m_T	Media thickness	L
n	Defined number (in summation etc.)	
q	Particle charge	C
r	(1) Polar coordinate	L
	(2) Distance between particle and collector centres	L
r_f	Fibre radius	L
r_c	Fluid cell radius around a cylinder	L
r_p	particle radius	L
r_g	Granule radius	L
r_o	Radius of a porous cylinder	L

s	Perimeter length	L
t	Time	T
t_s	Seam thickness	L
w	Channel width	L
w'	Channel width with increasing load	L
x	Cartesian coordinate	L
x_o	Initial value of x	L
Δx	Channel elemental length	L
y	Cartesian coordinate	L
y_w	Defined channel dimension	L
y_o	Initial value of y	L
z	Cartesian coordinate	L
z_w	Define channel dimension	L
z_o	(1) Initial value of	L
	(2) Separation distance of two surfaces	L
α	(1) Defined constant	
	(2) Packing density	
α_L	Clogging parameter	T^{-1}
β	Defined constant	
$\beta_{1,2}$	Empirical constants	
γ	(1) Defined constant	
	(2) Particle collection efficiency	
γ_L	Clogging parameter	
δ	(1) Defined constant	
	(2) Diffusion boundary layer thickness	
ε	Media porosity	
$\varepsilon_{1,2}$	Empirical constant	
ε_o	Influence constant	
ε_c	Configuration factor, cell model	

ε_f	Configuration factor, fan model	
ϕ	Angle	
ϕ_c	Darcy constant	L^2
ϕ_D	Defined constant	
ϕ'	Defined constant	
ψ	Stream function	$L^2 T^{-1}$
θ	(1) Angle	
	(2) Polar coordinate	
$\hat{\theta}$	Critical angle	
λ	Mean free path of gas	L
$\lambda_{o,1,2}$	Parameters defining filter deposit	L^{-1}
λ_k	Permeability	L^{-2}
λ_c	Defined constant	
λ'	Empirical constant	
μ	Gas viscosity	$M\,L^{-1}T^{-1}$
η	Single collector efficiency	
η_o	Initial single collector efficiency	
η_T	Single collector efficiency including electrostatics	
η_s	Single collector efficiency accounting for adhesion	
η_f	Single collector efficiency, fan model	
η_D	Single collector efficiency due to diffusion	
η_R	Single collector efficiency due to interception	
η_I	Single collector efficiency due to inertia	
η_G	Single collector efficiency due to sedimentation	
η_E	Single collector efficiency due to electostatics	
η_a	Single collector efficiency of adhesion	

η_{DR}	Single collector efficiency from interaction of diffusion and interception	
ρ	Gas density	$M\,L^{-3}$
ρ_p	Particle density	$M\,L^{-3}$
ρ_f	Fibre density	$M\,L^{-3}$
ρ_b	Dust bulk density	$M\,L^{-3}$
σ	Dust load deposited	M
σ_s	Specific dust load	$M\,L^{-2}$
σ_m	Dust layer height	L
σ_k	Permeability coefficient	L^{-2}
τ	Defined constant	
ν	Kinematic viscosity	$L^2 T^{-1}$
ξ	Defined parameter	

INTRODUCTION

The aim of this work is to investigate the effect which media arrangement within a HEPA filter unit has on its performance. An increase in the surface area of the media offers potential advantages in life expectancy or system space. However, the influence of geometry has received very little attention and almost nothing is known about gas and particle distribution within the filter and the effect of channel size, shape and orientation etc. on this. Before an optimum cost effective design can be produced the factors which limit the area of media and govern performance of these units must be established.

In this work the behaviour of samples of media as loading progressed were studied first. This information was then used to construct a model of an entire filter unit which allows the prediction of the pressure drop characteristics. Experimental work was carried out on two very different but typical designs of media arrangement. The effect of arrangement on dust deposition and air distribution within the filter has been studied and the results incorporated in the theoretical model.

The first chapter of the thesis is a literature review on the subject of fibrous filtration. The conclusions from this, which are reported at the end of the chapter, add further justification for the work. The following chapters are on theoretical model development, experimental testing of fibrous media and the experimental testing of filter units. These divisions have been made for convenience and should not be regarded as mutually exclusive. Where appropriate references are made to other sections of the work showing the overall development of the research. The main conclusions and areas of further study to extend the developed models are summarised in chapter 5. Appendices are used to supply supplementary information.

Literature Review

1. Introduction

The realisation of the need and importance of fibrous filtration research first arose before and during the First World War (1914-18) with the development of chemical warfare. Early respirators were relatively crude relying on charcoal for gas absorption and natural fibres such as wool, cotton, animal hair and even feathers were used as particulate filters. Experimental observations, later supported by theory, showed that fine fibres were necessary and this lead to the use of asbestos, particularly blue asbestos, in the 1930's.

The impetus for further research was provided during the Second World War (1939-45). However the development of fibrous filters for absolute filtration began in the 1950's with the use of the then new man-made fibres. The usefulness of glass fibre was soon apparent with its very high retentive properties for a relatively low pressure drop. Since the 1950's, serious research has been carried out into attempting to understand fibrous filtration and hence maximise its effectiveness. Different industries obviously have different requirements but all essentially want maximum efficiency with minimum pressure drop for as long a period of time as possible. This time factor is especially important in the nuclear industry where there is a storage and disposal problem with contaminated waste. Hence filter unit design has become essential.

The medical aspect has also been influential. According to a relatively recent report by Heyder (64) the particle sizes most dangerous to the human respiratory system are those between 0.1 and 2 μm diameter. This has particularly significant consequences in the nuclear industry. Contaminated dusts of this size range or indeed radioactive aerosol (0.3 μm diameter mean Plutonium aerosols can exist in a stable form) must not be allowed to escape into the atmosphere. Therefore research by this industry has been extensive and contributed much to the present knowledge of high efficiency filtration.

Typical figures for media currently used in the nuclear industry are .002% penetration at 25mm water gauge pressure drop when clean, falling to 0% penetration at 125 mm water gauge pressure drop when the filter is removed. However the need for absolute filtration has developed in other industries, notably the health service and electronics industry. These often require even higher specifications than that quoted above and consequently improvements are continually being sought in filter characteristics. Therefore the understanding and prediction of fibrous filter behaviour is still very much an advancing science.

Similarly work has developed in other fields of air pollution. Particularly related to fibrous filtration in terms of mechanisms, influence etc. are fabric filtration and granular bed filtration. Absolute filtration along with the relevant aspects of fabric and granular bed filtration will be reviewed in this survey. Initially a summary of the measurement techniques for media penetration tests commonly used on laboratory and industrial scale is given.

1.1. Common techniques for penetration measurement

The need to measure the amount of penetration of an aerosol typical of a type the filter is likely to be challenged with is obvious. To enable penetration to be adequately quantified in the critical size range various aerosols have been developed of a polydisperse nature. Typical particle sizes are in the order .01 -2 μm diameter and mass mean sizes around 0.2 - 0.5 μm. The way these aerosols are used in full unit tests and in the laboratory is described below.

1.1.1. Standard tests on full size units

The standard aerosol employed varies from country to country. In the States Dioctylphthalate (D.O.P.) is used, the French prefer uranine dye, and the Germans paraffin oil. The British originally tested with methylene blue (to BS 2831) but now sodium chloride (to BS 3928) is more common. Dorman et al (35) reviewed all these methods and favoured the sodium chloride flame test as the better overall method

with good sensitivity. This was not entirely surprising due to an earlier paper by Dorman et al (34) where they favoured the salt test and also later in a general review of HEPA filtration (36) he restates this opinion for the testing of full size units. Table 1 overleaf, taken from Dorman et al (35) summarises the various tests methods and their effectiveness. It does show some considerable advantages for sodium chloride particularly with regard to sensitivity, time and operable temperature. These properties have resulted in the burning of salt sticks as the most common industrial testing technique. This gives a high concentration of particles overall and removes humidity and drying problems (e.g. Dorman et al (34), Webb and Poyntrig (166)).

1.1.2. Standard tests on filter media

These usually take the form of challenging a sample of filter media, in a filter holder, with an appropriate aerosol. Aerosols used on testing test range from such as atmospheric, polydisperse salt, D.O.P etc. to monosize latex particles - the later being particularly useful for examination of a monosized particle behaviour as by Davies (30). Commonly air is drawn through the media by a fan or vacuum pump but pressurised tests have been carried out, for example with atmospheric aerosol by John and Resich (69). The methods of generation are well reviewed by Kerker (74). Salt aerosol is particularly popular due to its ease of generation and availability. Kerker considers the Collision generator especially consistent in producing a particle size from .009 -.65 μm diameter. Liu & Pui (95) confirmed this. Usually salt is generated from solution (generally 10% concentration by weight).

1.1.3. Penetration Measurement

Some method of determining upstream and downstream concentrations, with respect to the filter, is needed if the penetration of media is to be quantified. In full size operation it is often by a measure of mass generated compared to mass collected after the filter. The latter is found either by a master filter for total collection or by taking a

3

Table 1. Comparisons of 5 test methods for HEPA filters

	AEROSOL STD NO.	Di-octyl phthalate (DOP)	Uranine NFX 44-011	Methylene blue BSS 2831:1971	Sodium Chloride	Liquid Paraffin Oil
1	Type, (solid or liquid)	Liquid droplet	Solid	Solid	Solid	Liquid droplets
2	Size and shape	Spherical. Droplet size centred on 0.3µm. Narrow size distribution	Heterodisperse, near spherical MMD 0.15µ g.s.d. 1.55	Heterodisperse near spherical MMD 0.6µm g.s.d. 2.5	Heterodisperse cubic crystals MMD 0.45µm, g.s.d. 1.8	Spherical, heterodisperse MMD g.s.d
3	Method of generation	Condensation by vapour quenching	Pneumatic atomisation of 1% aqueous solution	Pneumatic atomisation of 1% aqueous solution	Pneumatic atomisation of 10% salt solution	Pneumatic atomisation
4	Reproducibility	Frequent monitoring needed. Homogeneity cannot be checked	Solution strength, air flow and pressure must be constant	Solution strength, air flow and pressure must be constant	Reproducible with constant air supply pressure	Supply air pressure and liquid temperature must be constant
5	Effect on filter	Normally none. Excessive amounts cause deterioration in efficiency	No effect	No effect normally. Large quantities can change filter efficiency	None normally. Excessive amounts increase filter efficiency	Normally no effect. Large amounts can cause filter deterioration
6	Temperature compatability	Suitable for ambient temperature only	Suitable for ambient temperature	Suitable for ambient temperature	Can be used at temperatures up to 400°C.	Suitable for ambient temperature
7	Toxicity	Under review	Unknown	Used in pharmacology	Non-toxic	Not known
8	Normal concentration of test cloud, mg/m³ 1700m³/h test	100	0.012 (one generator in 1700 m³/h.)	0.5 (20 generators)	3.0 mg/m³	10-60 mg/m³
	DETECTION					
9	Sampling method (direct or indirect)	Direct	Indirect - membrane filter	Indirect - esparto filter paper sample	Direct	Direct
10	Method of analysis	Forward light scattering	Deposit dissolved in water and analysed by fluorimetry	Deposits are "steamed" and compared optically	Emission flame photometry	Light scattering. 45° forward angle.
11	Time taken for sampling and analysis	Immediate result; continuous display	Sampling time and time for washing off, dissolving and analysis needed	Time for "steaming" and comparison usually small compared with sampling	Immediate display	Immediate result
12	Discrimination against contamination	Does not discriminate against extraneous particles	Specific for uranine	Specific for soluble blue particles	Specific for sodium	Does not discriminate against extraneous particles
13	Type of result (mass or no. etc)	Dependent on no. of particles and their light scattering section	Mass (volume)	Mass (volume)	Mass concentration	Depends on light scattering properties of the particles
14	Dependence on particle size	Dependence is a complex function of particle size	Depends on sampling efficiency and washability of membrane filters	Sampling efficiency reduced for very fine particles	Independent of particle size within aerosol size range	Affected by changes in particle size distribution
15	Ultimate sensitivity, µg/m³	1.0	0.0012 (10 minute sampling time)	0.1 (15 minute sampling period)	0.01	9.0 (500 particles/cc 0.3-0.4µ) (Sartorius SM 16-175)
16	Method of standardisation	Electronic; assumes mono-disperse aerosol.	Dilute standard solutions	Direct volumetric comparison	Gravimetric; direct ratio	Electronic
17	Linearity of response	Linear with particle concentration provided particle size is constant	N/A	N/A	Linear response below 0.5 mg/m³	Linear provided filter does not modify particle size distribution
	EQUIPMENT					
18	Air treatment required	Filtration; pre-heating	Filtration. Humidity 80%	Filtration. Humidity 85%	Filtration; humidity below 40%	Filtration
19	Warming-up period required	45 minutes	Fluorimeter only	None	15 mins. (Flame photometer only)	Generator requires warming to 100°C
20	Time for 1 test, 0.01% 1700 m³/h excludes filter insertion	1 minute (Est.)	10 mins + time for washing and analysis	30 mins	1 minute	1 minute (Est.)
21	Mass of aerosol deposited in one test. (0.01% 1700m³/h.)	2.8g	0.0033	0.4	0.08g	0.28-2.2g
22	Services required	Electricity	Electricity; compressed air	Electricity; compressed air	Electricity; compressed air	Compressed air; electricity
23	Flexibility; adaptability for leak testing and on-site tests	Widely used for on-site and leak tests (with pneumatic generator)	Inconvenient for leak testing; used for plant testing	Inconvenient for leak testing	Used for on-site testing and for leak testing	Adaptable for leak testing
24	Capital cost (relative)	High cost	N/A	Low cost simple equipment	Medium	N/A

known sample from the main flow. With D.O.P. the concentration is measured upstream and downstream by a light scattering device, usually acting on a sample from the main flow. With salt aerosol, emission flame photometry is the common technique used to measure sodium aerosol concentration. These last two methods have the advantage of an immediate result. In the laboratory (although now also common for in situ tests in industrial work) a further extension of these methods is sometimes employed using specialist equipment not only to give concentration upstream and downstream but size distribution curves as well. Instruments such as optical particle counters (including white light and laser devices), electrostatic mobility analysers and condensation nuclei counters are used in this work. Section 1.1.4. discusses instrumentation in more detail.

A further external influence on instrument performance which can have serious effects is sampling. The three major factors that effect sampling efficiency are:

(i)   Radial dispersion in the duct prior to sampling
(ii) The efficiency of aspiration into the sampling tube
(iii) Deposition in the sampling line

The effectiveness of radial dispersion should always be verified by experiments but empirical guidelines are given in BS 2831. The subject was also recently reviewed by Cunningham and Green (25) who give further information. The efficiency of aspiration should ideally approach 100% for good sampling. This implies that isokinetic sampling is a general requirement although Stenhouse and Lloyd (145) have shown that anisokinetic sampling is acceptable for low stokes numbers. Deposition in sampling lines should be measured experimentally. As a general guideline lines should be short and free of bends. This problem has been examined by Landahl and Herrman (86), Thiagorajon (160) and Crane and Evans (24) amongst others.

1.1.4. Particle sizing equipment in high efficiency filtration

Originally particle sizing was by microscope grids but now sophisticated electronic equipment for sizing and counting dominates the scene. The main types for fine aerosol analysis fall into two catagories:- optical light scattering devices (white light or laser the latter of which have began to dominate in the last 3 years) for particles greater than 0.1 μm and electrostatic mobility analysers for finer particles, less than 1 micron. An accurate device used with monodispersed aerosols less than 1 micron diameter is the condensation nuclei counter e.g. Liu and Pui (95). More recently this has been successfully ~~this has been successfully~~ combined with electrostatic mobility classification to give a highly sensitive instrument for measuring particle sizes below 1 μm diameter. The equipment used for experimental work within the following chapters is a Royco instrument using white light along with a TSI electrostatic mobility analyser, as designed by Knutson & Whithy (78). This review will concentrate on these.

Lieberman (92) in his review of Royco optical particle counters, explains how the operating principle depends on passing single particles through a narrow slit of light. The light scatter produced depends on particle size and is detected using a photomultiplier tube. The output voltage from the photomultiplier tube is then referred to a pulse height analyser. Obviously there needs to be a calibration between the pulse voltage and particle size. This is usually achieved using monodispersed polystyrene latex particles of known size.

The limitation of optical counters such as the Royco is dependant on the noise from the photomultiplier tube in relationship to the particle size which coincides with this. Generally this limit is between 0.1 - 0.5 μm depending on the clarity of the tube and type of light used. One further note of caution is with regard to inflexions which appear in the calibration curve (particle size vs. voltage) for particles between 0.6 and 1.2 μm diameter. However, inspite of these

problems the Royco optical particle counter has been shown to be a suitable particle sizing and counting device for in situ filter testing, Lieberman (94). It is also successful in continuous monitoring or even with adaption to liquid filtration testing as detailed by Lieberman (93).

Obviously with optical devices being limited at best to 0.1 μm diameter particles, an instrument capable of size analysis below this is necessary. The development of such an instrument, that was relatively simple in operation, was by Knutson and Whitby (78). They determined a method of aerosol classification by electric mobility which consists of introducing a high charge onto the aerosol so all aerosol particles are charged to saturation point. The aerosol is passed down a column which has a central electrode at a voltage which will effectively force the collection of aerosol particles above a certain size. Remaining particles reach a master filter, dissipate their charge and consequently produce a current relative to the number of particles above the threshold size. Hence by starting with the smallest size it is possible to change the voltage in predetermined steps, after the required time intervals to reach stability, to find particle counts in various size ranges. Knutson and Whitby calculated theroetically the requirements in terms of time, voltage and consequential multiplication factors to enable evaluation of particle concentration. Pui and Lui (125) have also worked on the calibration for the TSI 3030 electrostatic mobility analyser. Their factors for calculating particle counts are those used in the experiments of this research. The main problem with using this instrument, for high efficiency testing, is that insufficient quantity of aerosol penetrates the filter to give a consistent determinable reading. This severely limits the instrument's applicability. Thus alternative methods or adaptation of the technique is required for analysis of penetration in ultrahigh efficiency filters.

1.2. Clean Filter Media

Work, both theoretically and experimentally, has significantly progressed since Lamb (85) and Langmuir (87). However the areas studied have still generally been those originally suggested by Langmuir namely flow field derivations, capture mechanisms and pressure drop.

1.2.1. Flow Field model within fibrous media

The first attempt at modelling the flow of a fluid around a fibre was by Lamb (85). Davies (28), and Natanson (104) extended Lamb's analysis, to apply at higher Reynold's numbers (< 0.5). All these are "isolated fibre" models in that they are solutions to the problem of flow round an single cylinder in an infinite medium. The effect of Reynolds number on streamline tortuosity is taken into account. However, in a typical HEPA filter the fibre Reynolds number is very low and the proximity of neighbouring fibres has a more significant effect on the field. Fibre interference models are hence more applicable to modern theories of fibrous filtration.

The cellular models published by Happel (60) and Kuwabara (81) describe the flow through banks of parallel cylinders. A filter mat is considered to consist of a number of cells, each cell comprising a single fibre surrounded by an annular envelope of fluid. The diameter of the cell is determined by the proximity of neighbouring fibres and is thus related to the filter packing density. The flow pattern within the cell is related to the cell diameter thus the model in its fundamental concept takes into account the effect of neighbouring fibres. However, each cell may be considered as an independent entity and the field inside is considered in isolation from the rest of the filter.

The physical basis for the model is an assemblage of cylinders moving from right to left in a fluid; the fluid will be displaced above and below the cylinder as shown in figure 1. Due to the opposite directions of neighbouring zones of fluid displacement the boundaries indicated approximate to conditions of zero shear stress.

From this physical model both Happel and Kuwabara postulated the mathematical model shown in figure 1a. The cylinder, moving from right to left, is surrounded by a concentric cell of fluid, such that the ratio of fluid to solid in the cell is the same as the relative volume in the whole assemblage of cylinders.

A general solution of the creeping motion equation in cylindrical polar co-orindates (r, θ) is given by both Happel and Kuwabara as:

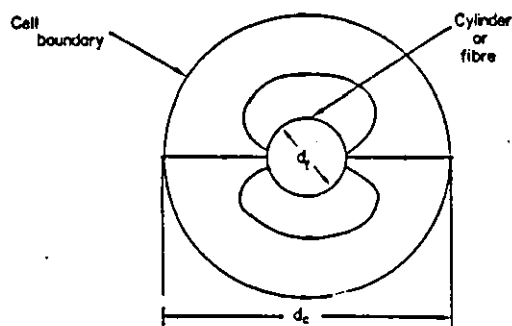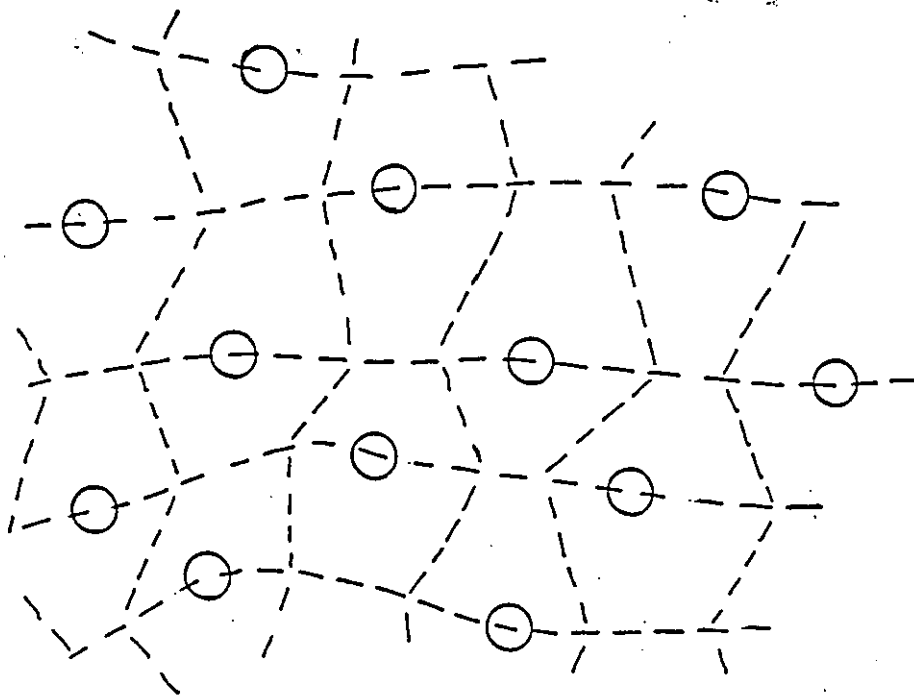# FIGURE 1: Lines of zero vorticity in the Kuwabara flow field model

Fig 1a   Mathematical model.

$$\psi = \left(\frac{A}{r} + Br + Cr \ln r + Dr^3\right) \sin \theta \qquad (1-1)$$

where the polar velocities (U_r, U_θ) are:

$$U_r = \frac{1}{r} \frac{\partial \psi}{\partial \theta} \qquad U_\theta = - \frac{\partial \psi}{\partial r}$$

As the inertia forces in the fluid are assumed negligible and omitted from the Navier-Stokes equation to obtain the creeping motion equation, the model suffers from the disadvantage that it is only applicable at low Reynolds numbers.

Both Happel and Kuwabara applied boundary conditions to solve equation 1-1.

Expressions for A, B, C, D, u and v are given the table below:

Happel (60)

$A = N^4 d_f^2 U_0 / 4J$

$B = \{[1 - 2\ln(d_f/2) - N^4(1 + 2\ln(d_f/2))]U_0/J\} - U_0$

$C = [2(N^4 + 1)] U_0/J$

$D = -4U_0/Jd_f^2$

where $J = 1 + 2\ln N - N^4(1 - 2\ln N)$

$u = \frac{A}{r^2}\left(1 - \frac{2y^2}{r^2}\right) + B + C\left(\frac{y^2}{r^2} + \ln r\right) + Dr^2\left(\frac{2y^2}{r^2} + 1\right) + U_0$

$v = \left(\frac{xy}{r^2}\right)\left(\frac{2A}{r^2} - C - 2Dr^2\right)$

where $r^2 = x^2 + y^2$

Kuwabara (81)

$u = \frac{A}{r^2}\left(1 - \frac{2y^2}{r^2}\right) + B + c\left(\frac{y^2}{r^2} + \ln r\right) + Dr^2\left(\frac{2y^2}{r^2} + 1\right)$

$v = \left(\frac{xy}{r^2}\right)\left(\frac{2A}{r^2} - c - 2Dr^2\right)$

Where $r^2 = x^2 + y^2$

$A = (1 - 2N^2)r_f^2 U_0/J$

$B = (4N^2 \ln r_f + 2N^2 - 2)U_0/J$

$C = -4N^2 U_0/J$

$D = U_0/Jr_f^2$

$J = 1/N^2 + 3N^2 - 4 - 4N^2 \ln N.$

Solutions for the cellular flow field.

The ratio of cell to cylinder radius (N) is related to α, the volume fraction of fibres, or packing density, of the filter mat. As α is increased N decreases and the extent to which the streamlines diverge is accentuated, this effect being similar to that caused by an increase in Reynolds number. For a real filter the relationship between α and N is complex but for an array of equidistant parallel cylinders the packing density is given by:

$$\alpha = \pi/4N^2 \qquad\qquad (1-2)$$

These models by Happel and Kuwabara are often referred to as unit cell models and have been used extensively. Stenhouse and Harrop (143) tested the validity of the theory with model filters and found reasonable agreement. In comparison with real filters, however, there was pressure drop variation in the real filters not present in the model filters or predicted by Happel or Kuwabara. They concluded this was due to the amount of filter homogenity which was considerably less in real filters than model filters. Similarly they surmised that this was the reason for the discrepancy between model filters and theory.

Fuchs and Stechkina (50) stated that the cellular model lead to better agreement with experimental values for efficiency and resistance than the isolated cylinder models. However, there were still significant discrepencies which were attributed to random fibre orientation, filter inhomogeneity and errors in the measurement of porosity.

In much later work Kirsh and Stechkina (76) developed the parallel cylinder idea to the fan model. This is shown in figures 2,3,4. Using this model they could get much closer to real filter results. Figure 5 shows how they determined the influence of each mechanism in terms of velocity versus particle size. This is discussed further in section 1.2.2.1.
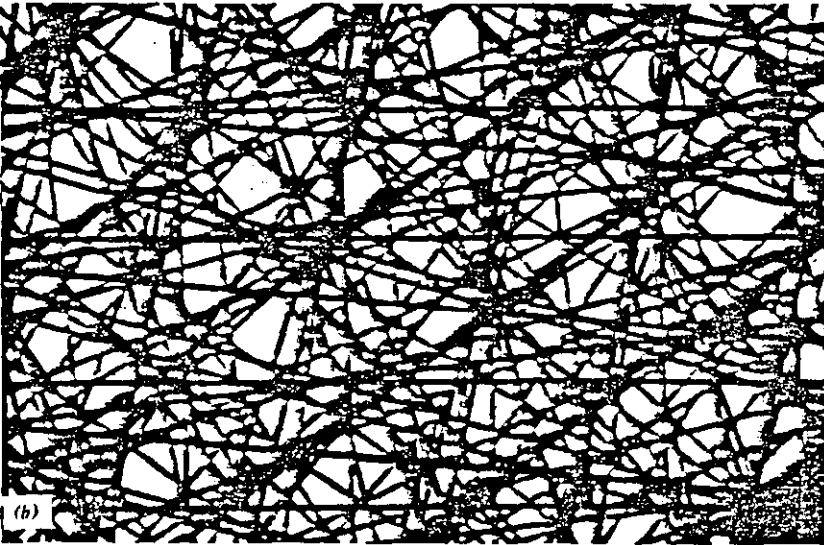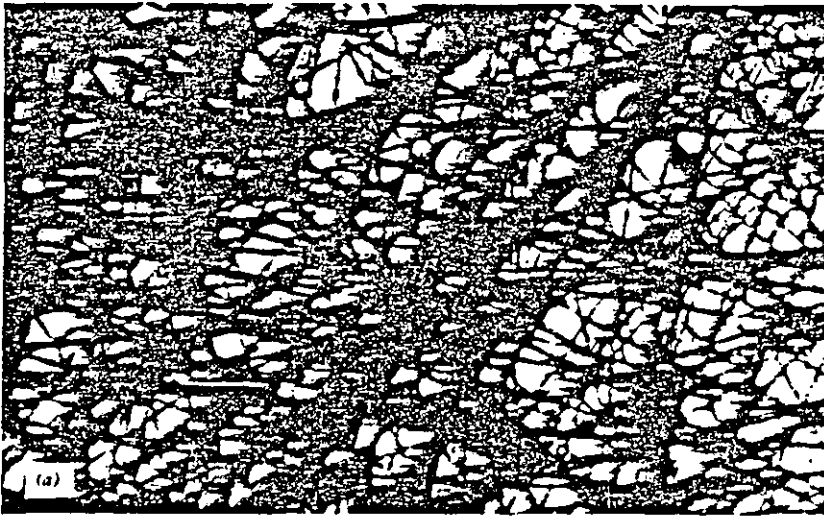
Figure 2 (*a*) A micrograph of a real filter. (*b*) Photograph of a fan model filter.   From Kirsh (76)
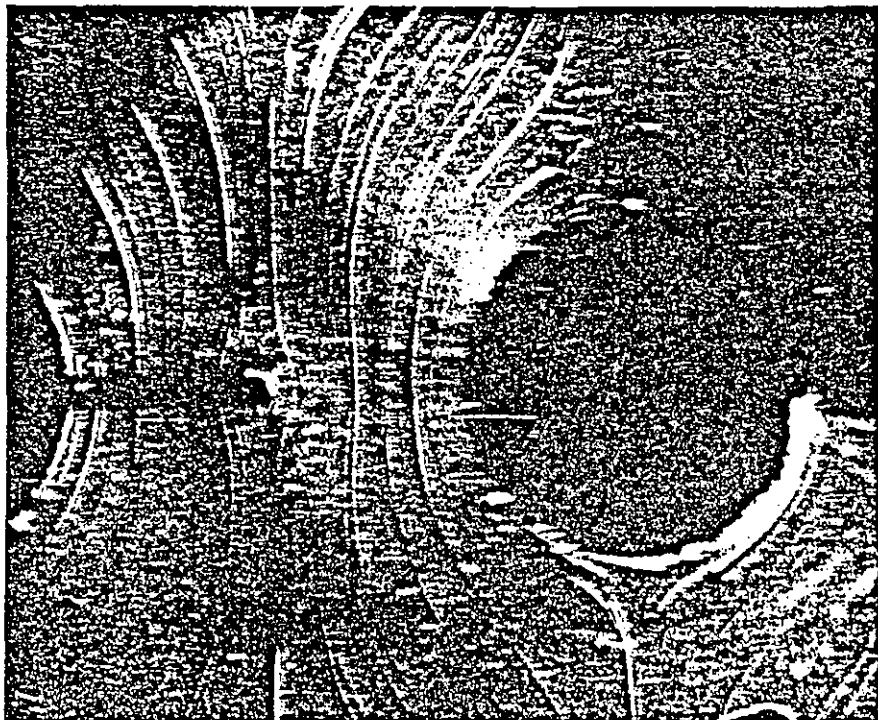
Figure 3. Photographs showing flow field in an array of cylinders of dfifferent radii
From Kirsh (76)

12
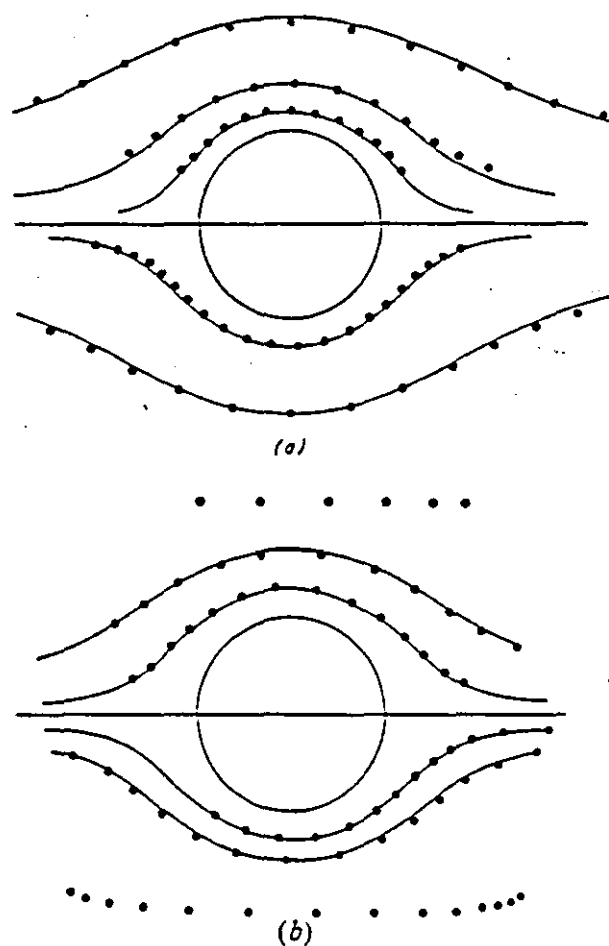
Figure 4 Flow field in the array of parallel cylinders with (a) $\alpha = 0.05$ and (b) $\alpha = 0.20$; curves: theory; points: experiment;

From Kirsh (76)

FIGURE 5: Domains of filtration mechanisms — Kirsh (76)

▥ Diffusion
⊟ Interception
▨ Inertia

14
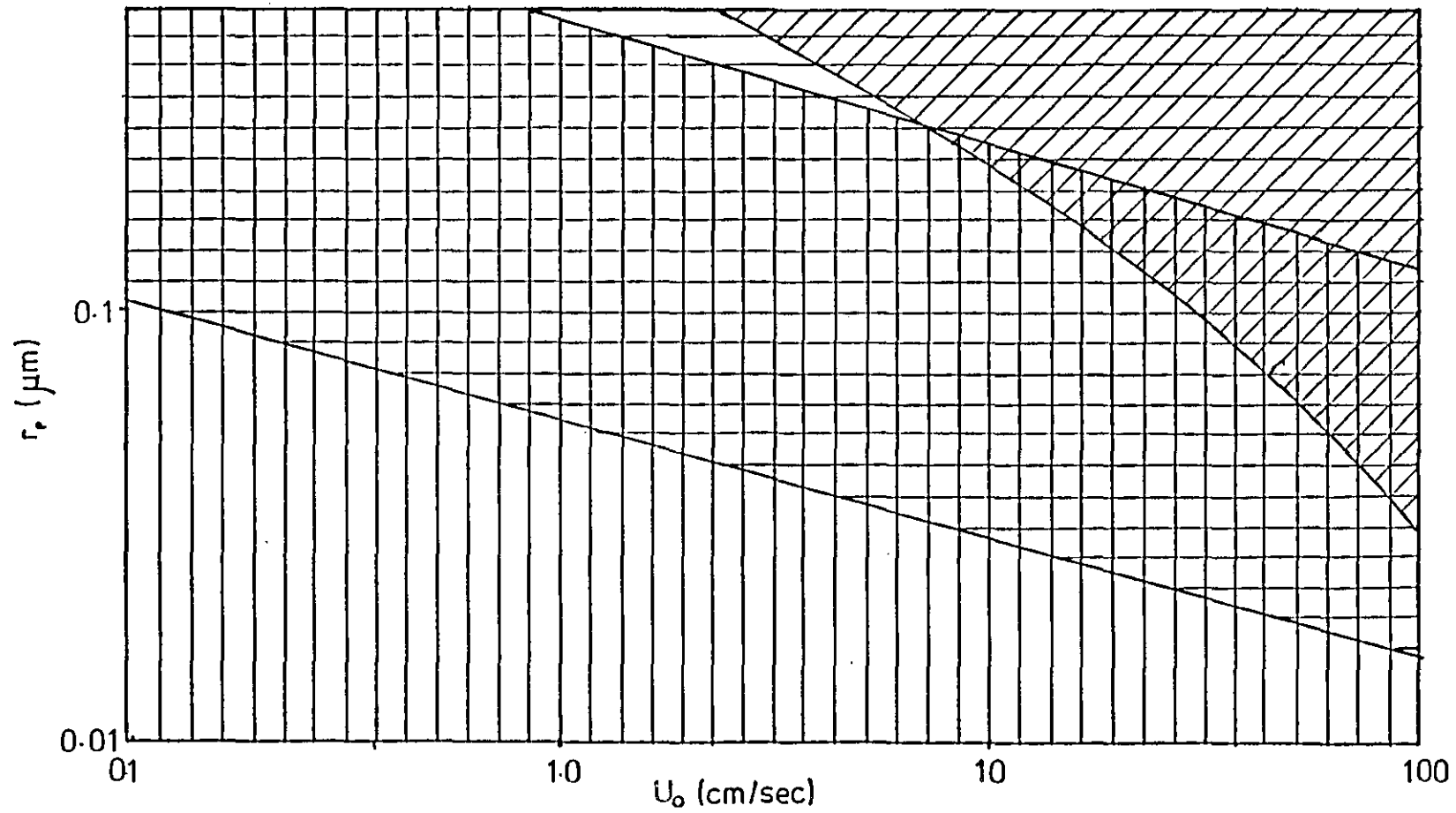
Tsiang and Tien (.162) have a preference for the parallel fibre concept in recent work. They consider that it has advantages over the unit cell model because there is no ambiguity with initial conditions for trajectory calculations. However, it over simplifies the real filter considerably and doesn't account for fibre interaction in an axial direction. This is clearly demonstrated by discrepencies with experimental work. Nevertheless Tsiang et al (163) decided to use this model as the basis for computer simulation work. The simulation incorporated the original ideas of Miyagi (101) for an infinite array of parallel fibres, to calculate particle trajectories. These are in the usual form except they assume, due to low Stokes number, the particles will follow streamlines and hence they use fluid velocity as an approximation to the particle velocity. The model proceeds to develop a dendritic build up approach and its consequences will be discussed further in sections 1.2.2.1. and 1.3.3.

Finally the most recent work on fibrous filter flow fields has extended some of the ideas of previous work particularly with respect to fibre interference. Brown (15) has preliminarily developed a model to describe flow through a fibrous filter incorporating the idea of the variational principle. This means he has modelled the flow field allowing for the interference of other fibres dependent on their distance from each other. However, as yet, only one dimension has been accounted for i.e the fibres are treated as flat in the direction of flow. Also calculations are at zero Reynolds number. This approach will need to be developed further before the results can be suitably compared.

1.2.2. Efficiency of clean fibre media

1.2.2.1. The normal collection mechanisms

The collection efficiency of a fibrous mat, E, is related to that of a single fibre within it, η, by :

$$E = 1 - \exp \left\{ \frac{- 4\alpha \ Ln}{\pi d_f (1-\alpha)} \right\} \qquad (1-3)$$

η is the single fibre efficiency which is the volume of gas cleaned divided by the fibre swept volume. Particles are removed from the gas by a number of mechanisms, the most important of which are diffusion, inertia and interception.

Up to the 1950's, the main work on efficiency of fibrous filtration had been done by Langmuir (87). However, new ideas were beginning to develop around 1950, such as those of Landahl and Herrman (86), Ramskill and Wendell (132) and Davies (28), with regard to inertia, or Johnstone and Roberts (70) and Stairmand (139) with regard to diffusion. A review by Chen (20) in 1955 gave a very effective summary of the state of the science at that time.

The next major work was by Natanson (103). He considered diffusional collection for a cylinder in potential flow conditions. He found:-

$$\eta_D = 4 \pi^{-\frac{1}{2}} Pe^{-\frac{1}{2}} \qquad (1-4)$$

under conditions that $Pe^{-\frac{1}{2}} < 1$ and $R \ Pe^{\frac{1}{2}} < 1$.

Friedlander (48) also considered efficiency by diffusion. He looked at the rate of mass and heat transfer to single spheres and cylinders for low Reynolds numbers. He used boundary layer theory and velocity distributions derived from the Navier Stokes equation to evaluate the effect of Peclet and Reynolds numbers on the Nusselt number. From these results he estimated single fibre efficiency due to diffusion and interception showing the dependence of diffusional collection on Peclet number to the negative two thirds for the first time. Further work, Friedlander (49) and Pasceri and Friedlander (113) results in a simplified equation for use in design calculations. This involved the Schmidt number and is given as:

$$\eta = 6Sc^{-\frac{2}{3}}Re^{\frac{1}{2}} + 3R^2Re^{\frac{1}{2}} \qquad\qquad (1-5)$$

Stechkina and Fuchs (140) used a parallel cylinder system to consider the diffusion boundary layer (δ) and its relationship to diffusional deposition of particles. They found :

$$2\,k\,\eta_D = 2.3\delta^2 + .312\,\delta^3 \qquad\qquad (1-6)$$

where,

$$k = \text{hydrodynamic factor} = 2 - \ell n\ Re\ (\text{Lamb}\ (85\ ))$$
$$= -\tfrac{1}{2}\ \ell n\ \alpha - 0.5\ (\text{Happel}\ (60))$$
$$= -\tfrac{1}{2}\ \ell n\ \alpha - 0.75\ (\text{Kuwabara}\ (81))$$

They added this to the interceptive effect as defined by Langmuir (87) and included an interactive effect to result in:

$$\eta = 2.3\delta^3 + .312\delta^3 + 2(1+R)\ell n(1+R) - (1+R) + (1+R)^{-1} + .68\delta^{\frac{3}{2}}R^{\frac{2}{3}}$$

$$(1-7)$$

The concept of the fan model by Fuchs, Stechkina and Kirsh has given some of the most significant advances in the study of the effect of filter non-uniformity on filter efficiency. Kirsh, Stechkina and Fuchs (75), Kirsh and Stechkina (76) and Kirsh and Stechkina in Shaw's book (138) consider the fan model. An experimental model filter was built consisting of a number of grids, each of parallel wires which were placed closely in series so the fibres had a random orientation to each other. This simulates an ideal filter with regard to fibre orientation although it is still too uniform with regard to spacing. They showed experimentally the packing effect to be described by the hydrodynamic factor.

$$K_f = -\tfrac{1}{2}\ln\alpha - 0.52 + 0.64\alpha + 1.43(1-\alpha)\,Kn_f \qquad (1-8)$$

A correction factor, ε_f which can be used to compare the real and fan filters, is obtained from measurement of pressure drop in a real filter giving:

$$\varepsilon_f = \left(\frac{4\pi}{K_f}\right)\Bigg/\left(\frac{\Delta P\,\mathrm{expt}\ \pi d^2}{4U_0\ \mu\ \alpha\ L}\right) \qquad (1-9)$$

ε_f is usually in the range $1.13 - 2.25$ and the single fibre efficiency calculated using the fan model η_f is converted to the real efficiency by

$$\eta = \eta_f / \varepsilon_f \qquad (1-10)$$

The value for the single fibre efficiency of the fan model comes from the sum of the contributions:

$$(1-11)$$

$$\eta = \eta_D + \eta_R + \eta_{DR}$$

where,

$$\eta_D = 2.7 Pe^{-2/3}(1 + 0.39 K_f^{-1/3} Pe^{1/3} Kn_f) + 0.624 Pe^{-1} \quad (1-12)$$

$$\eta_R = (2K_f)^{-1} \left\{ \begin{array}{l} (1+R)^{-1} + 2(1+R)\ln(1+R) - (1+R) \\ +2.86 Kn_f (2+R)R(1+R)^{-1} \end{array} \right\} \quad (1-13)$$

$$\eta_{DR} = 1.24 K_f^{-1/2} Pe^{-1/2} R^{2/3} \quad (1-14)$$

This does not take the effect of inertial interception into account. Stechkina et al [141] calculated this for low Stokes numbers (less than 0.2) where:

$$\eta_I = \frac{I. St}{(2 K_f)^2} \quad (1-15)$$

and

$$I = (29.6 - 28\alpha^{0.62}) R^2 - 27.5 R^{2.8} \quad (1-16)$$

However the factor K_f varies slightly to that used in equation (1-8) and (1-12,14) and so the inertial efficiency should only be taken as an estimate.

Other models to evaluate diffusional and interceptive collection are available and well reviewed by Davies [28] and more recently Shaw [138]. The effect of inertial collection has been studied by several authors using numerical computation of particle trajectories.

Harrop andStenhouse (62) numerically solved the basic particle trajectory equations in the Happel-Kuwabara flow fields. They found for inertial interception a constant value was approached for Stokes numbers greater than 2-3. This steeply reduced for values between 2 and 0.5 (although less significantly below Stokes numbers of 1). They also considered the relationship of efficiency with packing density and found efficiency decreasing as packing density reduced. However these results were with zero Reynolds number calculations which will under estimate the efficiency especially with low levels of inertia.

This approach of using trajectory equations was continued by Griffin and Meisen (56) when they looked at inertial and interceptive impaction at moderate Reynolds numbers. Particles were considered to be suspended in a fluid moving steadily through a random array of parallel cylinders, with the flow field solution subject to Kuwabara's zero vortocity boundary condition. Efficiencies were then found as functions of Reynolds number ($0.2 < Re < 40$) , particle inertial parameter ($0 < St. < 1000$), interception parameter ($.001 < R < 1$) and packing density ($10^{-4} < \alpha < .111$). Results are expressed graphically in figures 6, 7 and 8.

Emi et al (39) carried out some similar work, their results showing the considerable difference (particularly at low Reynolds numbers) between isolated fibre and neighbouring fibre effects. With the latter included (accounting for packing density) the predicted efficiencies were much higher. Hayashi and Uchiyama (63), although working with trajectories in a magnetic field, also found the importance of one fibre being in front of another fibre and its influence on the trajectory of a particle.

Emi et al (40) and (41) continued to work on flow field influence and applied Kuwabara's model to the convective diffusion equation. They solved this for a range of Peclet numbers from $1 - 10^4$ and extrapolated to cover higher Peclet numbers. The results gave diffusional collection efficiencies over a wide range of Reynolds numbers comparing with analytical solutions for creeping flow ($Re < 0.1$) by Stechkina and Fuchs (140) and potential flow ($Re \rightarrow \infty$) by

FIGURE 6 : Efficiency as a function of Stokes number
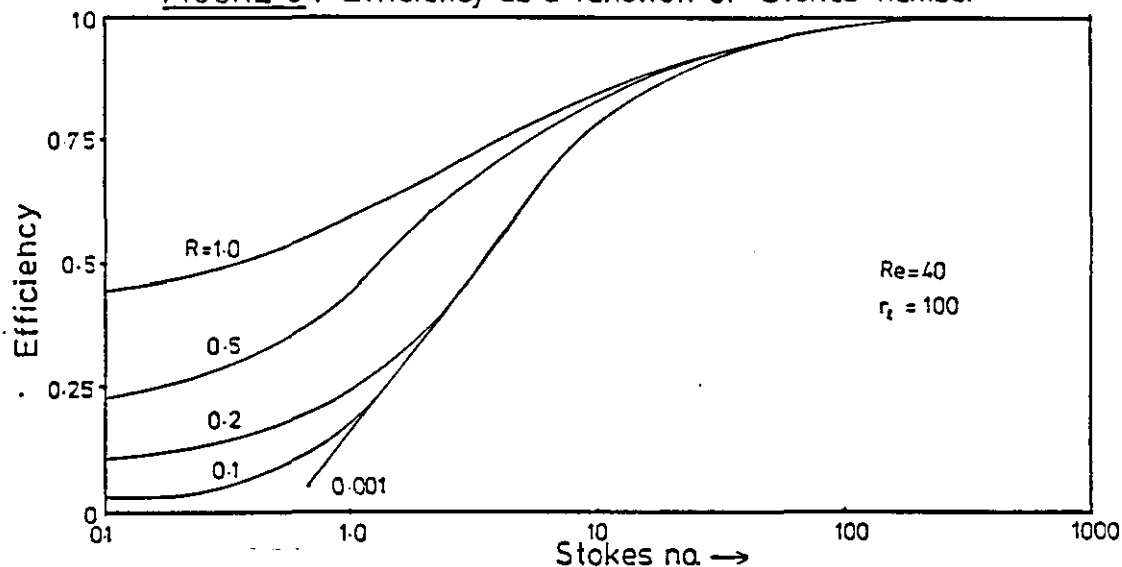
FIGURE 7: Efficiency as a function of Reynolds number
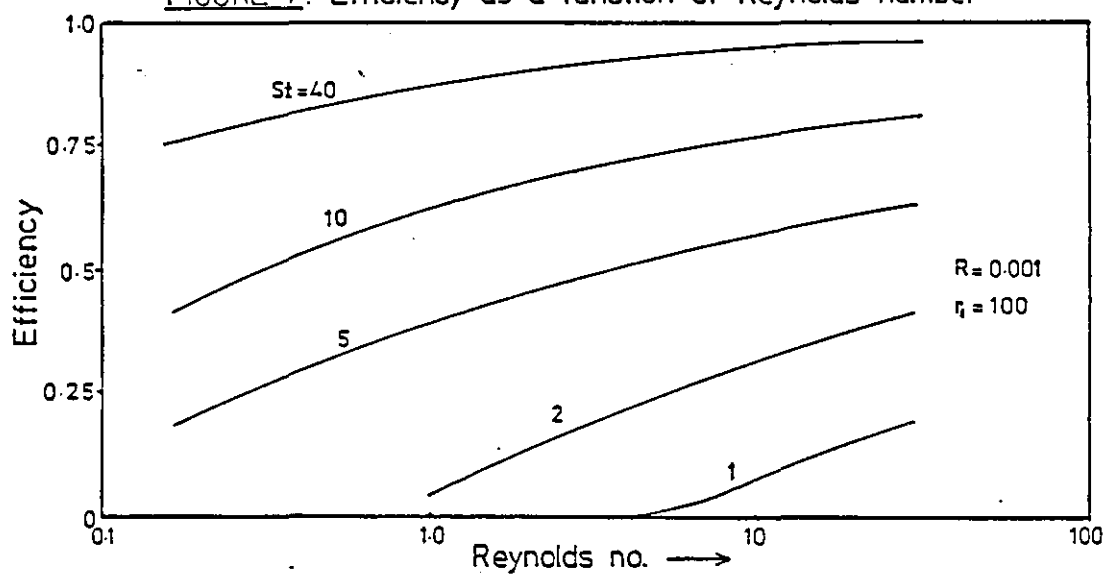
FIGURE 8 : Efficiency as a function of solids concentration

21
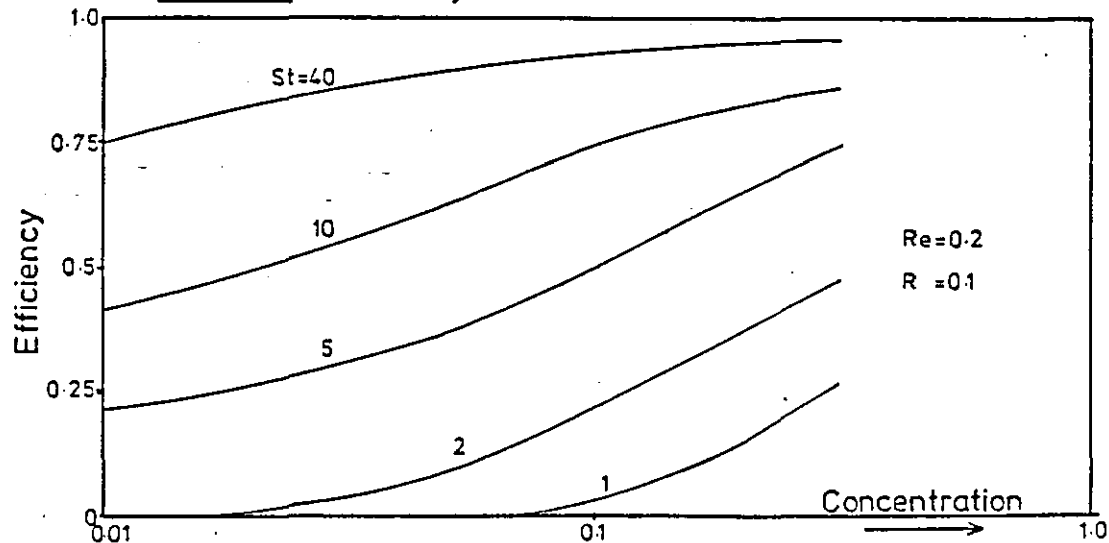
Natanson (103) at the extremes. Besides finding efficiency decreasing with Peclet number, they also showed that packing was an important influence on diffusional efficiency for low Peclet numbers whereas the Reynolds number effect was more significant at large Peclet numbers.

Ingham(68) carried out a more complex evaluation of diffusional deposition by taking the flow field around a cylindrical fibre but with a boundary layer for diffusion around the fibre. He determined diffusion at both the front and back of a fibre and obtained

$$\eta_D = (\Sigma_1 + \Sigma_2) \, Pe^{-\frac{2}{3}} \qquad (1-17)$$

for Pe > 1, Re < 100, Pe > Re

and where Σ_1 and Σ_2 are f (Re) and have to be numerically determined Σ_1 account for streamlines passing the fibre whereas Σ_2 accounts for eddies behind the fibre.

Lee and Liu (90) , (91) were interested in flow field effects particularly with interference from neighbouring fibres. They showed:

$$\eta_D = 2.6 \left(\frac{1 - \alpha}{K}\right)^{\frac{1}{3}} Pe^{-\frac{2}{3}} \qquad (1-18)$$

where $k = -\frac{1}{2} \ln\alpha - \frac{3}{4} + \alpha - \frac{\alpha^2}{4}$ (hydrodynamic factor)

and

$$\eta_R = \left(\frac{1 - \alpha}{K}\right) \frac{R^2}{1+R} \qquad (1-19)$$

Correlating with experimental results, where they had earlier shown the dependence of filter efficiency on particle size, velocity and filter solidity:

$$\eta = \eta_D + \eta_R = \beta_1 \left(\frac{1 - \alpha}{K}\right)^{\frac{1}{3}} Pe^{-\frac{2}{3}} + \beta_2 \left(\frac{1 - \alpha}{K}\right) \frac{R^2}{1+R} \qquad (1-20)$$

This holds well around the minimum efficiency point for $\beta_1 = 1.6$ and $\beta_2 = 0.6$.

The most penetrating size, has been examined by other workers. Dorman (33) in his review thought the most penetrating size to be between .05 and 0.3 μm with 0.1 μm diameter particles for standard HEPA filtration conditions. Kapoor et al (72) found 0.1 - 0.15 μm (average 0.13 μm) as the most penetrating size under normal filtration conditions. Kirsh et al (77) also showed the problem of theoretical predictions. They made predictions using the fan model including the mechanisms of interception, diffusion and their interaction. This gave a larger most penetrating size than experiment showed. One possibility could be that some of these problems are due to not accounting for inertia in the model. ~~attempting to predict the most~~. It is often regarded as unimportant for these small particles sizes.

Magee and Jonas (98) developed an empirical fit including inertia, from work of Dorman. This began with the relationship.

$$\ln P^* = 2 - K_I L U_o^x - K_D L U_o^{-y} - K_R L \qquad (1-21)$$

where,

P^* = % penetration

L = filter thickness

U_o = face velocity

K_I, K_D, K_R = characterisation parameters for inertia, diffusion, and interception respectively.

x and y = numbers theroetically determined or data fitted. Generally accepted $1 < x < 2, 0.5 < y < 0.6$

To find U_o for the maximum penetration a plot of $\ln P^*$ vs U_o was used but this was indeterminate and so an alternative technique was tried. They let $U_o^x = (U_o^{-y})^{-x/y}$ which by substitution and differentiation gave:

$$\frac{d \ln P^*}{d U_o^{-y}} = \frac{x}{y} L K_I \left\{ U_o^{x+y} - U_c^{x+y} \right\} \qquad (1-22)$$

and

$$K_D = \frac{x}{y} \, K_I \, U_c^{x+y} \tag{1-23}$$

By linear regression of $\dfrac{d \ln P*}{dU_o}^{-y}$ on U_o^{x+y} they obtained K_I from the slope and U_c at the intercept. Hence the filter could be characterised providing some experimental data was available.

Another important empirical model was that derived by Nguyen and Beeckmanns (106). It expressed the overall efficiency as

$$E = 1 - \exp \left\{ \frac{- \eta \alpha L}{d_f (1-\alpha)} \right\} \tag{1-24}$$

and takes the single fibre efficiency η to be equal to

$$\eta = \eta_I + \eta_R + \eta_D \tag{1-25}$$

Determination of η_I was based on Landahl and Herrmann's (86) work where they expressed this as :

$$\eta_I = \frac{St^3}{St^3 + 0.77 St^2 + 0.58} \tag{1-26}$$

From this it has been normal to modify η_I by multiplying by a power series of packing density (α). This can give inertial efficiencies greater than unity so the authors chose the alternative of multiplying Stokes number by a function of packing density

$$f(\alpha) = 1 + K_1 \alpha + K_2 \alpha^2 \tag{1-27}$$

They also multiplied the second term of the numerator by

$$F(Re) = 1 + \frac{K_3}{Re^{\frac{1}{2}}} + \frac{K_4}{Re^2} \tag{1-28}$$

Hence,

$$\eta_{\tau} = F(Re, St, \alpha) = \frac{St^3 \, F(\alpha)^3}{St^3 F(\alpha) + 0.77 \, f(Re) St^2 F(\alpha)^2 + 0.58} \qquad (1-29)$$

Having reviewed other work they also correlated

$$\eta_R = 7 \, R^3 \qquad R < 0.62$$
$$\eta_R = 1-R, \qquad R > 0.62 \qquad\qquad (1-30)$$

The exact forms of equations 1 - 30 is not essential as $\eta_R \ll \eta_I$ for most cases.

Therefore by comparing equation 1-30 with experimental works on real and model filters it is possible to obtain the regression coefficients K_1 to K_4 and hence complete the correlation.

Besides the fairly conventional approaches mentioned so far other suggestions and methods to calculate and account for filtration efficiency have been suggested. Bragg and Pearson (11) developed an analytical model assuming helical tubes to represent the flow passages in a filter. The model predicts efficiency due to diffusion and inertia and appears reasonable when compared to experiment for porosities between 0.7 and 0.994 and with fibre diameters greater than 5 μm. However doubt must be expressed in the model due to its improbable flowfield.

Radushkevich (131) also had a theory that ultra thin fibres present in multi component filters performed intensive Brownian vibrations due to which aerosol particles should be additionally captured from the gas flow. His calculations showed that for a single .05 μm diameter fibre fixed at one point the number of particles depositing within one second would increase 10 - 20 times compared with it being motionless. He attempted to confirm this hypothesis by showing that in experimental work ultra thin fibres gave higher than normal efficiencies. Sufficiently thin fibres of adequate length and with high porosity gave the best effect.

Cavanagh (19) strongly disagreed with Radushkevich's hypothesis and carried out several experiments to disprove it. He set up a system under the observation of a scanning electron microscope and took long exposure photographs to look for blurring. The only vibrations he encountered could be traced to electrostatic charges. He considers the whole idea of Brownian motion of a fibre a doubtful concept and that any vibrations of a fibre in a filter are far more likely to originate in normal mechanical ways.

This concludes the review of the general mechanisms found in fibrous filtration. However other factors have been found important such as electrostatics, material properties and the adhesive probability of a particle on a fibre. These influences will be discussed in the following two subsections.

1.2.2.2. Physical effects on collection efficiency

The effects of specific operating and filter media design parameters on performance is reviewed in this section. Also the actual physical conditions, temperature and pressure in particular, and the presence of electrostatics will affect the collection efficiency.

In his 1976 review Dorman (33) cited Chen's equation for the packing density influence obtained experimentally

$$\eta = \eta_o \ (1 + K'\alpha) \tag{1-31}$$

where, $K' \simeq 4.5$

Stenhouse et al (142), (149) found no evidence for packing density affecting single fibre efficiency while filtration was in the diffusive regime but as expected the overall collection efficiency would increase with increasing fibre concentration. In the inertial regime the effect on η is much more important.

The effect of fibre diameter has been examined by several authors. Radushkevich and Velichko (127) and Radushkevich and Kolganor (130) working with ultra thin fibres found little influence on efficiency. However, using coarser fibres Goldfield and Gandhi (55) showed mats of 1.4 μm fibres at velocities between 1 -18 m/s gave much lower penetration figures than larger fibres of 4.4 μm and in turn these fibres gave a much better performance than 7.8 μm fibres.

Masliyah (99) was particularly interested in elliptic fibres and compared these with normal circular fibres. He examined both diffusional and interceptive collection mechanisms and based his work on the Kuwabara cell model.

He found circular fibres were more effective in the diffusive regime but elliptical fibres had an advantage within the interceptive region.

Dorman (33) discussed temperature and pressure effects on the filtration efficiency. With regard to temperature he agreed with Pich assuming the only variable would be viscosity such that an increase in temperature would enhance diffusional capture but reduce inertial effects. He gives experimental evidence to this conclusion.

Stern et al (152) were interested in operating at reduced pressures and from their work drew several significant conclusions.

a) A minimum efficiency exists for each particle size at ambient and reduced pressures.

b) A unique velocity exists where collection efficiency is approximately the same for all particle sizes. This velocity shifts to lower values with reducing pressure.

c) For a given particle size and velocity, efficiency increases with pressure reduction.

d) In the inertial regime efficiency increases with particle size.

e) In the diffusional regime efficiency decreases with particle size.

f) For extremely low pressures 100% efficiency is feasible for submicron particles by either diffusion or impaction

g) In the diffusion regime alone no particle size of maximum penetration was found to exist.

The actual material used to make fibrous or fabric filters has also been shown to be important in its influence on particle collection. Subrahmaniam and Rao (153) showed that glass fibre is superior for normal use and in high temperature or acid conditions. Alkali conditions would probably require a synthetic fibre. In fabric work synthetic fibres are much more common. Turner (164) found that with bag filters nylon was very effective. Donovan et al (31) considered that addition of an expanded PTFE laminate, Goretex, to the top layer of a fabric filter greatly improved its overall performance. Mohammed and Afify (102) came to a similar conclusion using a Cerex scrimp on needle punched filters. Material and fibre geometry have also been shown to be significant.

Electrostatics is considered by many to be an important mechanism however the more important work has concentrated on fibre charging especially in the field of fabric filtration. Frederick (47), Koscianowski and Koscianowski (79) as well as Airman and Tang (2) and Ariman (5) have done some work looking at this. Important work has come from Lamb and Costanza (82), (83) and (84) and Miller, Lamb, Costanza et al (100) with regard to the role of fibre structure and electrostatics in fabric filtration. They found crimping fibres or using trilobal fibres increased the electrostatic effect to give lower penetration figures. They proved this by elimination of local differences in electrical potential by gold coating the fibres. The penetration improvement was reversed when they retested.

Ho and Wang (66) found that the single fibre efficiency of an 8.5 μm fibre with a flow velocity of 27 cm/s for 1-2 μm particles, could be increased an order of magnitude by introducing a 5 - 10 kV/cm electric field. Reid (133), in experimental work charged both particles and fibres equally and observed:

a) Deposition of a negatively charged particle on a negatively charged fibre is dependent on the magnitude of the ratio of the mat charge to that of an individual fibre.

b) Velocity decreased efficiency almost linearly as it increased.

c) Particle resistivity showed no trend on efficiency except some degradation of efficiency may be expected at lower resistivities.

d) Particle size influence on efficiency was greatest at particle sizes from 2 - 3 μm but negligible below 1 μm.

e) It was found the fibre electrical resistivity should maintain a high value to be effective in submicron range.

f) Both bed thickness and fibre volume density had dramatic effects on efficiency - increasing bed thickness with high velocity was especially effective.

g) The actual dust concentration had no direct effect on bed efficiency, although near saturation charge on the particles was required for the electrostatic charging to be most effective.

Loffler (96) and (97) tried to quantify the electrostatic influence.

He compared results from experiments with and without electrostatics and found:

$$\eta_E = \eta_T - \eta \qquad\qquad (1\text{-}32)$$

(η_T = single fibre efficiency with electrostatics present)

where

$$\eta_E = \frac{1.22(2 - \ln Re). N_{Qq}}{(\frac{1}{2} St \ Re^{-\frac{1}{2}})^{1.5} + 1}$$ (1-33)

N_{Qq} is the charge parameter

$$N_{Qq} = Qq/3 \ \pi \epsilon_o \mu d_f d_p U_o$$ (1-34)

where,

Q   = fibre charge per unit length, q = particle charge

ϵ_o = influence constant = 8.86 x 10^{12}

Recently Shapiro et al [137] carried out a study to find the relative effect of various electrical forces on aerosol filtration in fibrous and granular filters. They covered the engineering practical range of electrical field intensity and dust particle sizes. They found the coulombic force, was the most powerful force in most situations. However, the space charge effect and the image force can dominate some parts of the diffusional region while the dielectrophoris effect may be important for sufficiently large particles. Definitions of these particle forces are given below while their quantification is in table 2. Figures 9 and 10 give a good graphical representation of the various regimes of influence of these forces for spherical and cylindrical collectors respectively.

Definitions of the forces as applying to table 2 are:

a) Coulombic force due to collector charge
This is the attraction or repulsion between a collector charged by an electrostatic charge (Q) and a dust particle charged by a charge (q) when separated by a distance (r) between the centres of collector and particle.

b) Image Force
This is an interaction between a charged particle radius r_p and a neutral collector of radius R.

Table 2. Electrostatic forces—normalized with $E_0 q$ - from Shapiro (137)

Type of interaction	Spherical collector		Cylindrical collector	
	a. Force at $r = R + r_p$ Normalized with $E_0 q$	b. Normalized force for Saturation charges	c. Force at $r = R + r_p$ Normalized with $E_0 q$	d. Normalized force for saturation charges
1 Image force	$\dfrac{q a_s}{16\pi\varepsilon_0 E_0 r_p^2}$	$\dfrac{3}{4} a_s b_p$	$\dfrac{q a_c}{16\pi E_0 \varepsilon_0 r_p^2}$	$\dfrac{3}{4} a_c b_p$
2 Dielectrophoresis due to collector	$a_p \dfrac{r_p^3 Q^2}{2\pi\varepsilon_0 q E_0 R^5}$	$6\dfrac{a_p b_c^2}{b_p}\dfrac{r_p}{R}$	$\dfrac{Q_c^2}{E_0 q}\dfrac{a_p}{4\pi\varepsilon_0}\left(\dfrac{r_p}{R}\right)^3$	$\dfrac{3}{4}\dfrac{a_p b_c^2}{b_p}\dfrac{r_p}{R}$
3 Coulombic force	$\dfrac{Q}{E_0 4\pi\varepsilon_0 R^2}$	$3b_p$	$\dfrac{Q_c}{2\pi\varepsilon_0 E_0 R}$	$6b_p$
4 Space charge effect	$\dfrac{q R N_p}{3 E_0 \varepsilon_0}$	$3b_p \beta \dfrac{R}{r_p}$	$\dfrac{q N_p R}{2\varepsilon_0 E_0}$	$\dfrac{9}{2} b_p \beta \dfrac{R}{r_p}$
5 Coulombic force due to external electric field	$1 + 2a_s$	$1 + 2a_s$	$1 + a_c$	$1 + a_c$
6 Dielectrophoresis due to external electric field	$24\pi\varepsilon_0 a_p a_c E_0 \cdot$ $\cdot\dfrac{r_p^3}{Rq}(2a_s+1)$	$\dfrac{2a_p a_s r_p}{b_p R}(2a_s+1)$	$8\pi\varepsilon_0 a_p a_c \dfrac{E_0}{q}\cdot$ $\cdot\dfrac{r_p^3}{R}(a_c+1)$	$\dfrac{2}{3}\dfrac{a_p a_c r_p}{b_p R}(1+a_c)$

FIGURE 9 : Diagram of relative influence of the electrostatic forces for a spherical collector *
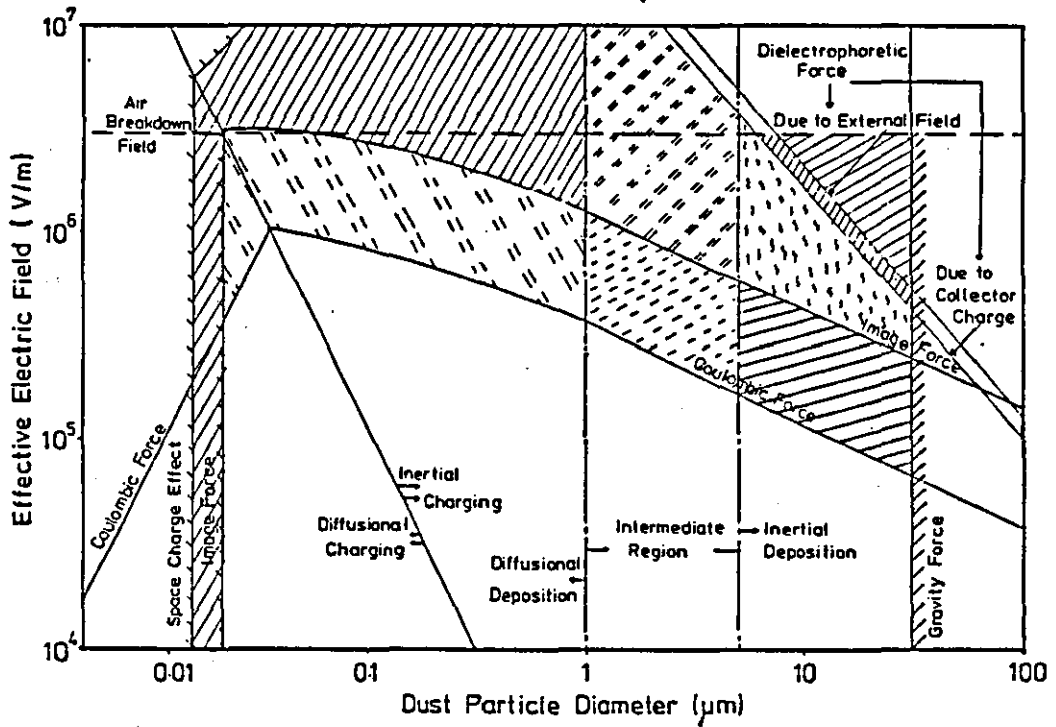

FIGURE 10: Diagram of relative influence of the electrostatic forces for a cylindrical collector *
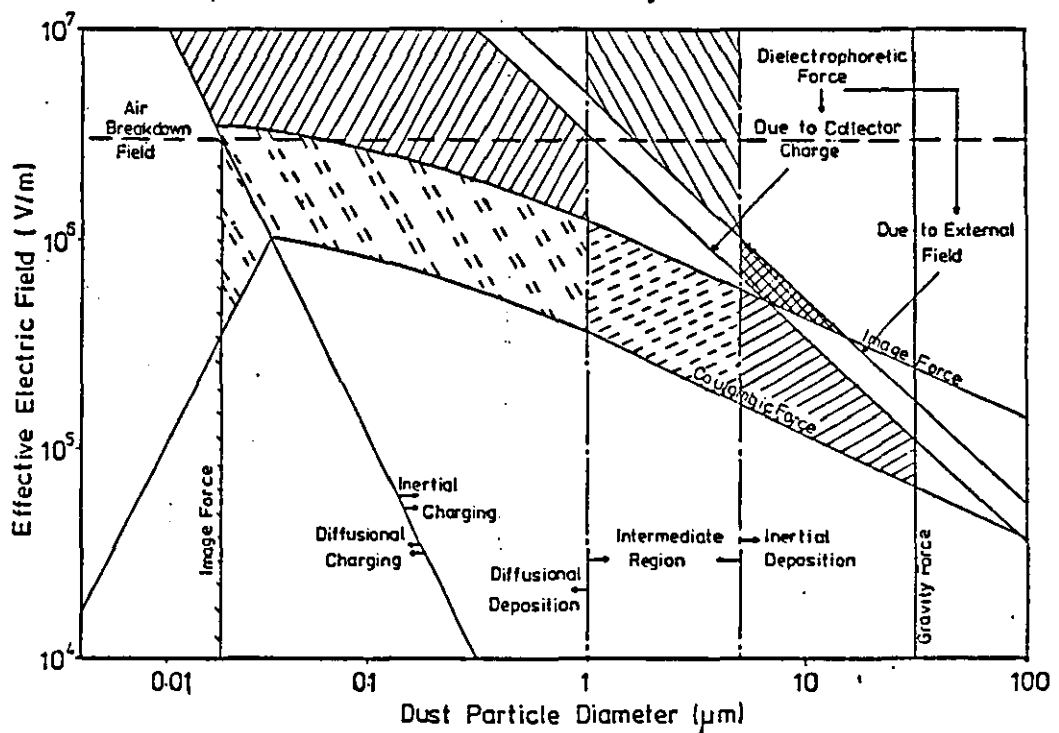
* Shapiro (137)

c) Space charge effect

This is when an uncharged sphere is in a cloud of charged particles of density N_p and a particle from the cloud experiences a net repulsion due to an uneven space charge distribution.

d) Coulombic force due to external field E_o

The force experienced by a charged particle in the vicinity of an uncharged collector due to charge polarisation induced by an external field.

e) The dielectrophoretic force

Present whenever there is inhomogenity in an electric field. An uncharged polarised particle experiences forces of different magnitude at its poles resulting in a net force. This force may exist due to an inhomogenity in the external field or one induced by collector charge.

1.2.2.3. The adhesion effect and its probability

So far the theoretical analyses given have implied a particle remains on the fibre after collision. Gillespie (52) in 1955 made one of the earliest suggestions that particles may not automatically stick to a fibre after colliding with it. However the concept of particle adhesion probability was not seriously considered for another fifteen years. Stenhouse et al (142) used wire grids coated with oil for some experimental work. The oil was to improve adhesion as they suspected many particles may bounce off the grids after collision. This they thought was particularly prevalent at higher velocities. Dorman (32) has similarly suggested precoating of fabric filters to improve collection efficiency.

From these initial observations several authors including Dahneke (26), Arziev et al (6), Stenhouse et al (144), (146), (147), (148), (151), Broom et al (13), (14) made a more thorough study. Significantly in his thesis Broom concludes:

(a) Adhesion probability decreased with increasing particle size and velocity. This was in accordance with theoretical reasoning, with impact velocity having an especially severe effect.

(b) The tangential component of the velocity was the most significant one with results indicating the adhesion mechanism could be considered on a scalar basis using this component.

(c) Adhesion probability for polymeric surfaces is lower than metallic surfaces due to a lower value of Hamaker constant and higher coefficient of restitution.

(d) Particle adhesion was virtually solely due to Van der Waals forces.

(e) The observed value for the coefficient of restitution with glass particles and a metallic surface was 0.5 whereas a value of 0.6 was seen with polymeric surfaces.

Loffler (96), (97) and Hiller & Loffler (65) showed in more recent work.

(a) For each filtration operation a 100% adhesion range exists but the particle size limits depend on the conditions.
(b) Particles will rebound even at very low velocity of only a few cm/s.
(c) Particle adhesion probability, when at constant flow, will increase with decreasing particle size, hardness or increasing fibre diameter.
(d) The rate of decrease of adhesion probability becomes smaller with increasing flow velocity.

Tashpolotov et al (158) further examined the role of Van der Waals force. Figure 11 shows the result of their theoretical analysis of the interaction energy of a sphere and an infinitely long fibre. This leads them to conclude that the range of action of intermolecular forces is significant in aerosol capture beyond the immediate surface of the particle and cylinder.

FIGURE 11: Energy of the molecular interaction of spherical particles with an infinitely long cylindrical fibre.

No.	r_p (µm)	r_f (µm)
1*	1*	1*
2	1	0·1
3	1	1
4	1	10
5	10	1
6	10	10··

* Retardation not considered
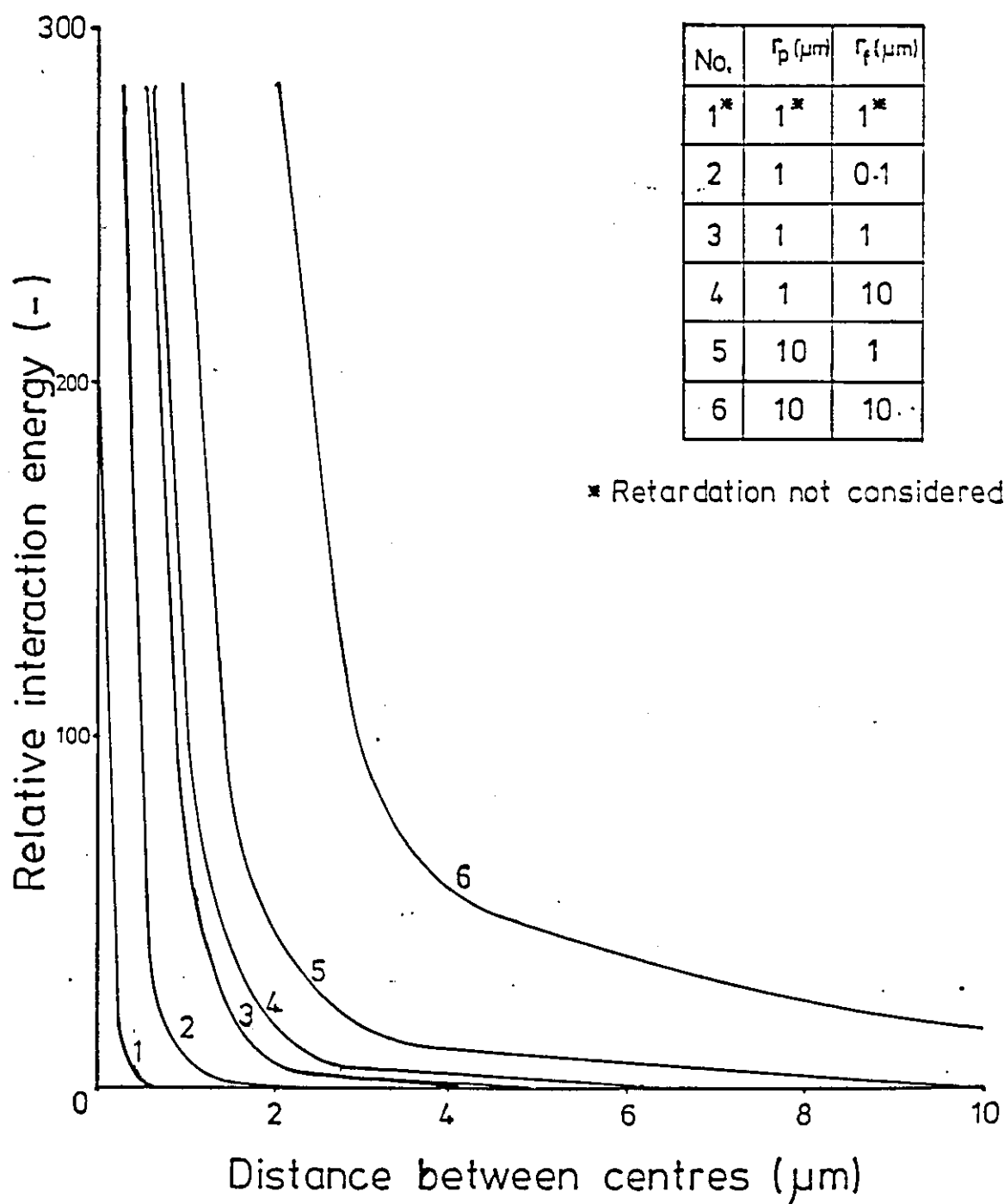
It is obvious from the above work of these various authors that particle adhesion should be virtually 100% in normal HEPA filtration conditions. Therefore further details of particle adhesion are not included in this review.

1.2.3. The Pressure Drop effect for Clean Media

Chen (20) was the first to include a review of this subject in his 1955 publication. He reports two approaches which had been considered to this time. First is the channel theory as used by Langmuir (87) which involves adapting the Kozeny-Carman equation to give:

$$\Delta P = \frac{16k''\mu\alpha\phi'U_oL}{d_f^2} \qquad (1\text{-}35)$$

where K'' = a numerical geometry factor

U_o = superficial gas velocity

$$\phi' = \left\{-\ell n\alpha + 2\alpha - \tfrac{1}{2}\alpha^2 - \tfrac{3}{2}\right\}^{-1}$$

Similarly Davies (28) worked empirically basing the results on Darcy's law to obtain.

$$\Delta P = \frac{\mu\ U_o\ L\ f\ (\alpha)}{d_f^2} \qquad (1\text{-}36)$$

where

$$f(\alpha) = 64\alpha^{1.5}\ (1+56\alpha^3)$$

The alternative approach of Chen is drag theory where the media is very porous ($\varepsilon > 75\%$) when the equations (1 - 35),   (1 - 36) appear weak. This lead to the equation

$$\Delta P = \frac{4\ C_{D\alpha}\ Re\ \alpha\ \mu\ U_o\ L}{2\ \pi\ (1-\alpha)\ d_{f_s}} \qquad (1\text{-}37)$$

where,

d_{f_s} = surface average fibre diameter

$C_{D\alpha}$ = The drag coefficient for an average size fibre in a filter of fibre volume fraction α.

Note that in experimental correlations the factor $(C_{D\alpha}Re/2)$ is usually used.

The next developments from Happel [59] and [60] evaluated the drag on a solid cylinder to be

$$F_D = 2 \pi \mu \phi_D \qquad (1-38)$$

where

$$\phi_D = \frac{-2 \, U_o}{\ln \dfrac{r_c}{r_f} + \dfrac{r_f{}^4}{r_f{}^4 + r_c{}^4} - \dfrac{1}{2}}$$

r_f=cylinder radius
r_c=fluid cell radius (around cylinder)

Also from the Darcy equation

$$\frac{F_D}{\pi r_c{}^2} = \frac{dP}{dx} = \frac{-\mu U_o}{\phi_c} \qquad (1-39)$$

So the Darcy constant becomes

$$\phi_c = \frac{r_c{}^2}{4} \left\{ \ln \frac{r_c}{r_f} - \frac{1}{2} \left(\frac{r_c{}^4 - r_f{}^4}{r_c{}^4 + r_f{}^4} \right) \right\} \qquad (1-40)$$

In his 1966 review Dorman[32] discusses the above equations and also includes a development by Fuchs and Stechkina [50] as a progression of Happel's work. This was

$$\Delta P = \frac{4 \, \alpha \, \mu \, L \, U_o}{r_f{}^2 \left\{ - \dfrac{1}{2} \ln (\alpha - \lambda) \right\}} \qquad (1-41)$$

where λ_c is a constant and for a value of $\lambda_c = 0.5$ there is good agreement with Langmuir.

Pich (123) considered pressure characteristics of fibrous filters over a wide range of Knudson numbers and concluded there were four different regimes and consquently four different pressure drop correlations.

(a) <u>Free molecule region</u> Kn > 10

$$\Delta P = 2.91 \ \beta \ \frac{(\alpha \ L \ Uo)}{r_f \ \bar{c}} \tag{1-42}$$

where,

$$\beta = \frac{1}{3} \ \rho_p \ \bar{c}^2$$

$$\bar{c}^2 = \frac{8kT}{\pi m}$$

(b) <u>The transition region</u> 10 < Kn < 0.25
No known equation or derived equation to describe this region

(c) <u>Slip flow region</u> $0.75 > Kn > 10^{-3}$
Providing $\alpha \ll 1$ then:

$$\Delta P = \frac{4 \ \mu\alpha Uo \ L}{r_f^2 \ (-\frac{3}{4} \ -\frac{1}{2} \ \ln\alpha \ + \ 0.998Kn)} \tag{1-43}$$

(d) <u>Continuum region</u> $Kn < 10^{-3}$

$$\Delta P = \frac{4 \ \mu\alpha Uo \ L}{r_f^2 \ (\ -\frac{3}{4} \ -\frac{1}{2} \ \ln\alpha)} \tag{1-44}$$

From analysis of these equations he determined that pressure drop is dependant on the gas properties (including actual pressure, temperature etc), the filter porosity and the flow character (as expressed by the hydrodynamic factor from the flow field).

Much of the fabric filtration work for clean filters appears to correspond to the principles of fibrous filters. For example the equation from Afify and Mohammed (1) is very similar to Davies work.

$$\frac{4 \, \Delta \, P \, r_f^2}{\mu \, Uo \, L} = 64 \, \alpha^{1.5} \, (1 + 56\alpha^3) \qquad (1\text{-}45)$$

The effect of physical conditions has also been examined in the fabric filtration field. Ariman and Helfritch (4) found increasing the relative humidity while loading reduced the rate of pressure drop rise. Aref'ev et al (3) tested fabric under vacuum conditions and found the permeability as an empirical fit to the equation:

$$\lambda_k = A + B/P \qquad (1\text{-}46)$$

where P was the absolute pressure. However as the constant A >> B/P then for pressures greater than atmospheric λ_k= A. Work on viscosity was carried out by Rudnick and Ellenbecker (135) showing the resistance $(\Delta P/U_o)$ varied proportionately with absolute viscosity - not kinematic viscosity as often reported.

1.3. Loaded filter media

Once aerosol or dusts begin to be captured by a filter then its characteristics change. It would be expected that both efficiency and pressure drop will increase and this is discussed below. Also as a consequence of particles sticking to a fibre the flow field will change and particles will not only be captured by fibres but also by the already captured particles on these fibres. This concept is often referred to as dendritic build up and is discussed in section 1.3.3.

1.3.1. The effect of load on filter efficiency

Apart from the general assumptions that efficiency will improve with load, little work, excepting dendritic simulations, has been carried out experimentally or theroetically in attempting to quantify

the effect. The main reason for this is probably that the critical parameter for filter design is minimum efficiency. If a filter becomes more efficient as it is loaded this can only be of benefit from the users point of view.

Raduskevich (128) studied the effect of load on efficiency. He assumed that the rate of accummulation of particles in a filter is due to both collection on the clean filter and on already deposited particles. He described the building of deposit with time in a filter as:-

$$\frac{\partial \sigma}{\partial t} = \frac{\eta U_o c \alpha}{\pi d_f} + \gamma a' U_o c \sigma \qquad (1-47)$$

where:

η = single fibre efficiency

γ = particle collection efficiency

c = concentration of air blown particles

σ = deposit within the filter

a' = effective area of unit deposit

He combined this with the continuity equation and solved these to obtain an expression for the influence of depth and time on the overall efficiency.

$$E = 1 - \frac{c}{c'}$$

$$= 1 - \frac{1}{1 + e^{c_1 t} (e^{\lambda_o L} - 1)} \qquad (1-48)$$

where,

$$C_1 = \frac{U_o \, C' \, a' \gamma}{(1-\alpha)}$$

$$\lambda_o = \frac{\eta \, \alpha}{(1-\alpha) \, \pi d_f}$$

Experimental results in the diffusion regime by Raduskevich (129) suggested that $a'\gamma$ is about the same order of magnitude as the cross-sectional area of the particles.

Davies (29) took a different approach to the clogging of filters. The resistance, R', to gas flow through a filter is related to the total aerosol penetration P. It was found experimentally that:

$$P^* = P_o^* \, \gamma_L \qquad -\left\{(R'/R_o')^{\frac{1}{2}} + 1\right\} \qquad (1\text{-}49)$$

and

$$\frac{1}{R'} \cdot \frac{dR'}{dt} = \alpha_L$$

$$(1\text{-}50)$$

α_L and γ_L are clogging parameters and are related to the single fibre efficiencies by:

$$\gamma_L = e^{\lambda_o L}$$

$$\alpha_L = \frac{2}{t} \ln \frac{\lambda_1}{\lambda_o}$$

where:

L = filter depth

t = filtration time

$\lambda_1 = \lambda_o (1 + K''\sigma)$

where σ is the deposit at time t. The factor K'' was found experimentally be about 5.

Expressions were derived to enable the mean efficiency and the quantity of deposit in a filter, over a period of use, to be calculated from the clogging parameters.

Stenhouse and Broom (150) carried out some work in the high inertia regime for feldspar dust of 2-22 μm, velocity 1 m/s and stainless steel fibres 145 μm diameter, packed at a volume fraction of .081 and 3 cm deep. They concluded that the efficiency did not vary significantly until a coating equivalent to a monolayer of dust covered the leading edge of the fibres. The efficiency then increased until maximum loading was reached. They also found that the actual improvement in efficiency was due to the collection to fine rather than coarse particles with the position of the grade efficiency curve highly dependent on the test dust size distribution. Under some conditions the addition of a small quantity fines can have a disproportionate effect.

1.3.2. The Effect of Load on Pressure Drop

Again with respect to fibrous filtration, with the exceptions of advances in dendritic theory, little has been done. Dorman (33) reports that initially pressure drop will rise linearly with load before a rapid exponential rise as loading moves towards completion. Davies (29) also experimentally studied clogging effects on filters as reported in section 1.3.1.

More work has been carried out in the fabric filtration field however due to the nature of this type of filtration i.e.the dust cake formed being periodically removed by pulsing; the work cannot be directly applied to fibrous filters. Hence for the purposes of this survey a detailed review is not included.

1.3.3. The dendritic model approach

In 1976 Franklin and Knutson (46) found that filtering with uranine dye aerosol gave a very steep rise in pressure drop. However after filtration was stopped and humid air passed through the filter this pressure drop suddenly fell almost to that of a clean filter. This did not happen with dry air. They hypothesised that this was due to dendrite bridges giving the high pressure drop and then being broken down by the water in the air due to the hygroscopic nature of uranine. The particles then redistributed themselves throughout the whole filter so virtually returning the filter to its original state.

Payatakes for a long time has been a major contributor to this type of work although never actually achieving a workable solution. His initial development with Tien, (110) was a model to predict a chain-like build up of particles on fibres with the intention of predicting the effect on filter pressure drop and efficiency. This resulted in a complex mathematical analysis requiring computer

simulation due to probability factors, time and age dependency. This is further complicated by the different collection mechanisms and this early model only considered interception. Furthermore as particles deposit the dynamics of the situation change and there is an influence on the flow field and collection area. Payatakes (111) and (112) considers particle-particle build up but results are still very unreliable especially with no consideration of other mechanisms such as dendrite collapse or re-entrainment through bounce etc. Later Payatakes and Bhutra (113) examined monodisperse aerosol particle deposition on a single fibre experimentally under conditions where inertial impaction as well as interception was important. Formation of dendrites on the fibre was observed and recorded photographically . A model known as the third approximation model was developed. This was also used by Payatakes and Graddon (115). Payatakes (114) discusses his results of these observations as showing that deposition on the actual fibre covers the whole front face of a fibre for interception alone ($\pi/2 < \theta < 3\pi/2$). However, when inertia is included there is a limiting angle for deposition. This angle $\hat{\theta}$ is greater than $\pi/2$ and so the region of deposition is between $\hat{\theta} \leqslant \theta \leqslant (2\pi - \hat{\theta})$. This idea lead to Payatakes concluding that particles skid off the fibre due to viscous interaction. Dahneke and Padilya (26') disagree suggesting bounce is the factor affecting particle distribution . This does seem more likely, although Payatakes defends himself, (116) with hydrodynamic theory. However even in his later work, (117) although introducing correction functions to efficiency and pressure drop dependent on deposited material, he does not appear to have solved the modelling of dendritic build up. Even these correction functions have to be evaluated from experimental work. An attempt is made from earlier work to extend it to calculating the correction functions for the initial period of dendritic deposition. He also tries to include Brownian diffusion. However these various works have not yet resolved the theoretical approach to dendritic deposition.

Bardet, Tien and Wang (8) studied the effects of air velocity and particle size on the structure of deposits on a fibre and capture efficiency experimentally.. With approximately 1300 to 17000 particles crossing a fibre the largest dendrite observed consisted of eight particles but with noticeably few consisting of more than two

particles. Only with further filtration do more dendrites of larger size gradually form. They also observed an increase in efficiency of collection with the increase in the number of particles collected.

Kanaoka, Emi and Ohta [71] attempted to predict change of efficiency and pressure drop with load by simulating dendrite growth. They used Kuwabara's [81] flow field to calculate particle trajectories although no allowance was made for change due to dendrite build up. Their simulation showed a linear dependence for increase in efficiency with load but the value of the slope, λ, varies with filtration conditions:

$$E_L = E (1 + \lambda'\sigma)$$ (1-51)

where,

E_L is efficiency with load

E is clean filter efficiency

σ is load

λ' is slope

This variation in the value of the slope disagrees with work by Yoshioka et al (168) who found the slope was constant with a value of 5 m^3/kg Kanaoka et al found the value of λ' very high for low Stokes numbers (56.1 at St = 0) and very low at high Stokes numbers (.0769 at St $\rightarrow \infty$). These figures are from the simulation with an interception parameter of .05. As the interception parameter increases λ' decreases e.g. for a value of R = 2, $\lambda' = 3.09$ at St = 0 and $\lambda' = .0482$ at St$\rightarrow \infty$. The overall effect of the simulation showed collection efficiency increased rapidly with dust load particularly in the low numbered Stokes region. This was verified by experiments on thin filters for light loads, although there was a slight underprediction at higher loads, probably due to the lack of correction of the flow field.

They also used drag theory to predict the effect on pressure drop. The equation used was of the form

$$\Delta P = \frac{4\alpha}{\pi d_f^2} \int_o^x F_D \, dx \tag{1-52}$$

F_D = the drag force of a fibre per unit length X.

and,

$$F_D = C_{Dm} \, d_{fm} \, \frac{\rho_c \, U_o^2}{2} \tag{1-53}$$

where C_{Dm} is the drag coefficient. The only other varying parameter is the fibre diameter (d_{fm}) which changes as particle loading is accounted for. These were correlated experimentally to show:

$$d_{fm} = d_f (1 + 0.28\sigma^{1.28}) \tag{1-54}$$

$$C_{Dm} = C_D (1 + .064 \, \sigma) \tag{1-55}$$

where,

$$C_{D_o} = \frac{24.8}{Re_f}$$

Re_f = Fibre Reynolds number

By using these correlations in the pressure drop equation (1-52) a reasonable agreement with experimental observation was found.

A separate dynamic simulation model, already discussed in section 1.2.1. and 1.2.2.1., was developed by Tsiang, Wang and Tien (163). This works with parallel fibre arrays and treats particle build up in three stages.

(a) Individual deposits
(b) Dendrite growth
(c) Filter cake formation as dendrite bridges form.

They observed this progression by taking micrographs at various stages. At low flow rates the comparison was good with high efficiency and cake formation stages rapidly reached. With higher velocities the increase in efficiency is more moderate and the maximum efficiency

reduces with increasing velocity, possibly due to re-entrainment. The comparison of this with the simulation was qualitatively reasonable but not quantitatively. In determining pressure drop the model is initially reasonable but at higher values considerably underpredicts.

The model's basis was Miyagi's [101] flow field for an infinite array of parallel fibres. This was used to calculate particle trajectories which are of the usual form except it is assumed, due to low Stokes numbers, particles follow streamlines and hence ... the fluid velocity can be equated with the particle velocity. Also neglected are the effects of deposited particles on the flowfield and collection by Brownian diffusion or gravity. Determination of whether a particle is captured is by considering the capture limit velocity - a particle being deposited if the velocity of a particle is slower than the limit calculated. The capture limit velocity is defined as

$$ V^* = \left\{ \frac{A_H (1-e^2)}{2\pi z_o \rho_p e^2} \right\}^{\frac{1}{2}} dp \tag{1-56} $$

where,

A_H = Hamaker's constant = 10^{-12} erg

Z_o = separation between surfaces = 4 Å

e = coefficient of restitution = .88 - .99 in general.

dp, ρ_p = particle diameter and density respectively.

The pressure drop effect was estimated by the contribution to the drag force given by:

$$ \triangle F_D = 6 \pi \mu r_p U_o \tag{1-57} $$

Assuming only the two closest deposited particles have any interaction effect on this drag factor then the correction for the ith particle with neighbours jth and kth particles gives:

$$ \triangle F_{Di} = \triangle F_D \, F(r_i, r_j) \, F(r_i, r_k) \tag{1-58} $$

47

where,

$$F(r_i, r_j) = \frac{Cos^2\phi}{1 + \frac{3}{2}(r_p/\ell_{ij})} + \frac{Sin^2\phi}{1 + \frac{3}{4}(r_p/\ell_{ij}) + \frac{1}{2}(r_p/\ell_{ij})^2}$$

$$F(r_i, r_K) = \frac{Cos^2\phi}{1 + \frac{3}{2}(r_p/\ell_{ik})} + \frac{Sin^2\phi}{1 + \frac{3}{4}(r_p/\ell_{ik}) + \frac{1}{2}(r_p/\ell_{ik})^2}$$
where,

ℓ_{ij} or ℓ_{ik} =   distance between centres of particles i and j (or k)

ϕ =   angle ℓ_{ij}(or ℓ_{ik}) makes with the normal flow direction.

This leads to an overall expression for pressure drop of

$$\frac{\Delta P - \Delta Po}{\Delta Po} = \frac{1}{F_{D,o}} \sum_{i=1}^{i=n} \Delta F_{D,i} \qquad (1\text{-}59)$$

From these various works it is obvious that the dendritic model approach is very ambitious and fraught with difficulties in obtaining good agreement with experimental data. However, the more recent developments of authors such as Kanaoka et al (71) and Tsiang et al (163) show far more promise of an eventual solution than Payatake's pioneering work. It is reasonable to conclude that the dendritic approach is a worthy one, and as a workable model will be useful for general application.

48

1.4. Packed and Granular Beds

The concept of a packed granular bed building up on a filter has already been mentioned. This completes the filtration process with the stages being.

(a) clean filter media
(b) penetration into the media
(c) build up of a cake on the media

To attempt to understand the effects of flow, efficiency and pressure drop in a complete filtration process this final stage is reviewed.

1.4.1. Flow Field Models

Originally a unit cell type model based on Kuwabara's (81) work was employed. However Payatakes et al (109) considered this unsatisfactory for granular type models and proposed the constricted tube model which is more realistic. This consists of unit cells having parabolic walls within a tube as in Figure 12.
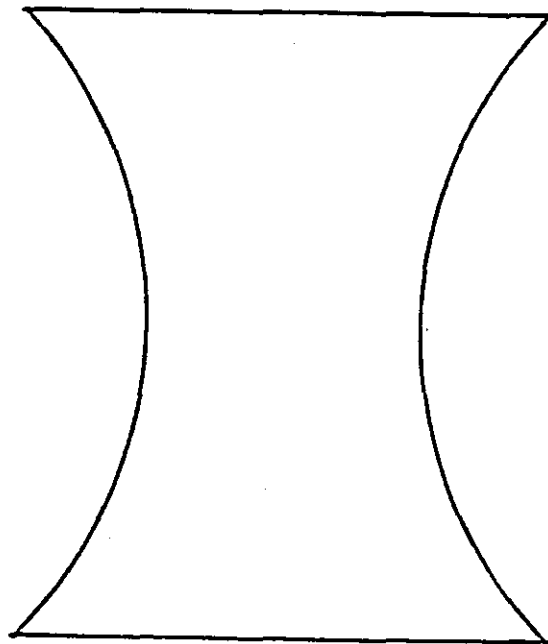
Figure 12 : Constricted tube model

Neale and Nader [105] developed a geometric model, based on the pore size of a unit cell, to study hydrodynamic transport processes. Although operating over the entire porosity range when the porosity is in excess of 0.7 there is good agreement with Happel's [60] free surface model. The actual mathematical solution is complex but consists mainly of an influence function which gives the deviation from Stokes law.

Tardos, Gutfinger and Abuaf (154) and (155) and Gutfinger, Tardos and Abuaf (58) use the approach.

For a general bed Tardos et al [155] gave a considerably simplified form of the influence functon as:

$$g(\epsilon) = \frac{k_\epsilon}{\epsilon} \qquad (1-60)$$

where

k_ϵ = 1.1 to 1.5 although 1.1 is generally used.

Obviously some measure of porosity (ϵ) is also required. This is commonly achieved by Fisher sub-sizer as detailed by Wasan and Wnek (165). In practice the empirical equation of Gebhart (51), Balasubramanian (7) and Thambimuthu (159) for diffusional collection is most suitable.

$$\eta_D = 4.36 \, Pe^{-\frac{2}{3}} \epsilon^{-1} \qquad (1-61)$$

Using the cell model of Happel (60) Tardos et al (155) derived

$$\eta_D = g (\epsilon) \, Pe^{-\frac{2}{3}} \qquad (1-62)$$

but with g (ε·) generally greater than $4.36/\varepsilon$ .Conversely using Payatakes (109) constricted tube model Chiang and Tien (21) have shown g (ε.) much closer to $4.36/\varepsilon$ hence showing the constricted tube model to be more realistic in this case. Chiang and Tien and also Pendse and Tien (121) examined the constricted tube model with parabolic, sinusoidal and hyperbolic tube wall geometries. The former gave the most acceptable results.

Paretsky (108)and Tardos et al (155) both attempted to use the cell model for evaluating the single grain efficiency due to inertia but neither found good agreement with experiment. Pendse and Tien (121) with Tien's (161) addition, however did develop a reasonable result with the constricted tube model giving:

$$\eta_I = (1 + .04Re)St.\pi^{-\frac{1}{3}}(0.75(1-\varepsilon))^{-\frac{2}{3}} \qquad (1-63)$$

Even so, the dependance on Stokes number is still too weak.

1.4.2. Efficiency mechanisms in granular beds

This, as with fibrous filtration, is a field which has been studied by many authors. The table in appendix 1.4 gives an overall review of the equations for each major mechanism - these being inertia, interception, gravity, diffusion and interaction between these. Developments in the effects of electrostatics have not been given but details of this can be found by reference to Coury (23) or work by Shapiro (137).

These equations have been reviewed by such as Kennard and Meisen (73), Pfeffer (122) and Clift (22). From these reviews and by considering the works given in appendix 1.4 certain equations are preferred due to their acceptable agreement with experiment . It is these equations which are used in the work of 2.1.

As the main emphasis of this review does not lie in considering packed bed efficiency the series of equations used in 2.1 are given below.

Lee and Gieske (89):

$$\eta_o = 2 \left(\frac{3\pi}{4}\right)^{2/3} Pe^{-2/3} \frac{(1-\alpha)}{k_g} \qquad (1-64)$$

$$\eta_R = \frac{3}{2} \frac{(1-\alpha)}{k_g} \cdot \frac{R^2}{(1+R)^m} \qquad (1-65)$$

$$\eta_G = \frac{\rho_p g d_p^2}{18\mu u_o} \qquad (1-66)$$

Where;

$$k_g = 1 - \frac{9}{5}\alpha^{1/3} + \alpha - \frac{1}{5}\alpha^2$$

$$m = \frac{1+2\alpha}{3-3\alpha}$$

Alternatively the following equations have been recommended

Wilson and Geankoplis (167)

$$\eta_o = \frac{4.36}{(1-\alpha)} Pe^{-2/3}$$

Tardos et al (156) and Pfeffer (122)

$$\eta_R = \frac{3.37}{(1-\alpha)^3} \qquad St < 0.02 \qquad (1-68)$$

$$\eta_R = \frac{1}{(1-\alpha)} \left(1 + 2R + R^2 - \frac{1}{1+R}\right) \qquad St \geq 0.02$$

Tardos et al (156)

$$\eta_G = St \cdot Ga \; (1 + St \cdot Ga)^{-1} \qquad (1-69)$$

Where Ga = Gallieo's no.

Thambimuthu (159)

$$\eta_I = \left\{ St / (St + .062(1-\alpha)) \right\}^3 \qquad (1-70)$$

Using either Lee and Gieske's equations, or the second series of equations given, the single grain efficiency can be found by summation of the individual mechanisms. The overall bed efficiency is then found by the same equation (1-3) as for fibrous filtration.

1.4.3. Pressure drop analysis for granular beds

Gebhart et al [51] experimentally determined the pressure drop relationship using glass bead media. They confirmed the Hagan-Poiseuille law for viscous flow where,

$$F(\Delta P) = \frac{\Delta P \, r_g^2}{\eta \, U_o \, L} \tag{1-71}$$

Rudnick and First [134] measured specific resistance of cakes of A.C. fine test dust in the velocity range 7 – 56 mm/s where all other factors were constant. They found that the normally used Kozeny Carman equation underestimated resistance, probably due to its assumption that the dust cake could be treated as a series of capillaries. The free surface model of Happel [60] was more suitable after particle size, shape and gas slip corrections had been taken into account.

On a similar approach, only for the low Knudsen number regime, Lee et al [88] developed a solution from the Kuwabara field:-

$$\Delta P = \frac{9 \, \alpha \, \mu \, Uo \, L \, (1 + 2Cm\lambda/r_a)}{2 \, r_g^2 \, (Kg + 3CmKg'\lambda/r_a)} \tag{1-72}$$

where,

λ = mean free path of gas

$\dfrac{\lambda}{r_g}$ is the Knudsen number

C_m is the dimensionless momentum accommodation coefficient of gas-material combination.

$$kg = 1 - \frac{9}{5}\alpha^{1/3} + \alpha - \frac{1}{5}\alpha^2$$

$$kg' = 1 - \frac{6}{5}\alpha^{1/3} + \frac{1}{5}\alpha^2$$

This solution shows that a substantial decrease in pressure drop is realised as Knudson number is increased.

Simpler correlations have been given by Schmidt and Gieske (136) and Kennard and Meisen (73) which can be used for general work,

(1) Schmidt and Gieske

$$\triangle P = 0.014 \, \mu^{.15} \, L \, \rho^{.85} U_o^{1.15}/r_g \qquad Re > 40$$

$$\triangle P = 0.170 \, \mu \, L \, U_o/ \, r_g^2 \qquad Re < 40$$

(1-73)

The Kennard and Meisen (73) equation takes porosity into account:-

$$\frac{\Delta P}{L} = 316 \, \frac{(1-\epsilon)^2}{\epsilon^3} \cdot \frac{\mu U_o}{d_g^2} + 1.73 \, \frac{1-\epsilon}{\epsilon^3} \, \frac{\rho U_o^2}{d_g} \qquad (1-74)$$

Tien (161) still prefers to use a form of the Kozeny-Carman equation in his modelling work i.e.

$$\frac{\partial P}{\partial L} = \frac{-150}{d_g^2} \, \mu U_o \, \frac{(1-\epsilon)^2}{\epsilon^3} \qquad (1-75)$$

However, he does develop some correction for this and uses Payatakes constricted tube model in his analysis.

Finally a point must be made, as observed by Tardos and Pfeffer (157), that these equations will fail if electrostatic forces are introduced, unless measurements of porosity etc. are taken with electrostatics present. Electrostatics tend to increase porosity and hence reduce pressure drop.

1.4.4. Loaded granular beds

Very little information is available on this. Pendse and Tien (119) and (120) have made an attempt with their dendritic build up model, being particularly interested in secondary (particle-particle) collection. However this still requires development.

1.5. Fibrous Filter Units

The units which are of interest to this work are HEPA filters. Burchsted (16) gives the fairly rigid specification of these filters as

(a)   For 0.3 μm diameter particles a minimum collection efficiency of 99.97%

(b)   When new at rated airflow capacity a maximum pressure drop of 25 mm W.G.

(c)   A maximum superficial velocity of 2.5 cm/s at rated airflow capacity.

Burchsted in fact points out that many so called HEPA filters do not acheive these requirements and quality assurance by manufacturing companies is not always what it should be.

The design and use of these filters is described below.

1.5.1.   Filtration unit research and design

Two main filter designs are currently in service although there are variations. Until a few years ago virtually only the American deep pleat filters were used having triangular channels of 30 cm long by 10 cm wide and 5 mm high. Filtration takes place through the channel base which consists of the appropriate media. The other surfaces are non-permeable and commonly formed by a aluminium spacer corrigated to the appropriated dimensions. The total area of media in one unit box of dimensions 600 x 600 x 300 mm, is typically 19 m^2. This contrasts to the more modern European design known as the minipleat filter which consists of several panels arranged in successive V's. Each panel contains pleats of a rectangular nature only 1 mm high and about 25 mm deep. All surfaces are filter media. The surfaces are spaced by string prebonded to the sheets of filter media before folding and assembly. These lengths of string are at 25 mm intervals and so this becomes the channel width once the media is

pleated. This allows about twice the area of media into the same volume as the deep pleat filter unit. There does however appear to be some discrepancies as to whether more media actually improves the filtration and enables the filter to achieve the same dust holdingcapacity. To consider this, the review will concentrate on the work which has been carried out both on these filters and on designs, theoretical and experimental, attempting to quantify the best filtration characteristics.

1.5.1.1. Clean Units

Gunn and Eaton (57) were interested in the effects on full size units and attempted to determine:-

(a) HEPA filter structure after exposure to abnormal conditions
(b) HEPA service life
(c) Particle size penetration

They concluded that separator type filters are stronger than the filters which have no spacers. The overall performance of filters appeared to be significantly improved by maximising the filter medium area and using smaller height separators. This tends to indicate that the mini-pleat arrangement should be successful. They also found that the particle collection efficiency for glass fibre HEPA medium dropped significantly when the velocity exceeded 2.5 cm/s. The most penetrating size at 2.5 cm/s was 0.16 μm.

Work on subjecting filters to sudden flow changes has been carried out by Gregory (54) and (55) . He examined filters under two types of pressure transient, i.e. shock pulse or tornado transient (which is much more progressive). He found the former did more damage when using the same maximum pressure but he made some other interesting observations. At high flowrates it was apparent that air passes only through the open ends of a filter and that the mat fibres may even open up to allow the air through closing after the passage of the transient to show no damage. Consequently the efficiency of the

filter is greatly degraded under these conditions. Also small amounts of particulate matter already collected were released, though nothing like the amount released with a reverse flow transient. This shows the danger in HEPA filter units being subjected to freak pressure build ups such as explosion conditions.

At standard conditions Belmont and Carpenter [9] developed a model for rectangular pleated filters of a HEPA nature. The model predicts a flow profile through the filter in two dimensions with analytical solutions. Figures 13 and 14 show the arrangement with the following equations as the solution.

$$\overline{V}_o = \overline{V}_i - 3(2\overline{V}_i - 1)\delta + \frac{3}{2}(2\overline{V}_i - 1)\delta^2 \qquad (1\text{-}76)$$

$$\overline{V}_i = \frac{7}{9} + C_1 \frac{\{C_2 - \tan(0.9\,\sigma_k \xi)\}}{\{C_1 + C_2 \tan(0.9\,\sigma_k \xi)\}} \qquad (1\text{-}77)$$

$$\overline{U}_o = \frac{0.9h\sigma_k C_1}{L} \left\{ \frac{1 + C_2 + \tan(0.9\sigma_k \xi)}{1 + C_2 \tan(0.9\sigma_k \xi)} \right\} \qquad (1\text{-}78)$$

or small σ_k (as HEPA filters)

$$\overline{U}_o = \frac{h}{L} \left\{ 1 + \frac{\sigma_k^2}{100}(81\xi^2 - 36\xi - 29) \right\} \qquad (1\text{-}79)$$

where,

$\delta = y/h$

$y = $ normal coordinate, $h = $ duct half height

$\xi = x/L$

$x = $ streamwise coordinate, $L = $ duct length

$V_o = $ outlet duct velocity, $\overline{V}_o = V_o/V_\infty$

$V_i = $ inlet duct velocity, $\overline{V}_i = V_i/V_\infty$

$U_o = $ velocity through medium, $\overline{U}_o = U_o/V_\infty$

$V_\infty = $ velocity approaching filter

$\sigma_k = $ permeabilty coefficient $= \dfrac{\rho K V_\infty L}{h \mu}$

FIGURE 13: Simplified model geometry for a pair of filter ducts

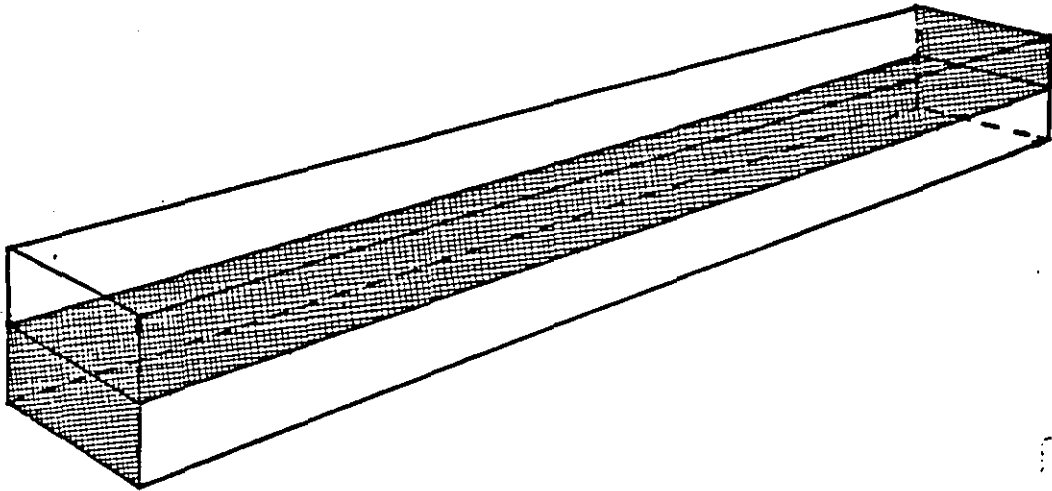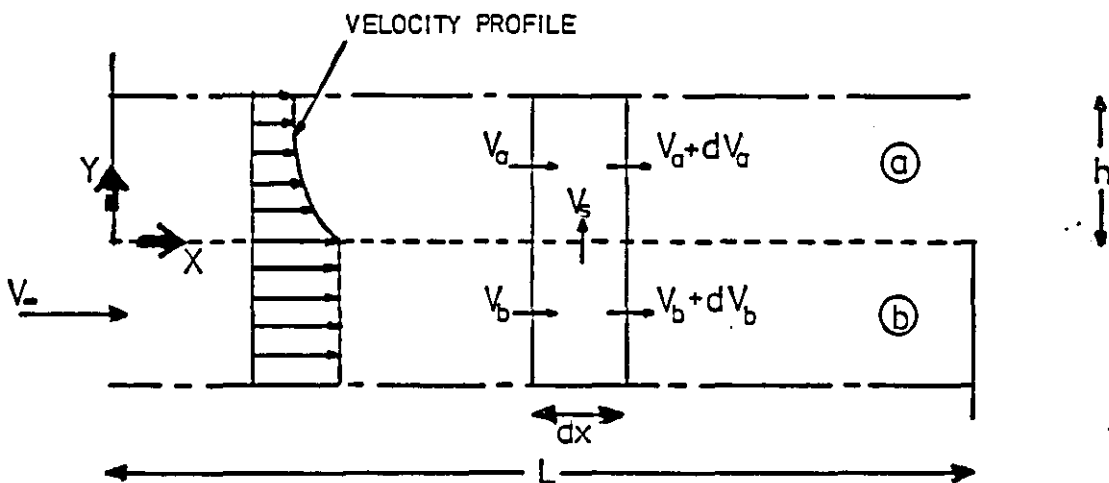# FIGURE 14 : Schematic sketch of filter duct

λ_k = permeability of filter meduim

$$= \frac{\mu\ V_\infty}{\triangle P} = \frac{B'}{L} \quad \text{in Darcy's law}$$

Also,

$$C_1 = \frac{2}{9} C_2$$

$$C_2 = \frac{-9 + \left\{81 + 56\ \tan^2(0.9\sigma_k)\right\}^{\frac{1}{2}}}{14\ \tan(0.9\sigma_k)}$$

From this model and profile, an estimation of the pressure drop using Darcy's law is given using a pressure coefficient:

$$Cp = \frac{\Delta P}{\frac{1}{2}PV_\infty^2} = \frac{2\overline{U}_o}{\sigma_k h/L} - 1 \qquad (1\text{-}80)$$

The model breaks down as $\sigma_k \to 0$ as V_o will be 1 but the profile across the channel will be zero. Also for larger σ_k the assumption of parallel streamlines is invalid so the model fails. However this is not the case with fibrous filters and this model certainly gives a novel approach to determining fluid flow patterns within fibrous filter units.

Raber [126] attempted to optimise the number of pleats in a deep pleat filter with respect to pressure drop and dust capacity. Simple one dimensional flow distribution theory, as widely applied to inlet and outlet manifolds of heat exchangers, was used. The pleat was considered to be triangular with angles between 0-90° but of real interest was data for angles less than 15° as these would be typical. Infact with usable designs only exhibiting angles between 1.1° and 4.4°, data for 0° angle was used in analysis, hence idealising the situation. Figures 15 a and 15 b show the pleat arrangement and dimensions. He used a momentum balance to evaluate pressure loss (due to flow change) and flow uniformity. Friction losses were ignored but pressure drop due to media, inlet and outlet manifolds and dust build
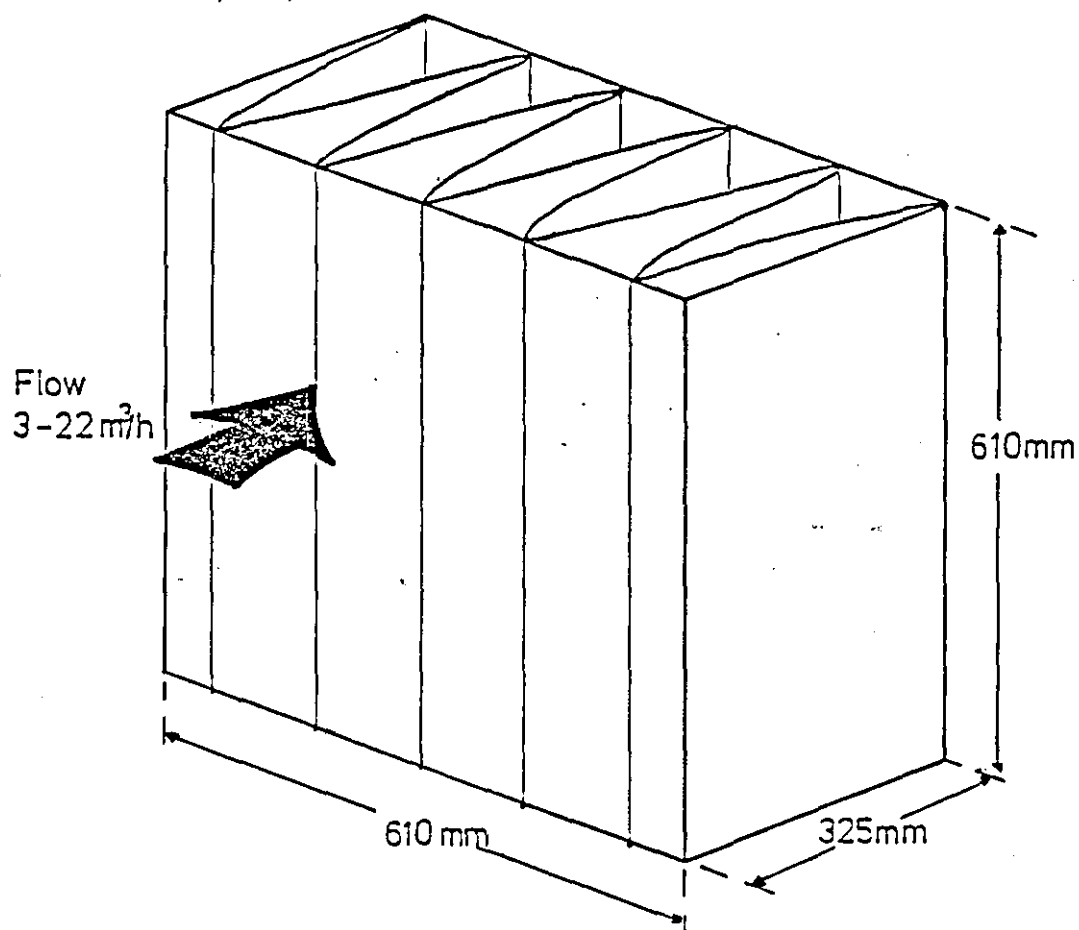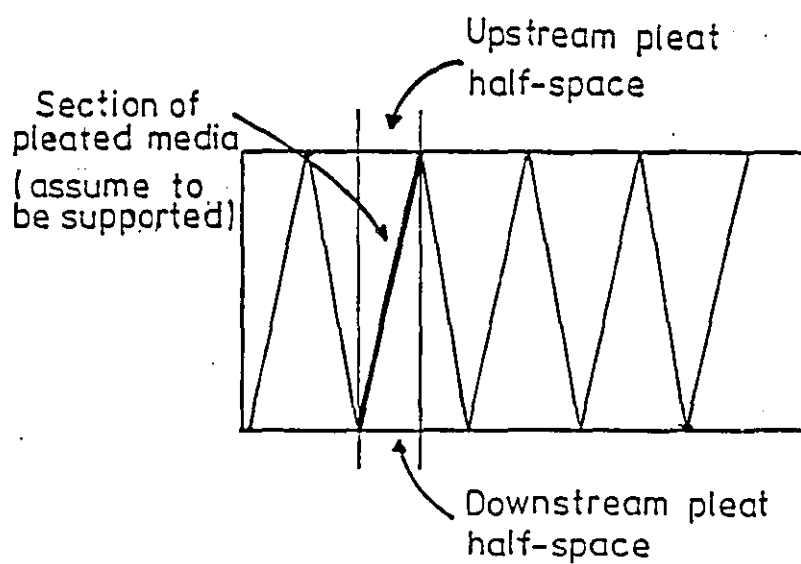
FIGURE 15a : Design envelope

Flow
3-22 m³/h

610mm

610 mm

325mm

FIGURE 15b: Typical half-pleat analysed

Upstream pleat
half-space

Section of
pleated media
(assume to
be supported)

Downstream pleat
half-space

up were determined experimentally for different pleat angles and included in analysis. He found lower pleat angles gave lower pressure drop build up rates.

Raber's results in optimising the number of pleats with respect to the various parameters are:

(a) Considering the best arrangement for low initial pressure drop gave an optimum of 17 pleats

(b) Flow uniformity increased with the number of pleats

(c) In terms of dust capacity an optimum of 22 pleats was found but in terms of specific load this varied between 18-22 pleats.

Some experimental tests he carried out with 16 pleated arrangements showed pressure drop to be under predicted from the above theoretical analysis by 15%. However, it must be noted that these results for Raber are unique and have not been substantiated by other work. It would also appear to disagree with other results in high capacity HEPA filtration where it is generally seen that the more filtration media exists the higher the dust capacity achieved upto certain, as yet undetermined, limits. Results (a) and (c) seem to contradict this suggesting a much lower area of media for an optimum arrangement -even 22 pleats would only be approximately 4 m^2 of filter media compared with typically 20 m^2 for traditional deep pleat and 35 m^2 for mini pleat. Hence Raber's work should be treated with some scepticism as to its actual practical use but the approach deserves consideration.

Work recently published by Burkhardt and Sharma (17), although largely irrelevant to HEPA filters due to the high face velocities used, did make an interesting conclusion. Generally Reynolds numbers used in media calculations are based on fibre diameter in the media. However they found it much more meaningful to base Reynolds number on the mesh (or pore) size. This conclusion came after observations of the non uniformity of local velocities after passing through a filter due to the filter's inhomogenity in pore size.

1.5.1.2. Loaded fibrous filter units

It is obvious that the rate of build up in pressure drop is the governing factor in the lifetime of a filter unit. The critical pressure drop used in the majority of industrial uses of the HEPA filters is 125 mm water gauge, at which point the filter is replaced. Of particular importance to the nuclear industry is being able to replace filters as infrequently as possible due to a waste filter storage problem as discussed in 1.5.2. This, therefore, in recent years has lead to the study of fibrous HEPA filter units under loaded conditions.

Hoppit (67) made measurements on various Vokes filters using carbon black as the charging dust, taken to represent particles after a prefilter. Before loading, D.O.P. and salt aerosol tests were made on the filter and repeated when a final pressure drop of 150 mm w.g. was reached. D.O.P. tests were also carried out during loading to find penetration variation with load. Three grades of filter media were used with initial D.O.P. efficiencies of 97%, 99.9% and 99.996%. At the final analysis the D.O.P. reductions in penetration were 99.5% for the low grade filter, 70.9% for medium grade and 50% for the higher grade paper. However the continuous testing showed this was not a linear decrease, infact with the two lower grades a minimum penetration point is observed. This is illustrated in figures 16, 17 and 18. Neither was a consistent pattern shown by comparison with salt aerosol penetration tests, probably due to the different size distributions of the two aerosols. The pressure drop versus load tests showed that the pressure drop initially rose exponentially followed by a steady linear increase, as has been observed when loading individual samples of media. The results are given in figure 19.

This latter result does not show agreement with First or Pratt's results in work on pressure drop-load characteristics of the last few years. Both do observe a sudden exponential increase, possibly to be followed by a more linear increase. However this is only after a

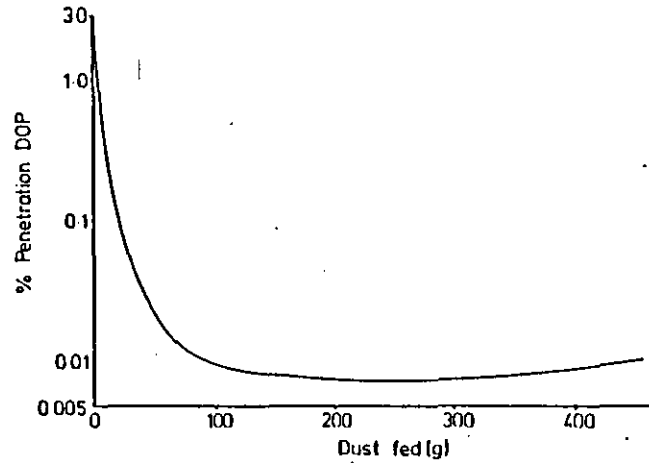FIGURE 16: DOP Penetration w.r.t. load for low grade filter media *

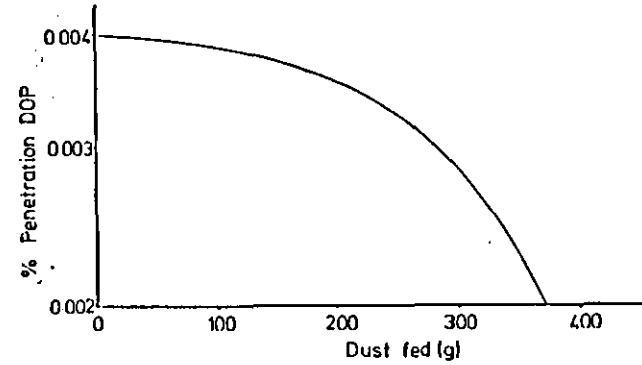FIGURE 18: DOP Penetration w.r.t. load for higher grade filter media *

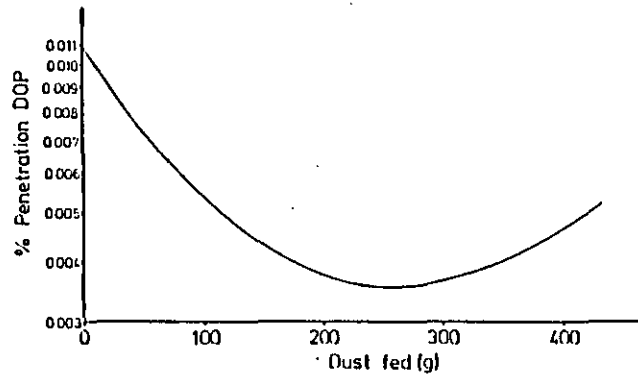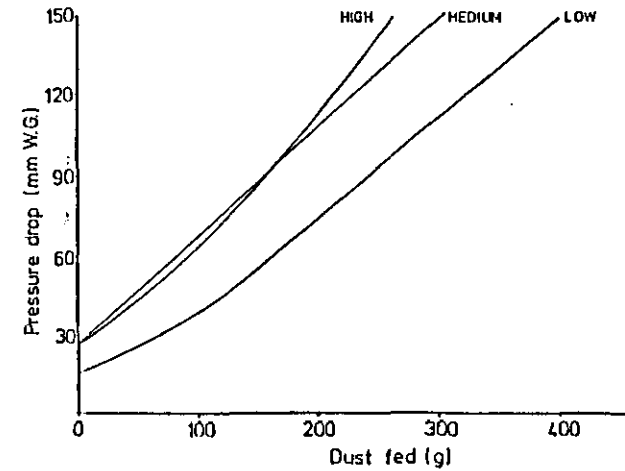FIGURE 17: DOP Penetration w.r.t. load for medium grade filter media *

FIGURE 19: Load vs. pressure drop for filters tested *

* From Hoppit (67)

period of fairly steady slow linear increase in pressure drop with respect to load, upto about 60 - 70% of the final load. This is discussed below.

First and Rudnick (43) began a long term experimental programme at the end of 1977. They set out with the objective of comparing American deep pleat designed filters with the European Luwa mini pleat filter. The American filter was run at 1700 m^3/h its rated flow, whereas the European filter was run at its rated flow of 3000 m^3/h and also a downrated flow of 1700 m^3/h. A rough theoretical estimate suggested the Luwa filter should last about three times longer than the deep pleat filter when run at its downrated flow - 1.8 times the amount of paper at 55% of the flow. Infact running the filters to 125 mm water gauge they found only a 1.6 times improvement in lifetime of a downrated filter with about the same dust loading in kg/m^2. The normally rated minipleat design lasted approximately as long as the deep pleat filter. The final specific dust loadings were:

Deep pleat at 1700 m^3/h gave a dust load of 0.038 kg/m^2
Mini pleat at 3000 m^3/h   "   "   "   "   0.033 kg/m^2
    "   "   " 1700 m^3/h   "   "   "   "   0.036 kg/m^2

It can therefore be seen that the minipleat design also collected about 1.6 - 1.7 times more dust.

The pressure drop/load relationship showed that, after an initial linear relationship, once a certain dust mass is reached the curve becomes non linear at an almost exponential rate. This suggests that the filtration on the media approaches cake filtration with a greater than linear pressure drop rise for increasing load and also that there may be bridging of filter pleats reducing the area of filtration. They also observed that the deposit in the deep pleat was very even, whereas a gradient could be seen with increasing deposit towards the back of the triangular prism shaped entrance plenums of the filter minipleat.

After these initial results First and Rudnick (44) continued their experiments. A more accurate quantification for expected improvement in filter life was developed giving the equation.

$$L_s = \alpha_r^2 \frac{(w_r \Delta P_m - \Delta P_o)}{w_r \Delta P_m - \alpha_r \Delta P_o}$$

(1-81)

where,

L_s gives the service life of an underated European design filter relative to the American design when at its rated flow rate.

α_r is ratio of filter paper area (Euro/Amer)

w_r is ratio rated air flow (Euro/Amer)

ΔP_m is maximum acceptable pressure drop

ΔP_o is ΔP of European design at its rated airflow

This equation assumes the pressure drop/load build up is linear. Allowing a maximum pressure drop of 125 millimetres water gauge and standard filters this equation predicts a 3.6 times longer service life for the downrated European filter.

The results for First's tests between 1977 and 1980 are given in table 6. A typical graph for pressure drop increase with load in figure 20 shows that the pressure drop build up was infact more exponential than linear particularly towards the end of the filter life when very rapid pressure drop rise was seen. Using this performance curve instead of assuming a linear relationship an extension to the service life by a factor of two was predicted. This was closer to the experimental value determined to be 1.6. First believes the reason the factor of 2 was not achieved was due to dust bridges forming between the pleats in the mini pleat design so effectively cutting off filtering area before full capacity is achieved. To counter this problem he suggests the use of prefilters to remove larger fibres and dust particles which he suspects are responsible for this clogging. Infact in his later paper with Price, First and Price (45) carrying out the same work but using prefilters no evidence was found to support this hypothesis . This leaves some doubt as to the actual cause of the bridging and loss of predicted service life.

TABLE 6: Summary of First's results 1977-1980 {From First (44)}

| HEPA Filter Brand	Airflow (cfm)		Startup Date	Initial Pressure Drop (in.w.g.)	Time to 3 in.w.g. (months)	Dust Weight (lb)				
	Rated Capacity	Test Rate				2 in. w.g.	3 in. w.g.	4 in. w.g.	5 in. w.g.	6 in. w.g.
American Design[a]	1000	1090	12/29/77	1.10	9.63	1.16	1.70	1.77	1.81	b
Luwa	1770	1000	12/29/77	0.49	16.3	2.87	2.95	3.02	3.19	b
Luwa	1770	1800	12/29/77	0.82	9.20	2.36	2.69	2.74	2.77	b
American Design[a,c]	1000	1090	11/17/78	1.10	9.07	1.72	2.14	2.23	b	b
Luwa[c]	1770	1800	11/17/78	0.92	10.6	3.63	4.03	4.25	4.33	b
Poelman	1770	1830	1/10/79	0.77	7.39	2.37	3.00	3.45	3.74	3.93
AAF	2000	2030	4/11/79	0.84	8.57	3.80	3.86	4.01	b	b
MSA	2000	1890	8/20/79	1.15	10.3	3.31	4.19	4.22	4.25	b

[a](with Luwa-type paper)
[b]not available
[c]replicated test

FIGURE 20: Performance curve for Luwa filter at 1000cfm
{From First (44)}
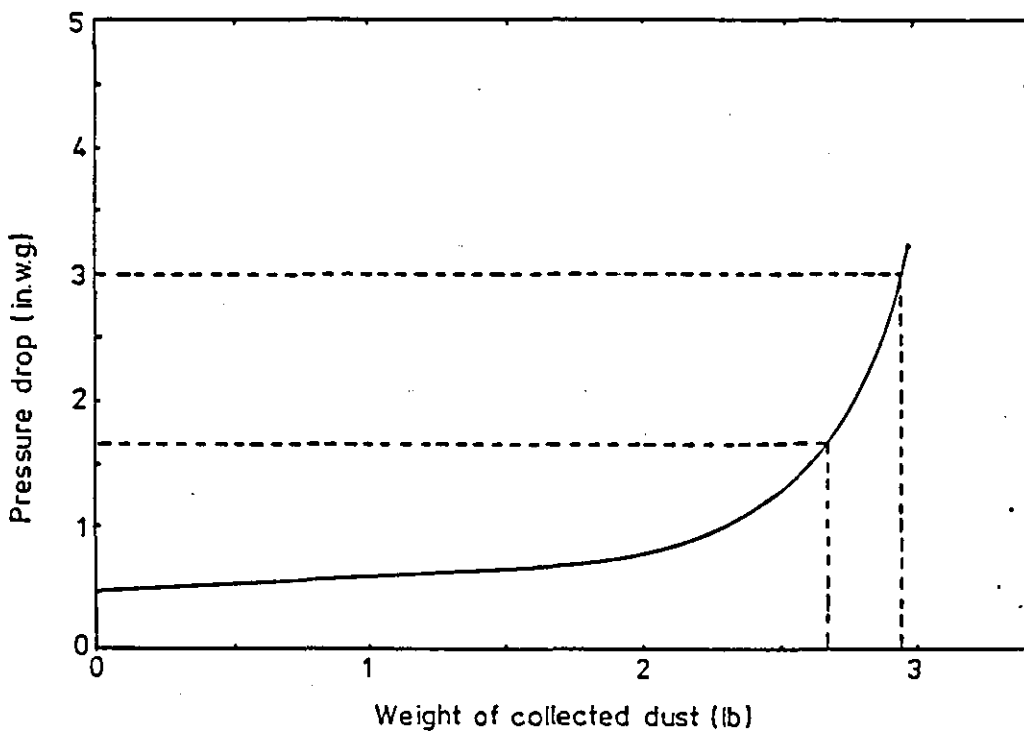
A graphical summary of all the tests First carried out in terms of life, with a summary of the local total suspended particulate matter at any one time, is given in figure 2 1.

Pratt (124) carried out tests on full size HEPA filters using BS 2831 No. 2. Alumina test dust and ASHRAE (carbon black) test dust for pressure drop against load of full and downrated flows. The results showed (see table 7) the downrated high capacity designs holding more dust due to their larger filter area. This enhancement was very aerosol dependant and with the finer ASHRAE test dust the increase in capacity at a given pressure drop is considerably less than would be expected by theory when used at the downrated flow. When a comparison was made between the deep pleat design and mini pleat design, both at their rated flow, there was suprisingly little difference with the amount of either test dust collected inspite of the area available for filtration being about double.

Figures 23 - 26 show the above results in terms of pressure drop with respect to load for the different filter types under the various filtration conditions. The characteristic exponential increase noted in First's work is seen although the initial proportional period found by First is not apparent. Study of these results leads to a conclusion that the aerosol type used is highly critical in its effect on filter performance. With the B.S. 2831 No.2. dust Pratt's experiments indicate that a minipleat design used at a downrated flow would significantly increase service life. However, with the fine ASHRAE dust this improvement is very marginal. Surprisingly with the minipleat designs operating at their rated flow Pratt has found only a very slight improvement in the total amount of dust collected over the deep pleat design, inspite of their greater area. Furthermore of the two types of minipleat filter used by Pratt the Luwa (as used by First) consistently gave a better performance. This was not expected on the basis of the physical parameters of the two designs and suggests that design can be optimised to increase dust holding capacity.
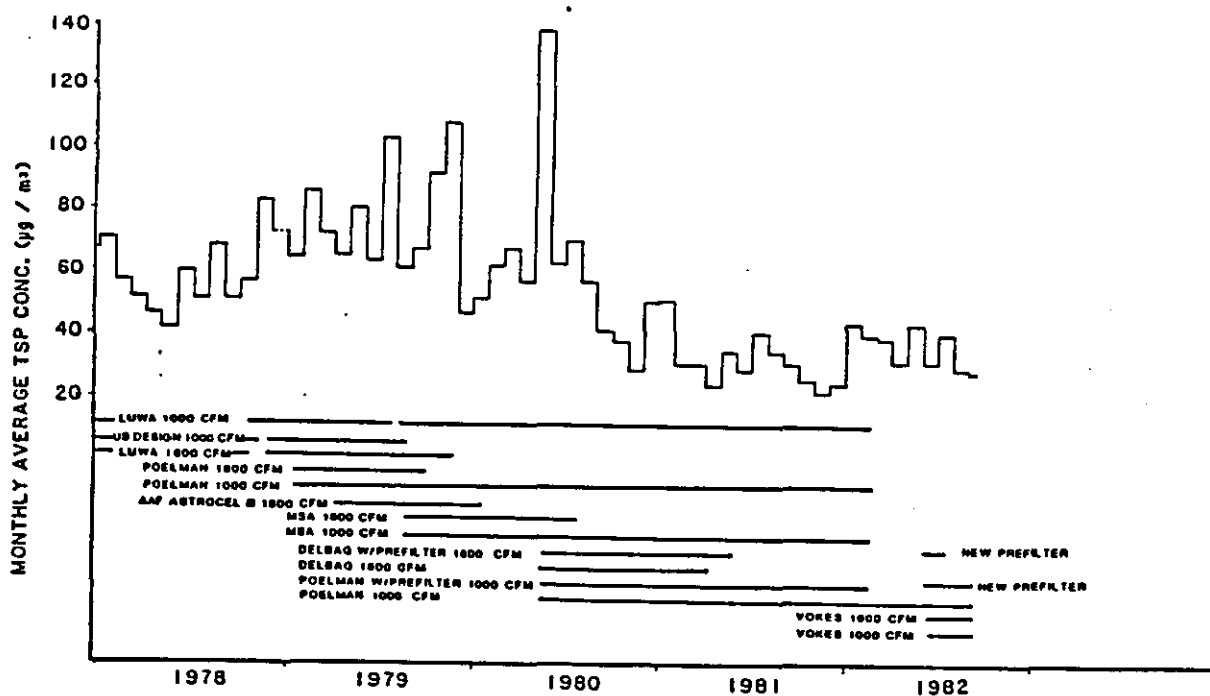
FIGURE 21: CHRONOLOGY OF TSP CONCENTRATION and HEPA FILTER TESTS — From First (45)

Table 7: Results of dust loading vs. pressure drop tests — From Pratt (124)

Filter Type	Sofiltra	Vokes	Luwa	Vokes	Sofiltra	Luwa	Sofiltra	Luwa
Flow m^3/h	1700	1700	1700	1700	3400	3400	3400	3400
Test Dust	BS No. 2	BS No. 2	ASHRAE	ASHRAE	BS No. 2	BS No. 2	ASHRAE	ASHRAE
Pressure drop with zero dust loading mm H_2O	11.5	23.5	12	24.5	27.5	28.5	28	28.5

Dust Loading – kg

Pressure Drop mm H_2O								
25	8	0.5	.75	–	–	–	–	–
50	15	4.3	1.65	0.6	7.2	6.0	0.75	0.7
75	20	6.5	2.2	1.1	9.6	10.2	1.2	1.3
100	24	8.3	2.55	1.5	10.8	13.0	1.4	1.8
125	26.5	9.8	2.85	1.9	11.4	15.0	1.5	2.25
150	27.8	11.2	3.1	2.25	11.7	16.5	1.6	2.6
160	28.2	11.8	3.2	2.35	11.9	17.2	1.6	2.7
200	–	–	3.6	2.75	–	–	–	–
250	–	–	3.8	3.2	–	–	–	–
300	–	–	4.15	3.55	–	–	–	–
350	–	–	4.3	3.8	–	–	–	–

Figure 23: Dust - load - pressure drop - B S nos 2 dust at 1700 m³/h. *

Figure 24: Dust load - pressure drop - ASHRAE dust at 1700 m³/h *

Figure 25: Dust load - pressure drop B S nos 2 dust at 3400 m³/h. *
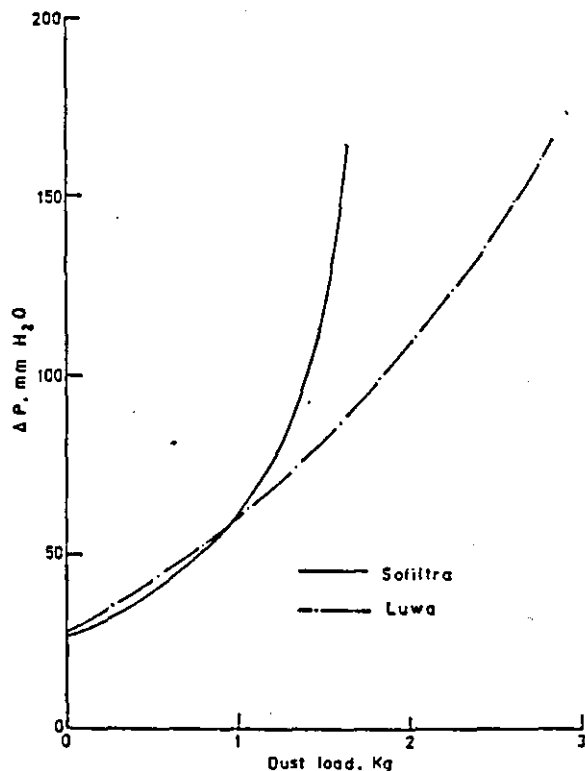
Figure 26: Dust load - pressure drop ASHRAE dust at 3400 m³/h *

* from Pratt (124)

1.5.2. Areas considered in Fibrous filter unit design

There have been virtually no analytical suggestions for filter unit design apart from the basic principle of trying to increase 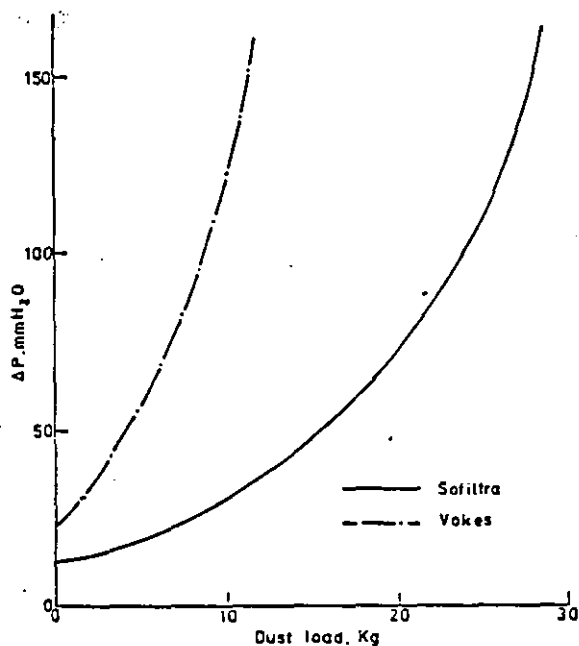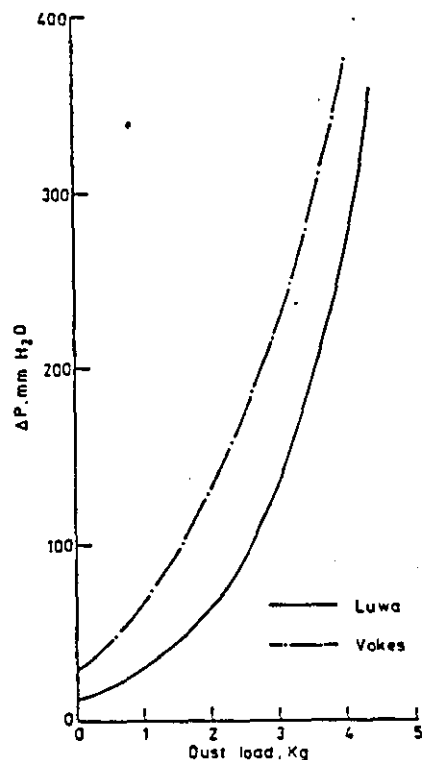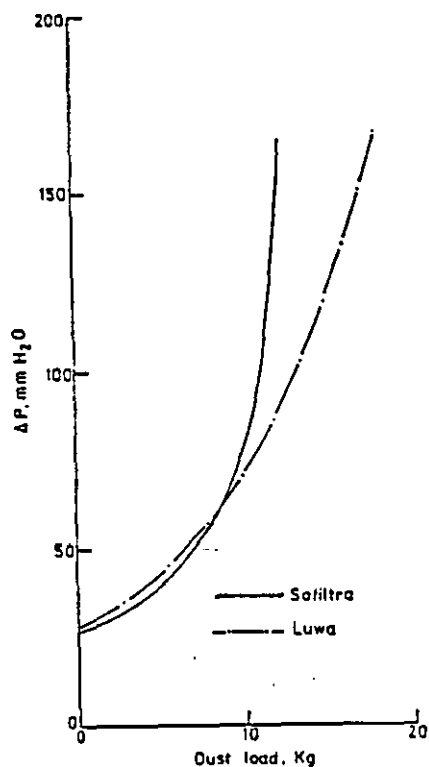the amount of filter media available for filtration and even this has not been seriously developed from a theoretical basis. Elliot and Horsley (37) and (38) did review alternative approaches for medium and long term improvement of filter units in the mid 1970's but this was more a series of suggestions. They state an idea of increasing the flowrate capacity for the same service life which is the governing principle of the mini pleat design developed around this time. They also suggested, as First and Rudnick (44), the reconsideration of the early practice of using pre-filters. However when tried by First and Price (45), as reported earlier, this did not appear to improve the situation. Significantly with regard to the nuclear industry they discuss the storage problem of used filters and waste disposal difficulties. Besides redesign of pleat arrangement to improve service life, so reducing filter turn over, Elliot and Horsley feel more emphasis is needed on containment case design. They suggest a case which allowed removal of the media and then reuse of the case after decontamination is a feasible consideration. This could reduce the bulk for disposal giving the possibility of crushing down and baling the medium and dust alone. With media, dust and support arrangements intrinsic in the filter only actually occupying 25% of the filter unit volume a four fold reduction in waste volume is possible by this approach. It is surprising that little or no work appears to have been carried out on this theme.

1.6 Summary and analysis of subjects for further work

From this review it is apparent the field of fibrous filtration, both theoretically and experimentally, is well documented with regard to clean media. Similarly work on collection mechanisms involved in granular bed filtration has been researched in some detail. Many authors also give pressure drop predictions for fibrous or granular bed filters.

Work on loaded filters, and their subsequent behaviour, is less thorough with regard to efficiency and pressure drop effects. Most work of this nature, with few exceptions, has concentrated on the field of fabric filtration or on the dendritic approach. However there is debate as to whether drawing parallels between fabric and fibrous filtration is valid and as yet there has been no successful conclusion to the development of the dendritic approach. An alternative concept considering a filter heavily load with dust as a combination of a fibrous filter and a packed bed is yet to be validated and even then could only in principle apply to coarse dusts.

In terms of filter design, apart from standard test procedures for HEPA filters, very little has been done either theoretically or even commercially. The main types of HEPA filter available are fundamentally deep pleat or a mini pleat arrangements which have been arrived at through convenience rather than development of research material. Even with these two designs there has been little attempt to study ways to improve performance. Those that have tested these filters disagree to some extent over the techniques of comparison employed and subsequently consistent results between workers have yet to be achieved.

It therefore appears that there is scope for further research into design of HEPA filter units and the arrangement of the media within these units from both theoretical and experimental aspects. If performance is to be improved then it is also important to understand the behaviour of loaded filter media. This indicates that a parallel study of loaded filter media performance, so the effects of this are predictable to a greater extent than at present, would be benefical. Such information should asssist in determining possible arrangements of media within HEPA filters.

2. Theoretical model development

The theoretical approach to modelling and understanding the major influences on dust deposition and pressure drop within HEPA filters had three major facets.

(i) By using current knowledge of fibrous media and granular bed efficiency and pressure drop characteristics, a model predicting behaviour of these filters in combination is developed.

(ii) The movement of particles in channels with filtration through a side wall is considered so indicating the influences and effects on dust deposition.

(iii) A model is developed to describe the pressure drop characteristics of both mini and deep pleat type filter designs accepting the individual media/dust pressure drop is known along with the dust distribution within the filter.

2.1. The loaded fibrous media model

The objective of this work is to predict the aerosol collection efficiency and pressure drop of a fibrous filter covered with a dust layer. The particles of the dust layer are assumed to have a mean diameter at least several times greater than the filter mean pore size. Hence the media and dust layers are considered to give separate efficiency and pressure drop contributions in series. This assumption is validated by visual observation of typical HEPA media loaded with a test dust such as BS 2831 No.2. (chapters 3 and 4). The mean media pore size is typically 1.5 μm and so this dust is virtually all removed by surface sieving.

The equations throughout this analysis are selected from work of other authors and have been referred to in the literature review. Alternative models or derivations are given where considered appropriate.

2.1.1. Filter media efficiency

Two models were considered as alternative methods for deriving the clean media efficiency.

(i)   The fan model by Kirsch, Stechkina and Fuchs (75)(77)   and described in Shaw's book (138).. The single fibre efficiency for the diffusive and interceptive mechanisms is:

$$\eta_D = 2.7 Pe^{-\frac{2}{3}} (1 + 0.39 K_f^{-\frac{1}{3}} Pe^{\frac{1}{3}} Kn_f) + 0.624 Pe^{-1} \qquad (2-1)$$

$$\eta_R = (2K_f)^{-1} \left\{ (1+R)^{-1} - (1+R) + 2(1+R) \ln (1+R) \right. $$

$$\left. + 2.86 Kn_f (2+R)R(1+R)^{-1} \right\} \qquad (2-2)$$

The interactive term is given as:

$$\eta_{DR} = 1.24 \, K_f^{-\frac{1}{2}} Pe^{-\frac{1}{2}} R^{\frac{2}{3}} \qquad (2-3)$$

All nomenclature is as defined in Chapter 1 for the fan model. Stechkina et al (141) also suggested the following equation for estimating the inertial contribution to collection efficiency for low Stokes numbers:

$$\eta_I = \frac{I.St}{(2K_f)^2} \qquad (2-4)$$

where nomenclature is as in Chapter 1. For conditions other than Stokes numbers > 0.2 the inertial term is neglected.

From these separate contributions the single fibre efficiency is assumed to be:

$$\eta = (\varepsilon_f)^{-1} (\eta_D + \eta_R + \eta_{DR} + \eta_I) \qquad (2-5)$$

where ε_f is a correction factor for non-uniformity and lies between 1.13 and 2.25. Ideally this value should be calculated from measuring the pressure drop and back calculating using the theoretical pressure drop given in equation (2 - 24). In the absence of pressure drop data the value of 2 can be used as an estimate.

The overall efficiency can then be found using

$$E = 1 - P^* = 1 - \exp \left\{ \frac{-4\alpha L \eta}{\pi d_f (1-\alpha)} \right\} \qquad (2-6)$$

where P^* is the filter penetration

(ii) As an alternative to the fan model the plain cellular model proposed by Stenhouse (144) can be used. This assumes the Kuwabara flow field applies throughout and gives the following:

76

$$\eta_D = 2.9 \, K^{-1/3} \, Pe^{-2/3} \tag{2-7}$$

$$\eta_R = (2k)^{-1} \left\{ (1+R)^{-1} - (1+R) + 2(1+R) \, \ell n \, (1+R) \right\} \tag{2-8}$$

and for $A \geqslant 1$

$$\eta_I = \eta_R + (1+R - \eta_R) \left\{ 1 - \frac{1}{A} \right\} \tag{2-9}$$

$A < 1$

$$\eta_I = \eta_R \tag{2-10}$$

where,

$$A = 0.45 + 1.4\alpha + (1.3 + 0.5 \, \log_{10}\alpha)St$$

$$
\begin{aligned}
K \quad &= \quad \text{the hydrodynamic factor} \\
&= \quad \frac{-3}{4} \frac{-1}{2} \, \ell n\alpha \qquad \alpha \leqslant .02 \\
&= \quad \frac{-3}{4} \frac{-1}{2} \, \ell n\alpha + \alpha - \frac{\alpha^2}{4} \qquad \alpha > .02
\end{aligned}
$$

In this case the single fibre efficiency is simply.

$$\eta = (\varepsilon_c)^{-1} (\eta_D + \eta_R + \eta_I) \tag{2.11}$$

77

Where ε_c is a configuration factor which is slightly larger than ε_f.

The overall efficiency can then be calculated from (2 - 6).

A correction for the adhesion effect is also facilitated. Stenhouse (144) redefined the single fibre efficiency as:

$$\eta_s = \eta \cdot \eta_a \qquad\qquad (2\text{-}12)$$

η_a is found from the empirical expression

$$\eta_a = .003 \, (f.St)^{-10} + .36 \exp\left\{- 1.7U_o \, (f.St)^{-.43}\right\}$$

$$(2\text{-}13)$$

For most systems the adhesion factor, f, is unity. The value of η_a lies between .004 and 1. However its value only deviates significantly from unity when the Stokes number exceeds 1.0 for most systems.

2.1.2. Granular bed efficiency

Two alternative methods for calculating the efficiency are proposed. The first is a method developed by Lee and Gieske (89) based on the Kuwabara flow field. Expressions are as given in Chapter 1 for single grain efficiency contributions by diffusion, interception and gravity.

$$\eta_D = 2 \left(\frac{3\pi}{4} \right)^{2/3} Pe^{-2/3} \frac{(1-\alpha)}{kg} \tag{2-14}$$

$$\eta_R = \frac{3}{2} \frac{(1-\alpha)}{kg} \frac{R^2}{(1-R)^m} \tag{2-15}$$

$$\eta_G = \frac{\rho_g \, dp^2}{18\mu Uo} \tag{2-16}$$

where nomenclature is as defined in chapter 1. Hence the contributions can be summed for the single grain efficiency

$$\eta = \eta_D + \eta_R + \eta_G \tag{2-17}$$

and equation (2-6) is used.

The second series of equations suggested for use in calculating granular bed efficiency are based on recommendations by several authors as predictions which give reasonable correlation with experimental data. Again details are given in the review of chapter 1. Generally accepted for the calculation of the single grain efficiency due to diffusion is the equation of Wilson and Geankoplis (167).

$$\eta_D = 4.36 \, (1-\alpha)^{-1} Pe^{-2/3} \tag{2-18}$$

Tardos et al (156) in agreement with Pfeffer (122) use the adaptable equation given below to calculate single grain efficiency from interception

$$\eta_R = 3.37 \ (1-\alpha)^{-3} R \ ; \ St < .02 \tag{2-19}$$

$$\eta_R = (1-\alpha)^{-1} \ (1+2R+R^2 - (1+R)^{-1}) \tag{2-20}$$

$$St \geqslant .02$$

For collection efficiency due to gravity Tardos et al (156) also derived.

$$\eta_G = St \ Ga (1 + St. \ Ga)^{-1} \tag{2-21}$$

Thambimuthu's (159) expression for single grain efficiency by inertia is preferred by Clift amongst others.

$$\eta_I = \left\{ St \ / \ (St + .062 \ (1-\alpha)) \right\}^3 \tag{2-22}$$

Once again the respective contributions are summed to give a single grain efficiency:

$$\eta = \eta_D + \eta_R + \eta_G + \eta_I \qquad (2\text{-}23)$$

and equation (2 - 6) is used to find the overall granular bed efficiency.

2.1.3. Pressure drop through the fibrous media

Three alternatives were proposed for calculating the pressure drop. The first to be used in conjunction with the fan model, the second with the cellular model and the other an empirical correlation of Davies for comparison.

(i) From the fan model

$$\Delta P = \frac{16 \; U_o \; \mu \; \alpha \; L}{K_f' \; d_f^2 \; \varepsilon_f} \qquad (2\text{-}24)$$

where all notation is as before except

$$K_f' = 0.5 \ln \alpha - 0.52 + 0.64\alpha$$
$$+ 1.43 \; (1-\alpha) Kn_f \; \varepsilon_f^{-\frac{1}{2}}$$

(ii) From the cellular model

$$\Delta P = \frac{16 U_o u \alpha L}{K_c d_f^2 \mathcal{E}_c} \qquad \qquad (2\text{-}25)$$

where,

$$K_c = \frac{-1}{2} \ln \alpha - \frac{3}{4} + \alpha - \frac{\alpha^2}{4}$$

(iii) From Davies's (29) empirical correlation:

$$\Delta P = \frac{64 u L \alpha^{1.5} U_o (1 + 56\alpha^{1.5})}{d_{fe}} \qquad \qquad (2\text{-}26)$$

where $0.006 < \alpha < 0.3$

d_{fe} is the effective fibre diameter and is usually greater than that measured by microscope.

2.1.4. Pressure drop through the granular bed

Three equations were suggested for comparison. These were: the well known Kozeny-Carman equation (18); Lee et al's (88) derivation for pressure drop in a Kuwabara flow field assuming low Knudsen numbers; the other equation was a semi-empirical correlation derived by Kennard and Meisen (73) based on the Ergun equation (42) as an alternative to the Kozeny-Carman equation.

(i) Kozeny-Carman equation

$$\Delta P = 180 \frac{\mu U_o}{dg^2} \frac{\alpha^2}{(1-\alpha)^3} L \qquad (2-27)$$

(ii) Lee et al's derivation

$$\Delta P = \frac{18\alpha u U_o L (1+4Cm\lambda/dg)}{dg^2 (Kg + 6Cm\ Kg'\lambda/dg)} \qquad (2-28)$$

where nomenclature is as defined in chapter 1.

(iii) Kennard and Meisen's correlation

$$\Delta P = 316 \frac{\mu U_o}{dg^2} \frac{\alpha^2}{(1-\alpha)^3} L + 1.73 \frac{\rho U_o^2}{dg} \frac{\alpha}{(1-\alpha)^3} L \qquad (2-29)$$

2.1.5. Calculation of overall efficiency and pressure drop

The media efficiency was computed for either the fan or cellular model. Similarly the granular bed efficiency was computed from either Lee and Gieske's model or the general series of equations. The overall efficiency of the combination was then found as

$$E = Eg + (1-Eg) \, E_f \qquad\qquad (2-30)$$

where E_g overall granular bed efficiency

E_f overall fibrous media efficiency

The pressure drops are assumed additive. To calculate the pressure drop, the equation corresponding to the model used to calculate efficiency was employed. Davies's empirical correlation was incorporated to give a comparison. Similarly for granular bed calculations consistency was kept by either using Lee and Gieskes' equations through out or the series of recommended equations with Kennard and Meisen's semi-empirical derivation. The Kozeny-Carman equation was used as a comparative solution.

2.1.6. Conclusions from the models used

The models were written into a computer programme. Results are in appendix 2-1. The model demonstrates that with the parameters expected for a high efficiency fibrous filter with a packed bed of mean size similar to BS 2831 No.2. dust, then very little can be expected to penetrate. Even the most penetrative aerosol sizes between .05 and .3 μm diameter would be effectively removed by either the media or bed alone. This confirms that filtration efficiency will improve with load whether this be depth or surface loading. The model also suggests that aerosols with a high concentration of particles

between .05 and .5 μm diameter will be needed in filter test work if effective efficiency results are to be obtained.

The calculated efficiencies are reasonably consistent as are computed media pressure drops. However the Kozeny-Carman equation predicts substantially lower granular bed pressure drops than the alternatives. Clearly the high voidage systems with such dust beds are outside the range of applicability of Kozeny-Carman equation. Brinkman (12) and Davies (27) made similar observations.

2.2. Analysis of particle trajectories within a deep pleat filter arrangment

2.2.1. Analysis of the concentration change in a channel by mass balance :

This was an initial estimation of the change in dust concentration with progression along a channel. It assumes the concentration of the dust will be reduced in two ways.

1. Filtration
2. Sedimentation

Inertia or any other flow effects are not accounted for. The evaluation was made with filtration assumed to be taking place through one of the side walls of a rectangular channel as shown by figure 2-1.

Taking an element Δx at the entrance of a channel of length L the concentration lost due to filtration through the element is

$$C_f = C_i \; \frac{\Delta x}{L} \tag{2-31}$$

where C_i is the concentration into the element.
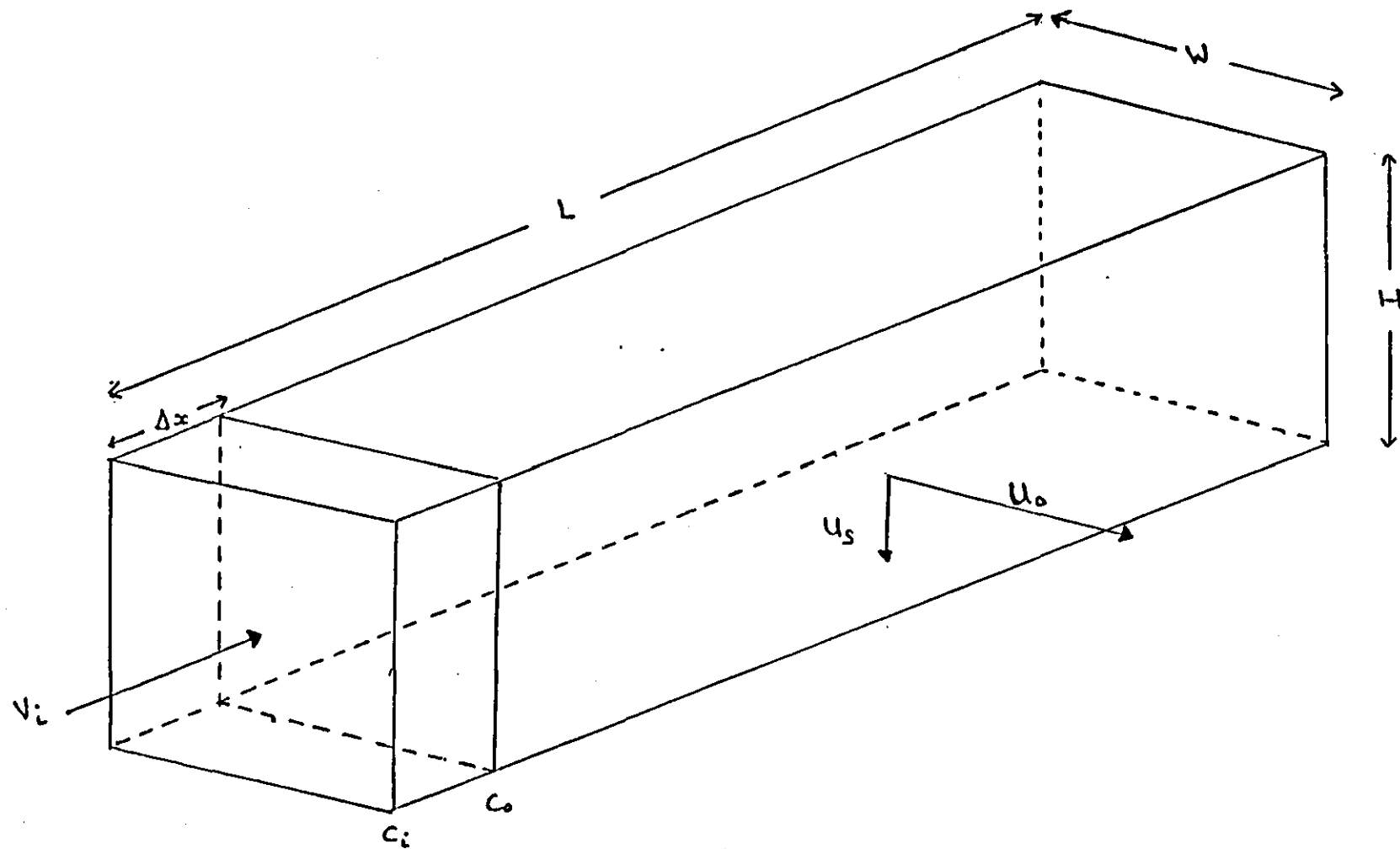
FIGURE 2.1   Rectangular filter channel with side wall filtration

The reduction in concentration due to sedimentation is:

$$C_s = C_i \times \frac{\text{Distance dust settles}}{\text{Distance available for settling}} = \frac{C_i U_s t}{H}$$

(2-32)

Obviously the settling velocity of a dust particle is size dependent. According to Stokes law the settling velocity is:

$$U_s = \frac{d_p^2 \rho_p g}{18\mu}$$

(2-33)

where

d_p = particle diameter, ρ_p = particle density, μ = gas viscosity, g = gravitational constant.

Time t can be evaluated by assuming a uniform fall off velocity of the gas along the channel length. Hence

$$V = V_i \frac{(1-x)}{L}$$

(2-34)

V_i = inlet velocity
x = distance along the channel

Also,

$$V_i = \frac{U_o L}{W}$$

(2-35)

U_o = filtration velocity
W = channel width

Considering the first element of the channel the average velocity can be found from

$$V_{av} = V_i \frac{(1- \frac{\Delta x}{2L})}{}$$ (2-36)

And so

$$t = \frac{\Delta x}{V_{av}}$$

$$= \frac{2 L \Delta x}{V_i (2L-\Delta x)}$$ (2-37)

So,

$$C_s = \frac{2C_i U_s L \Delta x}{H V_i (2L-\Delta x)}$$ (2-38)

There will also be some interaction as some dust will be removed by filtration before having the opportunity to settle out by sedimentation within the element. This can be expressed as

$$C_I = \frac{\Delta x \; h \; b \; Cav}{L \; H \; W}$$ (2-39)

where,

h = dust settling distance = $U_s t$

b = dust filtration distance = $U_o t$

Cav = average dust concentration in element Δx

$$= \frac{C_i - (C_i - C_o)}{2}$$

So using (2-37) and transposing (2-36)

$$C_I = \frac{2 (C_i + C_o) \, U_s \, \Delta x^3}{V_i \, (2L-\Delta x)^2 H} \qquad (2-40)$$

Now for the initial element Δx

$$C_o = C_i - (C_s + C_f - C_I) \qquad (2-41)$$

In the general case the height available for settling will be

$$H_s = H-F \qquad (2-42)$$

where F is the height the dust will have settled by distance x along the channel and can be found from the time to this point.

Further the average gas velocity can be generally defined as:

$$V_{av} = V_i \left\{ \frac{1 - (2n+1) \, \Delta x}{2L} \right\} \qquad (2-43)$$

where n is the number of elements previously considered. If the original concentration of the dust entering the channel is C' and equal elements Δx are taken for the full length of the channel then

$$C_o = \frac{C_i \left\{ \dfrac{1-C'}{C_i} \cdot \dfrac{\Delta x}{L} - \dfrac{2 \, U_s L \Delta x}{(H-F)V_i(2L-(2n+1)\Delta x)} + \dfrac{2 \, U_s \, \Delta x^3}{V_i H(2L-(2n+1)\Delta x)^2} \right\}}{\left\{ 1 - \dfrac{2 \, U_s \, \Delta x^3}{V_i H(2L-(2n+1)\Delta x)^2} \right\}} \qquad (2-44)$$

As expected in the absence of sedimentation this equation predicts a linear fall off in concentration with distance. As sedimentation increases the deviation from linearity increases. Computation shows that it becomes significant for aluminium oxide particles above about 5 μm diameter. The model is limited because of some of the assumptions made in its development. However the importance of sedimentation is clearly illustrated. With typical deep pleat filters the channels are separated by spacers which approximate to a triangular cross-section. Therefore it is essential to interpret the effect of these on sedimentation and so overall filter performance. Furthermore particle inertial effects were not considered. Therefore the following, more rigorous, model was developed to calculate particle trajectories in a deep pleat channel and so predict the overall dust distribution within the filter.

2.2.2. Particle trajectories in a triangular channel with side wall filtration

Figure 2.2 shows the geometry considered
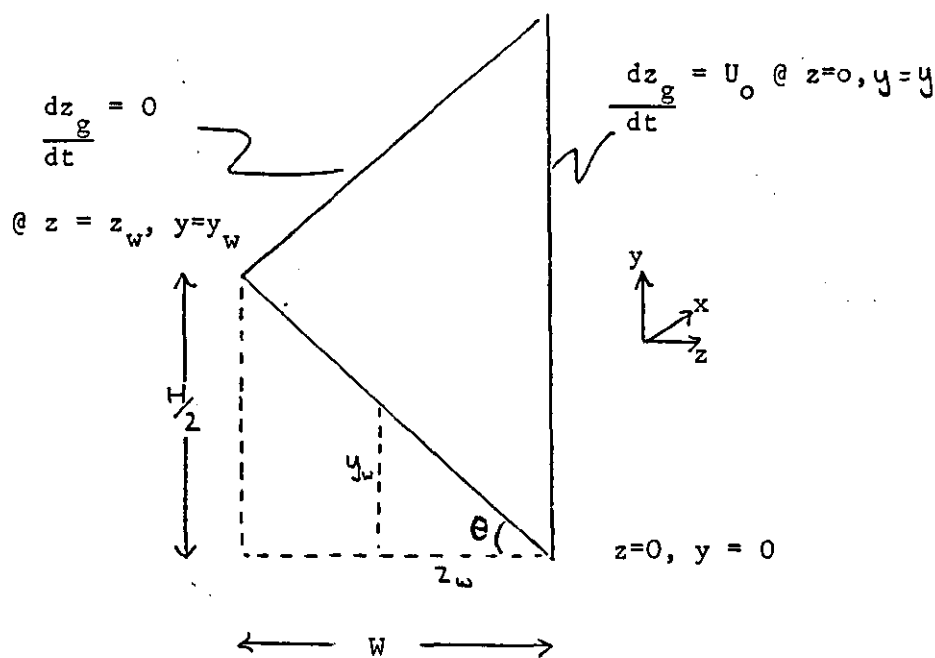
FIGURE 2.2 Triangular channel geometry

The general equation (neglecting electrostatic forces) for particle motion is

$$m_P \frac{d^2 x}{dt^2} = 3\pi\mu dp \ (Ug - Up) + m_p a$$

where,

m_p = particle mass $= \frac{\pi dp^3}{6} \rho_p$ for spherical particles

Ug = gas velocity

Up = particle velocity

a = any external acceleration force

In order to solve this to yield a particle trajectory the following assumptions are made.

(i) Flow is assumed laminar and stokes law applies.

This is reasonable as low Reynolds numbers exist for typical channel dimensions and flow rates.

(ii) Any particle hitting a surface will be retained on the surface. This is also reasonable as reentrainment and bounce would not be anticipated under normal operating conditions.

(iii) Particle motion is in the linear Stokes regime. The resultant coordinates considered are:

x direction = channel length

y direction = channel height

z direction = channel width

(iv) The y resolute of gas velocity is zero

(v) The particle settles in the y direction at its terminal velocity.

(vi) The z component of gas velocity is zero at the spacer surface from where it is taken to have a uniform acceleration to the filter surface. This results in a triangular profile in the y plane. This is clearly an over simplification. In reality an even velocity profile would be expected at the media surface in order to maintain a constant pressure drop at all points across it. However, this would involve a changing velocity and acceleration profile in both y and z directions. To obtain an estimation of the predominant mechanisms controlling filtration it was not considered necessary to include this additional severe complication.

(vii) The gas flux in the x direction is assumed to fall linearly with distance from the entrance.

The model described progresses logically from the above assumptions. Resolving in the y direction and including assumption (v).

$$\frac{\pi dp^3}{6} \rho_p \frac{d^2y}{dt^2} = 3\pi\mu dp \left(0 - \frac{dy}{dt}\right) - \frac{\pi dp^3}{6} \rho_p g \qquad (2-46)$$

which can be simplified to:

$$\alpha\frac{d^2y}{dt^2} + \frac{dy}{dt} + \alpha g = 0 \qquad (2\text{-}47)$$

where,

$$\alpha = \frac{\rho_p d_p^2}{18\mu}$$

This is solved using Laplace transforms (appendix 2.2.1) taking the initial conditions as

$$y(o) = y_o$$

$$\frac{dy(o)}{dt} = -\alpha g$$

The solution is

$$y(t) = y_o - \alpha g t \qquad (2\text{-}48)$$

In the z direction the triangular profile of the face velocity in assumption 6 can be expressed as:

$$U_o = 2\sqrt{2}\ Uoa\ \frac{y}{H} \qquad\qquad y \leqslant \frac{H}{2} \qquad (2\text{-}49)$$

where Uoa = average face velocity

The origin is at the bottom apex of the channel such that the centre line is at $y = \frac{H}{2}$ and

$$U_0 = 2\sqrt{2}\ \text{Uoa}\ \frac{(H-y)}{H}\ ; \quad y > \frac{H}{2} \tag{2-50}$$
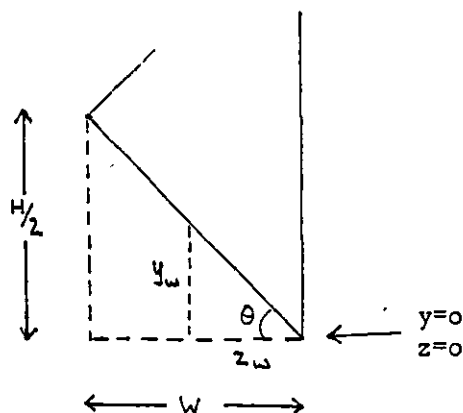
FIGURE 2.3

From Figure 2.3:

$$\tan\theta = \frac{H}{2W} = \frac{|y_w|}{|z_w|} \tag{2-51}$$

and gas velocity at any z

$$\frac{dz_g}{dt} = \frac{Uo}{|z_w|}\ (|z_w| + z) \tag{2-52}$$

Using (2-49) - (2-51) in (2.52)

$$\frac{dz_g}{dt} = k\ (1 + \gamma z) \tag{2-53}$$

94

·where

$$K = \frac{2\sqrt{2}}{H} U_{oa}.y \quad , \quad \gamma = \frac{H}{2Wy} \qquad \text{for } y \leq \frac{H}{2}$$

$$K = \frac{2\sqrt{2}}{H} U_{oa} (H-y) \quad , \qquad = \frac{H}{2W(H-y)} \text{ for } y > \frac{H}{2}$$

Combining equations (2-45 and (2-53) then:

$$\alpha\frac{d^2 z}{dt^2} + \frac{dz}{dt} - k\gamma z - k = 0 \qquad (2\text{-}54)$$

Solution (as in appendix 2.2.1) by Laplace transforms can be reached using the initial conditions.

$$y(0) = y_o \rightarrow k_o, \gamma_o$$

$$z(o) = z_o$$

$$\frac{dz(o)}{dt} = k_o (1 + \gamma_o z_o)$$

The solution is

$$z(t) = z_o + k\gamma t^2 + K (1-\alpha\gamma)t + \left\{ \alpha (K_o + K_o\gamma_o z_o \right.$$

$$\left. + \alpha K\gamma - K)(1-e^{-t/\alpha}) \right\}$$

$$(2\text{-}55)$$

By continuity and using assumption (vii) the gas velocity resolute in the x direction is:

$$\frac{dx_g}{dt} = \frac{2\,\gamma}{W}\,(L-x) \qquad\qquad (2\text{-}56)$$

where $\gamma = K\,(\,1 + \delta z)$

Therefore using (2-45) (2-56) becomes

$$\alpha\,\frac{d^2x}{dt^2} + \frac{dx}{dt} + \beta x - \beta L = 0 \qquad\qquad (2\text{-}57)$$

where

$$\beta = \frac{2\,\gamma}{W}$$

Again the solution (as in appendix 2.2.1) can be found by Laplace transforms from the initial conditions

$$y(o) = y_o \quad \rightarrow Ko,\ \delta o$$

$$z(o) = z_o \quad \rightarrow \gamma_o$$

$$x(o) = x_o$$

$$\frac{dx(o)}{dt} = \frac{2\,\gamma_o}{W}\,(L - x_o)$$

The solution is:

$$x(t) = x_o - \frac{\gamma}{W}t^2 + \frac{2\gamma}{W}(L+\alpha)t \qquad (2\text{-}58)$$

$$+ \left\{ 2\alpha (2\gamma_o L - \gamma L - \gamma_o x_o - V\alpha)(1-e^{-t}/\alpha) \right\}$$

Equations (2.48), (2.53) and (2.58) were solved by computer to yield the particle trajectories. Results are given in appendix 2.2.2.

The model provides only an approximate representation of the flow field in the channels of real deep pleat filters. However, because of the complex interactions of the mechanisms in the system the above analysis is necessary. Although the results are approximate they illustrate the relative importance of the contributing factors such that a number of conclusions can be drawn:

(i)   Particle inertia has a negligible effect for aluminium oxide particles less than about 25 μm diameter.

(ii) Sedimentation effects are apparent for aluminium oxide particles greater than about 5 μm diameter.

(iii) The spacers provide an additional surface for dust collection by sedimentation.   This effect diminishes with distance from the entrance. As the particles travel along the channel they move towards the filter face increasing the height through which they must settle.

(iv) The increase in the number of spacers by reduction of channel height would increase this sedimentation surface such that a higher proportion of particles would settle out. However there would be a consequential increase in the pressure drop. Mechanical constraints in construction and loss of area where spacers touch the media are important.

(v) The density of dust deposition on the filter face will decrease with distance due to sedimentation losses in the vertical plane. The deposition will be lowest on the top face of the media furthest from the entrance.

(vi) The major influence on filtration is the air velocity distribution. Sedimentation and inertial effects are minor compared with this and are indeed insignificant below the stated limits.

(vii) The model is limited by the use of the assumed simple velocity profile. It nevertheless provides an estimate of the limits of the sedimentation and inertia mechanisms in the channel.

(viii) The model is only applicable to a clean filter. Once deposits accumulate the air distribution will change to maintain an even resistance throughout the filter. This transient behaviour is not accounted for.

2.3. Theoretical analysis of pressure drop characteristics of a panel filter

The pressure drop resulting from the air flow through a panel filter can be considered to be due to the following factors:-

1. The media and dust collected on that media. This can be evaluated from empirical equations derived from experimental work.

2. The pressure drop due to air passing along a filter channel. With coarse dust (such as B.S. No.2.) being collected there will be a gradual restriction of available channel space as the dust layer grows. Hence the pressure drop will vary with load and this has to be accounted for.

3. The permanent head loss due to air accelerating into the channel entrance.

4. The permanent head loss due to the inlet and outlet effects of the filter casing. This is independent of the media arrangement.

98

The contribution to the total pressure drop under heading 1 is dealt with in chapter 3 and that under heading 4 is not relevant to the present argument. The contributions under headings 2 and 3 are dealt with below.

2.3.1. Flow through a channel between pleats

In the following analysis the air flow is considered to be between two parallel filtering surfaces which then form a channel.

a)   a mass balance is used to establish an expression for the average velocity in the channel, i.e. as a function of the distance from the entrance. For two infinitely wide parallel plates of total length L from the entrance, a differential mass balance yields

$$A_x dV = - U_0 s \, dx$$

where A_x = cross sectional area

U_0 = face velocity

s   = perimeter length

On integration this gives

$$\bar{V} = \frac{U_0 s}{A_x} (L-x) \qquad\qquad (2\text{-}59)$$

b)   The channel pressure drop for the above system is now calculated. Since the channel Reynolds number is in range 0 - 200 for a conventional type of deep pleat filter operated under normal conditions it is considered that it is most appropriate to apply viscous flow theory to the problem.   The equation of creeping motion,

$$-\frac{\nabla P}{\rho} + \gamma \nabla^2 V = 0 \qquad\qquad (2\text{-}60)$$

reduces to,

$$\frac{\partial^2 V}{\partial y^2} = \frac{1}{\mu} \frac{\partial P}{\partial x}$$

for steady flow between two infinite parallel plates integration yields

$$V = \frac{1}{2\mu} \left(\frac{\partial P}{\partial x}\right) y^2 + C_1 y + C_2$$

Applying appropriate boundary conditions at the centre $\frac{\partial v}{\partial y} = 0$ and at the wall ($V = 0$), this reduces to

$$V = \frac{1}{2\mu} \left(\frac{\partial P}{\partial x}\right)(y^2 - \delta^2)$$

y = distance from centre

δ = half the plate separation

By integrating the flow between the plates, the average velocity, $\overline{V}$ is found to be

$$\overline{V} = -\frac{\delta^2}{3\mu} \frac{dP}{dx} \qquad\qquad (2-61)$$

Comparing equation (2-59) and (2-61) the pressure drop across a differential element is

$$dP = \frac{3\mu Uo}{\delta^3} (x-L) \, dx \qquad\qquad (2\text{-}62)$$

Integrating across the length of the channel and expressing the channel width (i.e. wall separation) as w (w = 2δ) then the pressure drop is given by

$$\Delta P = \frac{12\mu UoL}{w^3} \qquad\qquad (2\text{-}63)$$

c)   Channel pressure drop in a loading filter.

Equation (2-63) gives the pressure drop for a channel width w. However in a loading filter w is a variable as the dust layer thickness increases. By allowing a dust layer height σ_H on each filtering wall, equation (2-63) is corrected for a loading channel to give:

$$\Delta P = \frac{12\mu UoL^2}{(w - j\sigma_H)^3} \qquad\qquad (2\text{-}64)$$

where j is the number of filtering surfaces involved in restricting the channel width. The dust layer height σ_H is obviously a function of the amount loaded and dust packing.

The filter arrangement involves both upstream and downstream channels. As loading proceeds the overall channel pressure drop will depend on the interaction between the separate upstream and downstream

contributions. This interactive relationship will be complex depending on the past history of the loading and the effect of the media and collected dust resistance. Obviously as the load increases the upstream channel becomes more resistant to flow along its length and so the gas will show a preference for filtering to the clean side towards the channel entrance. This will, however, have two counteractive effects by increasing both dust load and velocity which determine the contribution to pressure drop by the media and dust. Hence it would be expected that the gas flow will revert to filtering further down the channel where the overall resistance is lower. This is clearly a complicated progressive filtration model.

However, the experiments of chapter 4.1 show that the dust deposition is relatively uniform throughout the channel length except at the very beginning of the upstream channel. Furthermore, in numerical terms the clean channel pressure drop for practical filter designs is insignificant in comparison to the media resistance. Therefore for calculation purposes it is postulated that a sensible approximation is obtained by taking the dust layer height to be uniform throughout the channel and calculating the dominant upstream channel pressure drop on the basis of average flow through the channel. A small correction for the influence of the downstream channel under average flow conditions can then be included. This simplified analysis gives realistic predictions of the overall channel pressure drop for practical designs of filter systems.

d)   Defining channel width in terms of fixed parameters. It is necessary, for purposes of optimisation, to be able to define variables such as the channel width in terms of more obviously fixed parameters - although in optimisation these may themselves be allowed to vary. The channel width is certainly dependent on the amount of filter media within a filter unit. The area of filter medium in a concertina shaped section is:

$$A = \frac{H}{C}(2BL + CB) \qquad\qquad (2\text{-}65)$$

where L = depth of channel (thickness of concertina section)

B = width of section

H = length of concertina section

This leads to a solution for the channel pitch as:

$$C = \frac{2BHL}{(A - HB)} \qquad (2\text{-}66)$$

The face area of a concertina section is

$$A_f = HB \qquad (2\text{-}67)$$

Allowing the media thickness in the filter to be m_T then the pleat pitch size can be defined as:

$$C = 2(w + M_T) \qquad (2\text{-}68)$$

and hence using (2-67) and (2-68) in (2-66) the channel width is:

$$w = \frac{A_f L}{(A - A_f)} - M_T \qquad (2\text{-}69)$$

It is now a relatively straight forward exercise to calculate the channel pressure drop in a filter at a given load.

e)   Calculation of channel pressure drop in a deep-pleat filter.

Within a deep-pleat arrangement the length of a channel is equivalent to the depth of the filter unit i.e. L = D. A_f is the face area of the panel (BH) as below:
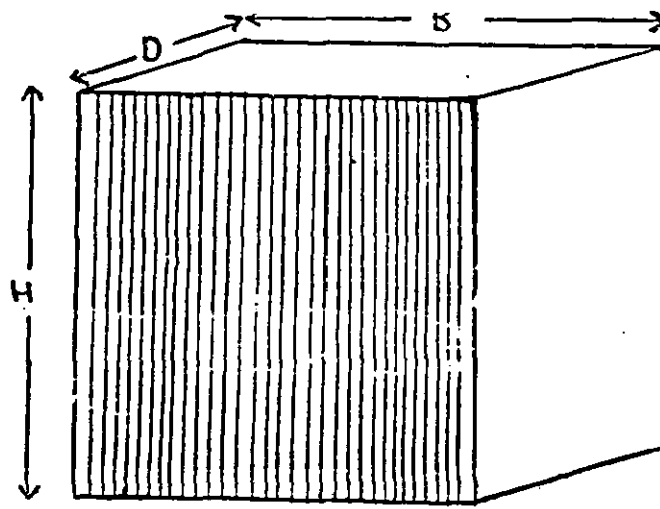
FIGURE 2.4a Sketch of deep pleat filter arrangement

Using (2-64) and (2-69):

(2-70)

$$\Delta P = \frac{12 \mu U_o D^2}{\left\{ \dfrac{A_f D - M_T - j\sigma_H}{A - A_f} \right\}^3}$$

where $j = 2$ for this derivation which has assumed filtration through
both parallel surfaces. It can be seen that the pressure drop is
defined in terms of basic filter unit dimensions, constants (media
thickness and air viscosity), the area of media packed into the filter
unit, air velocity through the media and dust layer thickness. For
the purpose of internal layout optimisation on standard units, these
last three would be the expected variables. Dust layer thickness can
be determined by considering the weight of dust, area it covers and
bulk density. Due to the presence of spacers giving a triangular
cross-section to the filter channels, a correction is necessary when
calculating the dust layer height. Thus for a deep pleat filter:

$$\sigma_H = \frac{h}{2w} \left\{ w - \sqrt{w^2 - \frac{4Aw}{h}} \right\}$$

(2-71)

where,

$$A = \sigma_s w / \rho_b$$

σ_s = specific load

ρ_b = bulk density

h = channel height $= 2w / \tan \theta$

where θ is the angle between the media and spacer in radians.

In calculating the specific load it is important to introduce a correction for the area lost due to contact between the media and spacers. This is found from first calculating the number of channels and pleats.

$$N_{channels} = Int \left\{ H/(2 m_T + h) \right\}$$
$$N_{pleats} = Int \left\{ B/(m_T + w) \right\} \qquad (2\text{-}72)$$

Hence the area available for filtration after accounting for spacer/media contacts is:

$$A_{avail} = A - 2N_c N_{Pl} M_T D \qquad (2\text{-}73)$$

assuming the spacer/media contact width is the same as the media thickness.

The face velocity is then corrected to:

$$U_o = \frac{A}{A_{avail}} \times U_{ospecified} \qquad (2\text{-}74)$$

However for the purposes of calculating the channel width C the total media area, A, must still be used.

f. Calculation of channel pressure drop in a mini pleat filter
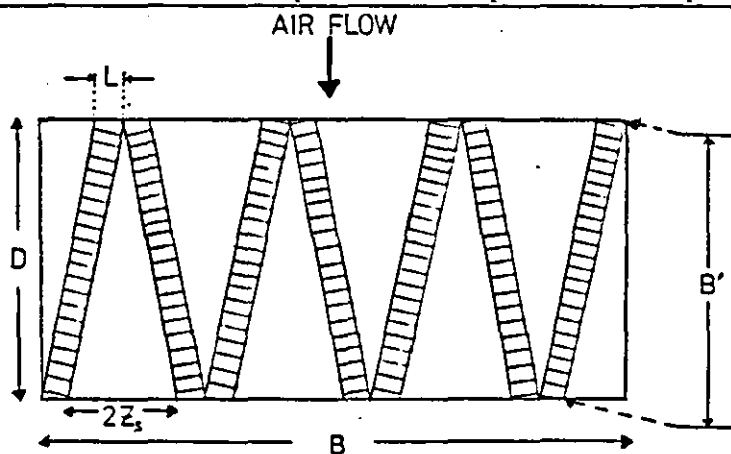
Figure 2.4b

Sketch of mini pleat filter arrangement - plan view, n = 7

105

Panels (or concertina sections) of thickness L (i.e. the channel length) are arranged in 'V's covering the full depth of the filter unit. Assuming there are n filter panels within the filter units it is possible to define A_f and L as follows – other variables and constants can be treated as before. Allowing the separation distance between two panels to be equivalent to $2Z_s$, as in the sketch above, then L is given by:-

$$L = \frac{B - n Z_s}{n}$$
(2-75)

The panel length will have also changed. This can be redefined as B' and be derived from considering a right angle triangle.

$$B_1 = \sqrt{D^2 + Z_s^2}$$

Therefore:

$$A_f = nB_1 H$$

$$= nH (D^2 + Z_s^2)^{\frac{1}{2}}$$
(2-76)

For the minipleat design the calculation of dust layer thickness is simplified due to the rectangular shaped channels. Hence:

$$\sigma_H = \sigma_s / \rho_b$$
(2-77)

The area available for filtration is governed by the area occupied by the stitching seams. The number of seams is found by:

$$N_{seams} = \frac{(D^2 + z_s^2)^{\frac{1}{2}}}{h + t_s}$$

where,

    h is the channel width

    t_s is the seam thickness

From this the area is found as:

$$Aavail = A (1 - N_s t_s (D^2 + z_s^2)^{-\frac{1}{2}}) \qquad (2\text{-}78)$$

To simplify the programming aspects in calculating the channel pressure drop, the available channel height for air to pass through is determined. Note due to the different orientation of the mini pleat filter this channel height is equivalent to the channel width, w, quoted for the deep pleat arrangement. Initially the total free height unoccupied by media is found as:

$$H_f = \frac{A_f (B - nZ_s) - AM_T}{n (B - nZ_s) (D^2 + Z_s^2)^{\frac{1}{2}}}$$

By calculating the occupied height from this the number of channels are found and the initial channel height simply given as;

$$W = \frac{H_f M_T}{(H - H_f)} \qquad (2\text{-}79)$$

The pressure drop due to the channel is now calculated.

2.3.2. Pressure drop contributed from air accelerating into the channels

This is an irrecoverable head loss due to the energy dissipated when air accelerates from the main volume into the individual channels. This is expressed as a pressure loss.

$$\Delta P_J = \frac{F' \rho V_i^2}{2} \qquad (2-80)$$

where,

V_i = channel entrance velocity

$$= \frac{Q}{A_f (\frac{1}{2} - \frac{\sigma_H}{W})}$$

ρ = air density
F' = a loss factor, typically 0.4
Q = flowrate

Therefore,

$$\Delta P_J = \frac{0.4 \ Q^2}{A_f^2 (\frac{1}{2} - \frac{\sigma_H}{W})^2} \qquad (2-81)$$

2.3.3. Total pressure drop

As previously stated this is defined as the sum of the individual pressure drops.

$$\Delta P_T = \Delta P_{ch} + \Delta P_{md} + \Delta P_J \qquad (2-82)$$

where

ΔP_{ch} channel pressure drop - section 2.3.1.

ΔP_J entrance loss - section 2.3.2.

ΔP_{md} media and dust pressure drop

          with increasing load - section 3.4.

Figure 2.4 shows the results of initial calculations made with this theory using a deep pleat filter but without the discussed corrections for area and dust layer height. Loading was assumed to be with BS 2831 No.2. dust. Different areas of media and gas flowrates were used in calculating the load at 100 mm water gauge. The expression load ratio is used so that data can be easily compared to that of the standard filter design with 20 m^2 of media and 1700 m^3/hr. rated flow. This is a load ratio of 1. The dotted line is where experimental data has been extrapolated beyond the measured range quoted in section 3.4.

This graph indicates that there is an optimum area of media for the standard type of design. However further interpretation is not justified without experimental validation. This leads to the experimental programme of 4.2 in which the pressure drop characteristics of deep pleat and mini pleat filters were measured. Figures A2.3 - 1 to 6 in appendix 2.3 show the comparison of the above theoretical model with experiment. The corrections to area and dust layer height were included in these computations. Figures 2.5 and 2.6 give a summary of this for an assumed bulk density of 700 kg/m^3 as suggested by the measurements of bulk density of dust collected in a deep pleat filter (section 3.5). Equations for the pressure drop characteristics of BS 2831 No.2 dust were used in the computations but alternative equations for other dust could be used if their pressure drop response to load was known.

FIG.2·4c : Variation of load of B.S. NO.2 with area at different flowrates – deep pleat filter.

(Load figures given as a ratio to the load predicted in a standard 20m² filter at 1700m³/hr.)

--- Points beyond tested range of empirical data

Load Ratio at 100 mm W.G. compared with 20 m² filter at a flow of 1700 m³/hr.

Filter Area (m²)

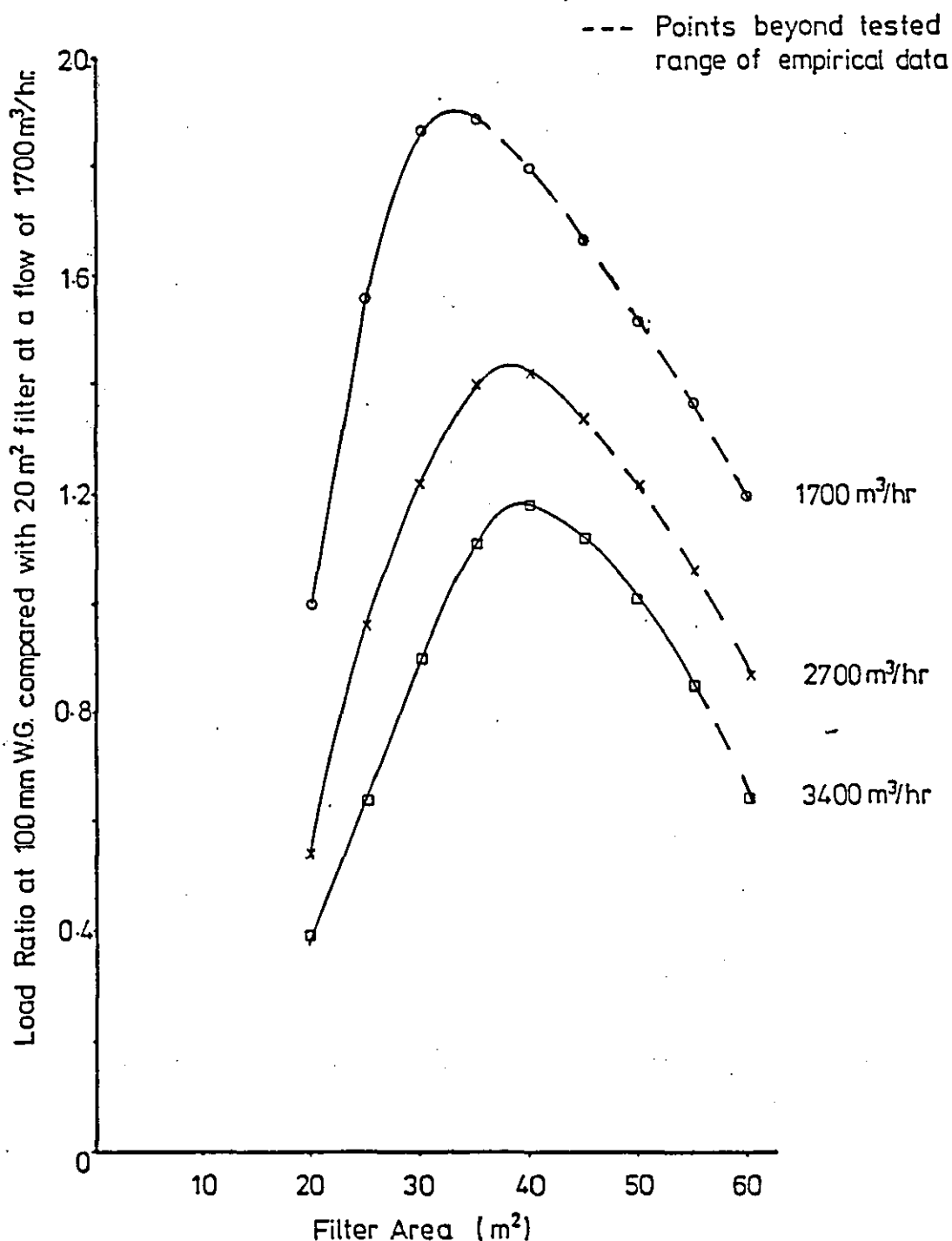1700 m³/hr

2700 m³/hr

3400 m³/hr

FIGURE 2.5 : Comparing theory and experiment for a deep pleat filter with BS2831 No.2 dust.
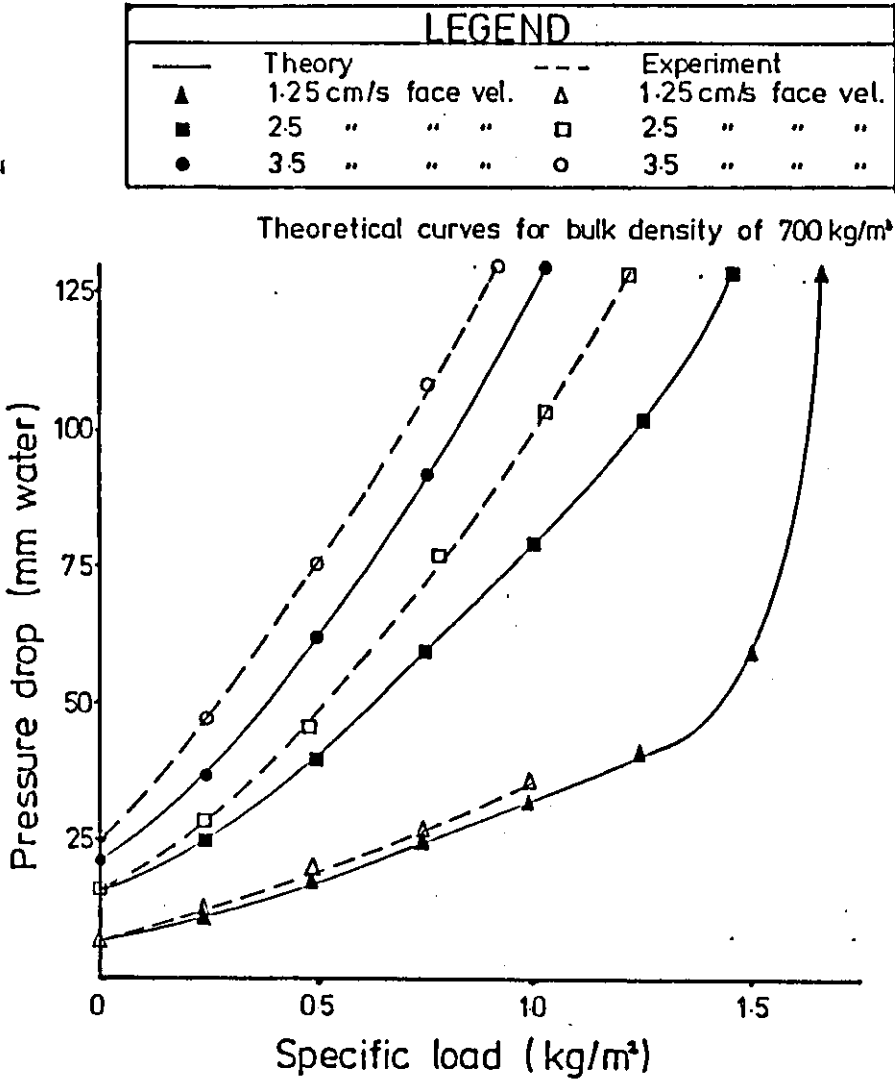
FIGURE 2.6 : Comparing theory and experiment for a mini pleat filter with BS2831 No.2 dust
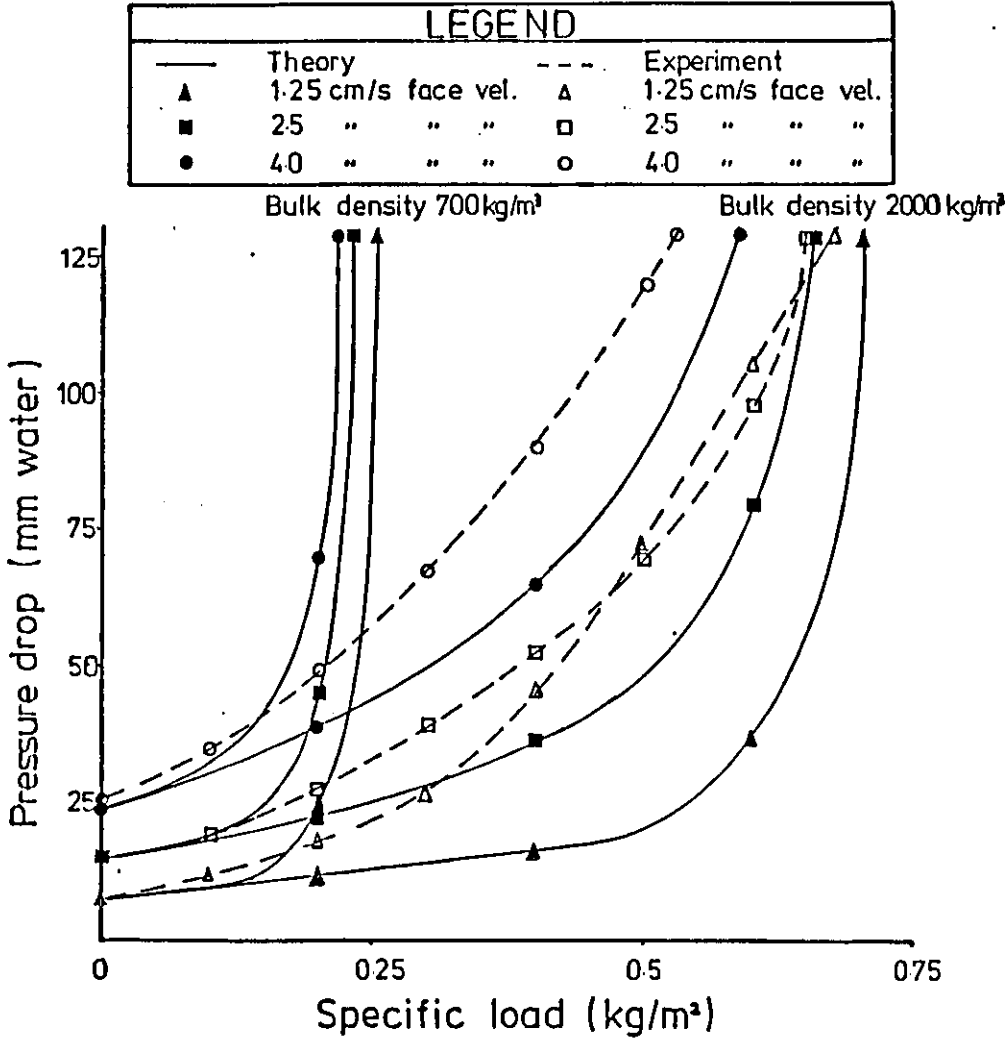
The deep pleat arrangement gives reasonable agreement considering the number of assumptions made. However the minipleat response is unsatisfactory suggesting further influences are present. Using experimental evidence from section 4.2. the theory has been developed for both filter designs to account for observed effects.

2.4. Modifications to deep-pleat theory

The results of experiments from 4.2 lead to the following improvements in the theory described in section 2.3.

(1) Considering the flow through a triangular channel rather than the parallel plate situation previously used.

(2) Considering the entrance effect on particle trajectories and subsequent dust deposition on the filter face and within the entrance.

2.4.1. Flow through a triangular channel

Happel and Brenner (61) derived an equation for flow through a triangular cross-section using a similar approach to that in 2.3. The solution is for an equalateral triangle of side length b and involves the summation of a complex series. Manipulating the result, as in 2.3, to yield an equation assuming side wall filtration at a mean face velocity V, gives:

$$\Delta P = \frac{320 \mu U_o L^2}{\sqrt{3}\ b^3}$$

(2-83)

However in a real situation the cross-section of the channel will usually be non-equalateral, although always an isoceles triangle. In practice this triangle is sufficiently close to equalateral for the equivalent area dimensions to be used. Therefore b is estimated from:

$$b = \left\{ \frac{2}{\sqrt{3}} \; w \, h \right\}^{\frac{1}{2}} \qquad\qquad (2\text{-}84)$$

The channel width and height will vary with the dust layer thickness. Equation 2.72 gives the dust layer height for channel width W (i.e. pleat spacing) and height h (i.e. pitch of spacer folds). Hence channel width at any instant is:

$$w' = w - \sigma_H \qquad\qquad (2\text{-}85)$$

where σ_H is the dust layer thickness.

As the angle of the spacer to media, Θ, is known, channel height any any instant is:

$$h' = 2w' / \tan\theta \qquad\qquad (2\text{-}86)$$

assuming the dust layer is flat.

Using (2-86) in (2-84) gives

$$b = 2w' \left(\sqrt{3} \, \tan\theta \right)^{-\frac{1}{2}} \qquad\qquad (2\text{-}87)$$

Substituting into (2-83) gives the general equation

$$\Delta P = \frac{320 \; \mu \; U_o \; L^2}{\sqrt{3} \left\{ 2w' \left(\sqrt{3} \, \tan\theta \right)^{-\frac{1}{2}} \right\}^3} \qquad\qquad (2\text{-}88)$$

2.4.2. Particle trajectories and consequential dust deposition at the channel entrance

In this section inertial migration of particles close to the front folds of the media is considered. Firstly the flow field is evaluated.

For a deep pleat filter the approach velocity, V_i , is typically 1.4 m/s. The following sketch shows how the folds of media of the filter face are considered to be porous cylinders of radius r_o . The spacing from centre to centre is taken as $4r_o$ and with infinitely thin media this will give a channel width of $2r_o$
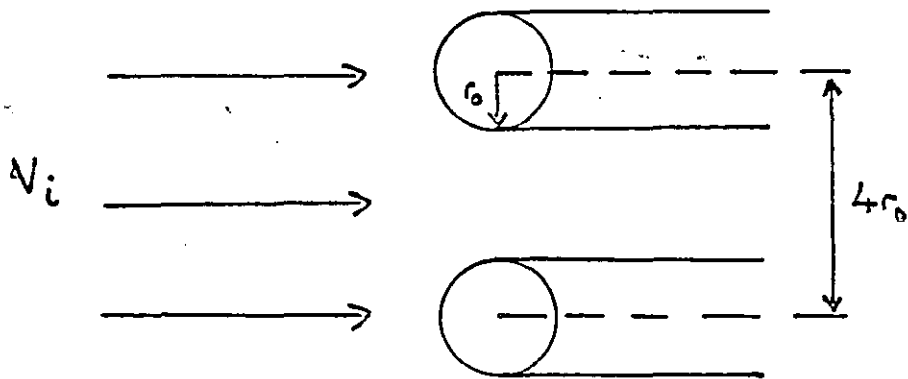
In a typical deep pleat filter design the cylinder Reynolds number is about 450. Hence a potential flow field analysis is applicable.

The flow has two major elements to be considered:

a)   Flow normal to the cylinder surface

b)   Flow round the cylinders

a)   <u>Flow normal to a porous cylinder surface</u>
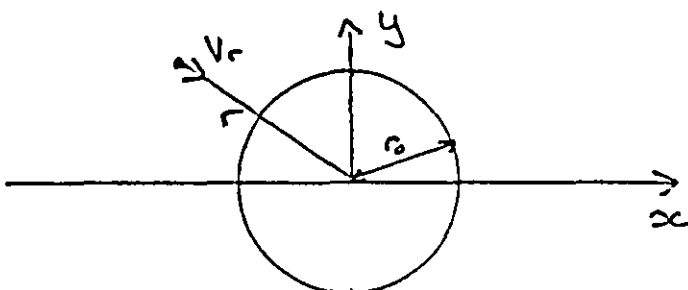
Consider a line source at the centre of the cylinder. This will result in a radially inward velocity, U_r, which has the value of U_o, the filter face velocity, at the cylinder surface. So,

$$U_r = \frac{U_o r_o}{r}$$

In Cartesian coordinates this gives

$$U_f = \frac{U_r x}{r} = \frac{U_o r_o x}{r^2} \qquad\qquad (2-89)$$

$$V_f = \frac{U_r y}{r} = \frac{U_o r_o y}{r^2} \qquad\qquad (2-90)$$

b) Flow round the cylinder

This can be described by the two resolutes, Bird, Stewart and Lightfoot (10   )

$$U_c = V' \left(1 + \frac{r_o^2}{r^2} - \frac{2x^2 r_o^2}{r^4}\right) \qquad\qquad (2-91)$$

$$V_c = V' \frac{(-2r_o^2 xy)}{r^4} \qquad\qquad (2\text{-}92)$$

where

$$V' = V_i - \frac{\pi}{2} U_o$$

The term V' therefore accounts for the flow into the cylinder. If the cylinder was non-porous then $V' = V_i$. Note the centre spacing of the cylinders has been assumed at $4r_o$ as stated before. If the spacing was nr_o then the $\frac{\pi}{2}$ term would become $\frac{2\pi}{n}$.

Hence the overall flow field can be defined as

$$V_x = U_f + U_c = \frac{U_o r_o x}{r^2} + V' \left(1 + \frac{r_o^2}{r^2} - \frac{2x^2 r_o^2}{r^4}\right) \qquad\qquad (2\text{-}93)$$

$$V_y = V_f + V_c = \frac{U_o r_o y}{r^2} - V' \frac{(2r_o^2 xy)}{4} \qquad\qquad (2\text{-}94)$$

where,

$$V' = V_i - \frac{\pi}{2} U_o$$

$$r = (x^2 + y^2)^{\frac{1}{2}} .$$

Now in the non linear regime (where Stokes Law is no longer applicable) the trajectory equations are

116

$$M_p \frac{dU_x}{dt} = 3\pi\mu dp f_f (V_x - U_x) \qquad (2\text{-}95)$$

$$M_p \frac{dU_y}{dt} = 3\pi\mu dp f_f (V_y - U_y) \qquad (2\text{-}96)$$

where U_x, U_y = particle velocity resolutes
V_x, V_y = gas velocity resolutes
f_f = friction factor

Now,

$$\frac{3\pi\mu dp f_f}{M_p} = \frac{0.75 \, C_D \, |\bar{V}_{rel}| \, \rho}{dp \, \rho_p} = \Upsilon \qquad (2\text{-}97)$$

where C_D is the drag coefficient which is a function of the particle Reynolds number based on the resultant velocity:-

$$|\bar{V}_{rel}| = \left\{ (V_x - U_x)^2 + (V_y - U_y)^2 \right\}^{\frac{1}{2}} \qquad (2\text{-}98)$$

C_D is evaluated using Kurten et al's (80) empirical equations which give a maximum error of $\pm$ 4%.

$$Re_p < 0.1$$

$$C_D = \frac{24}{Re_p} \qquad (2\text{-}99)$$

$$0.1 < Re_p < 4000$$

$$C_D = \frac{24}{Re_p} + \frac{6}{Re_p^{0.5}} + 0.28 \qquad (2\text{-}100)$$

where,

$$Re_p = \frac{\rho |\bar{V}_{rel}| \, dp}{\mu}$$

Now equations(2-95) and (2-96) can be integrated once with respect to time to give

$$U_x = V_{x_o} - (V_{x_o} - U_{x_o}) \, \exp\left\{-\Upsilon \Delta t\right\} \qquad (2\text{-}101)$$

$$Uy = Vy_o - (Vy_o - Uy_o) \, \exp\left\{-\Upsilon \Delta t\right\} \qquad (2\text{-}102)$$

where,

Ux, Uy are particle velocities to be calculated at anew position

Ux_o, Uy_o are present particle velocities

Vx_o, Vy_o are gas velocities calculated from flow field equations with present position coordinates x_o, y_o

Particle trajectories were calculated from the above equations using finite difference analysis and results are presented in appendix 2.4.1. These clearly demonstrate that some dust will be collected on the front folds of media which agrees with experimental observation.

Furthermore many dust particles will be deflected such that a concentration profile of dust will exist at the channel inlet. This profile shows a high concentration of dust close to the filter surface and consequently it is anticipated more dust will deposit towards the beginning of the channel again as observed in practice. There will be some compensatory effect as the build up of dust towards the entrance will create a higher resistance for gas flow through the dust/media layer. Hence a higher proportion of the gas flow, with the suspended particles, will tend to filter further along the channel. It can also be seen from the results that the particle size effect is important. This, together with the continuous change of r_D as the dust layer height grows, further complicates the prediction of the overall dust deposition within the channel due to entrance effects.

The entrance effect will also be interactive with the complex flow variations due to pressure drop differences in a loading upstream channel compared with its corresponding clean downstream channel. This was discussed in 2.3.1 (c). Then a simple approximation was postulated and a similar approach would appear justifiable to account for the above.

It is postulated that the channel is divided into three equal sections. The first of these is taken as the initial third of the complete channel, the second is the centre section and the third the end of the channel. Using experimental data obtained in section 4.2 the average proportion of the total amount of dust depositing in each section was calculated. The flowrate through the media of each section is then found by successive iteration. This is based on the pressure drop through each section being equal and the sum of the individual flowrates through the media being equal to the overall flow. The media/dust contribution to pressure drop is based on the velocity through the particular section of media whereas the channel contribution is taken to be based on the total flow through the section. This is the overall flowrate from the inlet to outlet of the channel. It is assumed that the dust layer is evenly deposited over the area of the particular section being considered. Hence the overall pressure drop (i.e. any section pressure drop) is evaluated for a three stage non-uniform dust deposition within a channel.

2.4.3. Conclusion from deep-pleat theory model incorporating modifications

The results shown in appendix 2.4.2 and figure 2.7 account for the described effects. The results can be seen to be in close agreement with experimental results for B.S. 2831 No.2. dust. The error present is easily accounted for by experimental error in flowrate measurement of $\pm$ 5%. All curves fall into this error band.

It is concluded that the theoretical model gives good predictions of deep pleat filter pressure drop behaviour. Unfortunately there is a dependence on empirical equations when considering the dust/media pressure drop, dust bulk density and dust deposition distribution. Chapter 5 includes suggestions for further work to eliminate this empiricism using theoretical approaches.

2.5. Modifications to the mini pleat filter theory

Experimental results showed that the theory developed to model dust deposition in a mini pleat filter arrangement required further additions or corrections. The improvements considered are discussed in this section.

2.5.1. Flow through a rectangular channel

The derivation of equation 2 - 64 was based on flow between infinitely wide parallel plates. Mini pleat channels are actually rectangular. Flow for rectangular channel is described by Happel & Brenner (61) as:

FIGURE 2·7: Comparing theory and experiment for a deep pleat filter with BS2831 No.2 dust
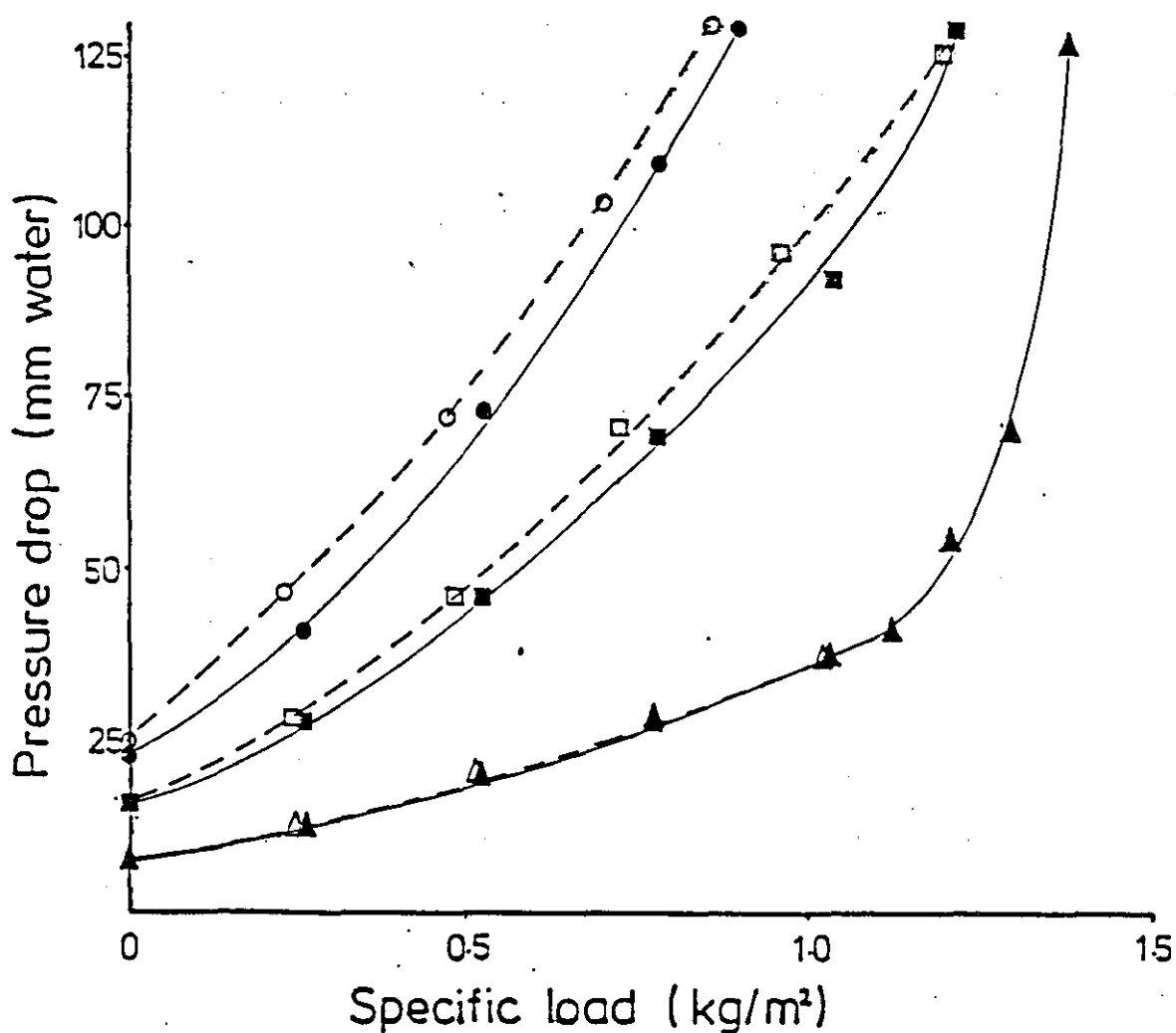
$$Q = \frac{\Delta P}{24\mu L} \ wh \ (w^2 + h^2) - \frac{8\Delta P}{\pi^5 \mu L} \sum_{n=1}^{\infty} \frac{1}{(2n-1)^5} \times$$

$$\left\{ w^4 \tanh\left(\frac{(2n-1)\pi}{2}\right) + h^4 \tanh\left(\frac{(2n-1)\pi w}{2h}\right) \right\}$$

(2-103)

where Q = $U_o wL$

U_o = face velocity,

h = channel width

w = channel spacing

L = channel length

This equation is now incorporated to describe the pressure drop due to flow through the channel. The summation is made for the first five terms, beyond which errors are negligible.

2.5.2. Deposition on the filter face

With the mini pleat design a significant area for filtration is actually on the filter face. Furthermore considering the entrance effects described in 2.4.2, it follows that a dust deposit would be expected on the filter face. This is observed in practice, 4.2. It would also be expected that as the channel clogs across its width, dust will build up on the front face by depositing on the dust blocking the channel due to both filtration and impaction.

In attempting to model this deposition it was simply assumed that the quantity of dust depositing on the dust face would be sufficient to maintain an equal pressure drop with that of the main filtration within the channel. The area this dust was depositing over was considered to increase in proportion to the dust layer build up within the channel. Hence when the channel is blocked filtration is still occuring through the filter face.

2.5.3. The development and effect of holes within the deposited dust

It was clearly observed in the experiments of 4.2, that holes formed within the channel where no dust deposited. For the purposes of including this effect within the context of the developed theory the model is adapted to include a permanent clear hole inside the channel.

The gas is considered to take three routes through the filter as shown in the sketch. These comprise of:

i)   Filtration through the end folds of the pleats.

ii) Passage through the rectangular channel which progressively fills with dust.

iii) Passage through a central hole which remains clean.

The pressure drop through each passage is the same and as the filter becomes loaded the flow through each will alter. If in general, then

$$\Delta P = \frac{Q}{\sum\limits_{j=i}^{iii} \frac{Q_j}{F_j(Q_j)}} \quad , \quad Q = \Sigma Q_j \qquad (2-104)$$
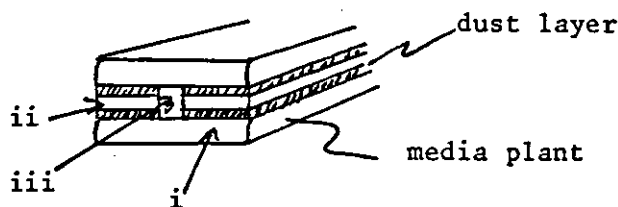
$F_i(Q_i)$ is the empirical expression for the pressure drop through loaded media as described in 2.5.2. $F_{ii}(Q_{ii})$ is as given in 2.5.1 for a loaded porous rectangular channel. $F_{iii}(Q_{iii})$ is for a clean square rectangular channel also under 2.5.1. Equation 2-104 was solved by successive approximation.

It is feasible that inertial classification and hence dust removal occurs as the dust laden gas enters the observed holes. The

concept is supported by the observation of "Beehive" shaped deposits round the edges of the holes. The object of this section is to explore the phenomenon theoretically. Particle trajectories are computed for a simple flow field representing that upstream of the hole entrance.

The potential field, generated by considering a point source in a planar transverse flow, is used. The velocity resolutes along the centre line of the hole in the direction of flow are:-

$$V_x = V_t + V_r \frac{x}{r} \qquad\qquad (2\text{-}105)$$

$$V_y = \frac{V_r y}{r} \qquad\qquad (2\text{-}106)$$

where r = radial distance from point source

   V_r = radial velocity into point source

   V_t = transverse flow velocity

Taking into account a flow balance and the physical dimensions of a mini pleat arrangement as shown in the sketch,

n sections
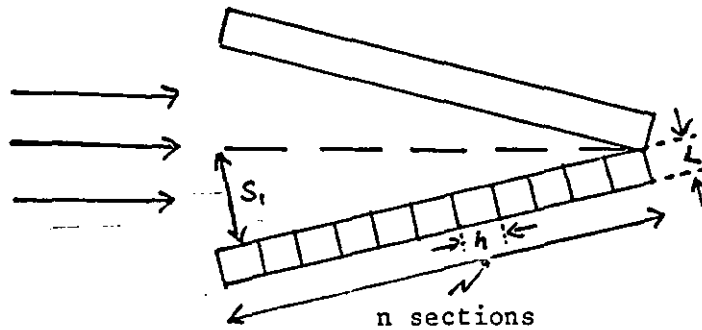
then,

$$V_x = 2LhU_o \left\{ \frac{n}{c.s_1} + \frac{x}{2\pi r^3} \right\} \qquad (2\text{-}107)$$

$$V_y = \frac{2LhU_o y}{2\pi r^3} \qquad (2\text{-}108)$$

where   C = the channel pitch

The trajectories in this field were computed using the techniques described in 2.4.2 above. Applying typical dimensions and operational conditions, deposition on the surface due to inertial classification is predicted. Some results, shown in terms of trajectory start and end points for different sizes, are shown in appendix 2.5.1. The trajectories shown in figure A2.5-1 illustrate the mechanism more graphically and confirm the mechanism of "beehive" formation.

Individual "beehives" were removed and analyzed by Coulter Counter. The results shown in appendix 4.2.2 clearly show this to be coarser than the dust collected within the channels. This gives further confirmation of the mechanism.

2.5.4. The channel expansion effect

It was observed that during use the upstream channel expanded. This was measured experimentally for a fully loaded filter as about 20%. The measurement procedure is given in appendix 4.2.2. However an exact value of the expansion is difficult to determine as it will vary with load and flowrate. Unfortunately the expansion when air is flowing through the filter cannot be quantified by the present experimental technique. Therefore, although it is expected that this will enhance the expansion effect, no real value can be given. It would be realistic to expect that this expansion is achieved gradually as the dust load, and consequently pressure drop, increases. However, the effect is most important as clogging approaches the point where the channel pressure drop becomes most significant. This is inversely proportional to the cube of the channel separation so a similar cubic relationship was assumed for channel expansion:

$$W = W_o + C_1 \sigma_H^3 \qquad \qquad (2\text{-}109)$$

where, W = the channel spacing of the media

σ_H = the dust layer thickness

W_o = W @ $\sigma_H = 0$

By accounting for the dust layer thickness and allowing W_e to be the final channel expansion as a fraction of the original channel separation, then the spacing for flow at any instant is:

$$W_s = W_o - 2\sigma_H + \frac{8W_e}{(1+W_e)^3} \frac{\sigma_H^3}{W_o} \qquad \qquad (2\text{-}110)$$

This expression is used in the final model to calculate the channel pressure drop. A further 50% increase in expansion was allowed over the experimental value in the general calculations. This was to allow for the extra expansion anticipated when air is flowing through the filter. When the effect of varying the channel expansion between 20 - 40% is examined (as illustrated in appendix 2.5.2) it is seen to have only a minor influence on the overall pressure drop-load response. Hence the figure used for the expansion is considered within acceptable limits.

2.5.5. The bulk density effect

The bulk density within a mini pleat arrangement could not be measured experimentally. An estimate, given in appendix 4.2.2, shows a figure of about 800 kg/m^3 but an error of upto 25% could exist in this value.

The bulk density will probably vary with load and also the high local velocities created within the channel causing the hole formation and inertial classification. The effect of variations of the bulk density, ρ_b, on the overall computed pressure drop is shown as most significant in appendix 2.5.2. It is reasonable that the bed compaction should increase with pressure drop during loading. This is easily illustrated by computation.

The model was adapted to allow variation of the bulk density linearly from an initial to a final value such that:

$$\rho_b = \rho_o + (\rho_f - \rho_o) \frac{2\sigma_H}{(\overline{1+W_e}) W} \qquad (2-111)$$

This is an entirely speculative equation but the term reflects the effect of pressure drop without introducing the need for a further interactive calculation for such a basic approximation. Results were calculated assuming values in the range below:

Face velocity (cm/s) U_o	Bulk Density (kg/m^3)	
	Initial (ρ_o)	Final (ρ_f)
1.25	700	900
2.5	700	1000
4.0	850	1000

These figures gave acceptable responses for the pressure drop-load characteristics suggesting that the basic approach is suitable. However, further understanding of the evaluation of the bulk density variation is desirable in future studies to remove this approximation.

2.5.6. Conclusions from the mini-pleat theory model incorporating the modifications

Appendix 2.5.2 shows the results of the complete programme containing the modifications. Figure 2.8 shows the much closer match between theory and experiment than previously obtained. The channel pressure drop is still extremely influential in the final analysis causing a slight but now acceptable under-prediction of the dust holding capacity of the filter. This could be reduced by increasing the bulk density effect but this was felt unacceptable without experimental evidence. Other empirical approximations, particularly that of the holes formed in the channel and the expansion effect, also justify further investigation. Furthermore it is suspected a swirling effect exists within the channels such that dust is deposited due to centrifugal motion as well as filtration. However absolute confirmation of this has not yet been achieved.

FIGURE 2·8 : Comparing theory and experiment for a mini pleat filter with BS2831 No.2 dust
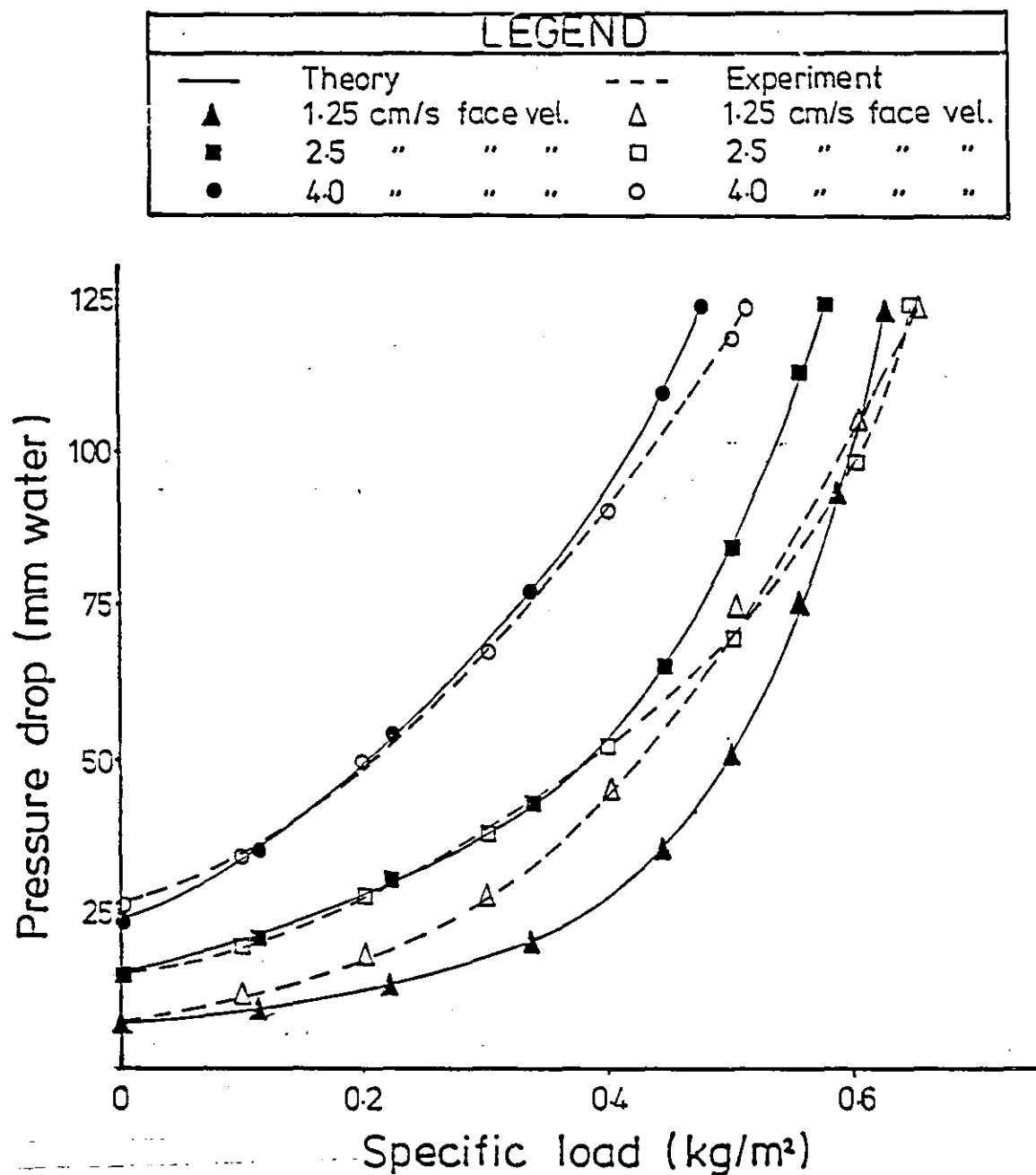
Consideration of the above effects may lead to further improvement in the theoretical prediction. This is discussed in chapter 5.

3. Experimental testing of fibrous filter media

The objective was to measure the aerosol penetration and pressure drop characteristics of both clean filter media and media loaded with dust. The experimental apparatus, procedure, test programme and results are described in this chapter.

3.1. Apparatus and experimental procedure

The rig was designed and constructed as shown in Figure 3.1. It was necessary for the design to comply with following requirements:

(i)   In order to measure filter efficiency a fine aerosol capable of penetrating the media is necessary.

(ii) To determine pressure drop a fine, but concentrated, dust dispersion is needed to load the media.

Figures 3.2. - 3.4. detail the design of the dispersion section, filtration section and radioactive source container. The source (Krypton 85 β) was used to eliminate any electrostatics which may be present. A photograph of the completed rig is shown as figure 3.5. The design meets both the specified requirements. The appropriate operation of the rig for measurement of filter efficiency or pressure drop characteristics is described below.

3.1.1. Efficiency testing of fibrous media

To measure penetration through the media a suitable aerosol has to be generated. The design, as shown by figure 3.1, allows for a polydisperse salt aerosol to be generated using a Collision generator, as specified by BS 3928, operating on 4.4 bar compressed air. Alternatively a monosized aerosol of latex particles can be produced using a Wright nebuliser operating on 2 bar compressed air. In each

FIGURE 3·1: Design of rig for testing fibrous media samples for efficiency and pressure drop characteristics
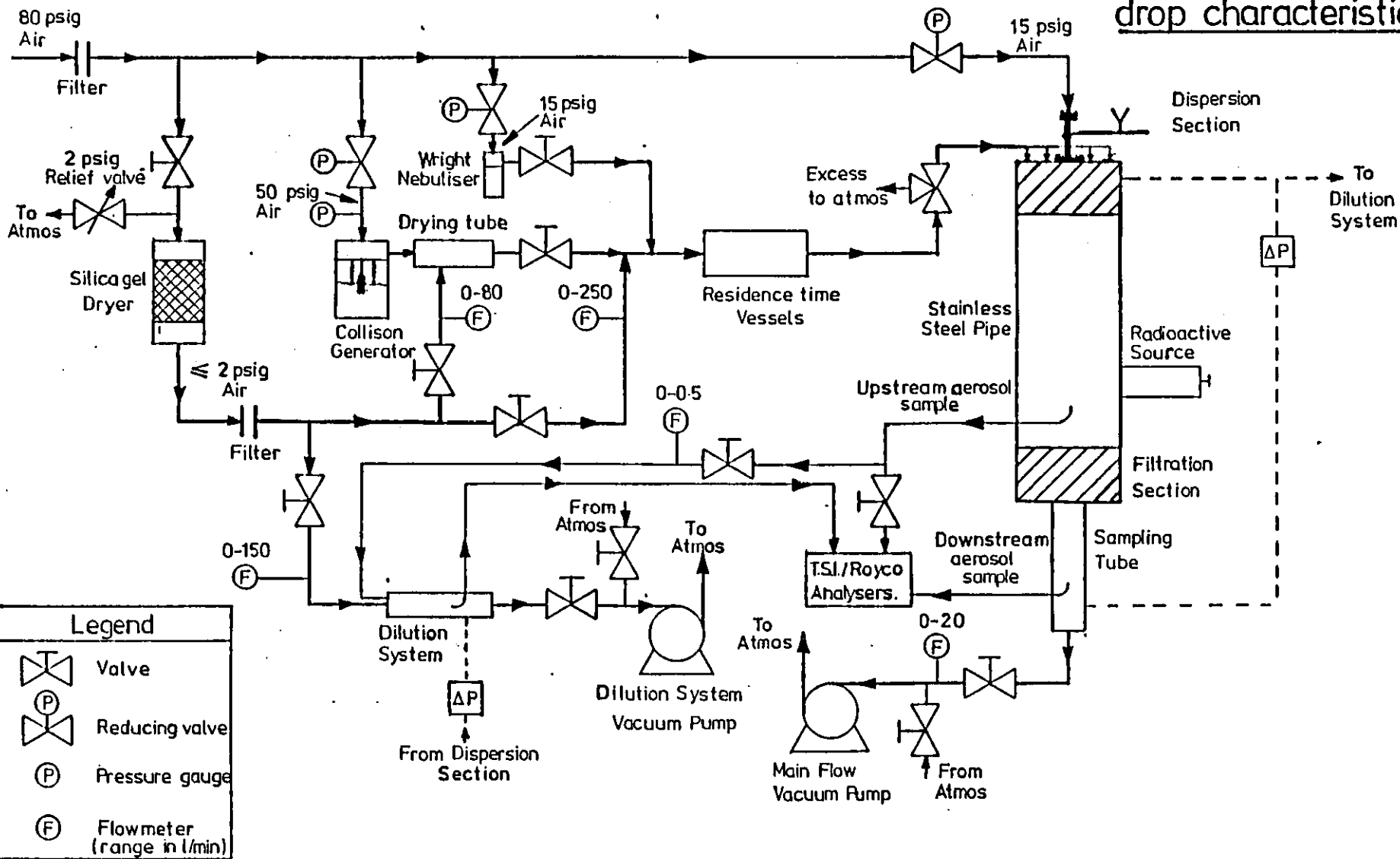
FIGURE 3·2

DISPERSION SECTION

Vibrating spatula

Compressed air
@ 10 psig for
dust dispenser

Dust dispenser

Clean air from aerosol
generation section

4" dia.

Stainless steel pipe
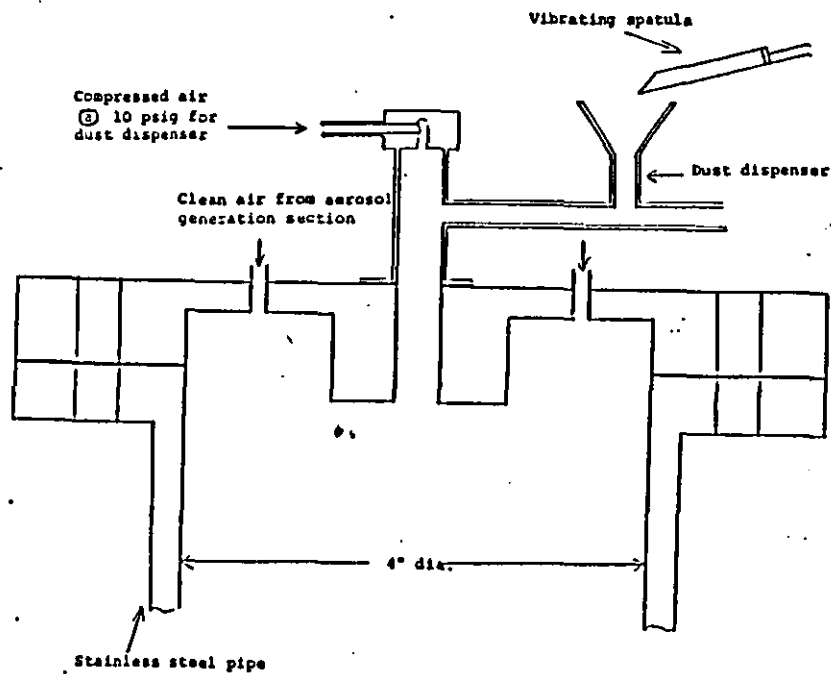
NOTE:

1. Original design contained a plate of 1/8" thickness with a 2" hole in the
centre to be fitted between top piece and stainless steel pipe flange.
This would have given a 1/4" annular gap around the dust dispenser
entry to the pipe with objective of improving mixing. It was, however,
found unnecessary.

2. Clean air (or aerosol) is fed through four inlet tubes into the top piece.
Only two are shown above.

FIGURE 3·3

FILTRATION SECTION

Main air flow

Stainless steel
pipe

Seal for sampling
probe

Constrictor

Sampling probe

Filter paper

'O' ring to
give good seal

Filter support

Baffle

Filter holder

Sampling Probe

Sealant

Pressure tapping

FIGURE 3·4 .

3/8" mild steel back plate

1/8" hinged steel flap which
falls when source is pulled back

Stainless steel
pipe wall

Smooth brass
holder for
tight fit

Ni/Cr container
of source

Radioactive
source
(Krypton 85)

134

Stop to
locate source
flush to pipe
wall

Surround box 3/8" mild steel
(Box also surrounded by lead
sheet totalling 5/8" thickness)

Guider - extends to wall
where grooves are cut for
the guider to run in so
keeping the source central
at all times

case a fine spray is produced and the superflurous water evaporated in the air stream. Conditions were maintained such that following complete evaporation, the relative humidity of the suspending air did not exceed 50%. Two residence time vessels, arranged in series to avoid bypassing, are included to provide a time for water evaporation which is well in excess of that specified by BS 3928. These vessels also have a flow stablising effect and hence the aerosol which is drawn off can be expected to be consistent.

The concentration of aerosol may be varied by the addition of dilution air before the residence time vessels. With the Collision generator this air is also used for the primary drying tube. The air is dried and filtered before contacting the aerosol in order not to contaminate, or effect the drying time, of the aerosol.

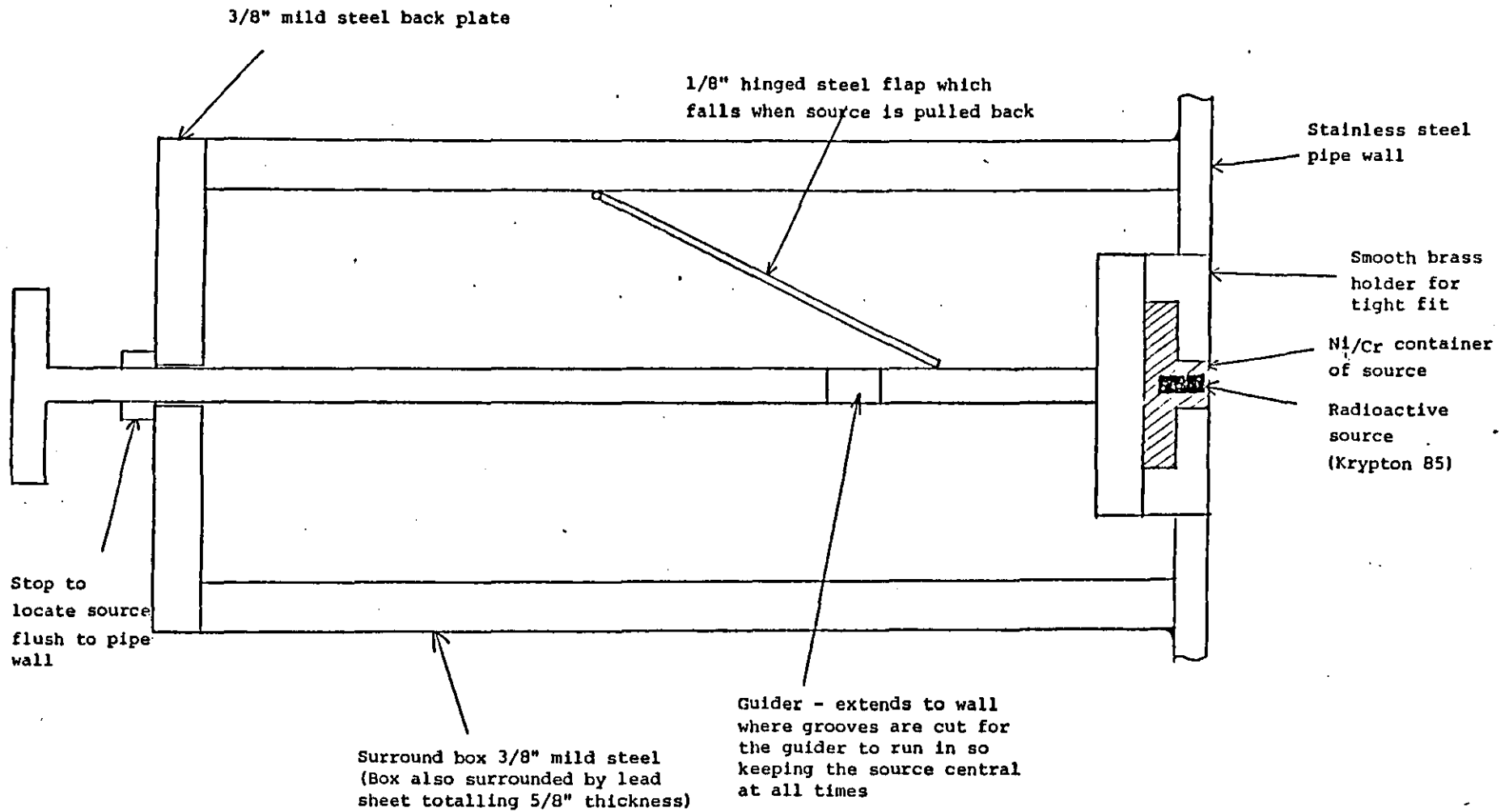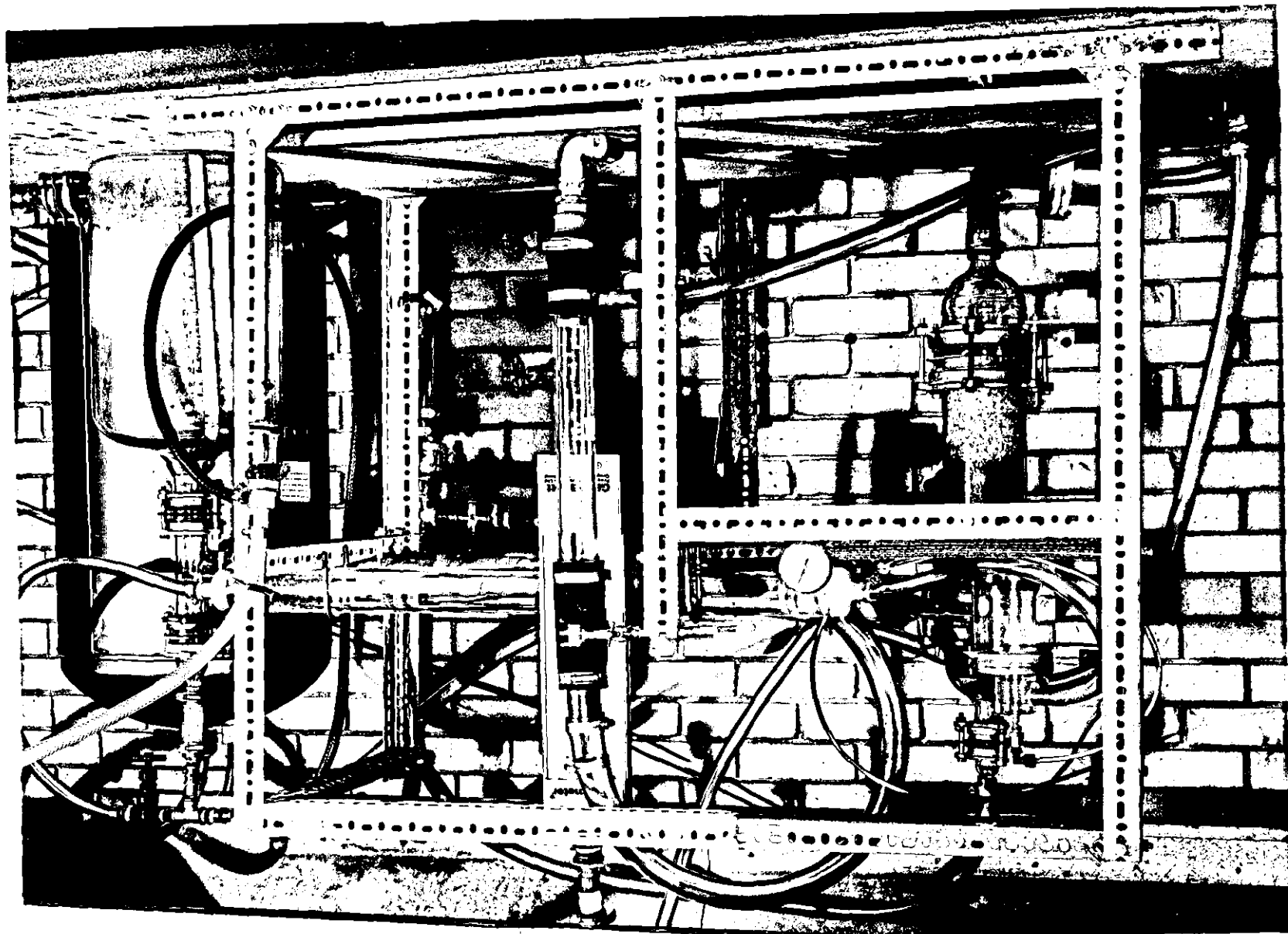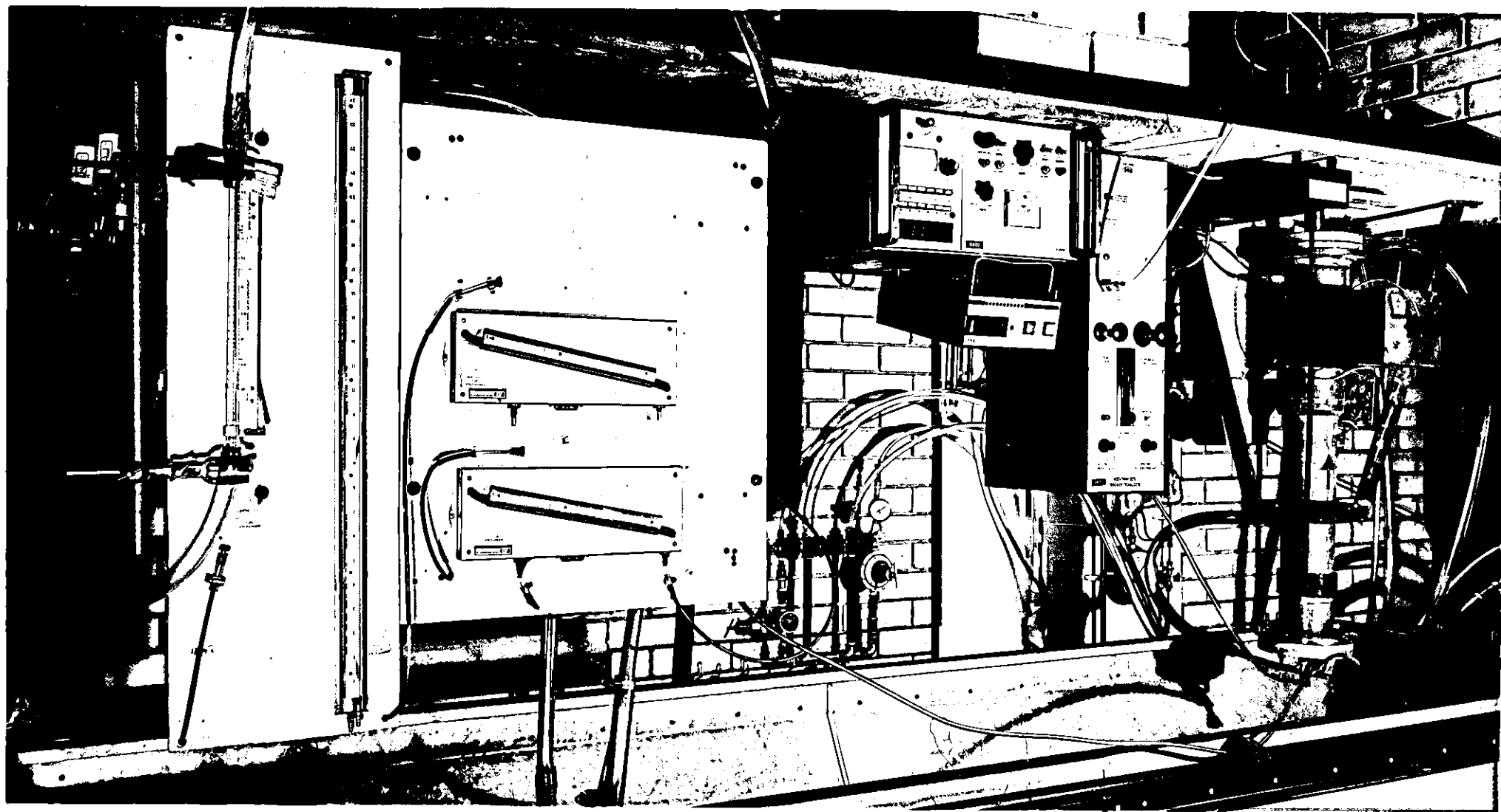The amount of aerosol required for filtration is drawn by vacuum pump into the stainless steel pipe. The excess passes to atmosphere via a three way valve and exhaust hood which covers all the apparatus. The aerosol enters the 1200 mm internal diameter stainless steel pipe via a manifold designed to give an even air distribution, figure 3.2. The pipe was drawn for smooth walls and is about one meter long to ensure good radial mixing of particulates before the filter. The particulates in the air stream are exposed to an earthed Krypton 85 β source of ionising radiation immediately upstream of the filter, figure 3.4. This should effectively neutralise the aerosol.

Sharp smooth sampling probes are located centrally upstream and downstream of the test filter. Samples of aerosol can be taken directly to either a Royco 225/512 size analyser or a TSl 3030 electrostatic mobility analyser. Alternatively the sample may pass through the dilution system which enables high concentrations of aerosol to be measured. Dilutions of upto 500:1 are possible and tests showed losses within the system were negligible for particles less than 3 μm . This is greater than the largest particle size produced by either generator. The Royco 225/512 sizes and counts particles greater than 0.3 μm while the TSl 3030 is used to measure the concentration of particles in size ranges between 0.01 μm and 1.0 μm. The operation of this equipment is described in section 1.1.4.

The Royco was fitted with a new photomultiplier tube. A calibration was then carried out using monosized Dow latex spheres. This tube gave a very low background voltage enabling the calibration to go down to spheres of 0.235 μm diameter. The output voltage of the Royco was measured for each separate size of particle tested and recorded on a storage oscilloscope. The resultant calibration curve is shown as figure 3.6. This curve illustrates the expected inflexion for particles sized between 0.55 μm and 1.1 μm diameter. This restricts the size ranges available for analysis.

After removal of a sample the remaining aerosol in the stainless steel pipe is drawn into the filtration section. Here it passes through a circular disc of filter media of which an area of 36.3 cm^2 is exposed to the flow. The disc is fixed to a Millipore support plate and clamped and sealed into place as shown by figure 3.3. A mixing baffle is positioned downstream of the filter. This allows a representative sample of the filtered aerosol to be taken for analysis. Penetration as a function of particle size is determined by comparing before and after filtration samples.

The remaining gas flow passes through a rotameter enabling the face velocity to be determined by back calculation. The aerosol is dispersed into the atmosphere via the vacuum pump and exhaust hood.

3.1.2. Determining pressure drop characteristics of loaded media

A scaled down version of the BS 1701 dust dispersion unit was fitted into the top of the stainless steel pipe (Figure 3.2). Any excess air requirements, needed to produce the correct filter face velocity, could be provided by drawing air into the pipe via the manifold. Similarly the manifold acts as an escape for excess dusty air when operating under low flowrate conditions such that the air volume required to generate the dust dispersion is greater than that used in the filtering. This excess dusty air passes to the exhaust hood via the three way valve. The main flow is filtered after exposure to the ionising radiation to remove electrostatic effects. Tests showed a good dispersion on the filter indicating sufficient radial mixing in the pipe length available.

FIGURE 3·6: Calibration curve for Royco analyser 225

Output Pulse (Volts)

Particle Size (μm)

Photomultiplier tube
Noise level
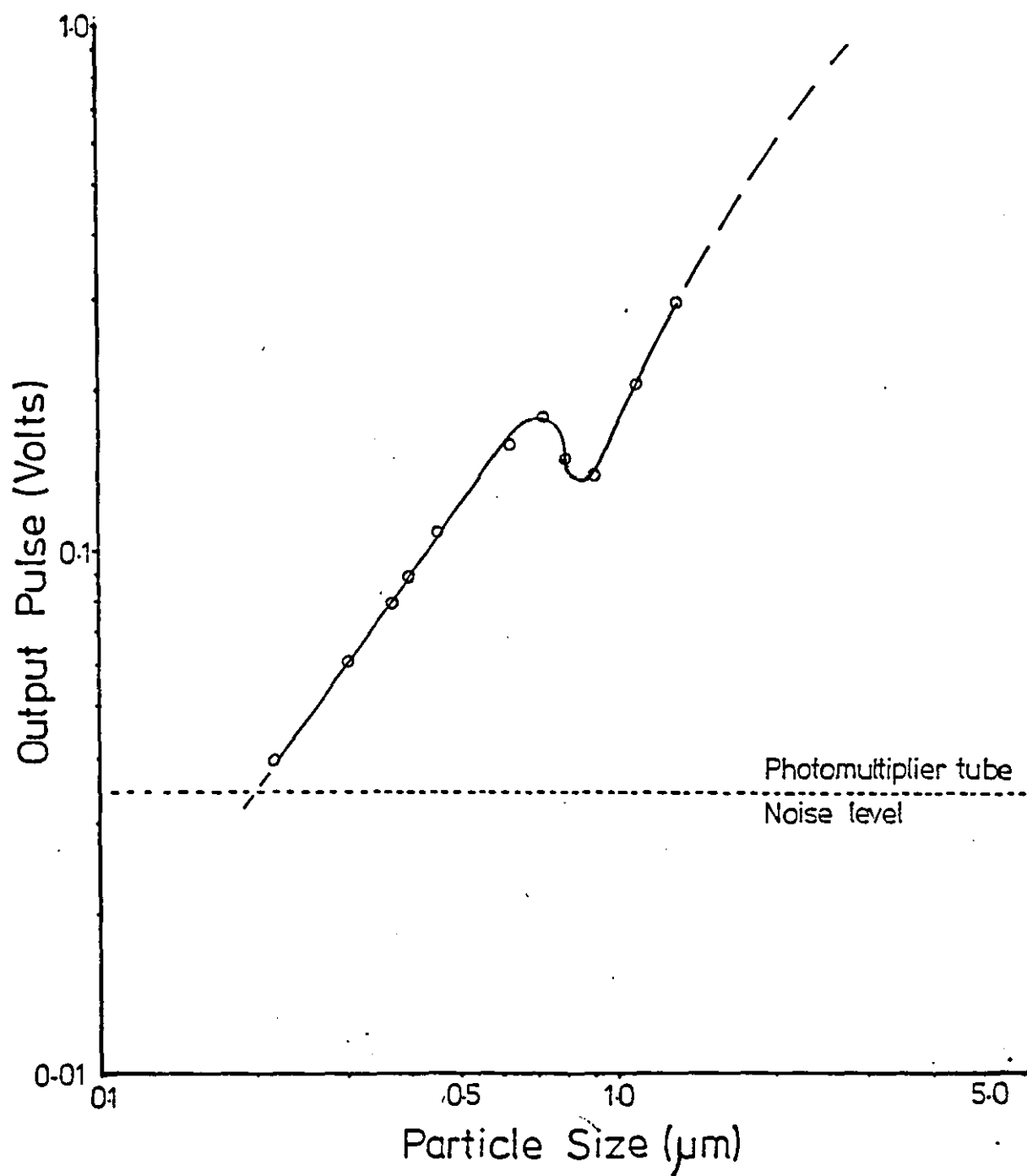
Small amounts of a dust were incrementally loaded onto the filter at a chosen face velocity. After each load the filter was removed, weighed and, with the filter back in position, the pressure drop measured for the velocity under examination.

It is possible to monitor efficiency changes with increasing load. The design further permits the loading of salt aerosol onto the media by using the Collision generator for long periods. It should therefore be possible to monitor efficiency and pressure drop with increasing load of a fine aerosol.

3.2. Efficiency testing of clean media

Tests were carried out on a range of media, obtained from Evans Adlard company, using the technique described in 3.1.1. Analyses characterising these samples are given in appendix 3.2.1. Early work showed measurement of very highly efficient media samples was inaccurate due to the low downstream concentrations obtained. These were such that even with very high concentrations of salt before the filter there was insufficient penetration to operate the TSI 3030 analyser and downstream results obtained from the Royco 225/512 were unsatisfactory in terms of statistical error.

Coarser samples of media were obtained with the objective of examining experimentally the general penetration behaviour of fibrous filter media. Results from this were used to verify the model described in section 2.1. Some sampling tests were made to examine the performance of the sampling system under different conditions. This is reported in appendix 3.2.2.

Scanning electron microscope photographs of a media sample are shown in figure 3.7. The characteristics of this media are summarised in table 3.1.

The size penetration curve for each media sample is given in figure 3.13. Media F38Z is omitted as particle counts were too low to be statistically acceptable. Downstream analysis was only possible with the TSI 3030 for the coarsest media. In this case a maximum

TABLE 3.1: Characteristics of Evans Adlard filter media from typical test data

MEDIA PROPERTY	UNITS	F38Z	F41Z	F43Z	F44Z	F45Y	F47W
Min. Efficiency by Sodium Flame	%	99.999	99.9	98.5	96.0	94.0	75.0
Sodium chloride aerosol penetration at 1.5 m/min. (2.5 cm/s)	%	0.0002	0.025	0.45	1.5	3.0	15
DOP aerosol penetration at 3.2 m/min/ (5.3 cm/s)	%	0.0015	0.11	1.5	4.3	8.0	31
Pressure drop at 1.5 m/min	N/m^2	210	127	77	58	47	27.5
Pressure drop at 3.2 m/min	N/m^2	448	271	164	124	100	59
Grammage	g/m^2	95	95	95	95	95	95
Thickness	mm	0.70	0.64	0.65	0.66	0.69	0.74
Mean fibre size at 50% cumulative number	μm	1.18	1.24	1.34	1.60	2.13	2.45
Specific area of paper	m^2/kg	10.5	10.5	10.5	10.5	10.5	10.5
Tensile MD (ambient)	KN/m	0.8	0.8	0.75	0.7	0.65	0.5
Tensile MD (550°C)	KN/m	0.45	0.45	0.45	0.45	0.4	0.35
Ignition loss (550°C)	%	4.5	4.2	4.1	4.2	4.1	4.1
Binder Type	—	Acrylic	Acrylic	Acrylic	Acrylic	Acrylic	Acrylic

FIGURE 3·7: Evans Adlard F38Z filter media

550 X
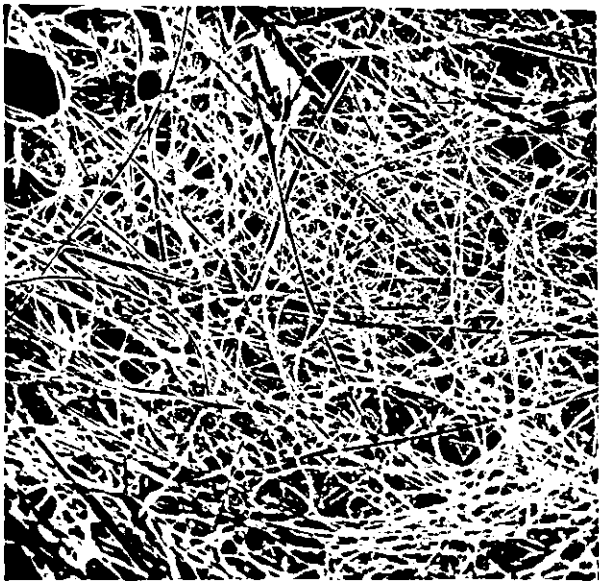
1100 X

2200 X
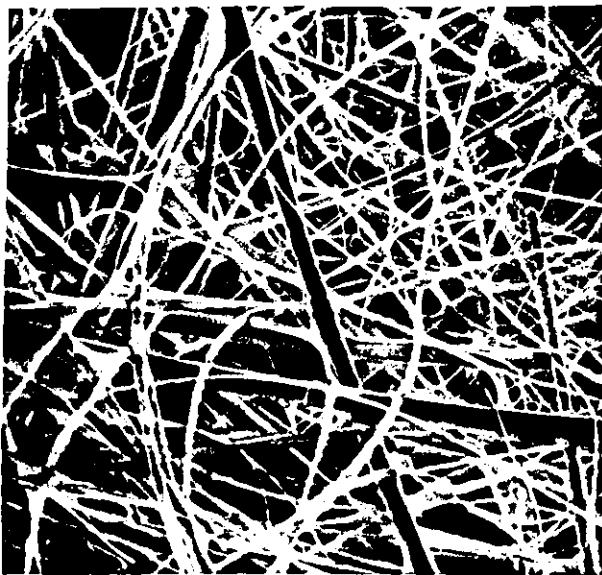
FIGURE 313: PENETRATION WITH PARTICLE SIZE

Various filter media

% PENETRATION

PARTICLE SIZE (µM)

F 47 W
F 45 Y
F 44 Z
F 43 Z
F 41 Z

• Royco results
• TSI 3030 results

143

Particle size ranges considered
- o 0.3 – 0.4 μm
- · 0.4 – 0.5 μm
- ▲ 0.5 – 1.2 μm
- □ 1.2 – 2.4 μm
- × Overall > 0.3 μm
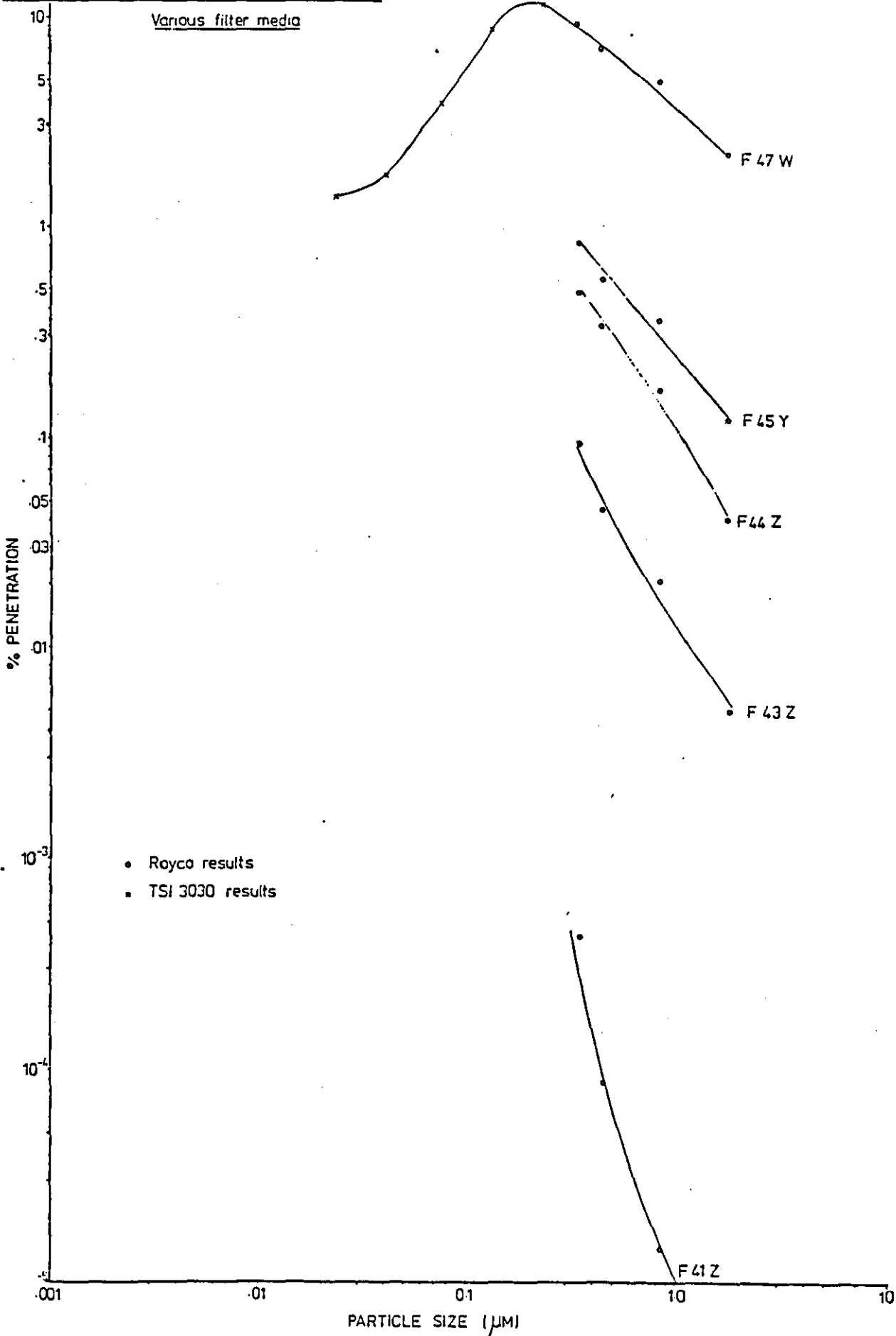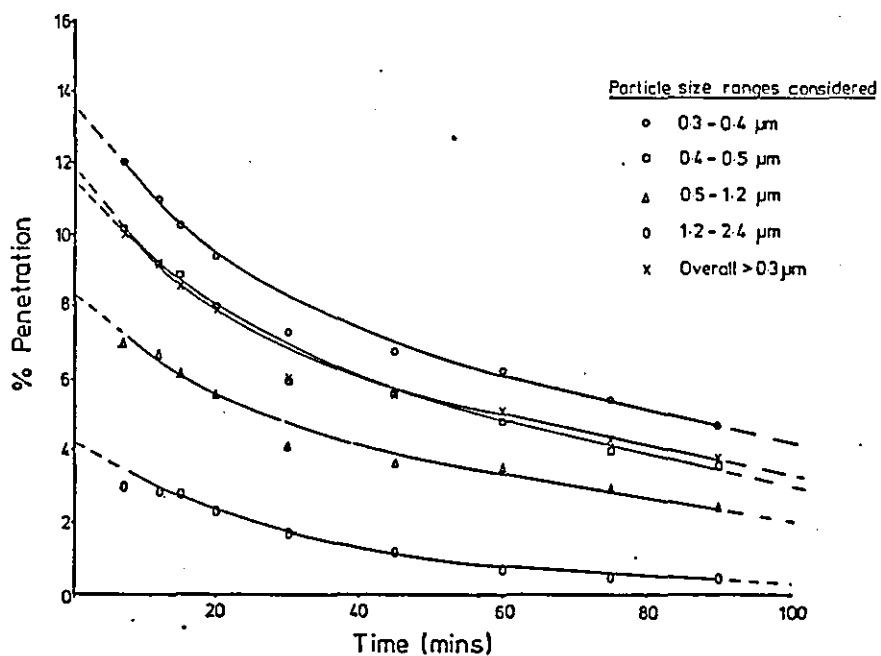
FIGURE 3.15: Penetration curves with loading for F47W filter – Run 2

Symbols as for run 1
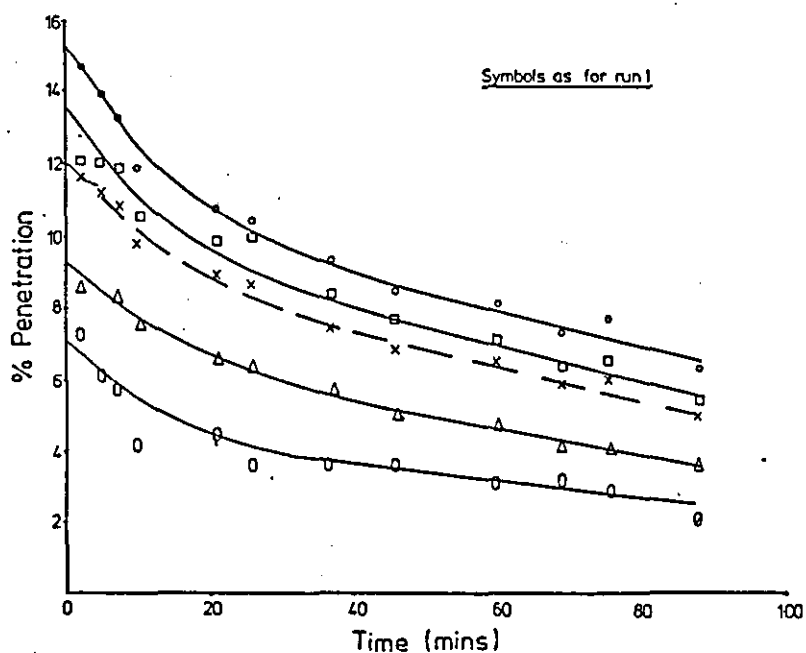
FIGURE 3.16: Penetration curves with loading for F47W filter – Run 3

Symbols as for run 1

Time (mins)
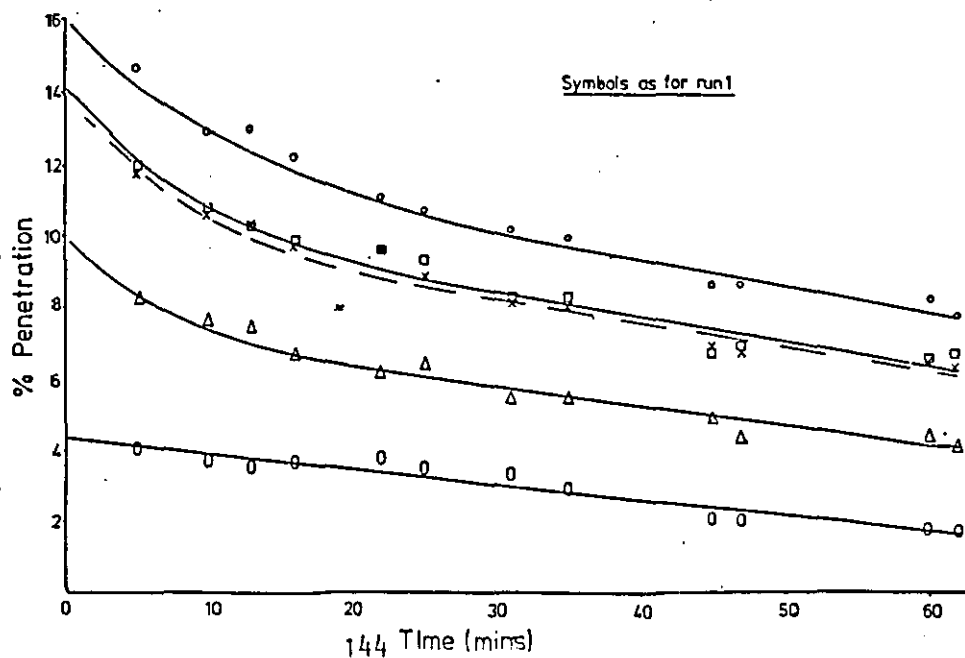
penetration with 0.2 μm particles is clearly demonstrated. The other media shows the expected trend in fall off of penetration with particle size.

3.3. Efficiency variation with aerosol load

Using the coarsest sample of media only and monitoring with the Royco analyser, penetration was measured with increasing load. Figures 3.14 - 3.16 show the results in terms of percentage penetration as a function of time. However, the aerosol concentration can be assumed constant - the maximum fluctuation about the mean was six percent. Therefore the specific load can be taken as directly proportional to time. Thus figures 3.14 - 3.16 can be interpreted as the effect on penetration with increasing specific load.

It is clear that the penetration falls off in an exponential manner with increasing load. It is also obvious that the penetration falls with increasing particle size over 0.3. μm diameter. This simply confirms it is the clean efficiency that is important in HEPA filter specification and that an aerosol with a high concentration of particles between 0.1 and 0.5 μm diameter is essential for testing purposes. The results also show that, because of the rapid initial reduction of penetration with load, care must be taken to measure filter penetration immediately the filter is challenged by the aerosol.

3.4. Pressure drop characteristics of the filter media with different loading and face velocity conditions

It is important to assess the influence of both velocity and dust size on the pressure drop - load characteristics of HEPA media. A range of dust fractions were used. Precut fine fractions of BS 2831 No. 2. dust and a dust sized at 1200 grid were supplied by AERE (Harwell). X-ray analysis confirmed these to be aluminium oxide. The size distribution of these dusts by cumulative weight percent, using Coulter analysis, is given in figure 3.17 showing mass mean particle diameters to be about 4.8 μm for the BS 2831 No.2. dust and 4.1 μm for the 1200 grid size dust. These size distributions have been

FIG 3.17 : Cumulative weight size distributions for dust samples used in loading tests

146
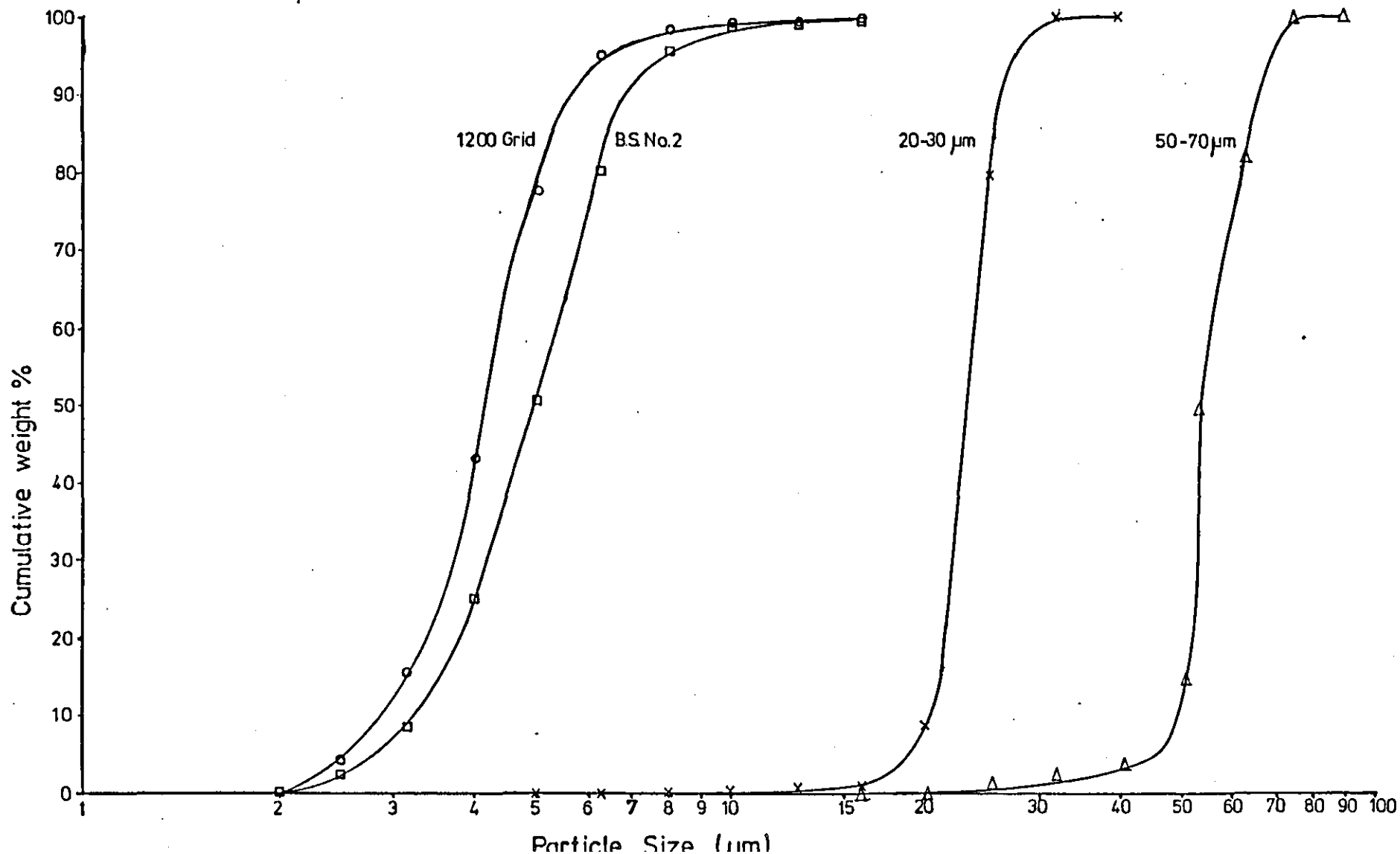
verified by both Andreasen pipette sedimentation and the Micrometrics sedigraph 5000 ET. These size analyses are in appendix 3.5.1 which includes the size distribution analyses of all the dusts used throughout this work.

Coarser fractions of alumina dust were obtained by air classification using an Alpine zig-zag classifier. However, due to excessive wear on the rotor blade of the Alpine, fractions could not be produced for sizes less than 20 μm diameter. The size analyses of the fractions of this dust used for the experimental tests are also shown in figure 3.17.

Before continuing with the major programme, samples of clean HEPA filter examined were examined for their pressure drop-velocity response. The average of these results is shown in figure 3.18 with error bands indicated. The response can be seen to be virtually linear over the range of   0 - 10 cm/s face velocity. Some preliminary test work was also made using BS 2831 No.2. dust to establish an experimental procedure. This is described below.

3.4.1. Initial tests with B.S. 2831 No.2. dust

The effect of dust load increment size on the pressure - drop load response was examined. Pressure drop was monitored as loading progressed at a fixed face velocity. For each run different load increments were used. The response was identical whatever the load increment. An example is given in Figure 3.19.

The electrostatic effect was considered. Test runs were carried out with an earthed radioactive source exposed to the dust stream in order to neutralise any electrostatic charge on the particles. Runs were made with and without the source and the results compared. Under the experimental conditions of this work no effect on pressure drop with load was observed (Figure 3.20).

Tests were made using dust which had been heated, to eliminate any possible moisture content. This was compared with normal ambient temperature dust loading results. Again no difference was observed in the result (Figure 3.21).

FIG.3.18 : Pressure drop variation with face velocity
for a clean filter

Pressure drop (mm water)

Face velocity (cm/s)
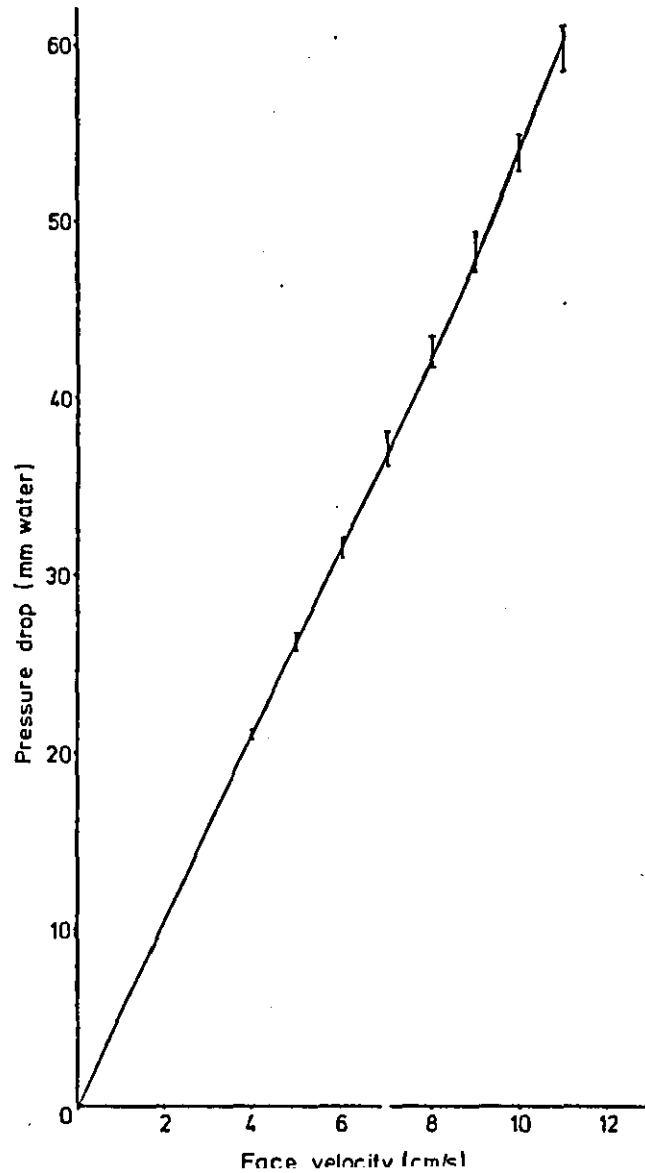
FIG. 3.19 : Effect of using different load increments
on presure drop-load relationship

Velocity 5.1 cm/s

o Small incments

□ Large increments

Pressure drop (mm water)

Specific load (kg/m²)
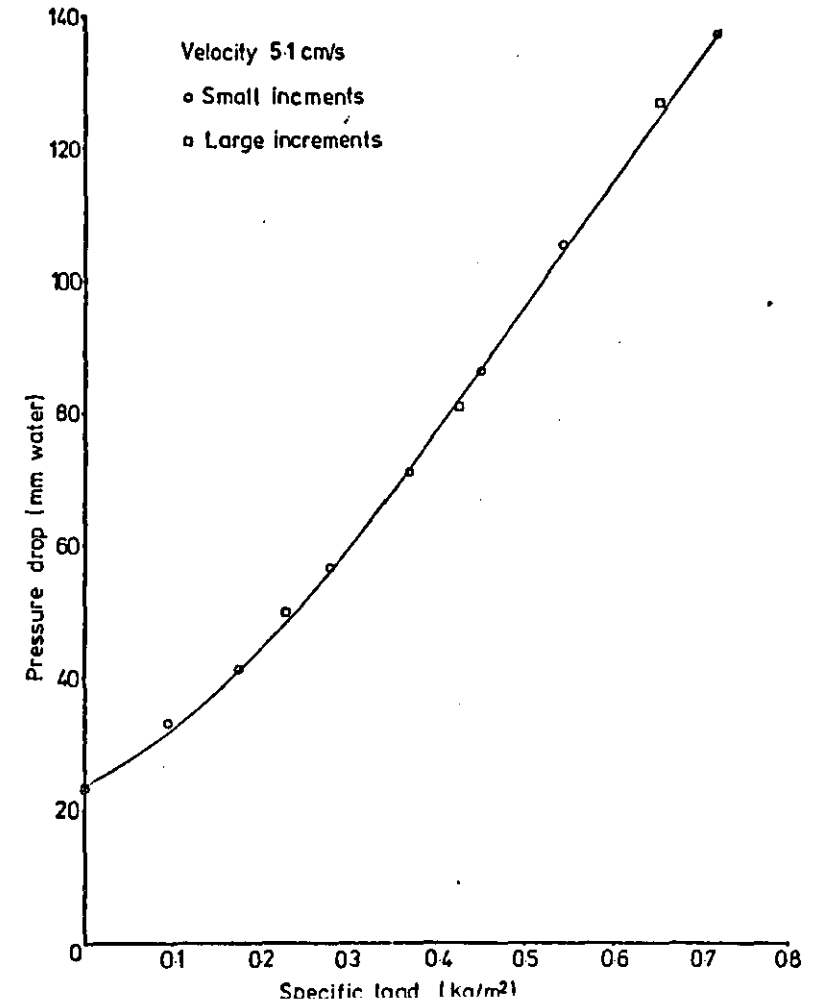
FIG. 3.20 : Comparison of load tests made with and without the dissapation of electrostatic charges

Face velocity when loading of 3.25 cm/s

o Normal dispersion
o Dispersion in the presence of electrostatic eliminator
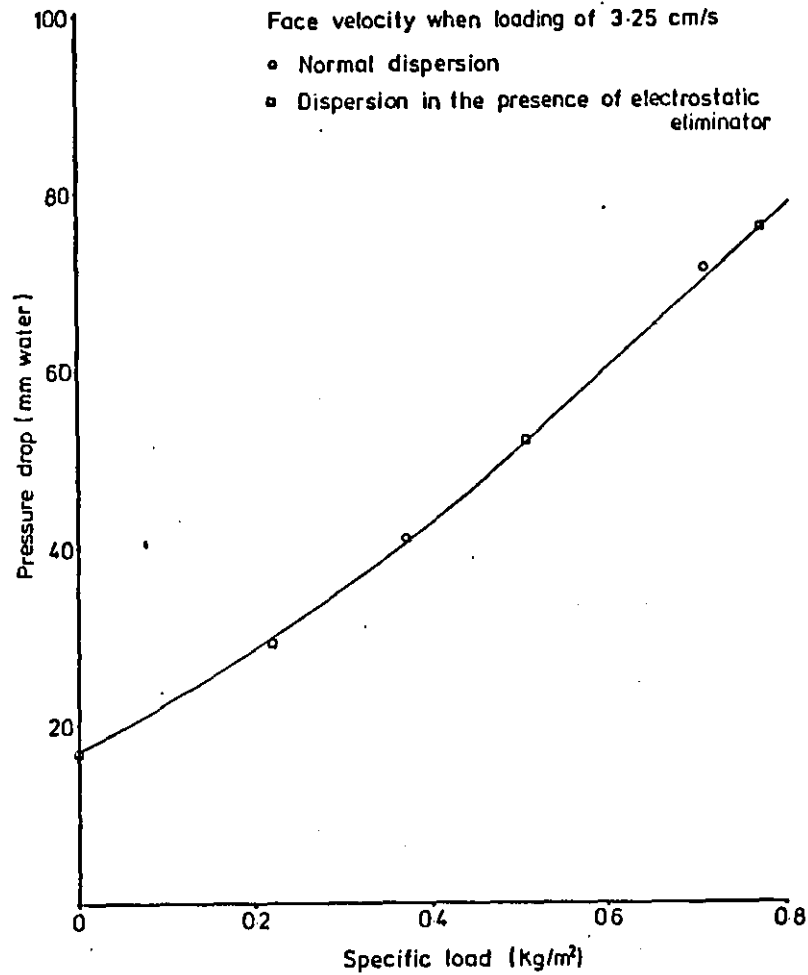
FIG. 3.21 : Comparison of loading with hot and cold dust

Face velocity of 5.1 cm/s
2nd Batch of B.S. No. 2 dust

o Hot dust
o Cold dust
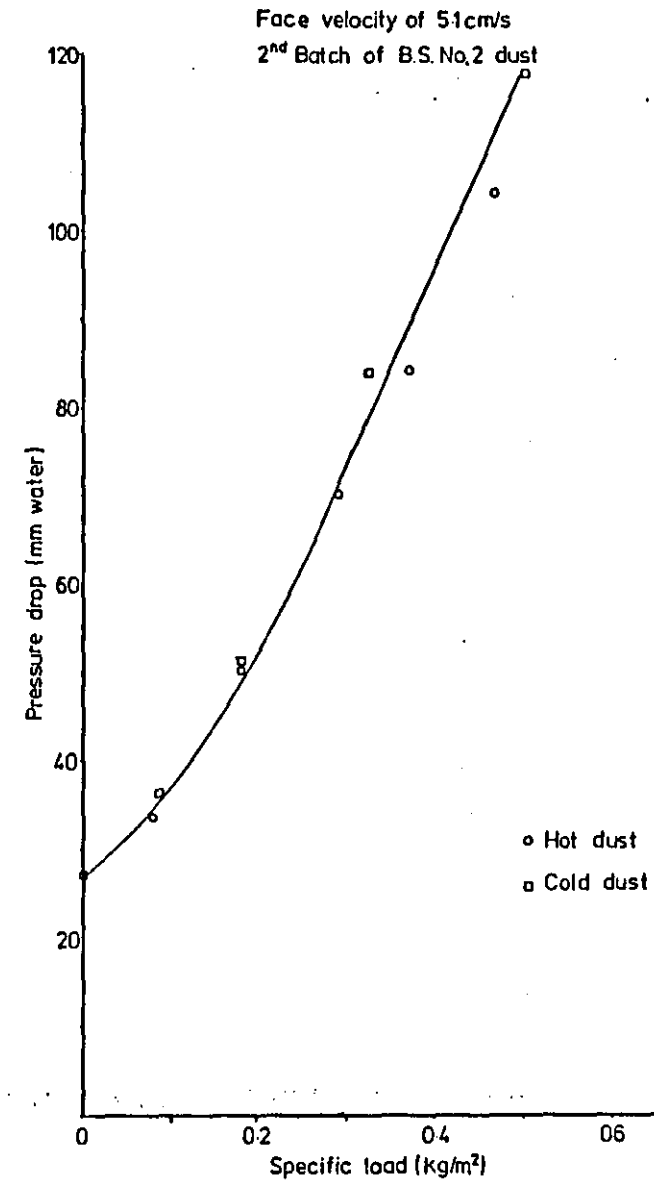
FIG. 3·22 : The effective increase in pressure drop after a velocity surge (hysterisis effect)

Dust originally loaded at 2cm/s

% Increase in pressure drop (permanent)

% Increase in velocity
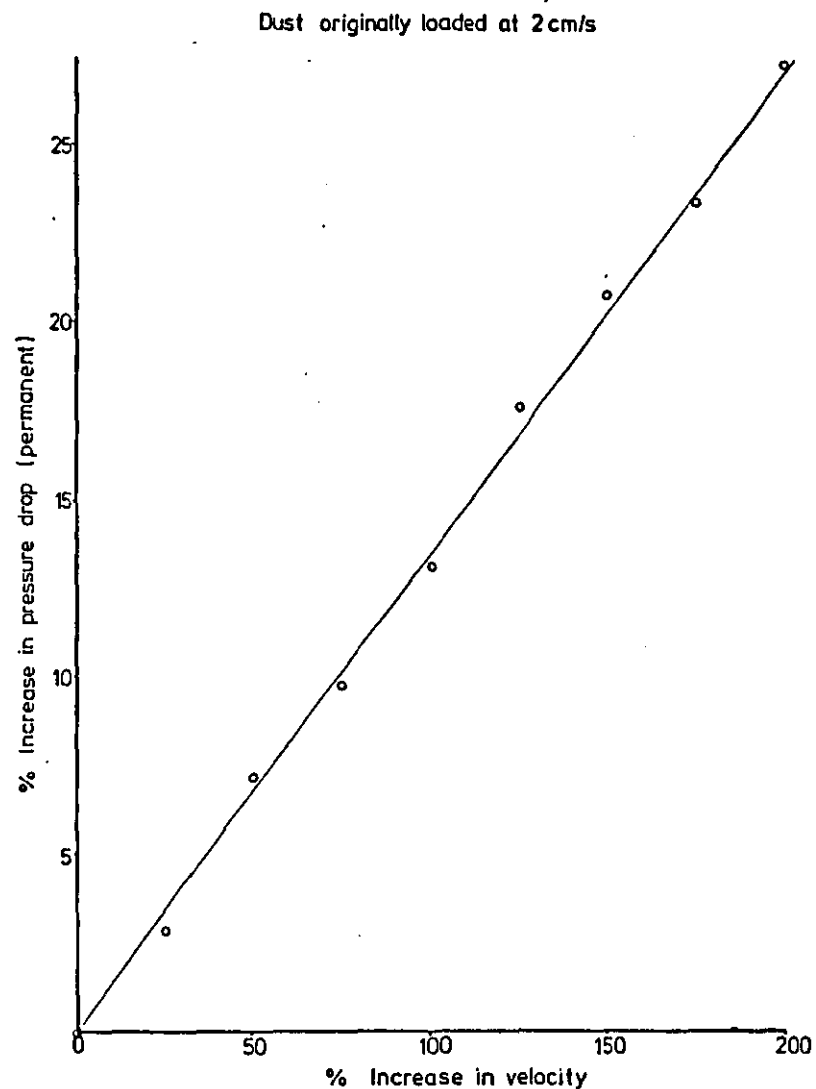
FIG. 3·23 : Load vs. pressure drop with intermittent rapping

Face velocity 5·1 cm/s

Prolonged rap

Short rap

Pressure drop (mm water)

Specific load (Kg/m²)
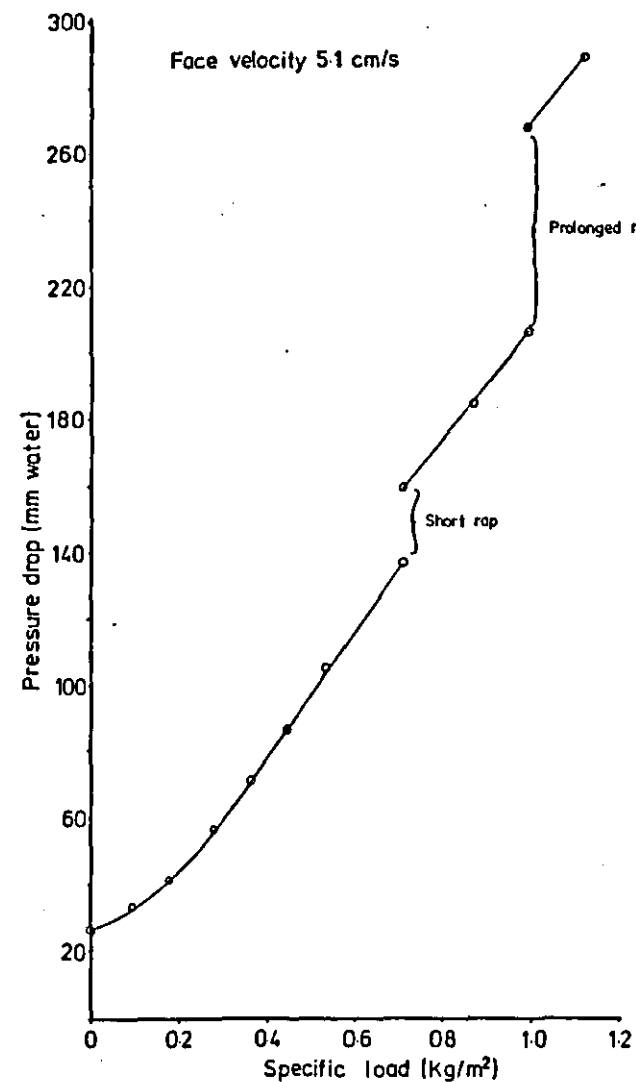
A hysterysis effect was observed as the velocity was increased and decreased. Dust was loaded at a relatively low velocity and the pressure drop measured. The face velocity was then temporarily increased to a higher value before returning to the original operating velocity and remeasuring the pressure drop. This second pressure drop showed a permanent increase over the original figure, the extent of this increase being dependent on the percentage surge of velocity as compared to the operating velocity. The results are in Figure 3.22. This demonstrated the need for good flow control within the rig.

The effect of rapping was examined. The filter holder was gently tapped, after loading, so vibrating the filter. A permanent increase in pressure drop was observed. The magnitude depended on how hard or how many times the filter holder was knocked and a two to three hundred percentage increase in pressure drop was easily obtained. An example of this test is shown in Figure 3.23. It stresses the need for careful handling of the filter and the need to avoid vibration of the apparatus.

From the results of these tests the following experimental procedure was developed:

1. Fix filter media sample to the filter support by means of silicon rubber adhesion to prevent its movement during testing.
2. Weigh filter and support.
3. Place filter and support in filter holder and secure to stainless steel pipe base.
4. Set face velocity and measure clean pressure drop.
5. Place radioactive source in the exposed position.
6. Load required quantity of dust.
7. Pull back radioactive source to safe position.
8. Remove and weigh filter and support.
9. Replace filter and support, resecure holder check face velocity reading and measure pressure drop of loaded filter.
10. Repeat from 5 until maximum load or pressure drop is reached.

3.4.2 Pressure drop with load experiments

Tests were conducted for pressure drop variation with specific load for the four dusts chosen. Standard HEPA filter media was used throughout. Several runs were carried out for each dust at each velocity to verify reproducibility. Face velocity was varied between 2 and 10 cm/s taking 3 to 5 velocities in this range for each dust.

The results for B.S 2831 No.2. dust are shown graphically in figure 3.2.4. Best fit equations, for all the data, were determined by a computer curve fitting routine. Results from the experimental data, and fitted by this routine, are given in appendix 3.4.1. The equations for each dust giving the result in terms pressure drop for any velocity and specific load within the stated range, are given in table 3.2.

These results show a strong dependance on dust size and face velocity. The latter of these was accounted for in the curve fitting but the results from this are only applicable to each dust independently. The relationship produced by the pressure drop response to increasing load clearly splits into two regimes. The initial portion, or primary regime shows the pressure drop to be exponentially increasing followed by a secondary regime where the relationship is one of proportionality. The extent of the primary regime depends on dust size such that it is less significant with increasing size.

The secondary portion of the curve (or total response in the case of larger dusts) is in line with the theoretical predictions of 2.1. However, the initial exponential responses of the smaller sized dusts requires further study. As the dust particles are greater than the pore sizes of the filter then penetration into the media would not appear a valid explanation. Observation through a microscope of the cross-section of a loaded filter, cut by a razor blade, equally demonstrates this and verifies the model of section 2.1. This observation also showed that the filter media was of varying thickness. Furthermore electron microscope photographs of the media had shown large variations in fibre sizes and pore sizes.

FIG. 3·24 : Relationship between specific load and pressure drop – face velocity ratio for different velocities

Best fit curves given from original data
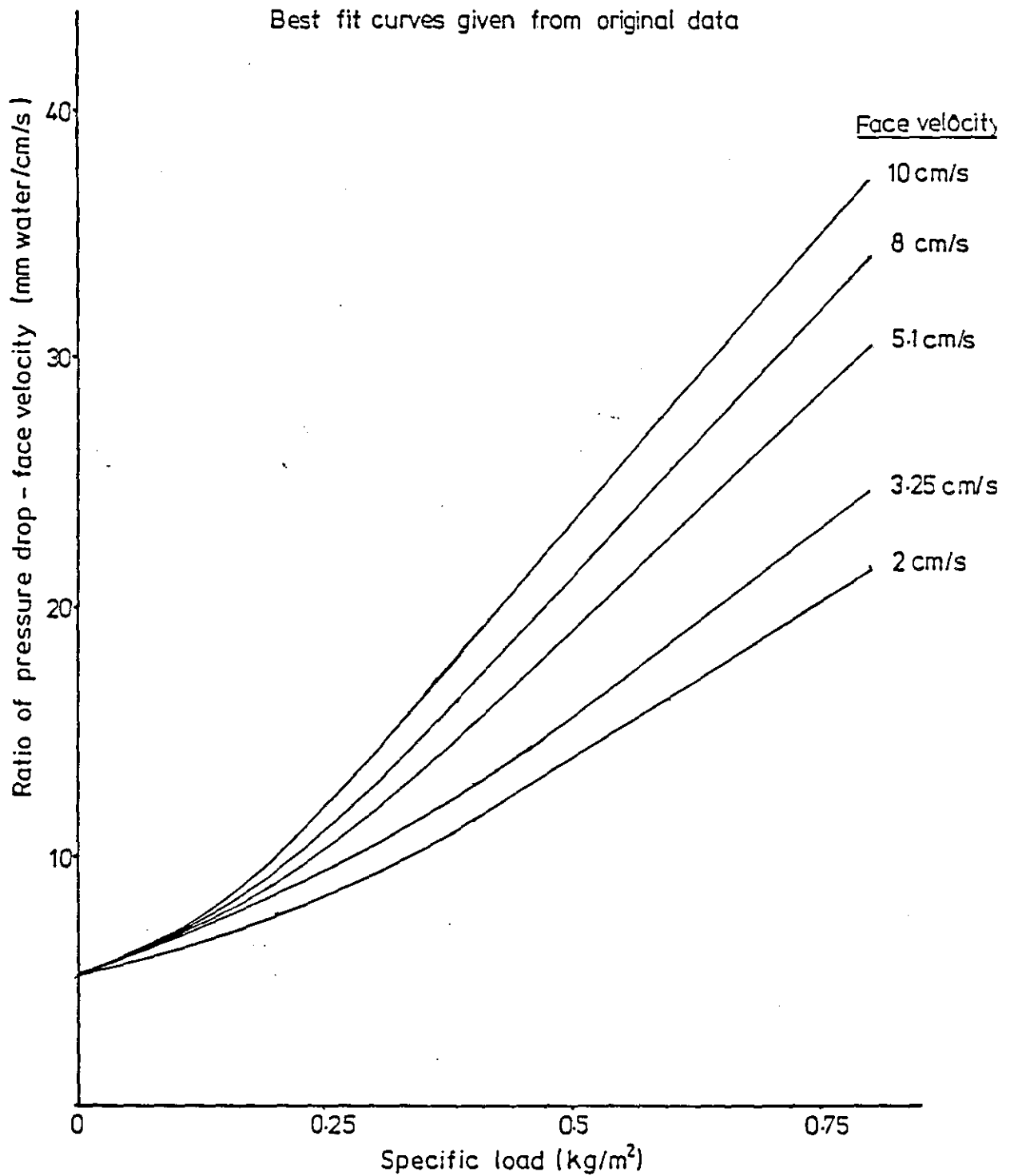
TABLE 3·2 Relationships evaluated between pressure drop, load and face velocity for the various test dusts.

Test Dust	Cut Point PD/V (mm water/cm/s)		Evaluated Relationship
1200 Grid	<	13.7	$PD = V \times (4.959 + .056\ V)$ $\times EXP\ [L \times (2.089 + .704\ V - .049\ V^2)]$
	> =	13.7	$PD = V \times [\ (4.484 - 1.236\ V)$ $+ L \times (7.093 + 16.376V - .929\ V^2)\ ]$
B.S.No.2	<	13.4	$PD = V \times (5.154 + .0274\ V)$ $\times EXP\ [L \times (1.390 + .308\ V - .015\ V^2)]$
	> =	13.4	$PD = V \times [(0.012 + L\ (17.758 + 4.810\ V$ $- .199\ V^2)]$
20 – 30 μm	<	5.9	$PD = V \times (5.050 + 0.25\ V)$ $\times EXP\ [L \times (.465 + .062\ V - 8.096\ V^2)]$
	> =	5.9	$PD = V \times [\ (4.510 + .067\ V)$ $+ L \times (5.349 - .132\ V + .015\ V^2)\ ]$
50 – 70 μm	> =	0	$PD = V \times [\ (5.050 + .054\ V)$ $+ L \times (1.508 + .0420\ V - .004\ V^2)\ ]$

PD = Pressure drop (mm water)
V = Face velocity (cm/s)
L = Specific load (kg/m^2)

Consequently it is reasonable to assume that initially local velocities, and so loadings, vary across the media in order to maintain an equal pressure drop at all points. In appendix 3.4.2 the above is assumed and the effect of having an uneven load on the filter calculated.

The derivation in appendix 3.4.2 accepts there will be an initial period of unsteady state filtration until such time that sufficient loading has taken place to equalise local velocities. Loading will then continue uniformly under steady state conditions and so obey Darcy's law. However, applying Darcy's law to the uneven loading, produced by the assumed initial period of unsteady state filtration, predicts a non-linear relationship between load and pressure drop. Furthermore the resulting rise of pressure drop with the load will be smaller than that of the purely linear response predicted by Darcy's law - the effect being more pronounced the greater the uneveness of load. Hence as the loading progresses the response becomes closer to Darcy's law until in the limit, when uniform loading conditions are reached, it will be obeyed.

A feasible explanation for the particle size effect on the significance of the primary section of the curve is that the less adhesive larger particles may be arranged more uniformly on the media surface in the initial stages. Further, the depth of irregularities on the clean media surface will be less important relative to the larger particle sizes. Another possible contributory mechanism may be the greater tendency of small particles to follow local velocity perturbations.

3.5. Measurement of dust bulk densities

The dust packing density, defined as the ratio of bulk density to particle density, affects the pressure drop per unit load and the volume occupied by unit load. Both of these are critical in determining the characteristics of panel filters. Clearly the packing density is affected by the relative importance of particle adhesion and mechanical forces during bed formation. These forces are in turn dependent on particle size, impact velocity and surface properties. It

was necessary to obtain data on the effect of the major operating variables on packing density. The series of tests outlined below, measuring the accessible parameter of bulk density, were undertaken to achieve this.

A simple test allowing dust to flow freely into a measuring cylinder was carried out. The weight per unit volume was calculated. The dust was further consolidated by continually vibrating the cylinder until no change in bed height was observed. Again the bulk density was calculated. This figure has been treated as a maximum consolidation value. Results for these tests are given in table 3.3. and shown in figure 3.25.

Tests were also conducted using the small scale rig. Dust was dispersed and loaded onto the media with a face velocity of 2.5 cm/s. Measurements were made at velocities upto 5 cm/s but no significant differences were noticed. Similarly tests with and without the presence of the radioactive source did not show variance beyond expected experimental error. Once the dust had been loaded, the media and dust layer were cut with a razor blade to give a cross-sectionhed view of the dust cake. This was examined using a travelling microscope with the height of the layer being measured at suitable intervals to give an overall average. From its average height and weight the bulk density of the bed was calculated. The results are given in table 3.4. and figure 3.25. An example with electrostatic forces neutralised is included in table 3.4. The mean of the dust size distribution is quoted and used in figure 3.25. The actual dust size distributions are given in appendix 3.5.1. The analysis by Coulter Counter is used.

It is obvious from figure 3.25 that there is a strong relationship between dust size and bulk density. The loading tests conducted at the realistic face velocity of 2.5 cm/s give the lowest figures for bulk density. In terms of channel clogging within HEPA filters it is obviously the minimum value of bulk density which will give the limiting worst case. Therefore it was assumed that the loading tests approached this lower limit and the relationship between dust size and bulk density was determined so the minimum bulk density of aluminium oxide test dusts could be predicted.

Table 3.3 : Bulk density measurements of aluminium oxide dust - free flow and consolidated

Dust	Weight (g)	Initial Volume (cm^3)	Final Volume (cm^3)	Free Flow bulk density (kg/m^3)	Consolidated bulk density (kg/m^3)
3μm	3.3	4.4	2.5	757	1332
B.S. 2831 N°2	4.09	4.4	2.4	930	1704
20-30μm	8.32	5.2	4.1	1600	2029
15-40μm	6.78	4.5	3.4	1507	1994
28-50μm	7.87	4.7	3.8	1675	2071
50-70μm	8.00	4.6	3.9	1739	2051
63-163μm	8.22	4.3	3.9	1911	2108

Table 3.4 Bulk densities of aluminium oxide dust collected on a Media disc

DUST LOADED	MEAN SIZE (μm)	WEIGHT LOADED (g)	SPECIFIC LOAD (kg/m^2)	AVERAGE DUST LAYER HEIGHT (6 READINGS) (mm)	STD. DEVIATION DEVIATION OF DUST LAYER DENSITY HT. (mm)	AVERAGE BULK DENSITY OF DUST (kg/m^3)
Abralox P3	3.2	1.78	0.42	0.89	0.16	478
Abralox P5	4.0	1.92	0.46	0.87	0.13	526
1200 Grid (Batch 1)	4.1	1.83	0.44	0.86	0.16	514
1200 Grid* (Batch 1)	4.1	1.30	0.31	0.60	0.06	518*
BS 2831 No. 2 (Batch 1)	4.8	1.60	0.38	0.56	0.07	681
BS 2831 No. 2 (Batch 5)	5.1	1.58	0.38	0.54	0.04	699
Abralox P15	10.8	2.85	0.68	0.82	0.15	828
20-30μm	22.8	4.53	1.08	0.78	0.04	1385
15-40μm	23.5	2.04	0.53	0.45	0.04	1085
28-50μm	37.7	5.40	1.29	0.78	0.21	1651
50-70μm[†]	52.3	7.12	1.70	0.89	0.26	1909

*Electrostatic effects removed.
†Powder too fluid for accurate measurements of dust layer height.

157

FIGURE 3·25: Alumina dust bulk density with particle size

Bulk density (kg/m³)

Particle size (μm)

o   Loading tests

□   Free flow

x   Consolidated dust
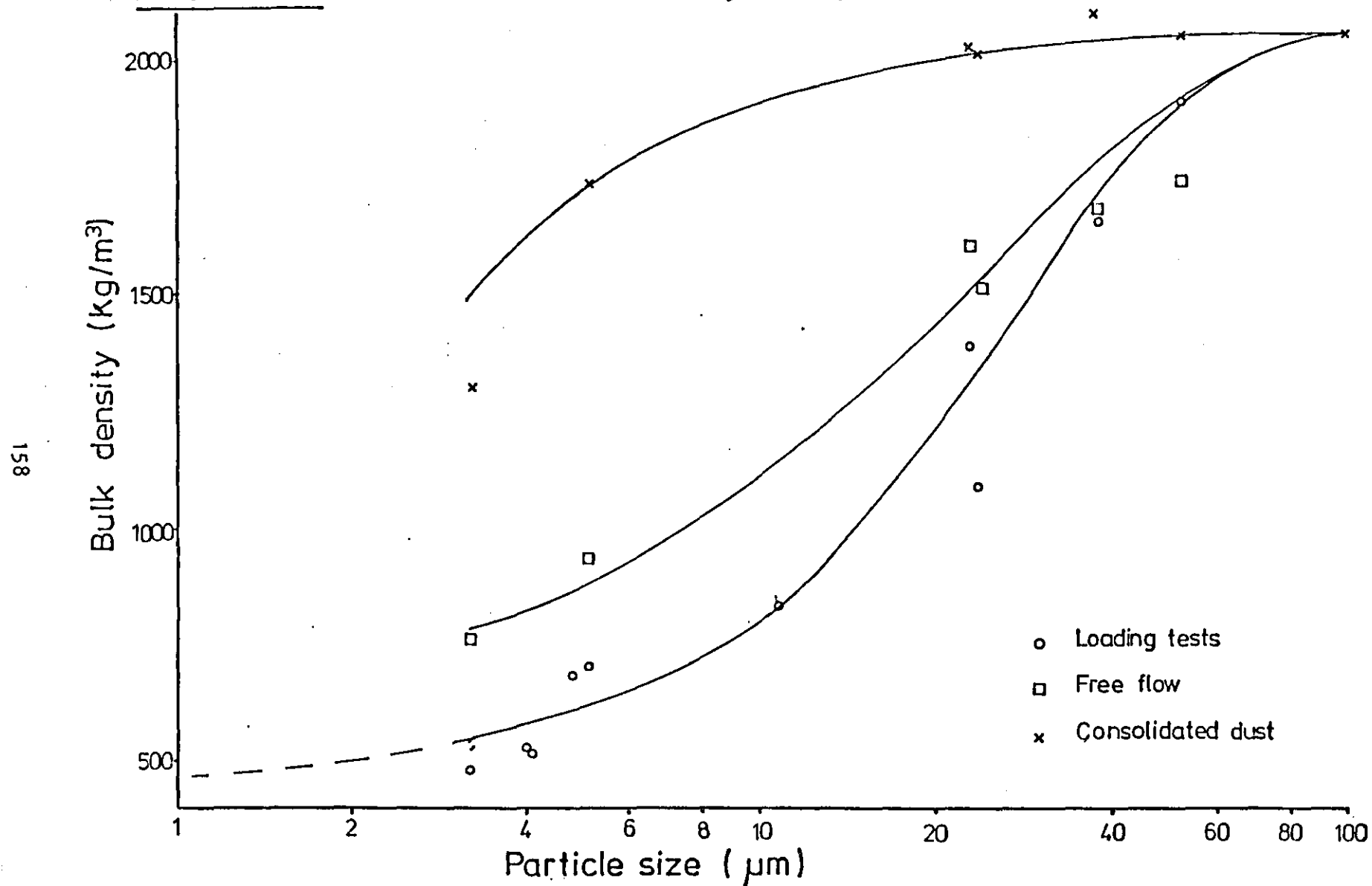
A curve fit was carried out beginning with a linear regression on a plot of

$$\ln \ln \left\{ \frac{1}{1-Y} \right\} \quad vs \quad \ln X$$

where, $Y = \dfrac{\text{bulk density} - \text{minimum bulk density}}{\text{maximum bulk density} - \text{minimum bulk density}}$

$X =$ mean particle size

This gives the constants in the Rosin - Rambler equation which has the form

$$\rho_b = (\rho_b max - \rho_b min)(1 - e^{-\left(\frac{dp}{dp_a}\right)^n}) + \rho_b min$$

where,

ρ_b = bulk density, dp = particle size

$\rho_b \ max$ = maximum bulk density

$\rho_b \ min$ = minimum bulk density

n = slope of the above linear regression

dp_a = particle size where $\ln \ln \dfrac{1}{1-Y} = 0$

i.e. $Y = 0.6321$

Using this analysis the following relationship was found

$$\rho_b = 1575 \left\{ 1 - e^{-\left(\frac{dp}{26.6}\right)^{1.45}} \right\} + 475$$

159

This is the curve drawn in Figure 3.25 and can be considered to give a good estimation of the bulk density of alumina dusts of a narrow size distribution within the limits of the data collected.

The bulk densities of dust collected in deep pleat filters during actual tests were measured. Complete channels were taken from each of the filters and cut into five equal sections across their width. The height of the dust layer across the channel width of 15 mm was measured at 3 mm intervals. This was done for B.S. 2831 No.2. dust samples which had been loaded at 1.25, 2.5 and 3.5 cm/s and also for the 3.2 μm mean diameter dust (Abralox P3) loaded a 2.5 cm/s. The results were in reasonable agreement with these obtained by the small scale work described above. Complete tables of the measurements that give details of the height profile of the dust layer with respect to both channel width and length, are given in appendix 3.5.2. From these results the figure of 700 Kg/m^3 for the bulk density was considered reasonable to use in deep pleat theory calculations.

It was not found possible to dissect the loaded mini-pleat filters for similar measurements without disturbing the dust. An estimate is also difficult because of the factors discussed in 4.2.3 as contributing to non uniform loading of the filter. In particular any remaining air spaces resulting from the holes observed in the filter face could not be measured. Similarly problems due to the apparent channel expansion and the large amount of dust impacted on the filter face complicate measurements. Attempts at measuring the bulk density assuming the channel to be full of dust and using its standard dimensions gave figures between 700 and 1000 Kg/m^3. Figures in this range have been used for theoretical calculations and their choice is discussed in 2.5.4.

CHAPTER 4

4. <u>Filter unit test work</u>

The objectives of this work were to find the limiting mechanisms controlling dust deposition within panel filter units. The observation and measurement of dust behaviour in a real system is an essential extension of the theoretical work described in chapter two.

The experimental programme consisted of two phases.

(i) To quantify the dust and air velocity distribution and dust classification within deep pleat filters.

(ii) To determine the pressure drop characteristics with increasing load for both mini-pleat and deep-pleat filter arrangements.

The experimental development, procedure, results and conclusions from these test programmes are described below.

4.1. <u>Dust and velocity distribution within deep-pleat filters</u>

4.1.1. <u>Experimental</u>

The theory given in section 2.2 was developed to predict particle trajectories within a deep-pleat filter. The following experimental programme was carried out to examine the air velocity and dust distribution and classification within a deep pleat filter. This would provide verification of some assumptions in the theoretical analysis.

A standard sized panel filter was divided into seven equal sections each for use in separate tests. Wooden slats covered six sections while the seventh was used. Inlet and outlet sections were built so they sealed tightly against the filter pleats and airflow could only pass through these inlet and outlet distributors.

The whole arrangement was held in place by a framework of angled irons and metal bars secured by wing nuts tightened onto screw threaded bars. These passed through the framework at each corner and across the filter width to a similar framework on the opposite side. Figure 4.1 shows the arrangement. Once a section has been used the distributors are moved across to one of the other sections and the wooden slats changed accordingly.

Figure 4.2 (a) shows the schematic layout of the apparatus and figure 4.2 (b) is a photograph of the rig. This allows either dust or aerosol to be generated and dispersed into the filter. The filter can be clean or loaded when the aerosol is passed through. The objectives were to examine dust distribution and classification by taking samples from the loaded filter. Since the aerosol capture efficiency in the media is virtually 100 percent, the local filter face velocity can be found from a quantitative analysis of aerosol deposited samples at various locations within the filter. A sub-micron aerosol which follows the air streamlines was used.

Initially methylene blue dye particles, produced by a Collision generator, were tried with the intention of extracting the dye and analysing it colourmetrically. However there were severe difficulties in successfully extracting all the dye from the media and dust and the subsequent results were too insensitive. Sodium chloride aerosol followed by extraction was used. Atomic spectroscopy was employed to measure the concentration of sodium ions in an extract solution made to a known volume. Unfortunately sodium ions leached from the media and any glassware used. This invalidated the results.

Finally magnesium chloride aerosol was used which has the advantage that it can be measured at even lower concentrations than sodium chloride using atomic spectroscopy. Figure 4.3a shows the calibration graph used to analyse results.

FIGURE 4·1: Support structure of filter unit

Inlet or outlet section

Angle iron

Metal bar

Wooden slats

Wing nut on threaded rod

(i) Front elevation

Angle iron

Metal bar

Wooden slat

Edge of inlet (or outlet) section

Wing nut on threaded rod

(ii) Side elevation

163
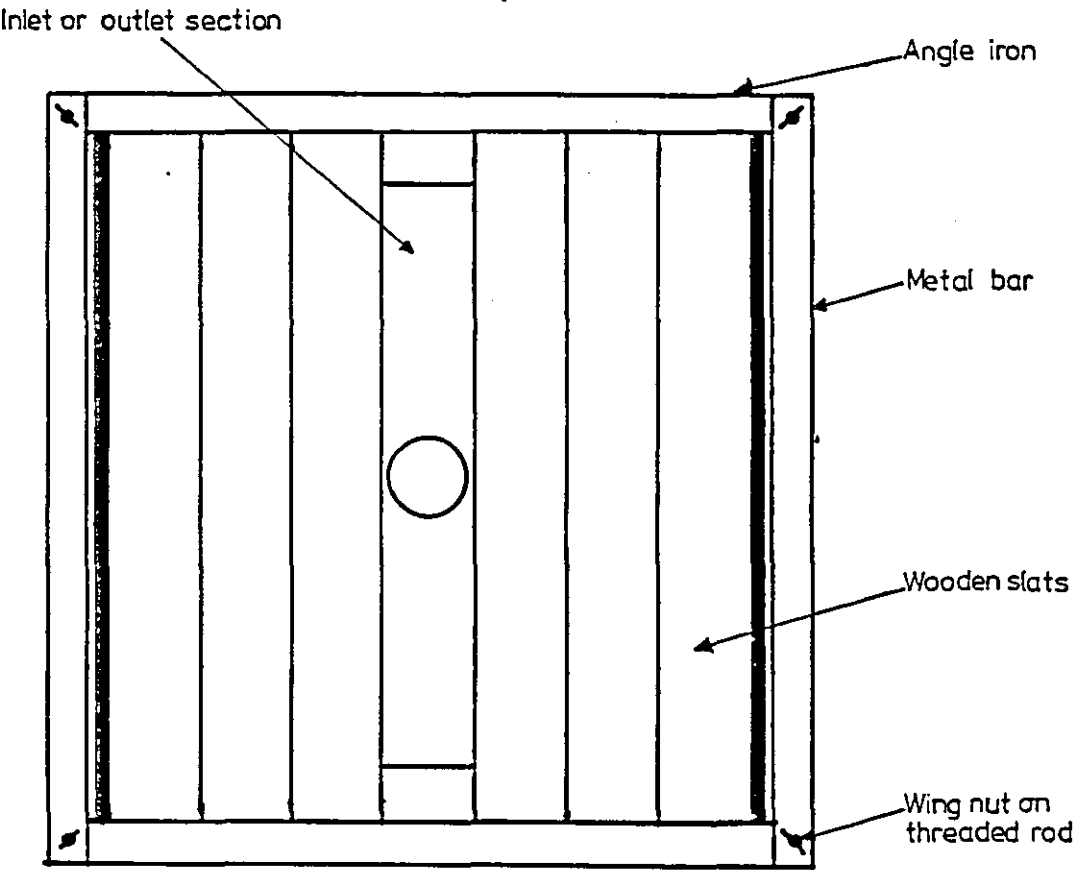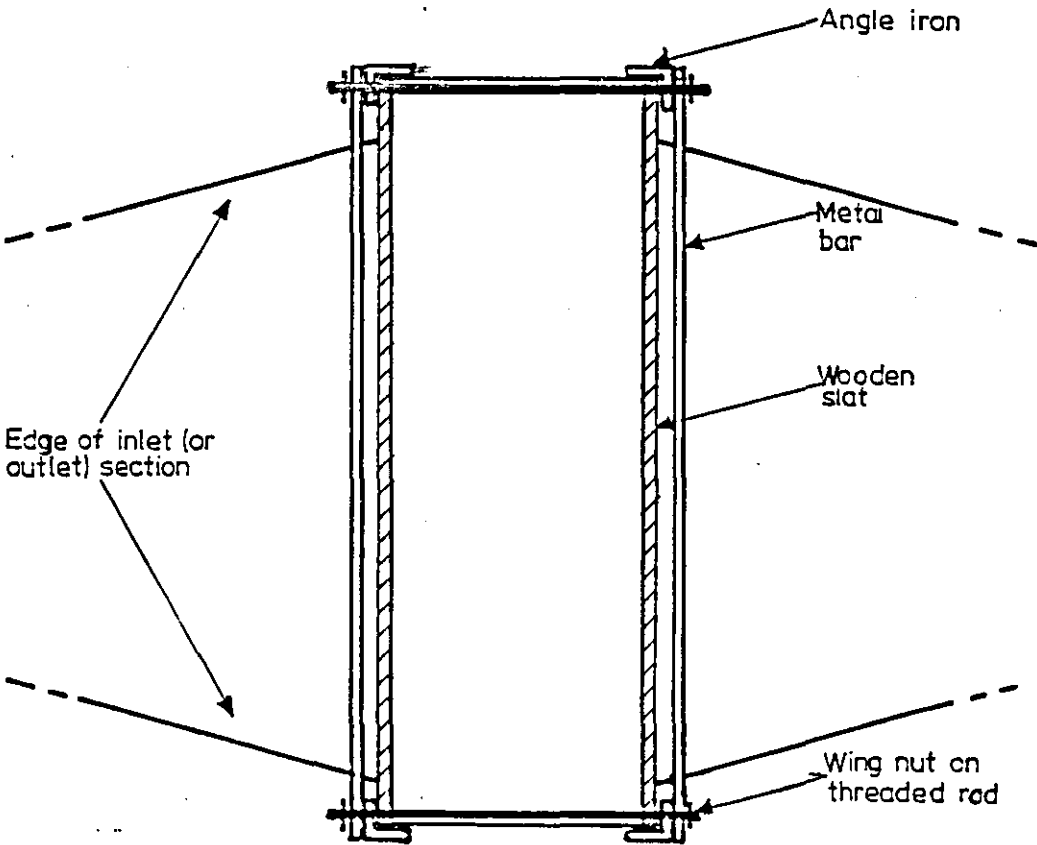
FIG 4.2 a : Design for Reconstruction of large Scale Rig

HONEYCOMBING
- for air distribution

To Atmos

ORIFICE PLATE

Mixing
Baffle

15 PSIG
Air

Dust

Flexitube

AEROSOL
GENERATORS

FILTER

Extra
Air

FAN

DUST
DISPERSER

50 PSIG Air
from compressor

Atmos air

RESIDENCE
TANK
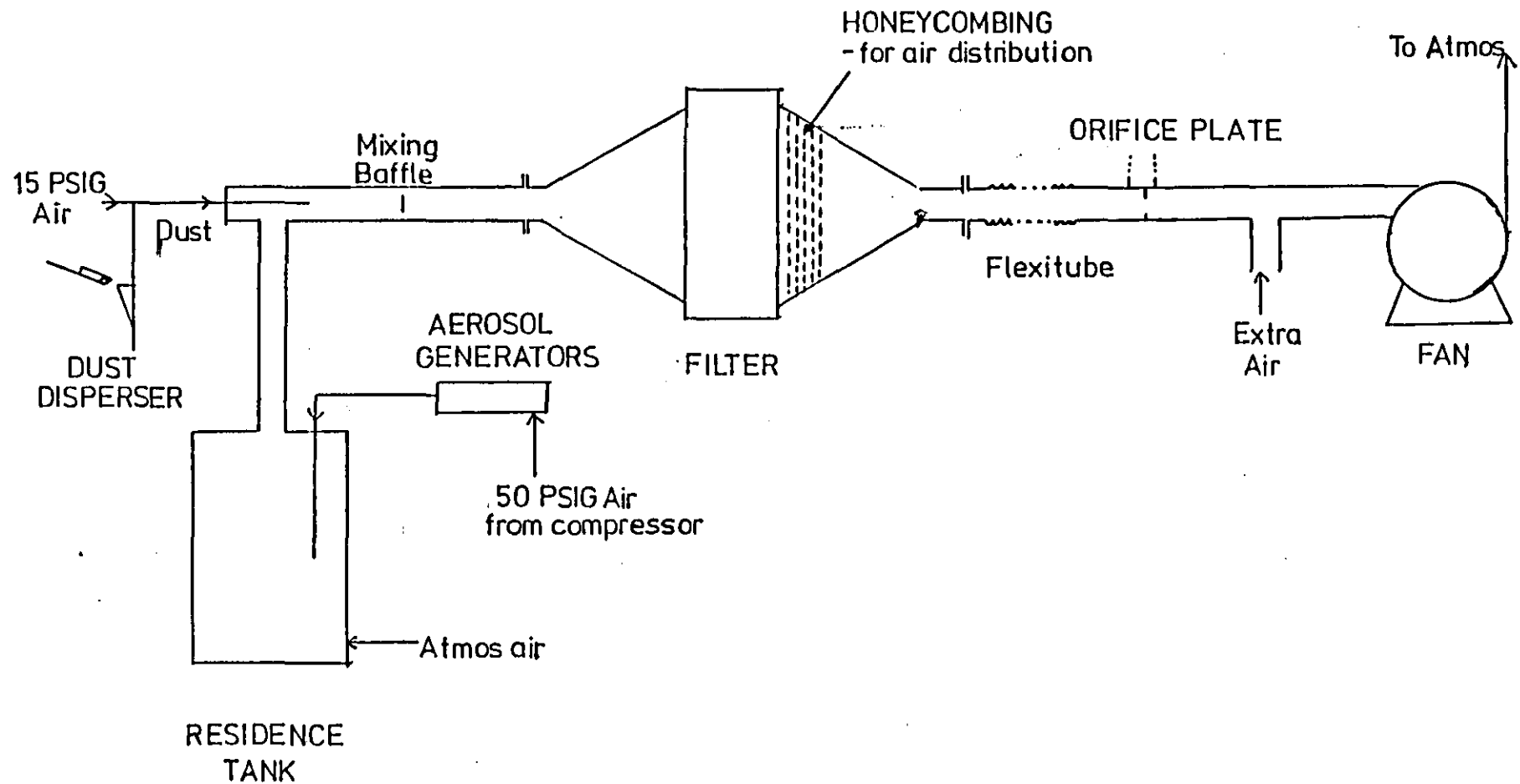
Initially small scale experiments were made to verify magnesium chloride's suitability in terms of particle size distribution, rate of generation and ease of extraction. From these experiments the generation time necessary to load a sufficient amount of aerosol for an acceptable level of detection was calculated. A generation time of approximately 15 hours was necessary for the area of media exposed to filtration when using only one generator. To improve on this a bank of generators was obtained. After relative humidity tests a suitable number of generators, which permitted sufficient drying, was found to be five. This reduced the run time required to three hours.

The experimental programme proceeded on the full size filter units as follows. A filter section was loaded with dust. When this was completed magnesium chloride was generated and filtered. After completion of both loading stages the filter was dismantled. Analysis was carried out on a complete sheet taken from a central pleat of the loaded section being examined (i.e. half of one complete fold of the filter media which was the height and depth of the filter unit in the deep pleat arrangement). Samples were taken from areas of the filter sheet and coded as shown in Figure 4.3b. Each sample was 3 channels wide and one third of the channel length. In the particular design examined this was an area of 27 cm^2 (3 x9 cm)

The following procedure was used for analysis of the samples.

1. Place sample in 100 cm^3 of distilled water.
2. Heat and boil for 15 minutes.
3. Allow $\frac{1}{4}$ hour minimum cooling time.
4. Filter using a 0.8 μm millipore filter of known weight.
5. Make the filtered solution upto 100 cm^3 and retain for analysis of its magnesium ion content.
6. Dry filter and weigh to obtain dust loading.
7. Use dust from the filter for a Coulter Counter analysis.

FIG 4.3b: Filter sheet sample positions

Airflow.

Top
T1 T2 T3
Middle
M1 M2 M3
Base
B1 B2 B3

Position 1 | Position 2 | Position 3
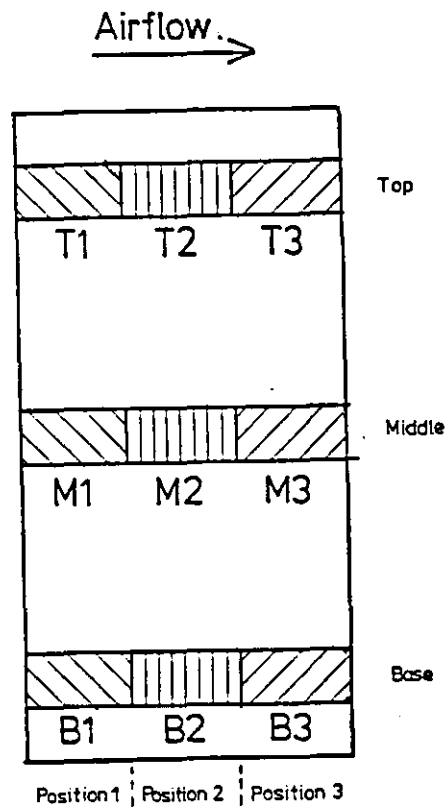
FIG 4.3a : Calibration Curve for Atomic Absorption Spectroscopy

Chart recorder scale (-)

Concentration of magnesium ions (ppm)

167
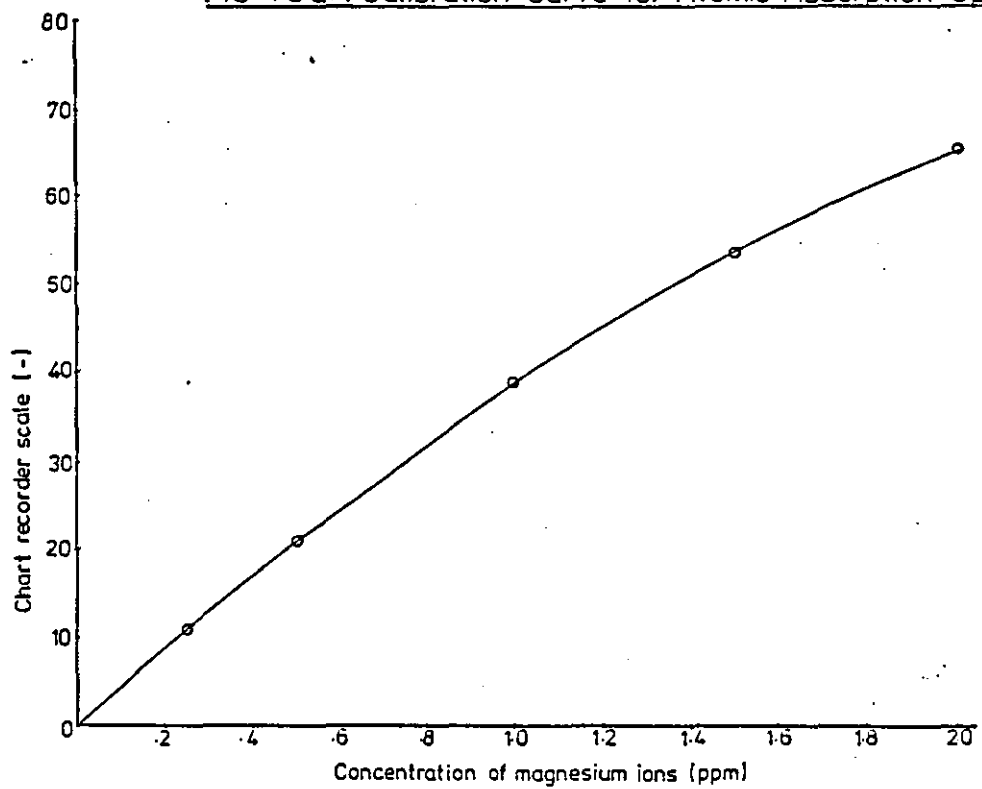
Photographs of some of the loaded filter sheets are presented in appendix 4.2.2. Coulter analysis of samples at different distances along the channel was also performed on the dust found on the corrigated aluminium spacer sheet of the filter. Photographs of these spacers are included with those of the filter sheets.

4.1.2. Results

A quantitative and qualative analysis was carried out on the experiments. This included early experiments performed with three different sized dust fractions and methylene blue dye aerosol as well as the tests with B.S. 2831 No.2 dust and magnesium chloride aerosol. A full set of results for each are presented in appendices 4.1.1. and 4.1.2 respectively. A summary describing the significant findings of all tests is presented below. Analysis and discussion of these results follows in section 4.1.2.2.

4.1.2.1. Summary of results

The results of earlier tests, given in appendix 4.1.1, showed a gravity effect present within the channel. Dust was found to be settling on the lower surface of the spacer, figure 4.6. . Figure 4.5 clearly shows the resulting ridge of dust formed at the media/spacer joint at the bottom of the channel as further evidence.

A methylene blue dye test on a clean filter indicated that the overall air distribution was uniform, figure 4.4. However, dust loading results were not so uniform. Figures 4.7 (a) and 4.7 (b) give the analysis of the dust weight collected with respect to channel length showing that in general more dust was collected towards the beginning of the channel. However a series of size analyses tests of dust in different areas of the channel proved inconclusive. Similar dust size distributions were found in all areas of the filter..
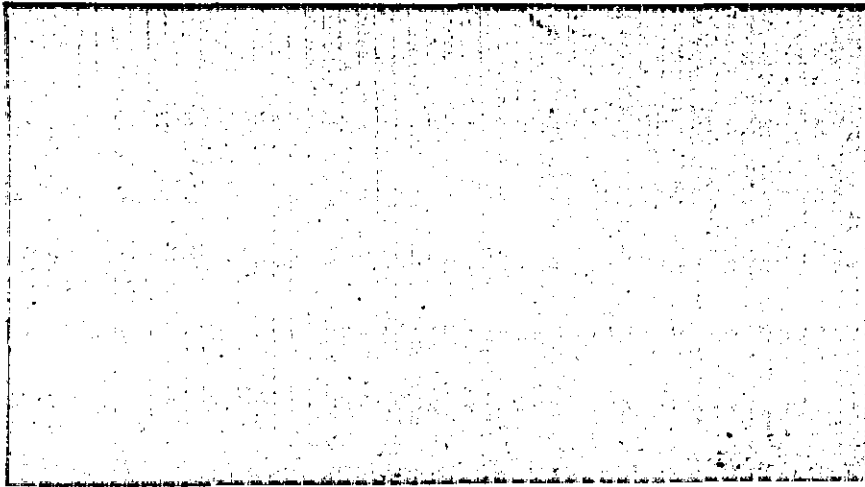
FIGURE 4.4: Clean sheet with filtered dye
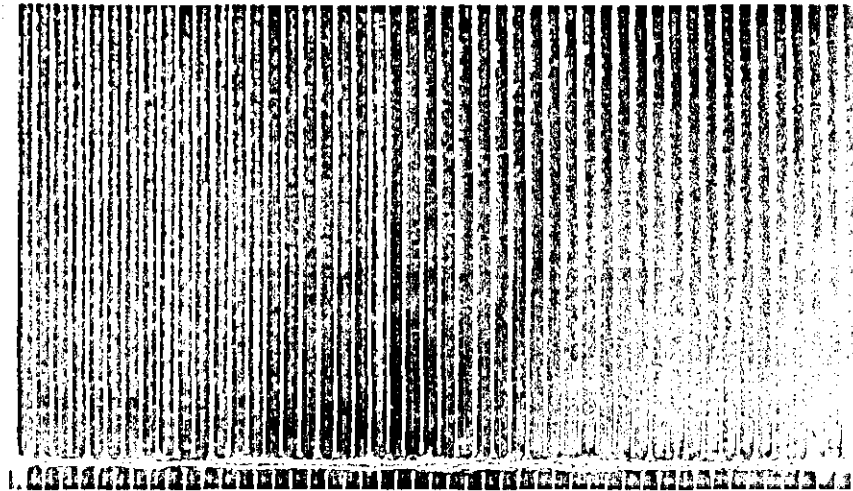
FIGURE 4.5: Loaded sheet with filtered dye
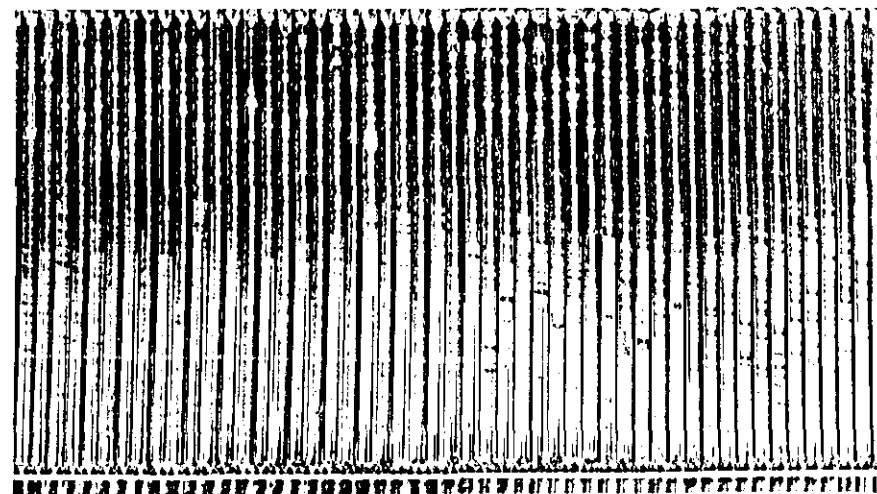
FIGURE 4.6: Dust collected on filter spacer

Plots of overall averages of % distance vs. % weight

FIG.4.7a : All Samples

□ Overall average
○ Base section 22% total wt.
× Centre „ 38% „ „
+ Top „ 40% „ „
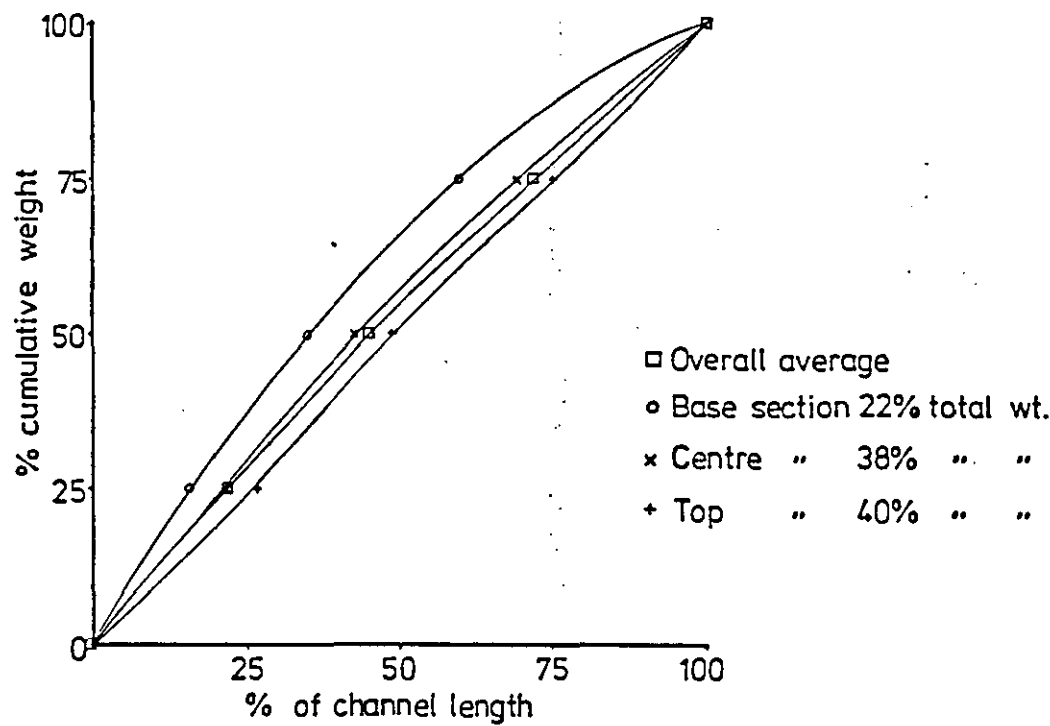
FIG.4.7b: B.S. NO. 2 Samples only

□ Overall average
○ Base section 20% total wt.
× Centre „ 32% „ „
+ Top „ 48% „ „
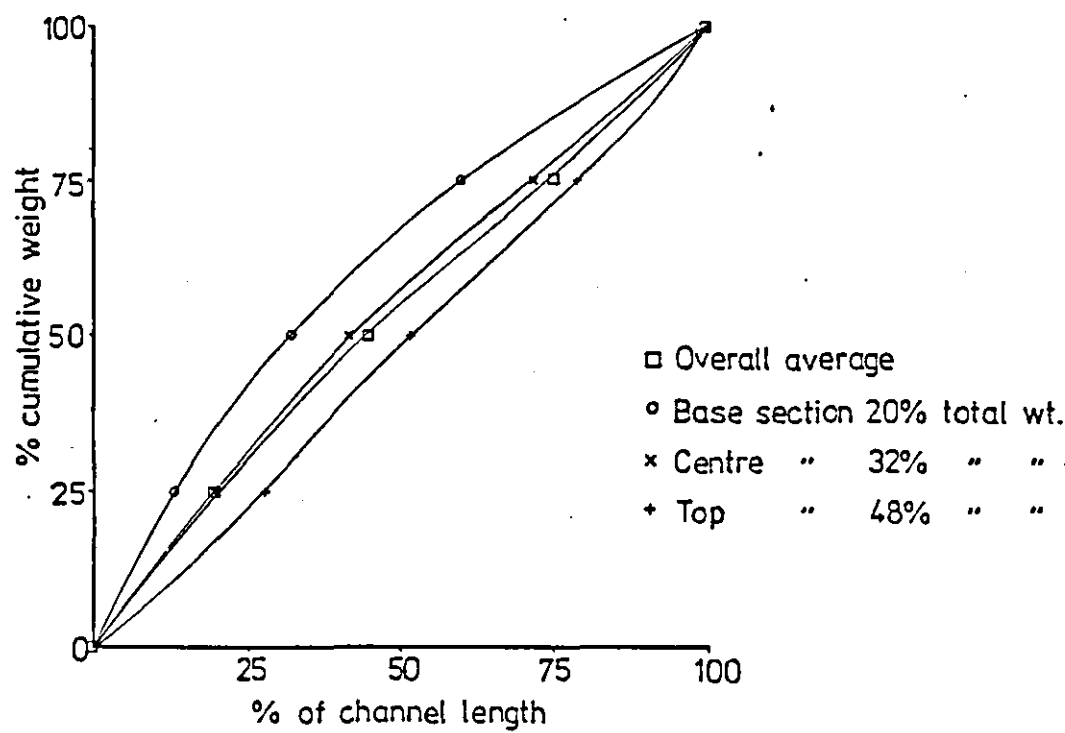
The magnesium chloride tests were more comprehensive. The range of specific loads examined is shown in table 4.1.

Sheet	Load (kg/m^2)
A	0
B	.036
C	.058
D	.084
E*	.104

Table 4.1. Overall dust loading for each filter sheet.

With sheet E some problems were encountered when carrying out the dust weighings. The membrane filters, onto which the dust had been filtered and dried, became electrostatically charged and in some cases dust was unavoidably lost. For this reason the figure presented in table 4.1 for sheet E is from a second sheet of this particular loading. However all other results presented refer to the original sheet. Table 4.2 presents the results from the atomic absorption tests, giving the concentration of magnesium ions, and also the dust loadings for each sample taken.

To obtain a clearer picture of dust deposition with distance from the channel inlet a further series of tests were carried out. Long strips 3 cm wide across the full height of a filter sheet were taken. Dust was removed and weighed in the usual manner. Strips were taken at distances of (1) 0 - 3 cm, (2) 8 - 11 cm, (3) 16 - 19 cm, (4) 24 - 27 cm down the channel from the entrance. The figures given in table 4.3 are for a lightly loaded (L) filter and a heavily loaded (H) filter.

A typical result for the Coulter analysis, carried out on the samples taken from sheets A - E, is given in figure 4.8. The full set of results, all of a similar nature, are in appendix 4.1.2. Further Coulter analysis was carried out on dust collected from a heavily

Table 4.2 Results from Atomic Absorption Tests

Sample	Hg^{2+} (ppm)	% of Av.	Dust load (kg/m^2)
A/B/1	1.4	88	
A/B/2	1.5	94	
A/B/3	1.5	94	
A/M/1	1.6	100	
A/M/2	1.6	100	
A/M/3	1.8	112	
A/T/1	1.6	100	
A/T/2	1.7	106	
A/T/3	1.7	106	
	Av = 1.60		
B/B/1	1.8	93	.036
B/B/2	1.9	98	.033
B/B/3	2.0	103	.032
B/M/1	2.1	108	.048
B/M/2	2.0	103	.036
B/M/3	2.1	108	.036
B/T/1	1.9	98	.037
B/T/2	1.8	93	.032
B/T/3	1.9	98	.032
	Av = 1.94		
C/B/1	1.9	99	.064*
C/B/2	1.8	94	.051*
C/B/3	1.9	99	.044*
C/M/1	2.1	109	.067
C/M/2	2.0	104	.063**
C/M/3	2.1	109	.061
C/T/1	1.8	94	.057
C/T/2	1.8	94	.057
C/T/3	1.9	99	.054
	Av = 1.92		
D/B/1	1.6	87	.087
D/B/2	1.6	87	.069
D/B/3	1.7	93	.067
D/M/1	1.9	104	.092*
D/M/2	1.8	98	.096*
D/M/3	1.9	104	.093*
D/T/1	2.0	109	.082*
D/T/l	1.9	104	.088*
D/T/3	2.1	115	.084*
	Av = 1.83		
E/B/1	1.8	105	.076 ?
E/B/2	2.0	117	.021 ?
E/B/3	2.0	117	.021 ?
E/M/1	1.7	99	.143
E/M/2	1.6	94	.122
E/M/3	1.5	88	.110 **
E/T/1	1.6	99	.077
E/T/2	1.6	94	.086
E/T/3	1.6	94	.098
	Av = 1.71		

Sample	Dust weight (g)	Dust load (Kg/m²)
L1	.50316	.0349
L2	.56620	.0392
L3	.46291	.0321
L4	.46023	.0320
H1	1.30689	.0908
H2	1.15177	.0800
H3	0.94984	.0660
H4	1.15431	.0802

Table 4.3 Dust loadings from long strips

loaded spacer. Dust was collected from the spacer at distances of 0 -
2 cm, 5 - 10 cm, 12 - 18 cm and 20 - 25 cm from the channel entrance.
These all gave similar size distributions but they were different from
those of the media samples. Figure 4.9 shows the comparison of the
typical dust found on the spacer to that found on the filter media. A
photograph of a relatively heavily loaded filter sheet is presented in
figure 4.10. Similarly a photograph of a spacer taken from this
filter section is given in figure 4.11.

4.1.2.2. Analysis of the results

The dust loading effect shows a general trend of relatively high
loading in the early section of the channel. This increase in load at
the entrance could be upto 30% greater than the rest of the filter,
although more commonly 10 - 15% increases were observed. It was also
noted that the further the loading progresses the more pronounced the
effect becomes. In fact with heavy loads some evidence of channel
blockage was observed. The centre and end sections of the channel are
more evenly loaded. Fluctuations in the specific load of dust beyond
the entrance section appear random and are in the order of 5 - 10%
which indicates uniform loading.

The atomic absorption tests on a clean filter indicated generally
uniform air distribution.

Clearly as zones of the filter become preferentially loaded then
the air face velocity in these zones will be reduced. Table 4.2
confirms this. If particle deposition on the media is a result of
filtration alone then the zones of media with a deeper dust layer, and
thus lower face velocity, will accumulate a lighter deposit. Therefore
it would be expected that the overall deposit will even out with time.
Since this is not the case at the channel entrance then obviously
additional mechanisms must be the cause of the extra deposition in
this region.

FIG.4.8: CUMULATIVE WEIGHT VS. PARTICLE SIZE
(SHEET B BASE)
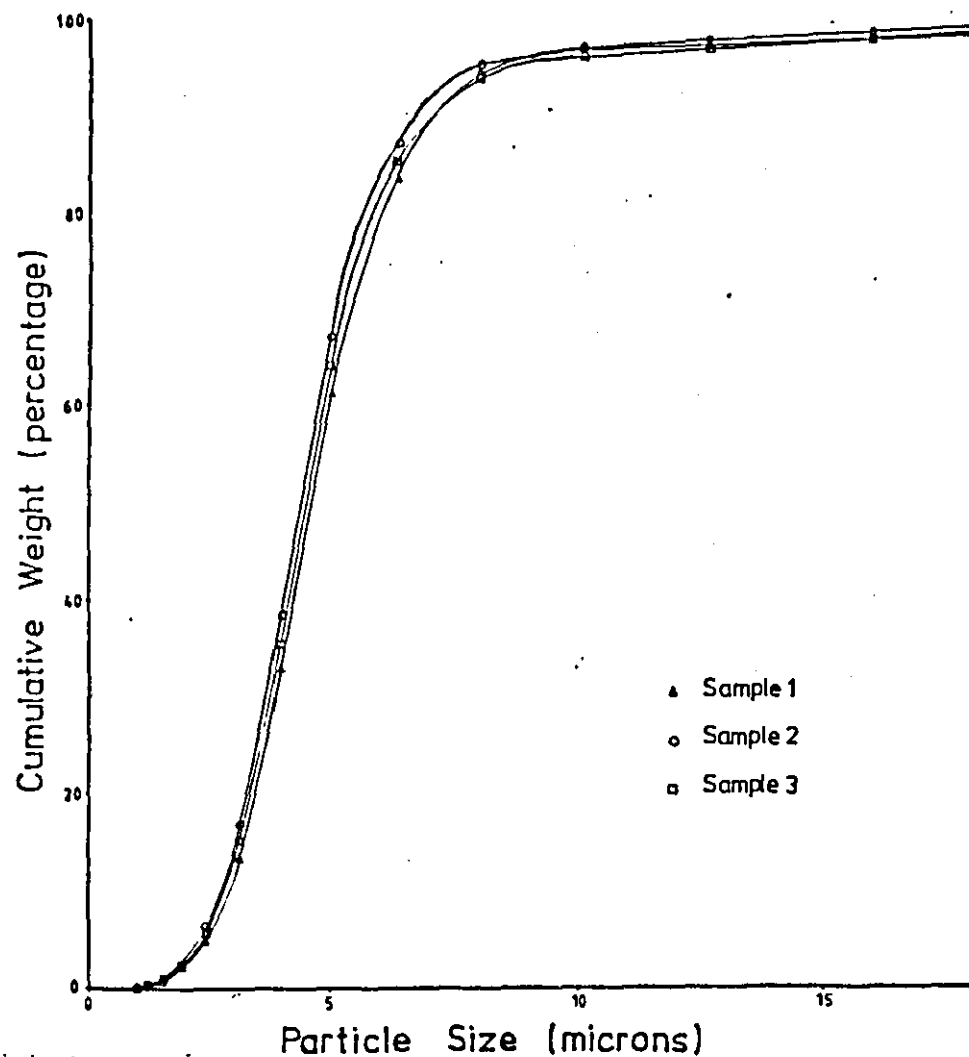
FIG.4.9: CUMULATIVE WEIGHT VS. PARTICLE SIZE

Comparison of typical sheet and spacer
dust size distributions

▲ Sample 1
○ Sample 2
□ Sample 3

○ Sample C/B/2
□ Sample B from spacer

Cumulative Weight (percentage)

Particle Size (microns)

175
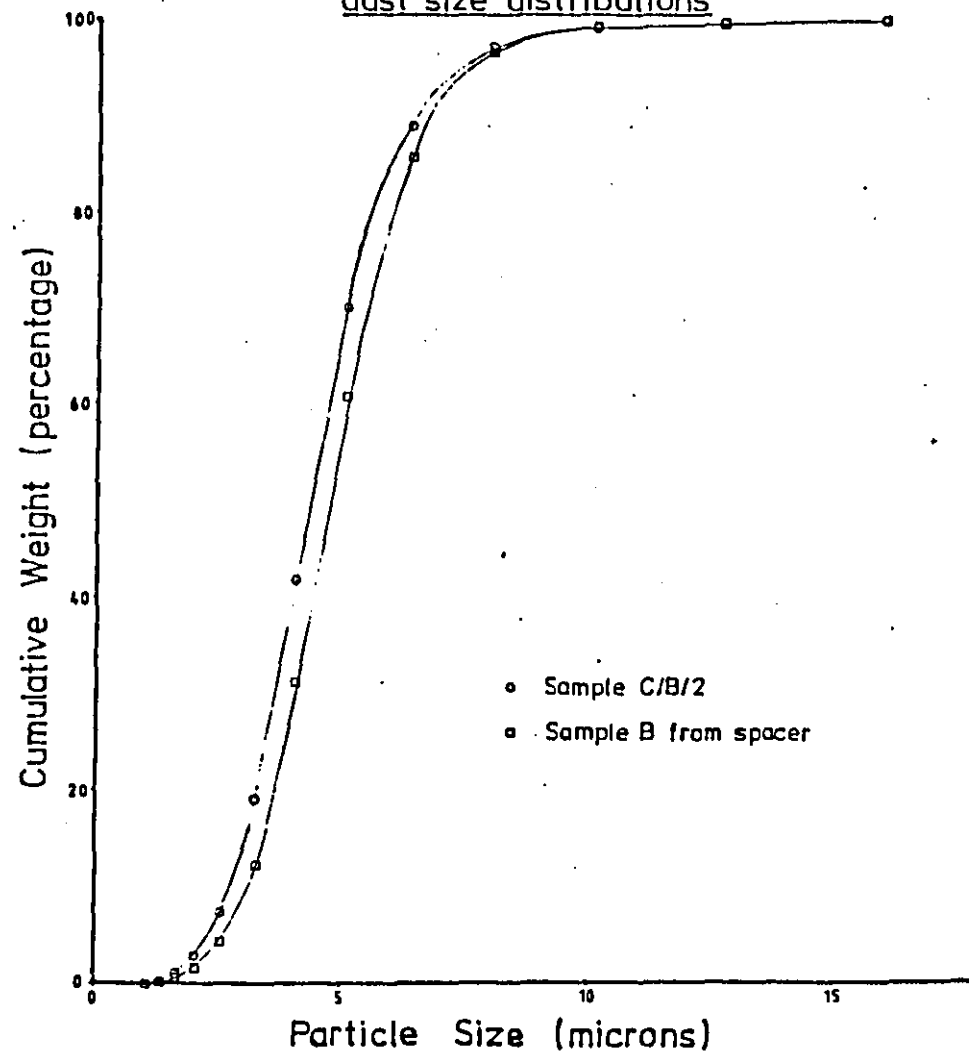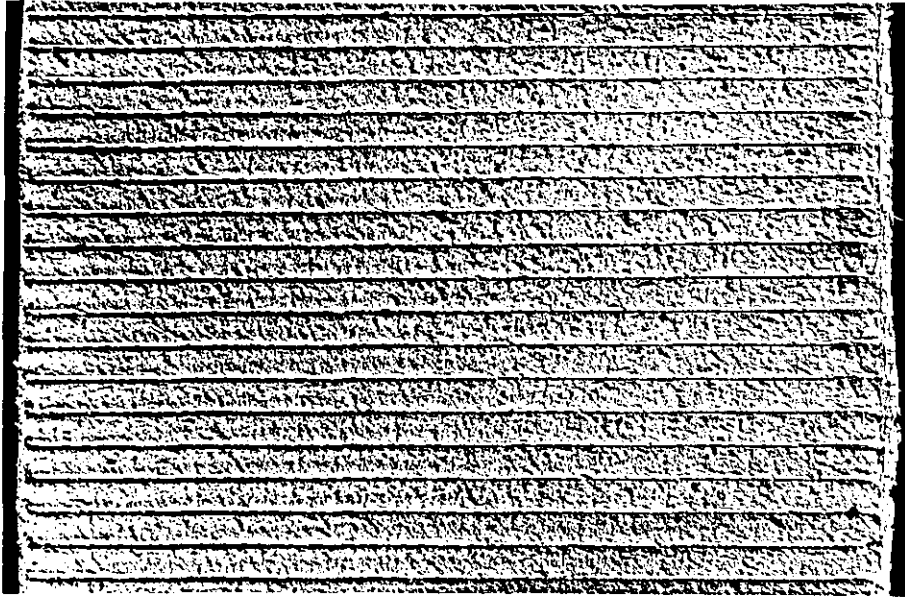
FIGURE 4.10: Loaded deep pleat filter sheet

FIGURE 4.11: Loaded deep pleat filter spacer

Coulter analysis showed that the size distribution of dust was
similar at all points in the filter. However, comparing the dust
collected from the spacer with the from the media shows that
significantly fewer fine particles are present on the spacer.
Typically the cumulative weight for upto 4 μm particles off the
filter sheet was 42% as opposed to 31% for the spacer. This agrees
with the concept of gravity sedimentation but shows little evidence
for inertial effects.

The photographs of filter sheets show indisputable ridges of dust
formed where the lower edge of the spacer joins the filter sheet.
This further strongly supports the idea of gravity settling. Also
observed on the top surface of the dust is a loose deposit of
agglomerated dust which decreases uniformly with distance from the
channel entrance. Similarly the deposit found on the spacer decreases
with distance. This can be explained by considering the loose deposit
to be the result of particles forming a layer on the spacer and then
breaking off as agglomerates and being reentrained temporarily into
the air stream before filtration.

Support to the hypothesis of an entrance effect is given by the
photographs. A high dust deposit at the immediate entrance of the
channel both on the filter sheet and on the spacer is clearly seen.

4.1.3. Conclusions

The overall results can be summarised as:

i)   The dust distribution is generally uniform in size and load
throughout the channel except at the entrance. Here an increase of
dust load of upto 30% but more commonly 15% is observed.

ii) The air velocity distribution, as indicated by the magnesium
chloride test, suggests that the airflow is uniform except at the
entrance. The results indicate more dust is present at the
entrance by a lower than average magnesium ion concentration

being found for these samples. The reduction is in the order of 10-15%.

iii) Gravity settling is shown by the evidence of ridges of dust where spacer edge meets the filter media. Furthermore the lower spacer surface is coated with dust. It is significant that this dust contains larger particles than that dust from the filter sheet.

These results demonstrate that inertia has little effect on dust deposition for particles less than 10 μm diameter. However gravity sedimentation is seen to have an important influence for particles over 5 μm, but this does not appear to be detrimental to the filtration. It is shown that the general design of the filter is successful in obtaining a uniform load distribution with the exception of the channel entrance. The significant increase in load at the entrance could lead to premature channel blockage. This suggests that difficulties may be encountered if channel height is significantly reduced.

It is concluded that the theory of section 2.2 reasonably predicts particle trajectories once within the channel to give uniform loading on the media with some deposition on the spacer, with progression along the channel, also indicated. This was borne out in practice. The entrance effect, however, had not been quantified and obviously needs to be accounted for. The theory of section 2.4 develops this aspect.

As a final important observation it was noted that the spacers themselves reduced the area of filter media available for filtration. This was where the triangular fold contacted the media. Also many spacers were misaligned with each other on opposite sides of the media. This accounts for upto a 10% loss in media area available and must be regarded as a significant feature in the design. It would become particularly important if, for example, the channel width was narrowed so introducing more spacer/media contacts.

4.2. Measurement of the pressure drop response of filter units

4.2.1. Experimental apparatus and procedure

The apparatus described in 4.1 was modified. Figure 4.12 gives the flow scheme and a photograph of the completed rig is presented in Figure 4.13. Sections of deep pleat filters can be tested or, by the insertion of a special support framework, panels of the minipleat type arrangement are studied. Figures 4.14 and 4.15, show the filter unit with and without the framework respectively. It can be seen that a port hole was cut into the side of the filter box so that the filter could be observed and photographed after each stage of loading. A second port hole was cut downstream of the filter to verify no dust was by passing the seals.

Loading was generally with B.S. 2831 No.2. dust but experiments at 2.5. cm/s were also carried out with the finer Abralox P3, a 3 μm mean particle diameter dust. A test was made to verify the dispersion of this dust. A membrane filter in a specially cut away holder was used as a sampling head on the end of a sampling probe. A sample of dispersed dust was taken isokinetically and examined under a microscope after clarification of the membrane with immersion oil. Figure 4.16 shows that the particles are discrete and so the dispersion can be assumed satisfactory. The test dust was heated to remove absorbed moisture and facilitate dispersion.

In order to examine the behaviour with even finer dusts an optional cyclone section was included. The objective was to take the fine fraction from a coarse dust while it was still in dispersion. A cyclone with a 50% cut point of about 1.5 μm was used.

Tests were carried out with a range of different face velocities, replicate tests being made as necessary to confirm reproducability. Dust was normally loaded until a pressure drop of 127 mm (5 inches) water gauge was achieved, the pressure drop being measured after each

FIG 4.12 : Revised arrangement for large scale tests

Fines

Cap

Dispersed dust

Cyclone

Excess air
requirement
taken from
atmosphere

Coarse dust
collected

Air flow to the cyclone is
controlled by varying the
height of the cap on the
excess air inlet.

ΔP

To atmos

Point where pipe can
be broken for direct
dust injection

Air
distributor

ΔP

Orifice
plate

Air
distributor

Filter
Section

Fan
(Flow through system
controlled by using a
bypass facility).

FIGURE 4.14: Position of minipleat filter and support frame

FIGURE 4.15: Filter box with deep pleat filter suport frame

FIGURE 4·16: Dispersed 3μm dust isokinetically sampled onto a membrane filter
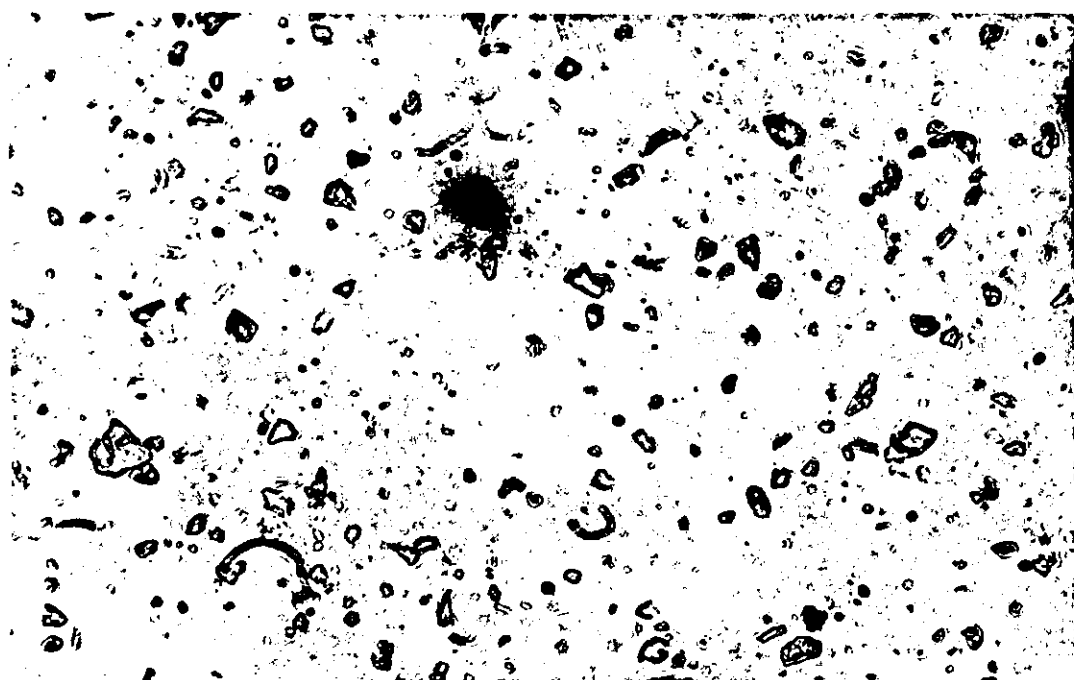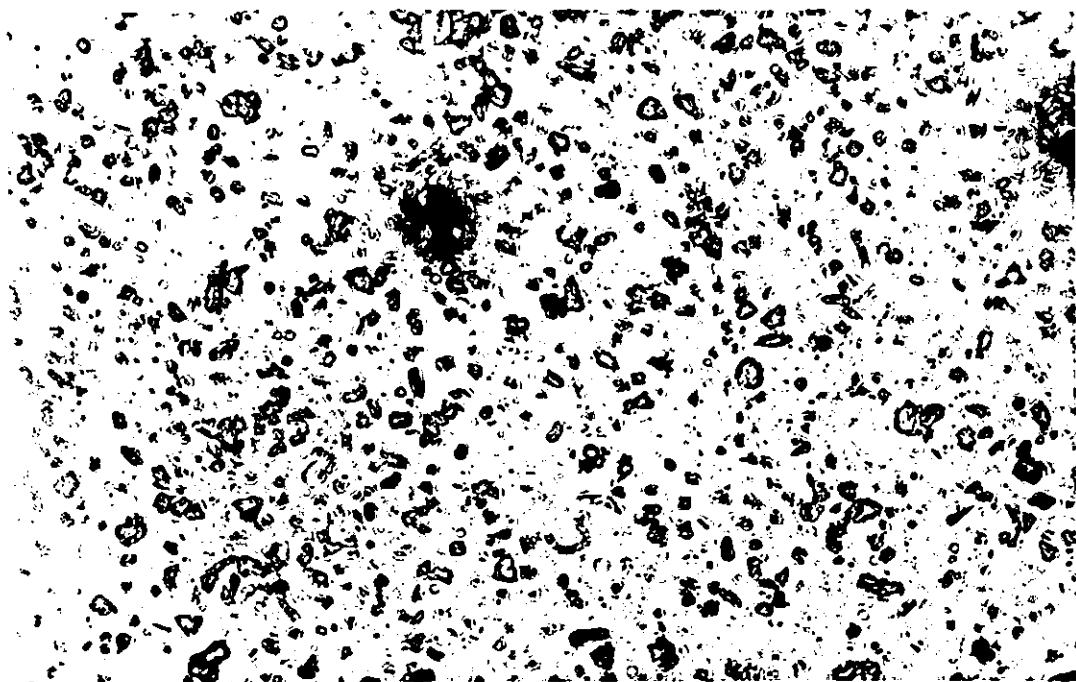
increment upto this stage. All increments were equal so that the amount actually loaded onto the filter could be back calculated by measuring the total weight of dust collected. Photographs were taken of the various stages of loading in the minipleat design. After the loading was completed photographs were also taken of the whole filter for both mini and deep pleat designs. This included close ups of channels to show the filtration mechanisms. Samples from various sections of the filter were also taken for Coulter analysis.

4.2.2. Results

A full set of tabulated results for each response is given in appendix 4.2.1. Figure 4.17 shows the resulting relationship for each dust graphically. The notation used is as follows

S	=	B.S. 2831 No.2 dust
F	=·	Abralox P3, 3 μm mean dust
C	=	Alumina 1200 grid after cycloning
1.25		
2.5		
3.5		Face velocity of filtration (cm/s)
4.0		
D	=	Deep-pleat type arrangement
M	=	Mini-pleat type arrangement

Therefore S2.5 M would represent a mini-pleat filter operating at a face velocity of 2.5 cm/s with B.S. 2831 No.2 dust being filtered.

Figure 4.18 shows the same curves with the pressure drop ratioed to the velocity term in an attempt to normalise the results with respect to velocity. Figure 4.19 gives a further plot which highlights the difference between the mini-pleat and deep-pleat arrangements. This considers the slope taken from the $\Delta P/U_0$ vs. specific load graph and plotted against specific load. It may be noted from the results that two loadings were not taken to completion. These were the cycloned dust at 2.5 cm/s and the B.S. No.2. dust at 1.25 cm/s in a deep-pleat filter. This was due to the large amount of

FIGURE 4.17: Filters tested for pressure drop response
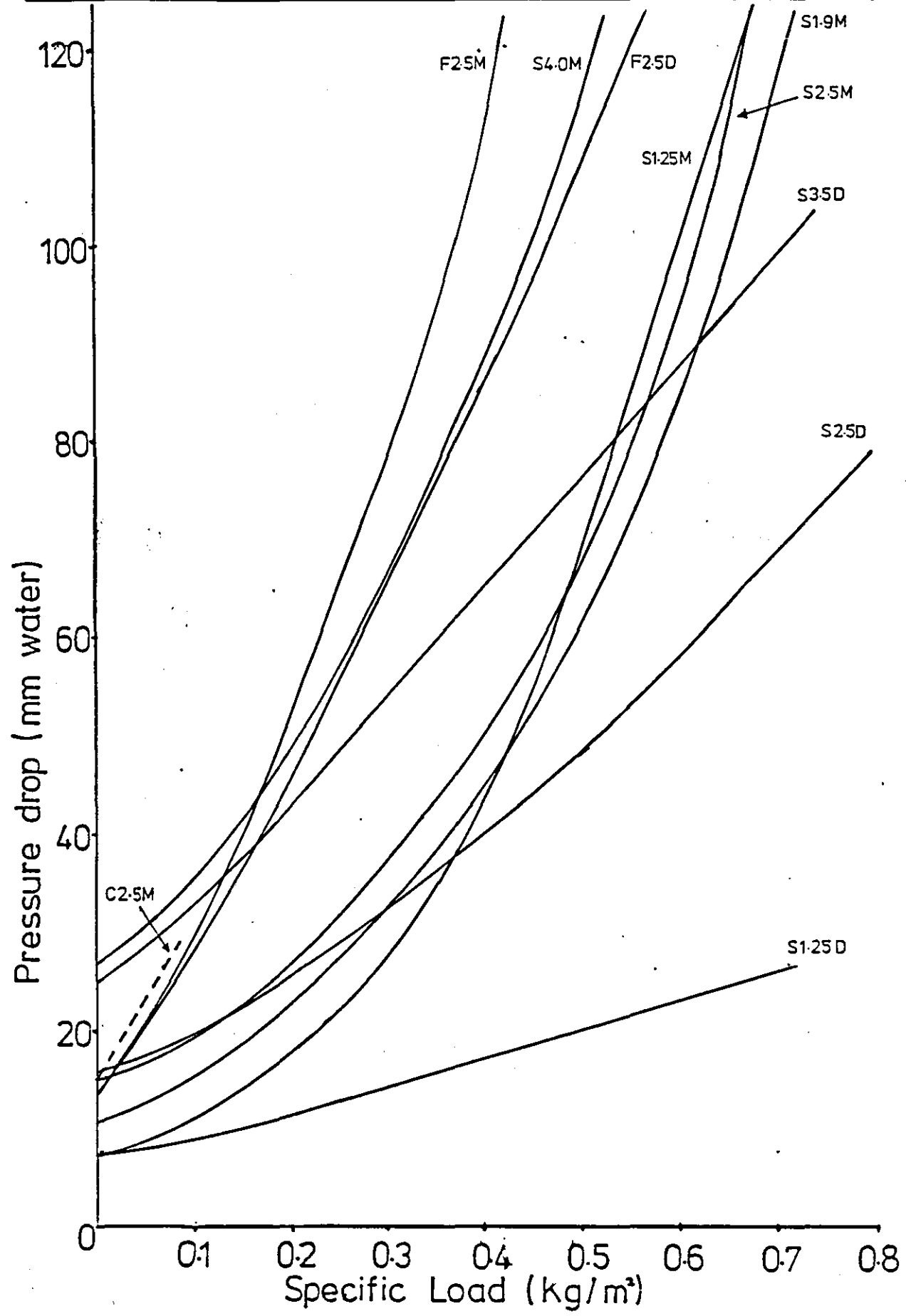
FIGURE 4.18: Comparison of filter tests eliminating the face velocity effect
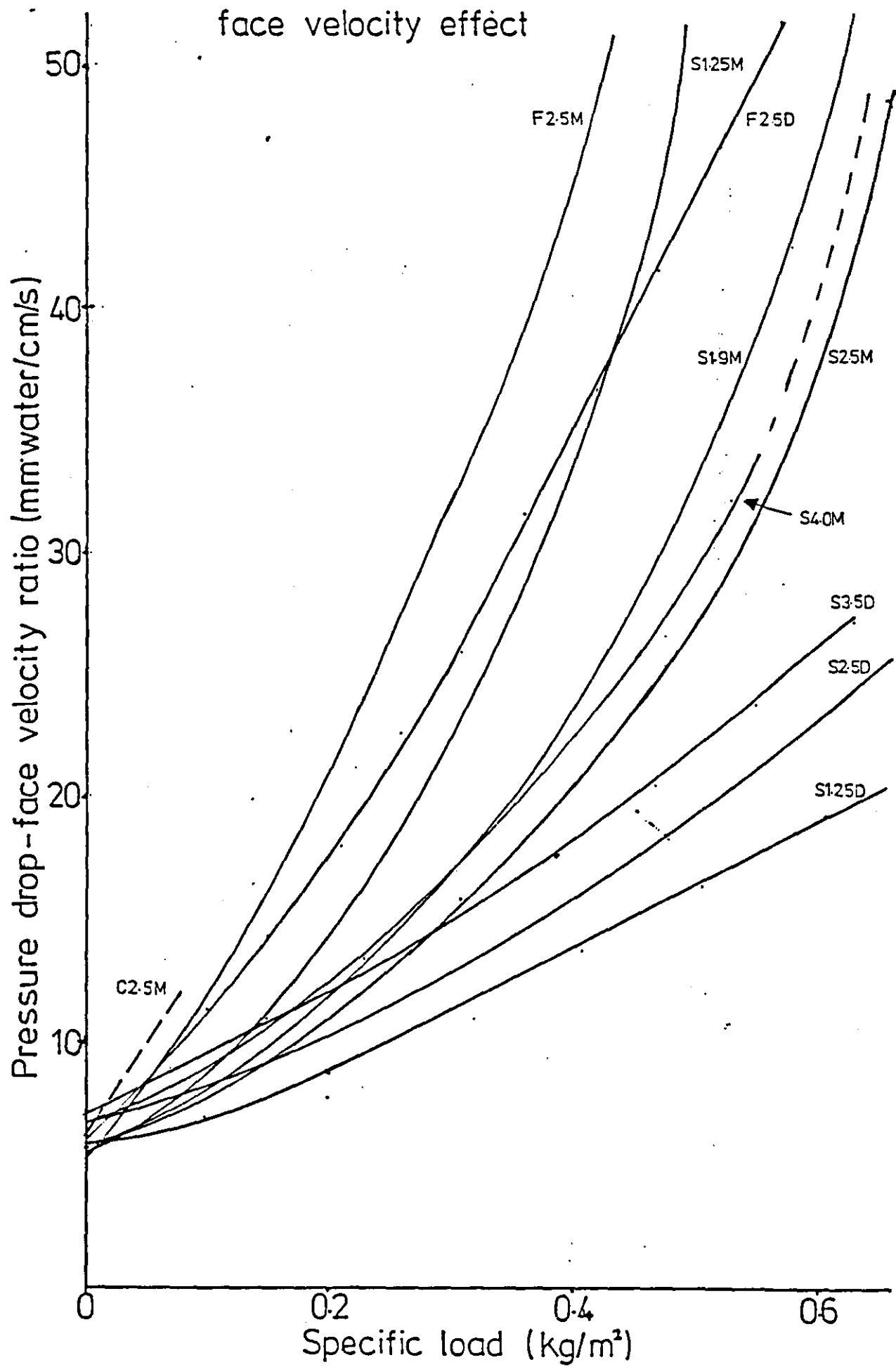
FIGURE 4.19: Specific load vs. slope of filter test plot after eliminating velocity effect
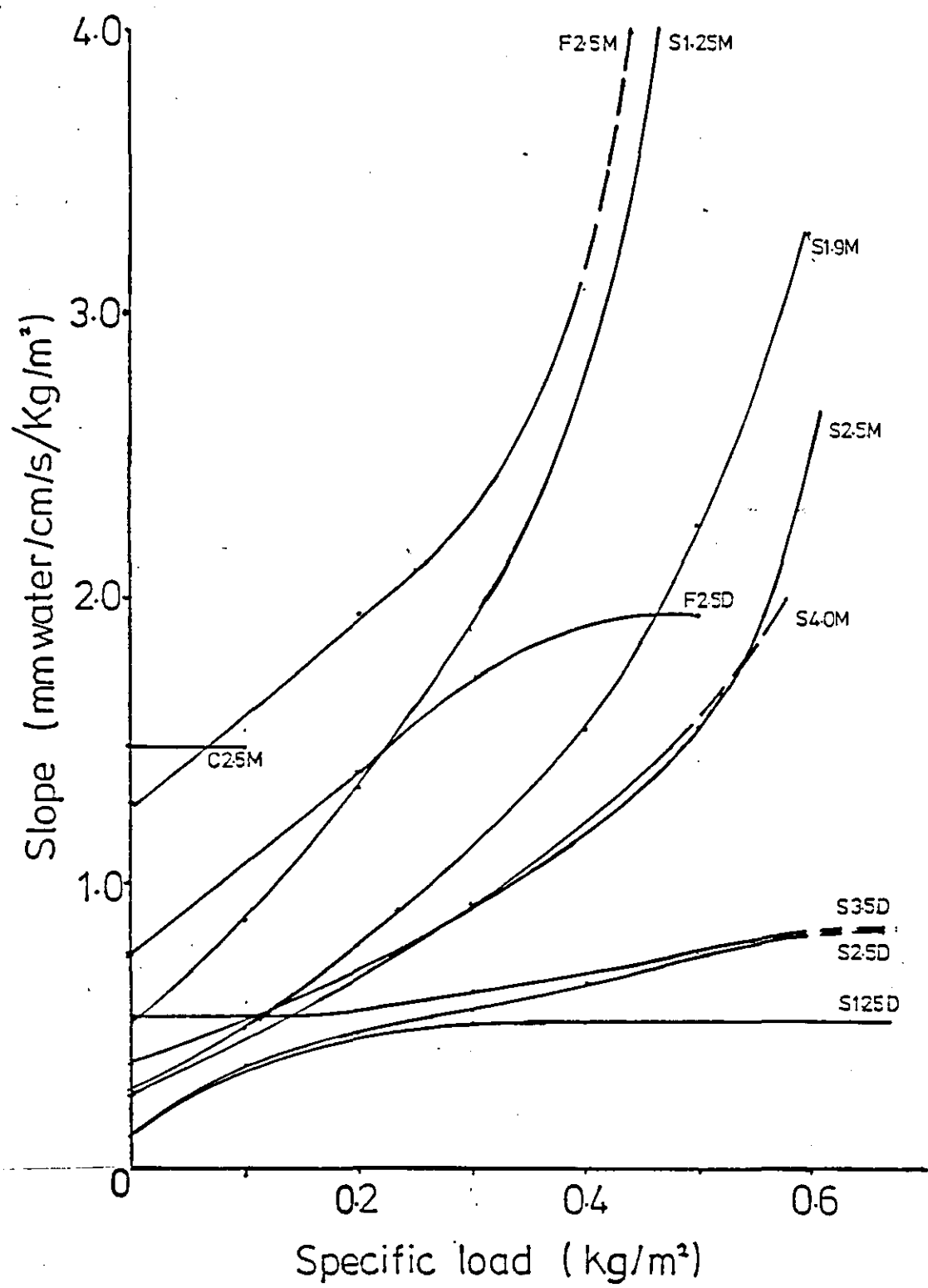
dust that was going to be required to reach the limiting pressure drop particularly with the cycloned dust. Only approximately 10% of dust fed was reaching the filter. The filtration was stopped when it was felt a reasonable trend could be observed.

In appendix 4.2.2 photographs of the various stages of loading of the mini pleat arrangement are given as well as photographs taken of completed filters, for both mini pleat and deep pleat designs with all dusts. Selected photographs are included in the following text to illustrate the major mechanisms observed. Figure 4.20 (a) - (i) show the progressive loading of a mini pleat filter at 2.5. cm/s with B.S. 2831 No.2 dust. Figure 4. 21 (a) - (c) shows the overall and close up views of this filter after loading was completed. Similarly figure 4.22 (a) - (c) shows overall and close up views of a deep pleat filter after completion of loading with B.S. 2831 No.2. Also figure 4.23 shows, close up, the cross-sectional view of channels from a fully loaded panel of a mini pleat filter.

Some random measurements of channel width in a loaded mini pleat filter are given in appendix 4.2.2. Furthermore, for the mini pleat design, analyses of the size distribution on the inside of the channel is compared with that collected on the filter face. Figure 4.24 illustrates this for B.S. 2831 No.2. at 2.5 cm/s. Dust size distributions measured with respect to position for a deep pleat filter showed no statistically significant variations. Tables are given in appendix 4.2.2. Analysis was also carried out on the dust weight with respect to position in a deep-pleat filter. The actual weights are given in appendix 4.2.2 and figure 4.25 illustrates the overall trends for each experiment.

FIGURE 4.20: Mini pleat filter showing progressive loading – face velocity 2.5cm/s
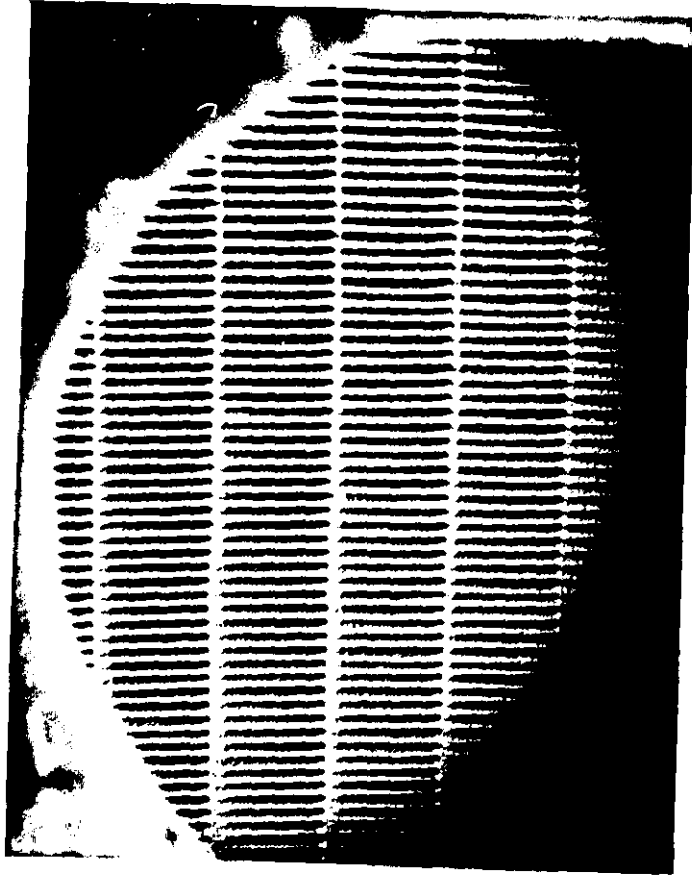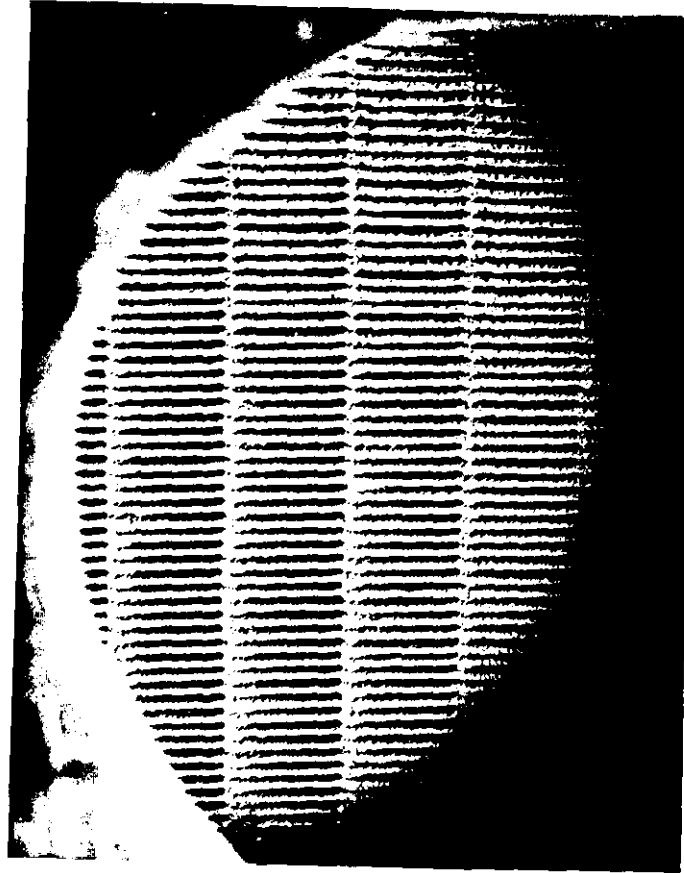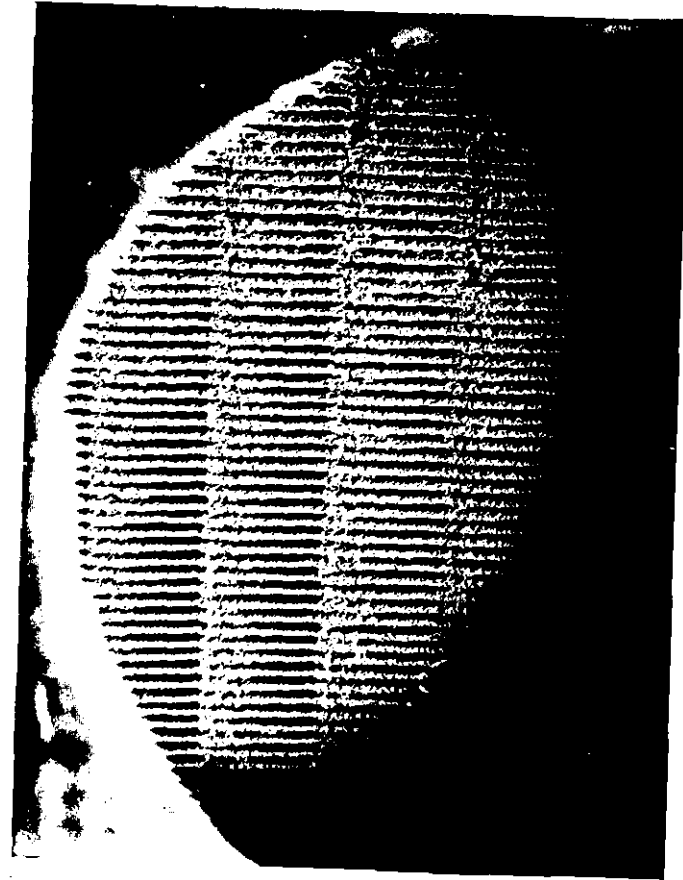
(a)   (b)   (c)

FIGURE 4.20: Continued
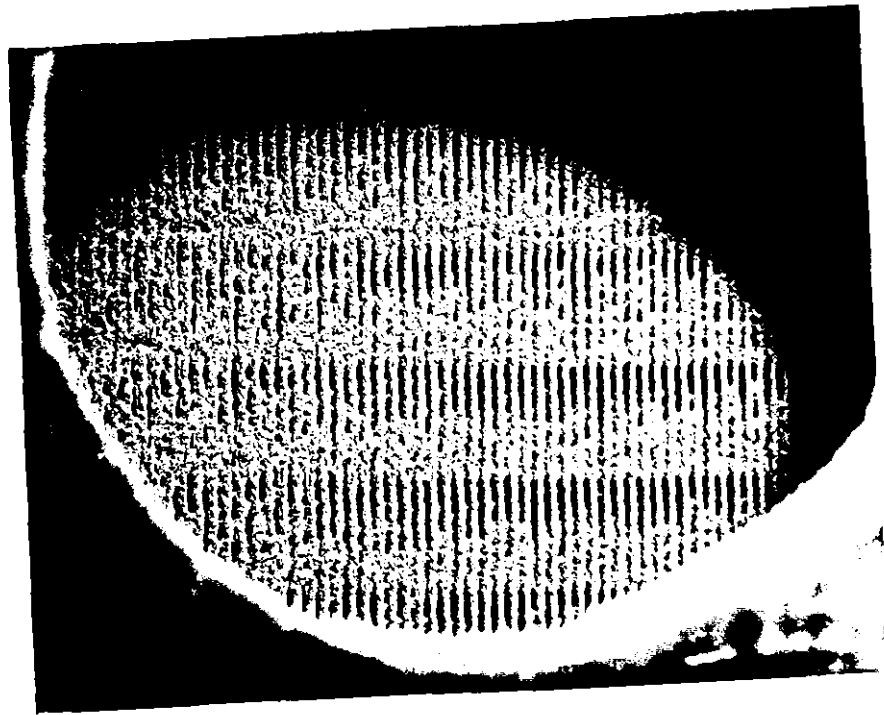
(d)
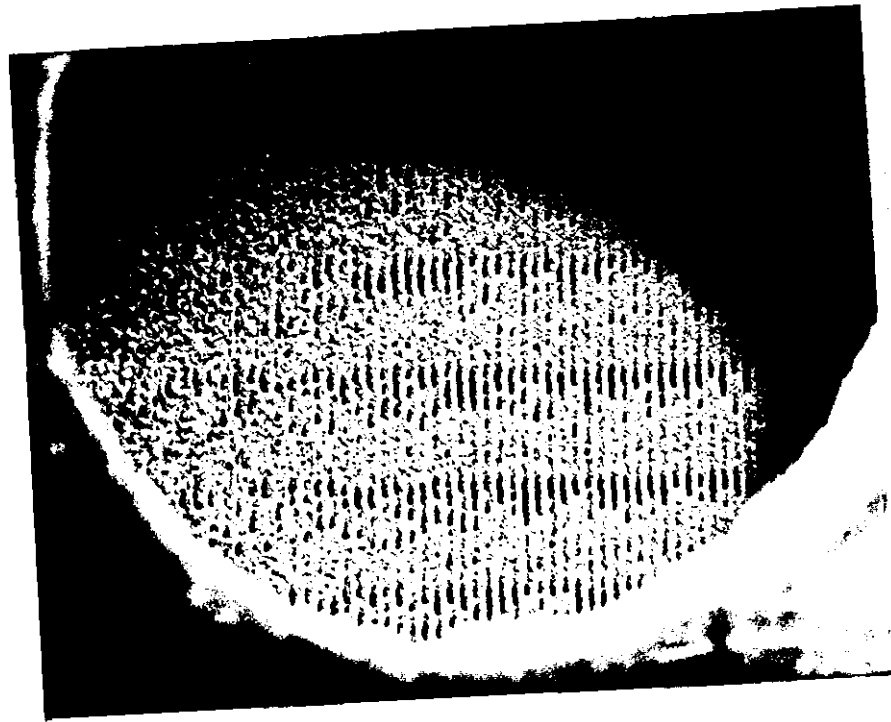
(e)
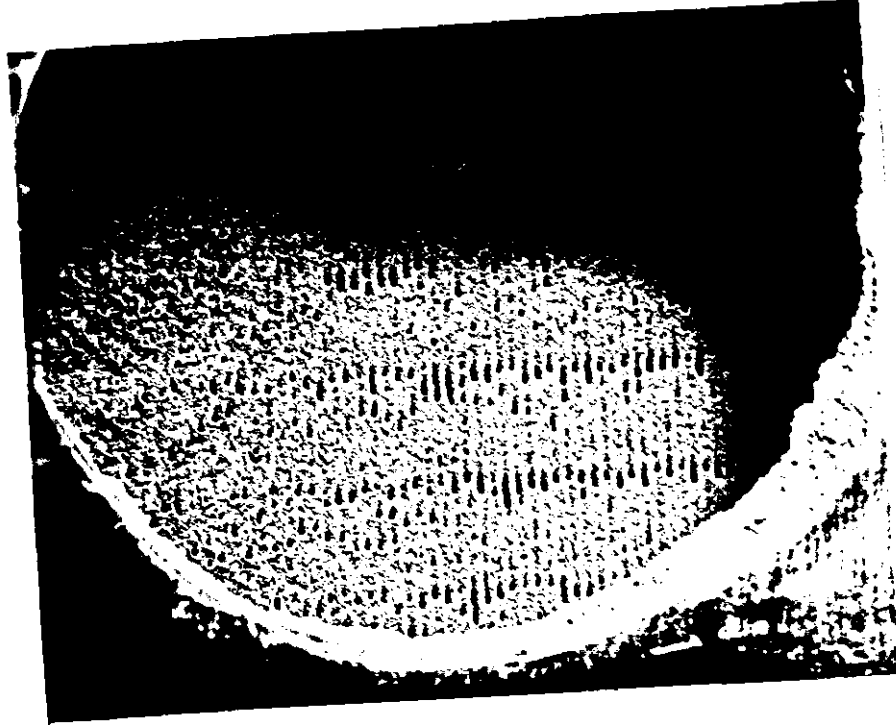
(f)

FIGURE4·20: Continued
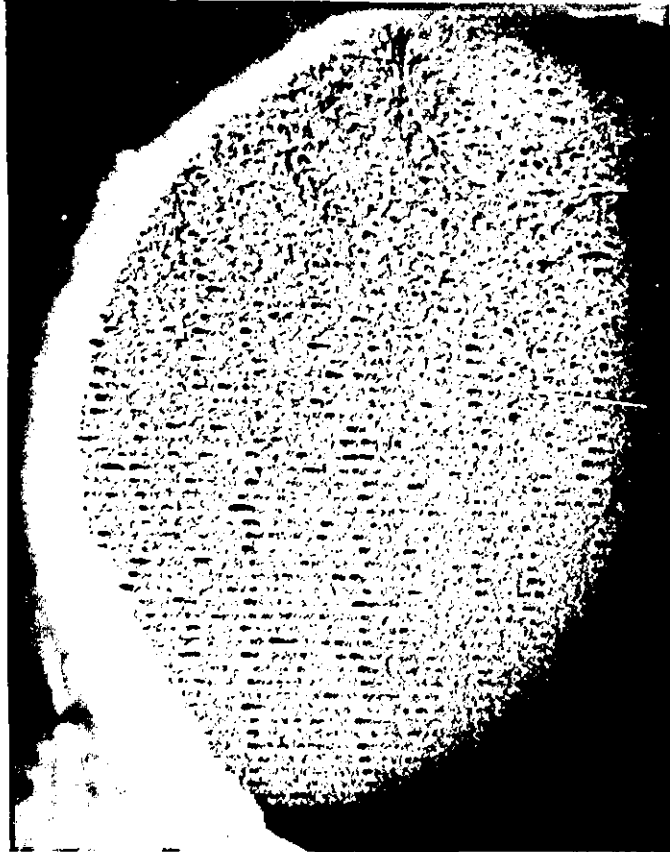
(g)

(h)
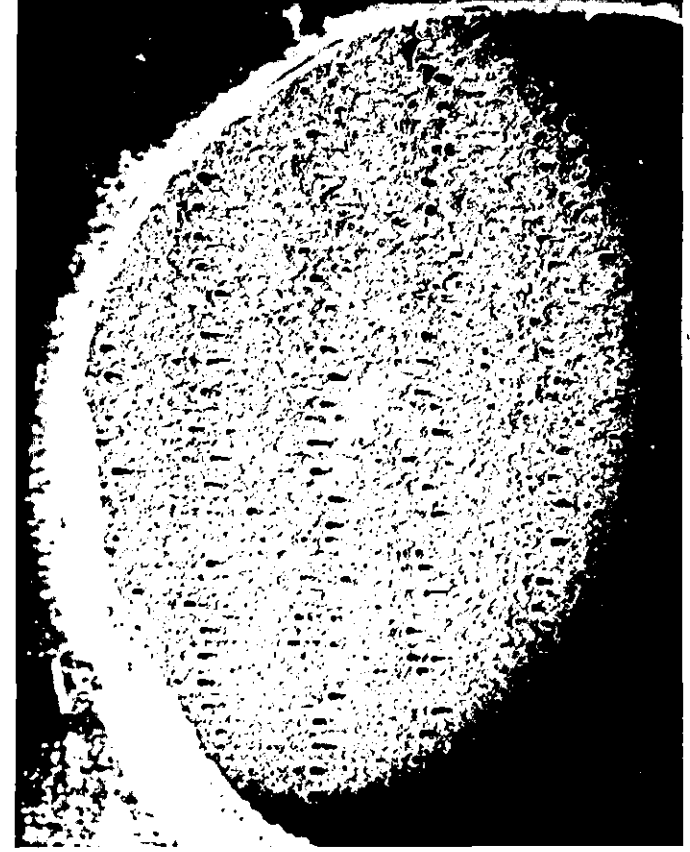
(i)

FIGURE 4.21: Complete loading of mini pleat filter — face velocity 2.5 cm/s
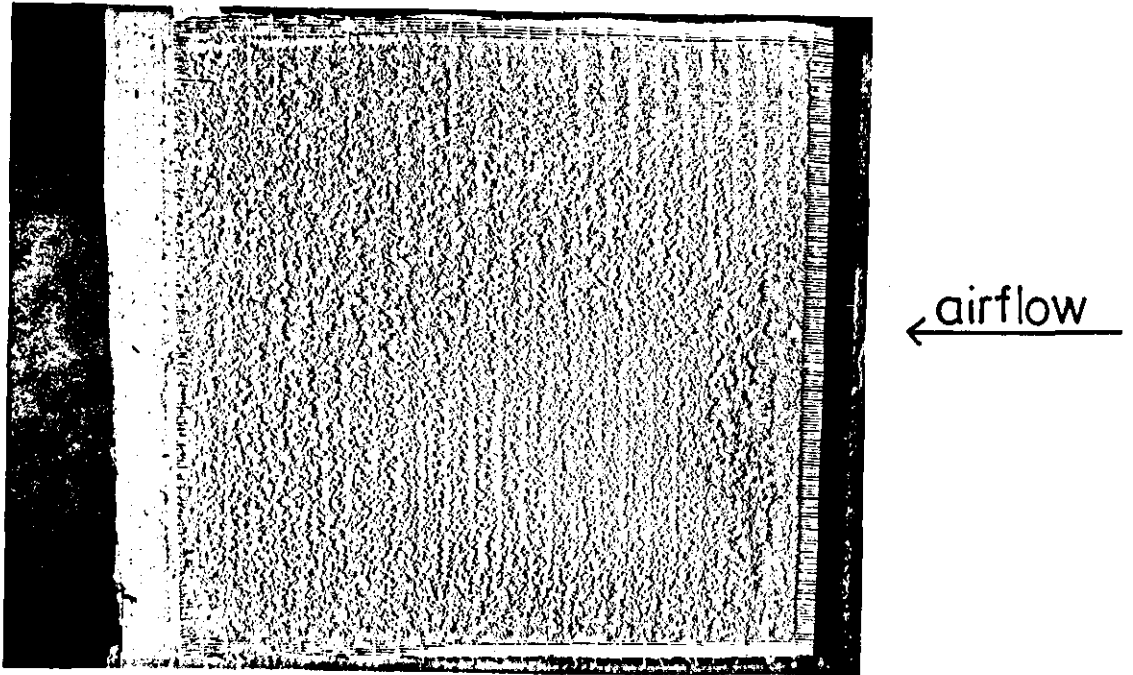
←airflow
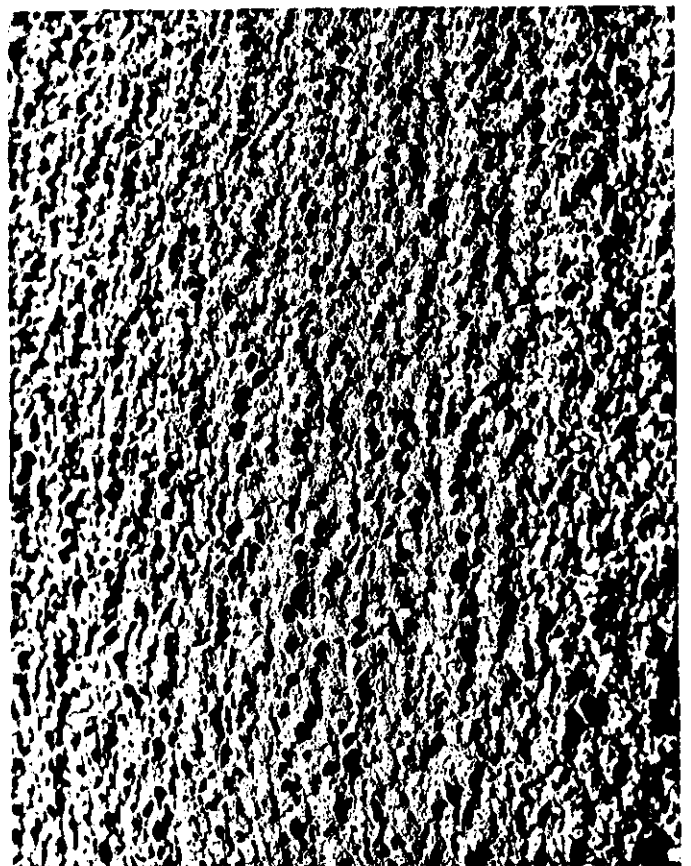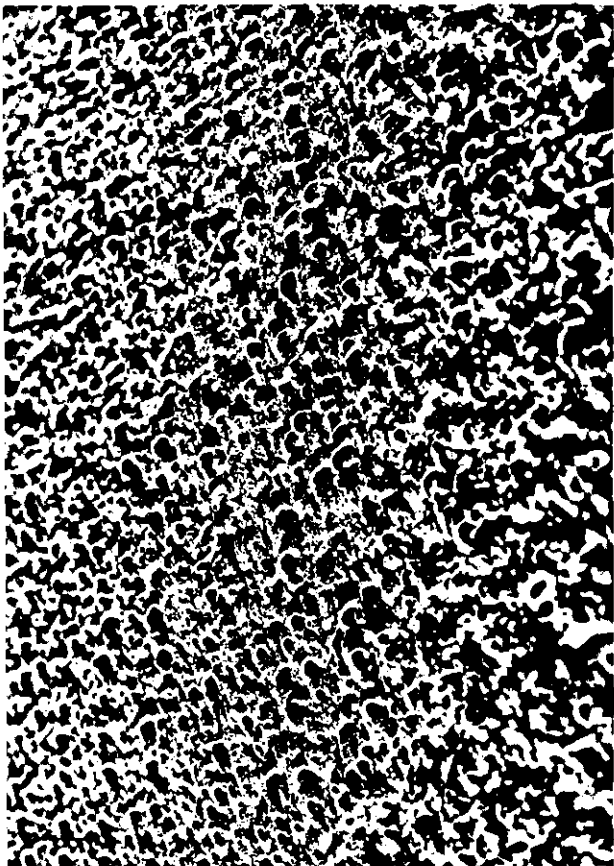
(a) Overall view

(b) + (c) Close up of filter surface

FIGURE 4.21: Continued

(d)+(e) View of holes formed on surface
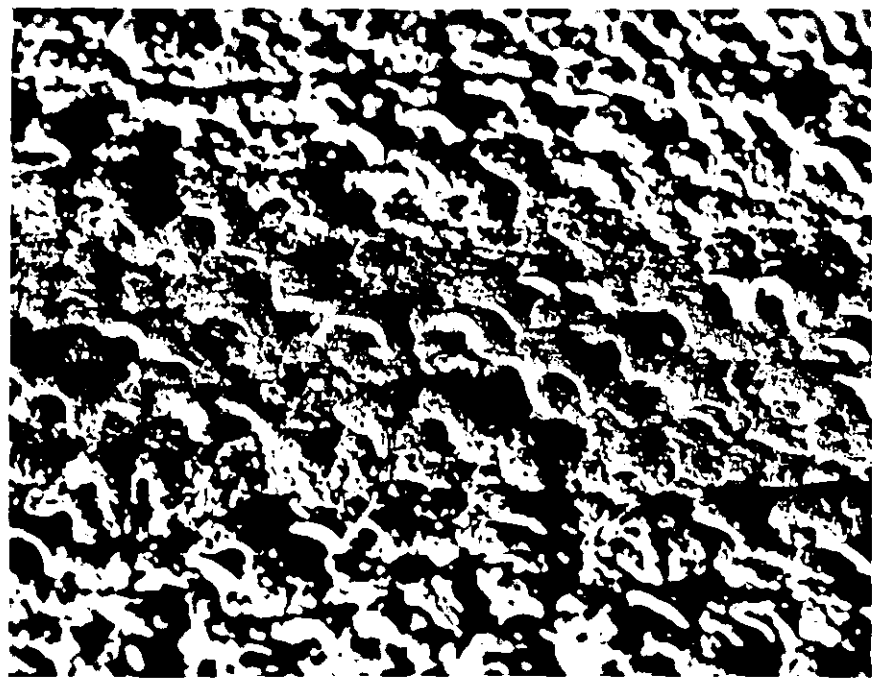
airflow

FIGURE 4·22: Deep pleat filter loaded at 2·5cm/s
(BS 2831 No.2 dust)
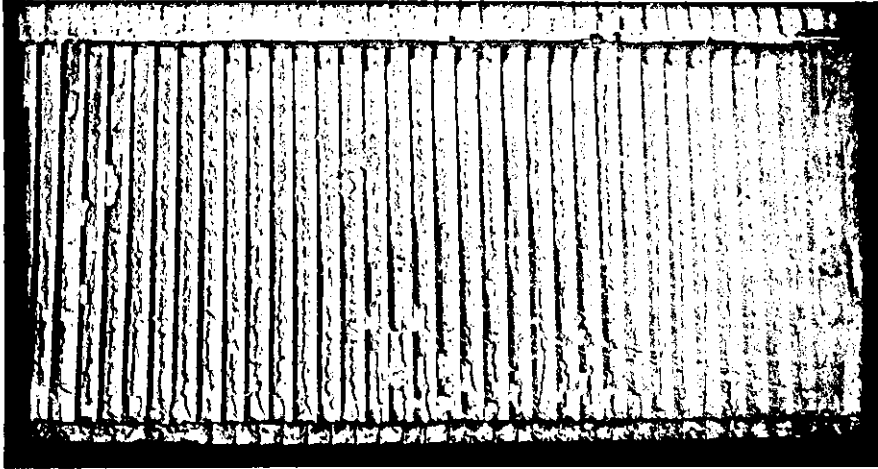
(a) Overall view - filter sheet
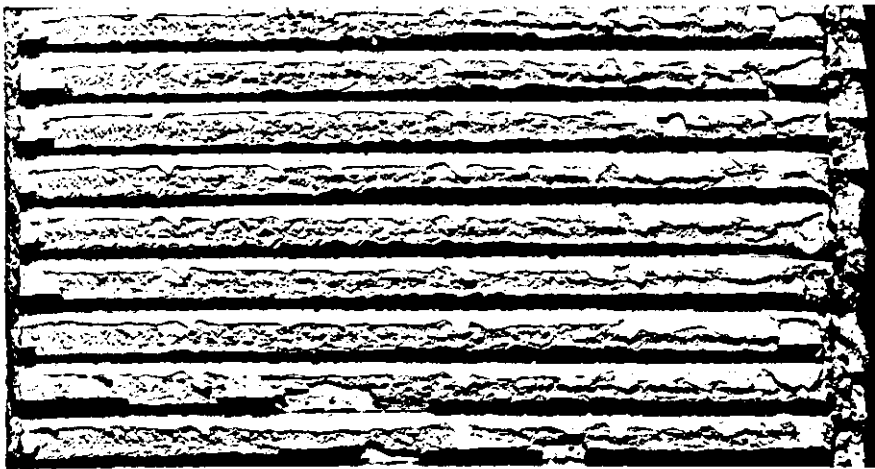
(b) Overall view - filter spacer

(c) Close up of channel entrance
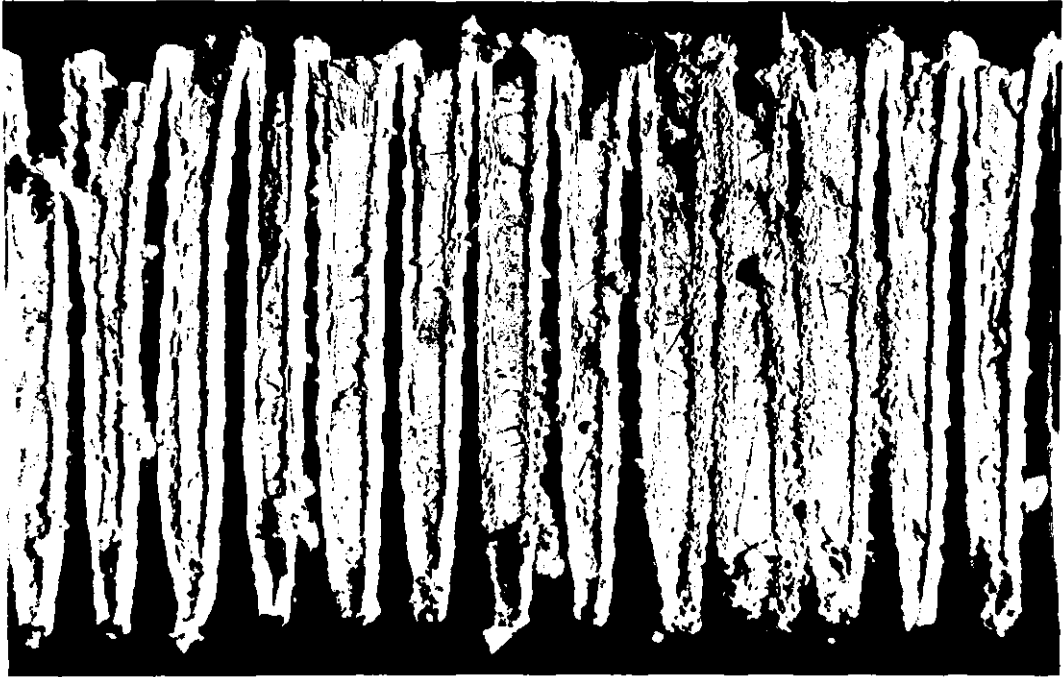
FIGURE 4.23: Cross-section view of loaded
mini pleat channels

FIGURE 4·24: Comparison of dust sizes found inside and outside a mini pleat channel

Legend:
- ○ Outside
- × Inside

Y-axis: Cumulative weight percent
X-axis: Particle Size (μm)
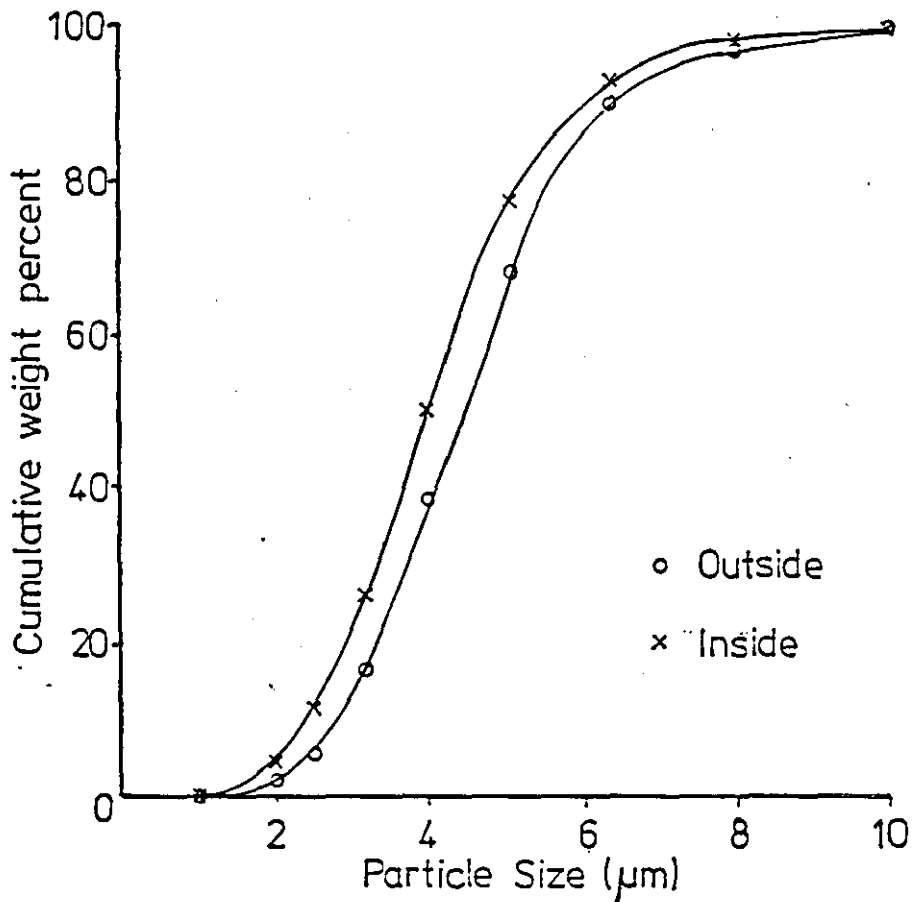
FIGURE 4·25: Dust weight distribution along a deep pleat filter channel

Legend:
- —— 3 μm 2·5 cm/s
- —·— BS No.2 1·25 cm/s
- — — " " 2·5 "
- ----- " " 3·5 "

Y-axis: % of total dust weight
X-axis: Channel section (Front, Middle, Back)
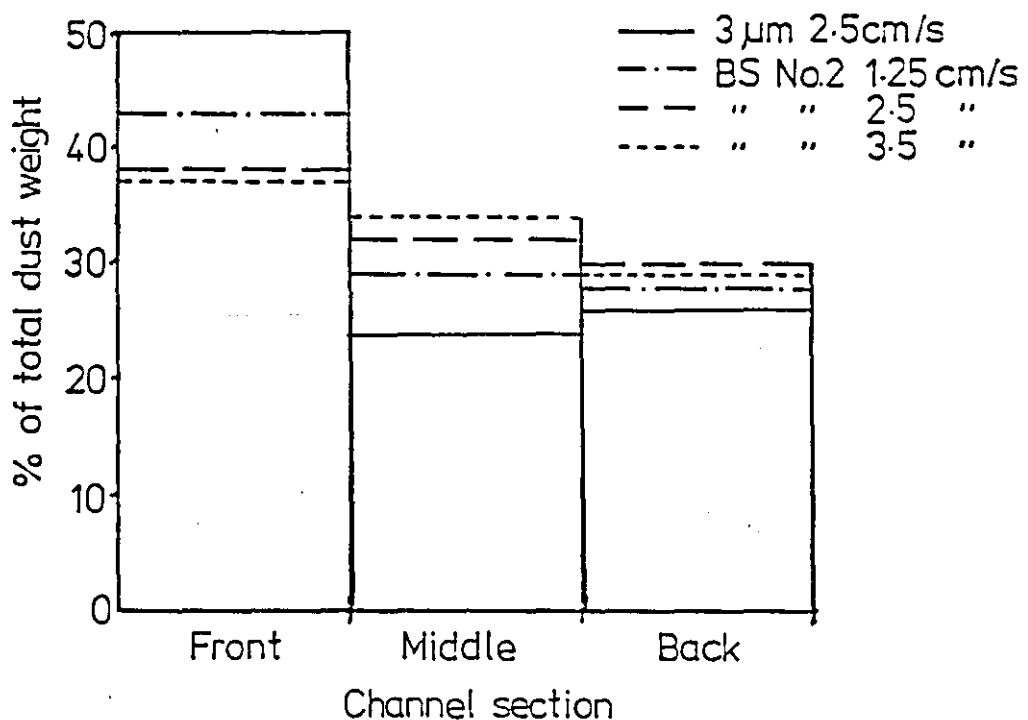
4.2.3. Discussion and conclusions

The pressure drop response to loading did not agree exactly with
the initial theoretical prediction (see figures 2.5 and 2.6 and
appendix 2.3). The deep pleat response. is reasonably close to theory
suggesting it will need only minor modifications. From the deep pleat
photographs and dust weight distributions two major effects should be
included in the theoretical derivation.

(i) The entrance effect, particularly with regard to build up on the
     outside of the entrance and the much higher dust loading found in
     channel entrance.

(ii) The effect of triangular channel flow in a real filter as opposed
     to the simple parallel plate model which had been used to
     calculate the channel pressure drop theoretically.

The deep pleat arrangement does filter uniformly as assumed in
theory. The gravity effect, although observed, does not appear to have
a large detrimental influence on this.

The minipleat design, however, did not show good agreement with
theory. The actual prediction was very dependent on dust packing
density but using a bulk density figure obtained from small scale
work, and similar to that measured from a deep-pleat filter, the
response was very different to experiment. Not only was the final
load under predicted but the response itself showed a far more rapid
asymptotic rise in pressure drop from a gradual start rather than the
steadily increasing exponential type curve observed in practice.

Considering the photographic and dust analysis evidence the dust
deposition is clearly non-uniform. Several factors are apparent:

(i) ·Dust is collected on the folds of media on the filter face as
     well as within the channel.

(ii) Dust shows preferential accumulation at the far edges of each channel where the stitching seams maintain the channel spacing.

As the loading progresses this deposition is increased eventually resulting in holes being formed towards the near edge of the channel. The tests were carried out with the channels in a horizontal orientation as is common practice. In a test with the mini pleat channels arranged vertically these holes were shown to be central.

The channels are rectangular sections bounded by the stitching seams which clearly produce end wall effects. It is postulated that circulating secondary flows are set up which cause centrifugal separation. When in the horizontal orientation the deposit will form preferentially on the far edge of the section due to the induced inertial behaviour of the gas entering the channel from the main flow. The channel will fill from both edges inwards and as the channel closes a hole will form close to the near edge. When in the vertical orientation the gas entry to the section will be symmetrical so the secondary flows will set up at each edge and the hole will form centrally.

An estimation of the feasibility of this hypothesis of centrifugal separation was made by comparing the channel section with a typical sampling cyclone. The important parameter governing a cyclone's performance is its Stokes number. A 4 cm diameter sampling cyclone could be considered to have a 50% cut size at 1.5 μm for unit density particles at inlet velocities of about 20 m/s. The channel section can be viewed as a 2 cm diameter cyclone with an inlet velocity in the order of 1 m/s (for 2·5 cm/s filter face velocity). For aluminium oxide particles a comparison of the Stokes numbers of these hypothetical cyclones gives a cut size in the order of 2 - 2.5 μm for the channel section. This indicates the possibility of centrifugal effects.

. The channel inlet area progressively reduces with load and hence the inlet velocity will increase so reducing the particle cut size for inertial classification. The hole will behave as a sampler in a cross

wind. In practice this entrance hole appears to diminish in size until preclassification occurs on the lip and almost clean gas enters the filter channel.

(iii) Deposition continues on the outside of the channels with the deposition around the holes being particularly prevalent. The holes continue to exist with a dust wall gradually forming round them and eventually this begins to cover the top surface while maintaining a side entrance to each hole.

(iv) It was experimentally found (appendix 4.2.2) that the dust on the outside of the channel was coarser than that inside, agreeing with the above.

(v) The above effects were observed to be velocity dependent. Increasing the velocity emphasised the deposition effect on the far side wall of the channel whereas at lower velocities the holes formed tended to be more central.

(vi) The pressure drop response was more rapid with finer dusts. This is expected because of the reduced permeability of a bed of finer particulates.

(vii) Noticeable at the lowest velocity of 1.25 cm/s was a deviation from the normal trend of the responses. After the onset of channel clogging the pressure drop rose relatively quickly. This could be due to a packing effect; the lower the velocity the more loosely packed the dust appears visually. However when tests were carried out experimentally measuring bulk density variation with velocities upto about 5 cm/s no significant difference was observed - section 3.5. It is possible that dust packing is affected by the velocity entering the channel as well as the face velocity through the media. In the case of the mini pleat configuration, inertial impaction of particles during formation of the dust layer may enhance packing. This effect was not covered by the experiments described in section 3.5 and will in any case be a complex function of loading - as entry velocity increases the influence of the mechanisms will

increase. Unfortunately it was not possible to dissect the mini pleat filter without significantly disturbing the dust layer so the voidage could not be measured and the dust packing determined accurately.

(viii) It was observed that the upstream channels full of dust expanded at the expense of those downstream. Therefore they were loaded with more dust than was anticipated from their original dimensions. This effect is difficult to quantify other than visually and will depend strongly on the load of dust, inertial level of filtration and mechanical properties of the filter. A sample was measured using a travelling microscope and expansion estimated at about 20% of the original channel volume (appendix 4.2.2).

From these observations the theoretical modelling of the deep and mini pleat filters can be improved. For the deep pleat filter an estimation of the entrance effects and using flow down a triangular channel are attempted. With the mini pleat design, deposition on the media folds on the filter face is taken into account. Also pressure drop due to flow through a rectangular channel of finite width is incorporated into the mini pleat analysis. An attempt to quantify the apparent inertial deposition due to centrifugal forces was considered feasible. However an empirical basis is used in the model presented due to the complex computing procedures required to develop a universal application of the effect.

The effects (vii) and (viii) are more difficult to include rigorously as they are dependant on the loading's past history. Consequently semi-empirical correction factors for the packing density and the extra load achieved in the channel, by expansion over its normal dimensions, are incorporated.

These conclusions therefore lead to the theoretical derivations of 2.4 and 2.5 and the resulting improvement in prediction of behaviour of deep and mini pleat design filters. It is these models which are referred to in chapter 5.

CHAPTER 5

5. Conclusions and recommendations for further work

The objective of this work was to determine the effects of media arrangement on the behaviour of HEPA filters. It is convenient to summarise the major conclusions of the work under a series of headings corresponding to the earlier chapters in the report.

5.1. Conclusions

5.1.1. Literature review

Use of the "mini pleat" concept of media arrangement in HEPA filter units allows a greater filtration surface area to be accommodated within the filter case. Published experimental evidence on the effectiveness of these designs was contradictory but strongly suggested that the benefit with respect to life expectancy is much less than would be predicted from a consideration of area enhancement alone. This relatively poor behaviour suggests that an optimum design may exist, the application of which could result in considerable financial savings. It is necessary, however, to establish the factors and mechanisms related to media arrangement which influence behaviour before any progress can be made towards this objective.

5.1.2. Loading characteristics of media

As dust accumulates on the surface of samples of media a linear relationship exists between load and pressure drop. Initially the relationship is exponential as the dust bed is established. The extent of this region depends on dust size and diminishes with increasing size. The effect of dust size and face velocity on the loading characteristics was measured and correlated. The density of the dust bed was also measured.

5.1.3. Behaviour of filter units

5.1.3.1. Dust distribution in deep pleat filter

Theoretical predictions for particle trajectories in a channel, of dimensions similar to that of a deep pleat channel, showed that:-

(i)   Particle inertia is negligible for aluminium oxide particles smaller than 25 microns diameter

(ii)   Particle sedimentation is evident for particles greater than 5 microns.

(iii)   The spacers which are present in deep pleat filters provide additional surface for filtration due to sedimentation effects alone. This sedimentation will reduce with respect to distance along a channel as particles will be drawn towards the filtration surface and hence the settling distance required to reach the spacer will increase (due to the triangular shape of the spacers). This sedimentation loss will similarly reduce the density of dust deposit collected on the media surface with respect to distance along the channel. However it could be anticipated that this effect will be self corrective due to increased resistance at points of higher dust deposit.

(iv)   The major overall influence on dust deposition is the air velocity distribution. All other effects are relatively insignificant by comparison.

Thus the theoretical prediction of dust deposition was a uniform deposit of similar size distribution with minor sedimentation effects apparent on the spacers. Infact experimental work on deep pleat filters, 4.1., generally confirmed this. The dust deposit was uniform in density and size distribution with one discrepancy. An increase in dust density was observed at the channel entrance. The magnesium chloride aerosol test verified the dust deposition was following the air flow distribution. This entrance effect is considered theoretically in 2.4 and discussed later.

The gravity effect was shown to exist in practice with dust collection observed on the spacers and at the joint between the spacers and media where ridges of dust were formed. That collected on the spacer was slightly coarser than on the media.

5.1.3.2. Pressure drop effects with increasing load for HEPA filters

Theory was developed to predict pressure drop build up in a HEPA filter assuming a uniform dust deposit on the filter media at all points, whether this be a deep pleat or minipleat design. In order to predict the pressure drop rise due to the media and dust deposit the experimental data on dust loading HEPA filter media samples (chapter 3) was used. Pressure drop lost due to air entering and flowing down a channel was also accounted for. This theory does indicate that there is an optimum area and arrangement of filter media which will minimise the rate of pressure drop build up for a given flowrate and aerosol challenge.

To verify the accuracy of the theoretical predictions experiments were carried out (section 4.2) in loading dust onto both deep pleat and minipleat designs of HEPA filters. Pressure drop was monitored with increasing load and observations (given as photographs in chapter 4) made during and after loading. Different test dusts and face velocities were used to examine dust size and velocity effects.

The results for the deep pleat design showed reasonable agreement with the theoretical prediction. The bulk density of the dust collected on the media surface was accurately measured enabling detailed prediction of the restriction in channel width as the dust layer built up.

There is an entrance effect. A build up of dust was seen outside the entrance and a higher deposit was found for the initial length of the channel. A theoretical trajectory analysis confirmed inertial impaction on the front edge of the pleat and a higher concentration of particles near the media surface at the channel entrance.

The results of the tests on the minipleat design of filter showed poor agreement with the initial theoretical predictions. Whereas it is reasonable to assume uniform dust deposition for a deep pleat filter the experiments on a minipleat filter clearly demonstrated this assumption does not hold. Several factors are apparent, as detailed in 4.2.3.

(i)   Excessive quantities of dust collected on the front folds of the media.

(ii)   Dust showed centrifugal action in entering the minipleat channels resulting in preferential dust deposition towards the far edge of the channel. This causes a premature blockage of the far side of the channel and the formation of holes towards the near edge. Eventually the dust forms a cap over the hole at the near side while maintaining a side entrance for air flow and deposition continues around this. At this point only very fine particles are entering the channel via the hole while the dust is inertially classified and deposited around the hole. This effect was also seen to increase with velocity.

(iii) Dust packing and so dust size and bulk density appear critical in the mini pleat design in terms of determining the rate of channel blockage and so pressure drop rise.

(iv)   Expansion of channels on the dust loaded side of the filter occurs at the expense of those downstream.

The theory was modified to include the above effects. The pressure drop loss due to flow down a channel was calculated on the basis of a rectangular channel. It was assumed that filtration could take place through the front face of the filter as observed and as would be expected from the predictions of trajectory analyses carried out for particles entering a deep pleat filter channel. Inertial deposition was confirmed theoretically as the mechanism responsible for the phenomena reported under (ii) above. A model of dust build up is proposed in which a permanent clear hole remains in the channel in which no dust is deposited whereas deposition continues uniformly on

the remainder of the channel's filtration area. Empirical corrections are also made for the observed channel expansion and the bulk density effect. It is shown in chapter 2 that after these modifications the minipleat theory model predicts, with reasonable accuracy, the pressure drop characteristics with increasing surface dust load.

The significant factors in determining filter performance have been shown as:-

    (i)   The media/dust layer pressure drop

    (ii)   The pressure drop due to flow along a channel

   (iii)   The entrance effect on dust deposition:

         a)   due to flow effects directly into the channel

         b)   due to induced centrifugal flow (mini pleat design).

    (iv)   the packing of the dust layer

    (v)   Pressure effects which may change channel dimensions (only observed in the mini pleat design).

Overall a model has been developed which accounts for these factors and will allow the study of different geometrical arrangements of filter media for either deep pleat or mini pleat configurations. However, the model has used experimental correlations and therefore recommendations for further work to eliminate or refine these have been proposed in 5.2.

It must be emphasised that the effects described vary with surface filtration. If depth filtration only was anticipated then the model could be used to predict the clean pressure drop of an arrangement. Beyond this all indications are that the filtration would continue with reasonable uniformity, whatever the media arrangement, and pressure drop would increase as predicted by tests on media samples under the same conditions of filtration. Hence the filter life could be maximised from its clean pressure drop alone.

5.2. Recommendations for further work

The application of this work and models developed would benefit from further research into the areas given below:

(i) A model which can predict the pressure drop increase as filter media of a given fibre size distribution is loaded with an aerosol of given size distribution. This will eliminate the need for the empirical correlations developed in chapter 3 which are dust and media dependent.

(ii) Detailed knowledge of the size distribution of the aerosol likely to challenge the HEPA filter. In the nuclear industry in particular this knowledge is needed. Once this aerosol size is established then the arguements for depth or surface filtration will be known and appropriate media arrangement designs could be examined.

(iii) Accurate knowledge of the relationship between dust bulk density, dust size distribution and face velocity is needed.

(iv) More detailed examination of the observed channel expansion effect in minipleat filters should be made. It would be particularly useful if it was known how the channel expanded with respect to loading.

(v) Tapered spaces may improve the deep pleat filter as this would allow an increase in channel entrance spacing and so compensate for preferential deposition near the inlet. It is suggested that a method be developed to cater for this adaptation in the deep pleat model.

(vi) As a general design point, it would be possible to increase the area available for filtration if the area covered by media/spacer contacts is reduced. Particularly in deep pleat designs up to 10% of the area may be lost due to misalignment of the spacers on the upstream and downstream sides of the filter channels.

(vii)   The volume of channel downstream from the media remains dust free. Designs developed should attempt to minimise this volume.

(viii)   The theoretical model should be developed further and design optimisation studies carried out to investigate the possible advantages to be gained. The cost effectiveness of developing custom made optimum designs could then be quantified.

(ix)   The analyses carried out on rectangular pleated units should be extended to include circular filter units.

REFERENCES

1. AFIFY E.M., MOHAMED M.H., "Collection efficiency and pressure drop of needle punched filters", J. Eng. Ind., 98 (2), 1976, 675-680.

2. AIRMAN T., TANG L., "Collection of aerosol particles by fabric filters in an electrostatic field"; ATMOS ENVIRON. 10 (3), 1976, 205-210.

3. AREFF"EV K.M., GOLOVANOV V.V., LESYUIS A.R., KHOMCHENKOV B.M., BEMEKHAN L., "Experimental determination of filter fabric gas permeability at low pressures", SOV. J. NON FERROUS MET, 17, (7), 1976, 29-30.

4. ARIMAN T., HELFRITCH D.J., "How relative humidity cuts pressure drop in fabric filters", FILTR. SEP. 14 (2), 1977, 127-130.

5. ARIMAN T., "Aerosol filtration by fibrous filters in an electrostatic field", MULTIPHASE FLOW AND HEAT TRAN SYMP., WORKSHOP MIAMI BEACH 1979. EXTENDED ABSTRACT: CORAL GABLES, UNIV. MIAMI, 1979, 527-528.

6. ARZIEV Zh, SADOVSKI B.F., IMON A.D., SEREBRYAKOA G.A., TEKENOV Zh.Tj. "The adhesion of aerosol particles to thin fibres", DOKL. PHYS. CHEM. 241 (1-3), 1978, 657-659.

7. BALASUBRAMANIAN M., MEISEN A., "A note on the diffusional deposition of aerosol particles in packed beds", J. AEROSOL, Sci.,6 (6), 1975, 461-463.

8. BARDOT D.T., TIEN C., WANG. C., "Accumulation of solid particles on single fibres exposed to aerosol flows"; A.I.Ch.E.J., 26 (2), 1980, 289-292.

9. BELMONT M. R., CARPENTER P.W., "A novel approximate calculation of the flow through absolute filters", PAP. FILTR, 2nd WORLD CONGRESS, LONDON 1979. CROYDON. UPLANDS. 1979.

10. BIRD R.B., STEWART W.E., LIGHTFOOT E.N., "Transport Phenomena" 1960,, J. Wiley, N. York.

11. BRAGG G.M., PEARSON B.M., "A model of aerosol filtration by fibrous filters", IND. ENG. CHEM., PROCESS RES. DEV. 18 (1), 1979, 171-177.

12. BRINKMAN H.C., "On the permeability of media consisting of closely packed porous particles" APPL. SSIENT. RES. 1A, 1948, 81-86.

13. BROOM G.P., "Ahesion of particles in fibrous air filters"; Ph.D. THESIS, LOUGHBOROUGH, 1978. BLLD D25448/79

14. BROOM G.P.; "Adhesion of particles in fibrous air filters"; FILTR. SEP., 16 (6), 1979, 661-669.

15. BROWN R.C., "The use of the variational principle in the solution of Stokes flow problems in fibrous filters", J.PHYS.D.APPL.PHYS., 16 (5), 1983, 743-754.

16. BURCHSTED C.A.: "Experience in the quality assurance testing of HEPA filters", FILTRATION 3rd WORLD CONGR., FILTR. SOC., 1982, vol 1, 15-22.

17. BURKHARDT W.M., SHARMA L.K.: "An experimental investigation of the flow behind fibrous filters"; FILTRATION: 3rd WORLD CONGR., FILTR. SOC., 1982, VOL 1, 43-51.

18. CARMAN P.C., "Fluid flow through granular beds", TRANS. I.CHEM.E. 15, 1937, 150-166.

19. CAVANAGH P., "Comments on: "The role of Brownian vibrations in ultrathin fibres in aerosol filtration" bu L.V. Radushkevich", J.COLLOID INTER. SCI., 37 (2), 1971, 501-502.

20. CHEN, C.Y., "Filtration of aerosols by fibrous media"; CHEM. REV., 55, 1955, 595-623.

21. CHIANG H.W. TIEN C., "Deposition of Brownian particles in packed beds", CHEM. ENG., SCI., 37 (8), 1982, 1159-1171.

22. CLIFT R., "Fundamental processes in gas filtration"; 8th AUSTRALIAN FLUID MECHANICS CONF., NEWCASTLE 1983, AUST.MECH.ENG.TRANSACTION.

23. COURY J.R., "Electrostatic effects in granular bed filtration of gases", Ph.D. Thesis, UNIV. OF CAMBRIDGE, 1983.

24. CRANE R.I., EVANS R.L.: "Inertial deposition of particles in a bent pipe"; J. AEROSOL SCI., 8 (13), 1977, 161-170.

25. CUNNINGHAM J., GREEN E. Private Communication.

26. DAHNEKE B., "The capture of aerosol particles by surfaces", J. COLLOID. INTER. SCI., 37 (2), 1971, 342-353.

27. DAVIES, C.N. "The thermosis of liquids through porous materials", DISC FARADAY SOC., 3, 1948, 86-129.

28. DAVIES C.N.: "The separation of airborne dust and particles", PROC. INST. MECH. ENG. 113, 1952, 185-198.

29. DAVIES C.N., "Aeorosl Science" 1966, Academic Press.

30. DAVIES W.I.; "Air filter media testing utilising uniform latex spheres", FILTR. SEP., 18 (2), 1981, 143-147.

31. DONOVAN R.P., DANIEL B.E., TURNER J.H.; "EPA fabric filtration studies part II: Performance of filter bags made from expanded PTFE laminate", USNTIS REP PB 263-132, 1976, 53p.

32. DORMAN R.G., In "Aerosol Science", ed., C.N. DAVIES, 1966. ACADEMIC PRESS, LONDON. 195-222.

33. DORMAN R.G., "Filtration theory", SEMINAR ON HIGH EFFICIENCY FILTR., AIX-EN-PROVENCE, 1976. LUXEMBROUG, COM. EURO. COM, 1977.

34. DORMAN R.G., EDWARDS J., POLYNTING R., "The sodium chloride aerosol test for high efficiency air filter installations", SEMINAR ON HIGH EFFICIENCY FILTR., AIX-EN-PROVENCE, 1976. LUXEMBOURG, COM. EURO COM, 1977.

35. DORMAN R.G., DYMENT J., POLYNTING R., WEBB I.J., "High efficiency air filter testing in factory or laboratory", FILTR. SEP. 15 (5), 1978, 410-416.

36. DORMAN, R.G., "High efficiency air filtration", PAP. FILTR. 2nd WORLD CONGR., LONDON 1979. CROYDON, UPLANDS, 1979, 223-228.

37. ELLIOT M.N., HORSLEY D.M.C. "Gas cleaning in nuclear power industry", PREP. REMOVAL FINE PART IN GAS STREAMS SYMNP. MANCHESTER, 1976 RUGBY, I.CHEM.

38. ELLIOT M.N., HORSLEY D.M.C., POWELL R.M., "Research and development topics in gas cleaning for fuel reprocessing plant", SEMINAR ON HIGH EFFICIENCY FILTR., AIX-EN-PROVENCE, 1976., COM. EURO. COM. 1977.

39. EMI H., OKUYAMA K., ADACHI M., "The effect of neighbouring fibres on the single fibre inertia-interceptive efficiency of aerosols"; J.CHEM.ENG. JAPAN, 10 (2), 1977, 148-153.

40. EMI H., KANAOKA C., KUWABARA Y., "The diffusional efficiency of single fibres for aerosol over a wide range of Reynolds numbers"; PORC. INT. CONF. POWDER AND BULK SOLIDS HAND AND PROC., PHILADELPHIA, 1979. CHICAGO, IND. SCI. MGI, 1979, 515-516.

41. EMI H., KANAOKA C.M KUWABARA Y., "The diffusion collection efficiency of fibres for aerosol over a wide range of Reynolds numbers", J. AEROSOLS SCI., 13 (5), 1982, 403-413.

42. ERGUN S., "Fluid flow through packed columns", Chem. Eng. Prog. 48(1952), 89-94.

43. FIRST M.W., RUDNICK S.N., "Performance of 1000 and 1800 cfm HEPA filters on long exposure to low atmospheric dust loadings", PAP. FILTR., 2nd WORLD CONGR., LONDON, 1979. CROYDON, UPLANDS.

44. FIRST M.W., RUDNICK .S.N. "Performance of 1000 and 1800 cfm HEPA filters on long exposure to low atmoshperic dust loadings II", AEC/ERDA/DOE 16th NUCLEAR AIR CLEAN CON.F. SAN DIEGO, 1980, USNTIS CONF. 801039, 682 - 696.

45. FIRST M.W., PRICE J.M., "Performance of 1000 and 1800 cfm HEPA filters on long exposure to low atmospheric dust laodings III", AEC/ERUA/DOE 17th NUCLEAR AIR CLEAN CONF.

46. FRANKLIN H., KNUTSON E.O., "A humidity effect in the resistance of loaded fibrous filters", ATMOS. ENVIRON., 10 (10), 1976, 911-912.

47. FREDERICK E.R., "Some recent experiences with fabric filters for particulate collection", J. AIR POLLUT. CONTROL ASSOC., 28 (4) , 1978, 401-404.

48. FRIEDLANDER S.K., "Mass and heat transfer to single spheres and cylinders at low Reynolds numbers", A.I.Ch.E.J.,3 (1), 1957, 43-48.

49. FRIEDLANDER S.K., 'Theory of aerosol filtration", IND. ENG. CHEM., 50 (8), 1958, 1161-1164.

50. FUCHS, N.A, STECHKINA I.B., "A note on the theory of fibrous aerosol filters", ANN. OCCUP. HYG., 6, 1963, 27-30.

51. GEBHART J., ROTH C., STANLHOFFEN W., "Filtration properties of glass bead media for aerosol particles in the 0.1 - 2 μm size range", J.AEROSOL SCI., 4, 1973, 355-371.

52. GILLESPIE T., "Role of electrical forces in the filtration of aerosols by fibre filters", J. COLLOID SCI. 10, 1955, 299-314.

53. GOLDFIELD J., GANDHI K., "Influence of fibre diameter on pressure drop and filtration efficiency of glass fibre media", J.AIR POLLUT.CONTROL ASSOC., 31 (1), 1981, 95-97.

54. GREGORY W.S. "Pressure transients across HEPA filters", SEMINAR ON HIGH EFFICIENCY AEROSOL FILTR., AIX-EN-PROVENCE, 1976, COM EURO. COMN.

55. GREGORY W.S., HORAK H.L., "HEPA filtration efficiency during large pressure transient", J.ENVIRON SCI., 22 (1), 1979,m 16-18+27.

56. GRIFFIN F.O., MEISEN A., "Impaction of spherical particles on cylinders at moderate Reynolds numbers", CHEM. ENG. SCI., 28, 1973, 2155-2164.

57. GUNN C.A., EATON D.M., "HEPA filter performance comparative study", PROC 14th ERDA AIR CLEAN. CONF., SUN VALLEY, 1976. USNTIS REP. CONF. 760822, 1976, 630-661.

58. GUTFINGER C., TARDOS G.I., ABAUF N.: "Analytical and experimental studies on granular bed filtration"; USNTIS REP PB-295-288, 1979, 243-277.

59. HAPPEL J., "Viscous flow in multiparticle systems: slow motion of fluids relative to beds of spherical particles"; A.I.CH.E.J., 4, (2), 1958, 197-201.

60. HAPPEL J., "Viscous flow relative to arrays of cylinders"; A.I.CH.E.J., 5 (2), 1959, 174-177.

61. HAPPEL J., & BRENNER H., "Low Reynolds Number Hydrodynamics" 1965 Prentice Hall.

62. HARROP J.A., STENHOUSE J.I.T.; "The theoretical prediction of inertial impaction efficiencies in fibrous filters"; CHEM. ENG. SCI., 24, 1969, 1475-1481.

63. HAYASHI K., UCHIYAMA S., "On particle trtajectory and capture efficiency around many wires"; IEEE TRANS. MAGN, MAG- 16 (5), 1980, 827-829.

64. HEYDER J., "Mechanisms of aerosol particle deposition", CHEST 80 (6: SUPPL), 1981, 820-823.

65. HILLER R., LOFFLER F., "Influence of particle impact and adhesion on the collection efficiency of fibre filters", GER. CHEM. ENG., 3 (5), 1980, 327-332.

66. HO C., WANG C., "Dust collection of particle inertia and electrical for.ces", US NAT. SCI. FOUND. AWARD NO. INT 78-21376. JAPAN SOC. PROM. SCI. GRANT NO. ENGR021.

67. HOPPIT B.; "A consideration of the changes in efficiency of absolute filters under various conditions of contaminant loading" SEMINARS ON HIGH EFFICIENCY AEROSOL FILTR., AIX-EN-PROVENCE, 1976 LUXEMBOURG, COM. EURO. COM, 1977.

68. INGHAM D.B., "The diffusional deposition of aerosols in fibrous filters ", J. AEROSOL SCI., 12 (4), 1981, 357-365.

69. JOHN W., REISCHL G., "Measurements of the filtration efficiencies of selected filter types", ATMOS. ENVIRON., 12 (10), 1978, 2015-2019.

70. JOHNSTONE H.F., ROBERTS M.H., "Deposition of aerosol particles from moving gas streams", IND. ENG. CHEM., 41 (11), 1949, 2417- 2423.

71. KANAOKA C., EMI H., OHTA M., "Peformances of dust loaded air filters", TRANS. UTILIS. PART. CONTROL TECH., 3rd SYMP. ERA, 1981 Vol. 3. USNTIS REP PB 149069, 280-281.

72. KAPOOR J.C., SUBRAMANIAN K.G., KHAN A.A.; "The particle size of test aerosol for HEPA filters", FILTR. SEP. 14 (2), 1977, 133- 134.

73. KENNARD M.L., MEISEN A., "Aerosol collection in granular beds", PAP. FILTR. 2nd WORLD CONGR. LONDON 1979. CROYDON UPLANDS, 1979.

74. KERKER M. "Laboratory generation of aerosols", ADV. COLLOID INTER. SCI., 5 (2), 1975, 105-172.

75. KIRSH A.A., STECHKINA I.B., FUCHS N.A., "Efficiency of aerosol filters consisting of ultrafine polydisperse fibres"; COLLOID   J. USSR, 37 (1), 1975, 31-36.

76. KIRSCH A.A., STECHKINA I.B., "The theory of aerosol filtration with fibrous filters", PAP, AEROSOL SCI. TECH. SYMP., ATLANTIC CITY, 1976. IN 'FUNDAMENTALS OF AEROSOL SCIENCE", N.Y. WILEY,   1978, 165-256.

77. KIRSCH A.A., ZHULANOV Y.V., "Measurement of the penetration of aerosols through high efficiency filters", COLLOID J. USSR, 39   (2), 1977, 246-251.

78. KNUTSON E.O., WHITBY K.J. "Aerosol classification by electric mobility: Apparatus, theory and applications", J.AEROSOL SCI., 6 (6), 1975, 443-451.

79. KOSCIANOWSKI J.R., KOSCIANOWSKI L., "Effect of filtration parameters on dust cleaning fabrics", USNTIS REP PB 251-145, 1975, 187p.

81. KUWABARA S., "The forces experienced by randomly distributed parallel circular cylinders or spheres in a viscous flow at small Reynolds numbers", J. PHYS. SOC. JAPAN, 14, 1959, 527-532.

82. LAMB G.E.R, COSTANZA P.A.: "Improving the performance of fabric filters", CHEM. ENG. PROG. 73 (1), 1977, 57-53.

83. LAMB G.E.R., COSTANZA P.A., O'MERA D., "Contributing role of single fibre properties to non woven fabric performance", PROC. FABR. FILTS. PART. COLLECT 3rd SYMP., TUCSON. 1977. USNTIS   REP PB 284 969, 1977, 235-249.

84. LAMB G.E.R., COSTANZA P.A., "Role of fibre structure and electro statics in dust cake formation"; TEXT. RES. J., 50 (11), 1980, 661-667.

85. LAMB H., IN "Hydrodynamics"; CAMBRIDGE UNIV. PRESS, 6th., 1932, 609-616.

86. LANDAHL H.D., HERRMANN R.G., "Sampling of liquid aerosols by wires, cylinders and slides, and the efficiency of impaction of the droplets", J. COLLOID INTER. SCI. 4, 1949, 103-135.

87. LANGMUIR I. "Report on smoke and filters"; OSRD REP. NO. 865, 1942, OFFICE TECH. SERV. WASHINGTON.

88. LEE K.W., REED L.D., GIESEKE J.A., "Pressure drop across packed beds in low Knudson number regime", J.AEROSOL SCI., 9 (6), 1978, 557-565.

89. LEE K.W., GIESEKE J.A.: "Collection of aerosol particles by packed beds", ENVIRON. SCI. TECH., 13 (4), 1979, 466-470.

90. LEE K.W., LIU B.Y.H.: "On the minimum efficiency and the most penetrating particle size for fibrous filters", J.AIR POLLUT. CONTROL ASSOC. 30 (4), 1980, 377-381.

91. LEE K.W., LIU B.Y.H. "Theoretical study of filtration by fibrous filters", AEROSOL SCI. TECH., 1 (2), 1982, 147-161.

92. LIEBERMAN A., "Royco Instruments particle counters : Capabilities and limitations", AEROSOL MEAS. PROC. WORKSHOP, GAINSVILLE, 1976. GAINSVILLE UNIV. FLORIDA PRESS, 1979; 183-193.

93. LIEBERMAN A., "Particle size distribution measurements made with Royco optical instruments", PROC. INT. CONF. POWDER AND BULK SOLIDS HANDLING AND PROC., PHILADELPHIA, 1979, CHICAGO, IND. AND SCI. CONF. MGT., 1979, 266-270.

94. LIEBERMAN A., "In place filter testing with optical single particle counters"; FILTR. SEP., 17 (6), 1980, 573-576.

95. LIU B.YH., PUI D.Y.H.: "A submicron aerosol standard and the primary absolute calibration of the condensation nuclei counter", J. COLLOID INTER. SCI. 47 (1), 1974, 155-171.

96. LOFFLER, F., "The influence of electrostatic forces for particle collection in fibrous filters", PROC. NEW CONCEPTS FINE PART. CONTROL, NOTRE DAME, 1978. USNTIS REP. PB 295095, 1978, 206-236.

97. LOFFLER F., "Particle collection from gases on fibre filters", CHEM-ING-TECH (Germnan), 52 (4), 1980, 312-323.

98. MAGEE W.S. (Jr.), JONAS L.A., "Aerosol filtration by fibrous filter mats", PAP, SYMP. REMOV. TRACE COUTAMIN. AIR, ATLANTIC CITY, 1974. WASHINGTON, AM. CHEM. SOC. SYM. SER., 17, 1975, 91-105.

99. MASLIYAH J.H., "Aerosol removed by diffusion and interception in mats of elliptic fibres", CAN.J.CHEM. ENG., 53 (5), 1975, 568-571.

100.MILLER B., LAMB., G.E.R., COSTANZA P.A., O'MEARA D., DUNBAR.: "Studies of dust cake formation and structure in fabric filtration", USNTIS REP. 297. 581, 1979, 48p.

101.MIYAGI Y., "Viscous flow at low Reynolds numbers past an infinite row of equal circular cylinders", J.PHYS. SOC. JAPAN, 13, 1958, 493-496.

102.MOHAMED M., AFIFY E., "Efficient use of fibrous structures in filtration", USNTIS REP. PB. 257 147, 1971, 146p.

103.NATANSON G.L.: "Diffusion precipitation of aerosols on a stream lined cylinder with a small capture coefficient"; DOKL. AKAD. NAUK. USSR, 112 (1-6), 1957, 21-25.

104.NATANSON G.L.; "Critical conditions in the sedimentation of aerosols in viscous flow around a cylinder and sphere", PROC. ACAD. SCI. USSR, 116 (1-6), 1957, 587-591.

105.NEALE H.N., NADER W.K., "Prediction of transport processes within porous media: creeping flow relative to a fixed swarm of spherical particles", A.I.Ch.E.J.20, 1974, 530-536.

106.NGUYEN X., BEECKMANS J.M., "Single fibre capture efficiencies of aerosols particles in real and model filters in the inertial interceptive domain", J. AEROSOL SCI., 6 (3,4), 1975, 205-212.

107.OWEN, R., STENHOUSE J.I.T., "Investigation of the effect of the arrangement of the filter medium on the performance of high efficiency filters, Report 6" AERE (Harwell) Contract ref. no. H2C 3655 EMR, July 84.

108.PARETSKY. L., "Filtration of aerosols by granular beds", Ph.D. THESIS, CITY UNIVERSITY OF NEW YORK, 1972.

109.PAYATAKES, A.C., TIEN C., TURIAN R.M., "A new model for granular porous media-Part 1: Model formulation"; A.I.Ch.E.J., 19, (1), 1973, 58-67.

110.PAYATAKES A.C., TIEN C., "Particle deposition in fibrous media with dendrite like pattern - a preliminary model", J. AEROSOL SCI., 7 (2), 1976, 85-100.

111.PAYATAKES A.C., "Model of aerosol particle deposition in fibrous media with dendrite - like pattern :- application to pure interception during period of unhindred growth", FILTR. SEP., 13 (6), 1976, 602-607.

112.PAYATAKES A.C., "Model of transient aerosol particle deposition in fibrous media with dendritic pattern", A.I.Ch.E.J. 23 (2), 1977, 192-202.

113.PAYATAKES A.C., BHUTRA S., "Experimental investigation of dendritic deposition of aerosol particles", J. AEROSOL SCI., 10 (5), 1979, 445-464.

114.PAYATAKES A.C., "Advances in dendritic deposition of aerosols by inertial impaction and/or interception", PAP. FILTR. 2nd WORLD CONGRESS, LONDON, 1979. CROYDON, UPLANDS. 1979.

115.PAYATAKES A.C., GRADON L., "Dendritic deposition of aerosol particles in fibrous media by inertial impaction and interception", CHEM. ENG. SCI. 35 (5), 1980, 1083-1096.

116.PAYATAKES A.C, "Discussion of 'Comments of the paper experimental investigation of dendritic deposition of aerosol particles" by B. Dahneke", J.AEROSOL SCI., 11 (5-6), 1980, 571-575.

117.PAYATAKES A.C., OKUYAMA K., "Effects of aerosol particle deposition on the dynamic behaviour of uniform or multilayer fibrous filters", J.COLLOID INTER. SCI. 88 (1), 1982, 55-78.

118.PASCERI R.E., FRIEDLANDER S.K., "The efficiency of fibrous aerosol filters: deposition by diffusion of particles of finite diameter", CAN.J.CHEM.ENG., 38 (12), 1960, 212-213.

119.PENDSE H., TIEN C., "Simulation model of aerosol collection in granular media", USNTIS REP. PB 81-113664, 1980, 50p.

120.PENDSE H., TIEN C., "Simulation model of aerosol collection in granular media", J. COLLOID INTER. SCI., 87 (1), 1982, 225-241.

121.PENDSE H., TIEN C., "General correlation of initial collection efficiency of granular beds"; A.I.Ch.E.J., 28 (4), 1982, 677-684.

122.PFEFFER R., "Granular bed filters for the removal of particulates from gases", REP. DEPT. CHEM. ENG. CITY UNIV., NEW YORK, 1979.

123.PICH J., "Pressure characteristics of fibrous aerosol filters", J. COLLOID INTER. SCI., 27 (4), 1971, 912-917.

124.PRATT R.P., "A preliminary assessment of the dust loading vs. pressure drop characteristics of high capcity HEPA filters", AEC/ERDA/DoE 16th NUCL. AIR CLEAN. CONF., SAN DIEGO, 1980. USNTIS CONF. 801038, 697-707.

125.PUI D.Y.H., LIU B.Y.H.; "Aeorosl generation and calibration of instruments", TSI Q. 5 (2), 1979, 5-12.

126.RABER R.R., "Pressure drop optimisation and dust capacity estimation for a deep pleated industrial air filter using small sample data", PAP FILTR., 3rd WORLD CONGRESS. FILTR. SOC., 1982, VOL. 1. 52-59.

127.RADUSHKEVICH L.V., VELICHO M.V., "Theory of precipating highly disperse aerosols from a stream onto an ultrathin cylinder", DOKL. AKAD. NAUK., 146 (2), 1962, 406-408.

128.RADUSHKEVICH L.V., Bull. Acad. Sci.,USSR, (3), 367.

129.RADUSHKEVICH L.V., Colloid J., USSR, 26 (2), 194.

130.RADUSHKEVICH L.V., KOLGANOV V.A., "Study of collection of highly disperse aerosols from a gas stream on ultrathin cyclinders",   In "AEROSOL PHYSICAL CHEMISTRY", ED. K. SPURNEY, 1965.

131.RADUSHKEVICH L.V., "On the role of Brownian vibrations in ultrathin fibres in aerosol filtration", J. COLLOID INTER. SCI. 34 (2), 205-209.

132.RAMISKILL E.A., WENDELL L.A., "The inertial mechanism in the mechanical filtration of aerosols", J. COLLOID. SCI., 6 1951, 416-428.

133.REID. D.L. "Electrostatic capture of fine particles in fibre beds", PROC. NEW CONCEPTS FINE PART. CONTROL, NOTRE DAME, 1978. USNTIS REP. PB. 292095, 1978, 305-319.

134.RUDNICK S.N., FIRST. M.W., "Specific resistance of filter dust cakes:-comparison of theory and experiments", PROC. FABR. FILT. PART. COLLECT 3rd SYMP., TUCSON, 1977. USNTIS REP. PB 284 969,   1977, 251-288.

135.RUDNICK S.N. ELLENBECKER M.J., "The role of viscosity in fabric filtration", J.AIR POLLUT. CONTROL ASSOC. 29 (11), 1979, 1161-1162.

136.SCHMIDT E.W., GIESEKE J.A., "Filtration theory for granular beds", J.AIR POLLUT. CONTROL ASSOC., 28 (2), 1978, 143-146.

137.SHAPIRO, LAUFER G., GUTFINGER C., "Electrical forces in aerosol filtration in fibrous and granular filters", ATMOS. ENVIRON., 17 (3), 1983, 477-484.

138.SHAW D.T. "Funadmentals of Aerosol Science ", 1978, JOHN WILEY & SONS INC.

139.STAIRMAND C.J. "Dust collection by imp.ingement and diffusion", TRANS. I.CHEM.E. (LONDON), 28, 1950, 130-139.

140.STECHKINA I.B., FUCHS N.A. "Studies on fibrous aerosol filters: I. Calculation of diffusional deposition of aerosols in fibrous filters", ANN OCCUP. HYG. 9, 1966, 59-64.

141.STECHKINA I. B., KIRSLCH A.A., FUCHS, N.A. "Studies on fibrous aerosol filters: IV Calculation of aersol deposition in model filters in the range of maximum penetration", ANN. OCCUP. HYG.,   12, 1969, 1-8.

142.STENHOUSE J.I.T. HARROP J.A. FRESHWATER D.C., "The mechanisms of particle capture in gas filters", J. AEROSOL SCI., 1, 1970, 41-51.

143.STENHOUSE J.I.T., HARROP J.A., "Particle capture mechanisms in fibrous filters", FILTR. SEP. 8, 1971, 169-175.

144.STENHOUSE J.I.T., "Mechanisms of fibrous filtration", Ph.D. THESIS, 1972, LOUGHBOROUGH UNIVERSITY OF TECH, D36643/73.

145.STENHOUSE J.I.T., LLOYD P.J. "Sampling errors due to inertial classification", A.I.Ch.E.SYMP. SER., 7, 1974, 137-140.

146.STENHOUSE J.I.T., LLOYD P.J. BUXTON R.E., "The retention of large particles (> 2 um) in fibrous filters", AM. IND. HYG. ASSOC. J., 37 (7) 1976, 432-436.

147.STENHOUSE J.I.T., FRESHWATER D.C., "Particle adhesion in fibrous air filters", TRANS.I.CHEM.E., 54 (7), 1976, 95-99.

148.STENHOUSE J.I.T., BROOM G.P., CHARD N.T.J., "An experimental study of high inertia fibrous filtration", REMOVAL FINE PART. GAS STREAMS SYMP., MANCHESTER, 1976, RUGBY. I. CHEM. E.

149.STENHOUSE J.I.T., FORMBY J., SINCLAIR I., "An experimental determination of the retention of submicron particles in fibrous materials", SEM.HIGH EFF. AEROSOL FILTRS., AIX-EN-PROVENCE, 1976. LUXEMBOURGH, COM. EURO. COM. 1977.

150.STENHOUSE J.I.T., BROOM G.P., "Dust loading characteristics of high inertial fibrous filters", AM. IND. HYG. ASSOC. J., 39, (3) 1978, 219-225.

151.STENHOUSE J.I.T.,"High inertia fibrous filtration", PROC.INT. CONF.POWDER AND BULK SOLIDS HAND. PROC., PHILIDEPHIA, 1979, CHICAGO, IND. SCI. CONF. MGT., 1979, 517-527.

152.STERN S., ZELLER M., SCHEKMAN A., "The aerosol efficiency and pressure drop of a fibrous filter at reduced pressures", J.COLLOID SCI., 15, 1960, 546-562.

153.SUBRAHMANTAM T.V., RAO A.P., "Fibrous filtration of gases", PROC. SEM. SOLID-GAS SEP., NEW DELHI, 1975, CHEM. AGE. INDIA, 217 (1), 1976, 110-115.

154.TARDOS G.I. GUTFINGER C. ABUAF·N., "High Peclet number mass transfer to a sphere in a fixed or fluidised bed", A.I.Ch.E.J., 22 (6), 1976, 11467-1150.

155.TARDOS G.I., ABUAF N., GUTFINGER C., "Dust deposition in granular bed filters - theories and experiments". J.AIR. POLLUT. CONTROL ASSOC. 28, 1978, 354-363.

156.TARDOS G.I. PFEFFER R., YU E., SQUIRES A.M., "Experiments on aerosol filtration in granular sand beds", J. COLLOID INTER SCI., 71 (3), 1979, 616-621.

157.TARDOS G.I., PFEFFER R., "Influence of electrostatic charges on the filtration efficiencies of airborne dust in a fluidised bed", CHISA 7th INT. CONGR., PRAHA, CZECHOSLOVAKIA, 1981, PAP B1.9. 31p.

158.TASHPOLOTOV I., SADOVSKII B.F., CHERNYAEVA G.A., "Role of molecular forces of attraction in the filtration of aerosol particles by fibrous filters", DOKL. PHYS. CHEM. 266 (1-2).

159.THAMBIMUTHUK.V.TANB.K.C.,CLIFT R., "Mechansims of steady state filtration of gases in packed beds". I.CHM.E.SYMP.NO. 59, 1980, SER. NO. 59, 1.3/1-1.3/12/.

160.THIAGORAJON V., YU C.P., "Sedimentation from aerosol flows in finite tubes in random orientation:, J. AEROSOL SCI. 9 (6), 1978, 543-546.

161.TIEN C., "Aerosol Filtration in granular media"; CHEM ENG. COM., 17 (1-6), 1982, 361-382.

162.TSIANG R.C., TIEN C., "Trajectory analysis of particle deposition in model filters composed of parallel fibres", CAN.J.CHEM.ENG., 59 (5), 1981, 595-601.

163.TSIANG R.C., WANG C.S., TIEN C., "Dynamics of particle deposition in model fabric filters", CHEM.ENG.SCI., 37 (11), 1982, 1661-1673.

164.TURNER J.H., "EPA fabric filtration studies part I: Performance of non woven filter bags", USNTIS REP. PB. 266, 271, 1976, 37p.

165.WASAN D.T., WNEK W., "Measurement of specific surface area" PAP.7th ANN FINE PART.SOC.CONF., PHILIDELPHIA, 1975, POWDER TECH. 14 (2).

166.WEBB I.J., POINTRIG R., "An improved sodium chloride particulate test for air conditioning filters", FILTR. SEP., 13 (6), 1976, 609-612+624.

167.WILSON E.J., GEANKOPLIS C.J., "Liquid mass transfer at very low Reynolds numbers in packed beds", IND. ENG.CHEM. FUNDAM., 5 (1), 1966, 9-14.

168.YOSHIOKA Y., EMI H., SONE H., CHEM. ENG. JAPAN 33, 1969, 1013.

Collection Mechanisms	No.	Reference Authors	Single granule collection efficiency equation	Remarks
INERTIA ONLY	–	Langmuir I. Blodgett KB	$1+0.75 \ln(2St)^{-2}/(St-1.214)$ $St^2/(St+0.05)^2$	Creeping flow Potential Flow $(St > 0.02)$
	103	Landahl H. Hermann K.	$St^2/(St^3+0.77\ St^2+0.22)$	$Re = 10$
	140	Paretsky LC	$2St^{1.13}$	$St < 4.4 \times 10^{-2}$
	12	Behie SW Beeckmans JM	0 $3.6 \times 10^{-3} - 0.232St + 2.42St^2 - 2.303St^3$ $St^2/(St+0.05)^2$	$St < 0.083$ $0.083 < St < 0.6$ $St > 0.6$
	95	Knettig P Beeckmans JM	$3.76 \times 10^{-3} - 0.464St + 2.42St^2 - 16.2St^3$	$0.0416 < St < 0.3$
	204	Thambimuthu KV et al	$\left\{St/(St+0.62\ \epsilon)\right\}^3$	Accounts for interference from other granules
	153	Pendse H. Tien C.	$(1+.04Re)St\pi^{-1/3}(0.75(1-\epsilon))$	"
INTERCEPTION ONLY –	102	Lamb H.	$2R$ $1.5\ R^2$	$St \to \infty$ $St \to o$
	135 60	Natanson GL Friedlander SK	$R^2(2-\ln Re)$ $2Re^{\frac{1}{2}}R^2$	

106	Lee KW Gieske JA	$\dfrac{1.5\,(1-\alpha)\,R^2}{k}$	Accounting for interference and using Kuwabara flow field.
71	Gutfinger C.	$1.5\,\{g(\varepsilon)\}^3\,R^2$	Correction function for interference from other granules
200	Tardos GI et al	$\dfrac{3.37\,\varepsilon^{-3}\,R}{\dfrac{1}{\xi}(1+2R+R^2-\dfrac{1}{1+R})}$	Creeping flow Potential flow

DIFFUSION
ONLY

	Langmuir I. Blodgett KB	$1.71\,Pe^{-2/3}/(2-\ell nRe)^{1/3}$	Re<7.39, Developed from Langmuir (104)
86	Johnson HF Roberts MH	$8\,Pe^{-1}+2.3Re^{1/2}Pe^{-5/8}$	Analogy with heat and mass transfer
181	Stairmand CJ	$2.83Pe^{-1/2}$	Potential flow
135	Natanson GL	$2.92\,Pe^{-2/3}/(2-InRe)^{1/3}$	Pe>> 1, Creeping flow.
214	Wilson EJ Geankoplis CJ	$4.36\,\varepsilon^{-1}\,Pe^{-2/3}$	From liquid mass transfer work. Accounrs for other granules. Other authors agree exp.
198	Tardos GI et al	$9.54\,Pe^{-2/3}$	Creeping flow

	171	Gutfinger C. Tardos G.I.	$4 g (\varepsilon) Pe^{-2/3}$	Correction function for interference from other granules
	106	Lee KW Gieske JA	$3.5 \left\{\dfrac{1-\alpha}{K}\right\}^{1/3} Pe^{-2/3}$	Accounting for inter. and using Kuwabara flow field
GRAVITY ONLY	140	Paretsky LC	$0.0375 (N_G + 0.21 N_G^{0.78})$	$N_G = U_s/U_o$
	200	Tardos GI et al	$St Ga/(St Ga + 1)$	
	108	Lee KW	$dp^2 \rho g/18\mu U_o$	
INTERCEPTION + DIFFUSION	60	Friedland SK	$6 Re^{1/6} Pe^{-2/3} + 3R^2 Re^{1/2}$	
INTERIA + INTERCEPTION	31	Davies CN	$0.16\left\{R + (0.5 + 0.8R)St - 0.105 RSt^2\right\}$	$Re = 0.2$
INTERIA + INTERCEPTION + DIFFUSION	31	Davies CN	$0.16\left\{R + (0.5 + 0.8R)(Pe^{-1} + St)\right.$ $\left. - 0.105 R(Pe^{-1} + St)^2\right\}$	
INERTIA + GRAVITY		Doganoglu Y.	$2.89 St + 6.87 N_G$ $5.83 \times 10^{-2} ReSt + 1.42 N_G$	$dg = 110$ $dg = 600$
INERTIA + INTERCEPTION DIFFUSION	175	Schmidt FW Gieske JA	$3.97 St + (8 Pe^{-1} + 2.3 Re^{1/8} Pe^{-5/8})$ $+ 1.45R + N_G$	
+ GRAVITY	89	Kennard ML Meisen A	$2.29 St + 9.64 Pe^{-2/3} + 3.61 N_G$ $+ 0.00157 St^{0.2} Pe^{03} Re^{-1.15}$	Semi empirical regression equation

Appendix 2.1

The following appendix presents the results of the theory described in 2.1. Tables are given showing the variation of penetration with certain parameters for each model. These are followed by graphical presentation of the pressure drop effects.

TABLE A 2.1-1: Penetration with particle size

Filtration conditions

    Filter Face velocity 2.5 cm/s
        Fibrous filter
        a) fibre diameter 0.5 μm
        b) packing density 4%
        c) depth of filter 500 μm
    Granular bed filter
        a) granule diameter 5 μm
        b) packing density 25%
        c) specific loading 0.5 kg/m^2

Particle size (dia) μm	Fibre Filter penetration % fan	cell	Granular Bed pentration % recommended	Lee	Combined penetration %
.01	–	–	.0001	–	–
.05	.0045	.0001	.0101	–	.0001
.1	.0502	.0001	.0029	–	.0001
.15	.0538	.0001	.0002	.0002	.0001
.2	.0212	–	.0001	.0011	–
.25	.0043	–	.0001	.0031	–
.3	.0006	–	–	.0053	–
.5	.0001	–	–	.0031	–
1.0	–	–	–	–	–

TABLE A 2.1-2: Penetration with face velocity

Filter conditions

   Challenge particle size 0.15 μm
     Fibrous filter
     a) fibre diameter 0.5 μm
     b) packing density 4%
     c) depth of filter 500 μm
   Granular bed filter
     a) granule diameter 5 μm
     b) packing density 25%
     c) specific loading 0.5 kg/m^2

Face velocity cm/s	Fibre Filter penetration %		Granular Bed pentration %		Combined penetration %
	fan	cell	recommended	Lee	fan + recommended
2	.0241	.0001	.0002	.0001	–
2.5	.0538	.0001	.0002	.0002	.0001
4	.1978	.0001	.0005	.0051	.0001
6	.4246	.0001	.0008	.0430	.0001
8	.6114	.0003	.0009	.1701	.0001
10	.7364	.0005	.0010	.3885	.0001

TABLE A 2.1-3: Penetration with increasing load

Filter conditions
   Face velocity 2.5 cm/s
   Challenge particle size 0.15 μm
     Fibrous filter
     a) fibre diameter 0.5 μm
     b) packing density 4%
     c) depth of filter 500 μm
   Granular bed filter
     a) granule diameter 5 μm
     b) packing density 25%

Specific load kg/m²	Fibre Filter penetration %		Granular Bed pentration %		Combined penetration %
	fan	cell	recommended	Lee	fan + recommended
0	.0538	.0001	0	0	.0538
0.25	.0538	.0001	.1534	.1233	.0001
0.5	.0538	.0001	.0002	.0002	.0001
0.75	.0538	.0001	.0001	.0001	−
1.00	.0538	.0001	−	−	−
1.25	.0538	.0001	−	−	−

FIGURE A2.1-1.: Prediction of pressure drop response with face velocity.

- Mean fibre diameter 0.5 μm
- Packing density 0.04
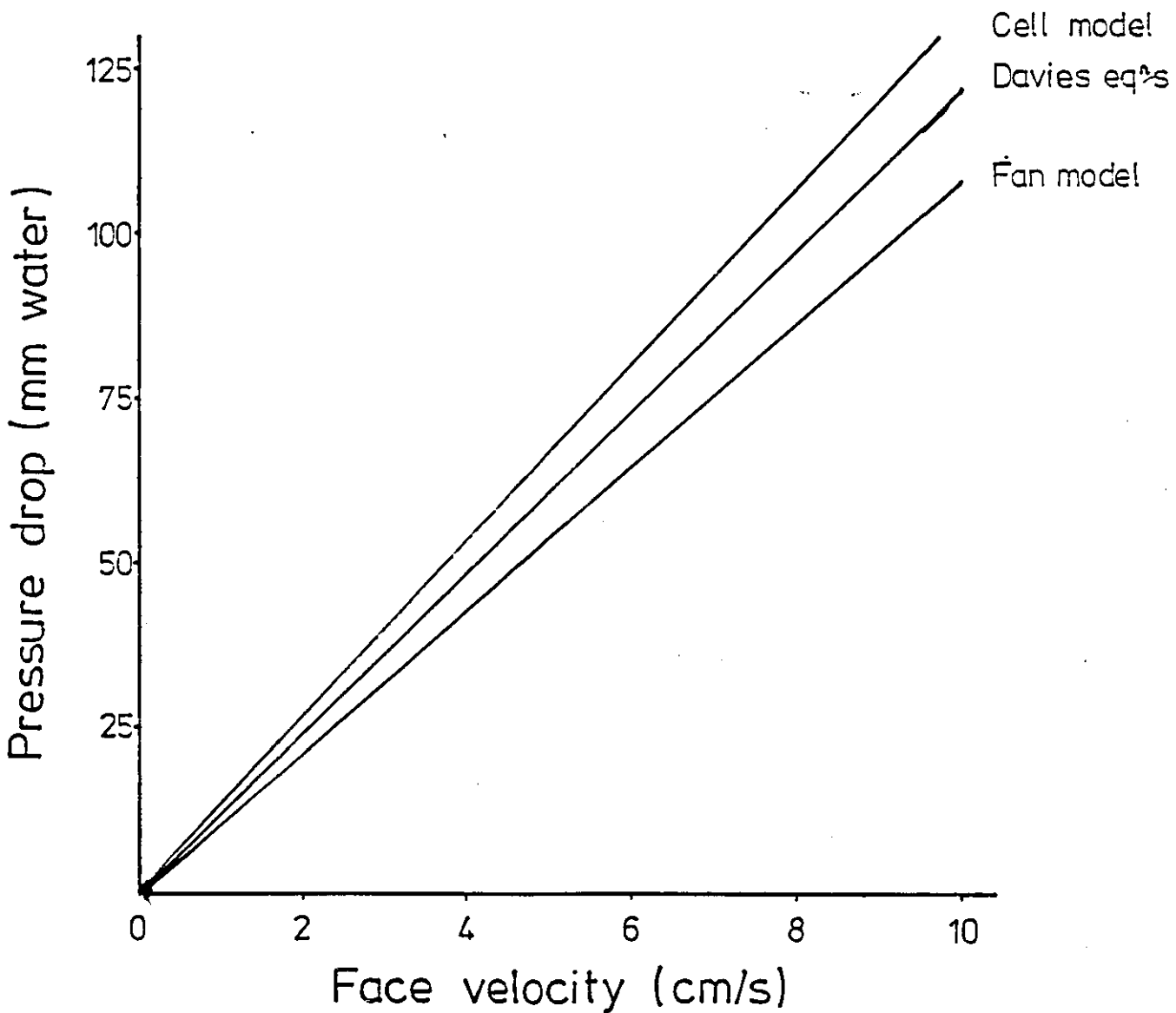
FIGURE A2.1-2: Prediction of pressure drop response with load for a bed of 5μm particles, packing density 0.25, at different face velocities.
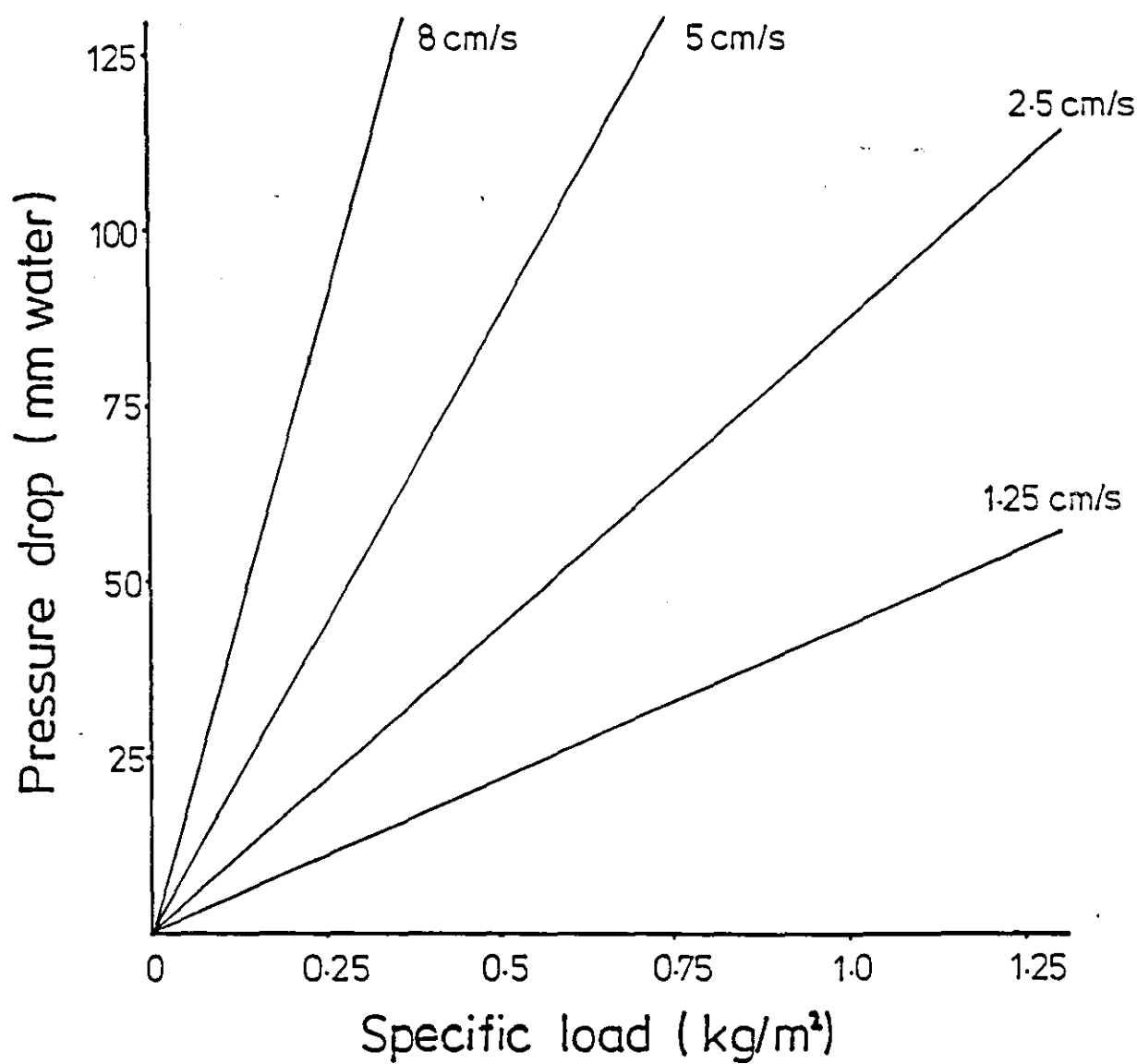
FIGURE A2.1-3: Prediction of pressure drop response with load, at 2.5 cm/s face velocity, for different particle sized beds.

(Packing density 0.25)
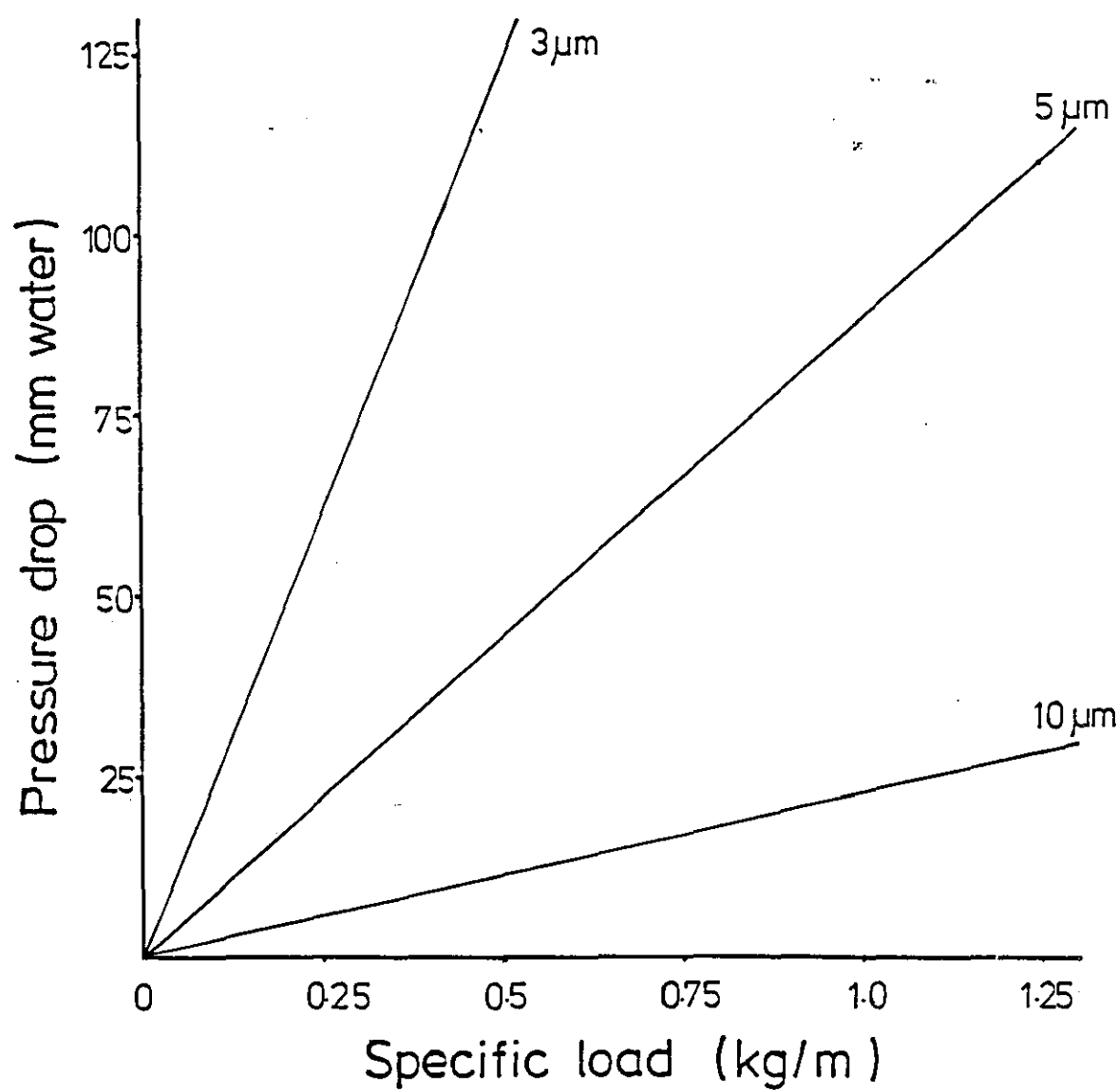
FIGURE A2.1 - 4 : Prediction of pressure drop response with load, at 2.5cm/s face velocity, for different packing densities.

(5μm particles assumed)
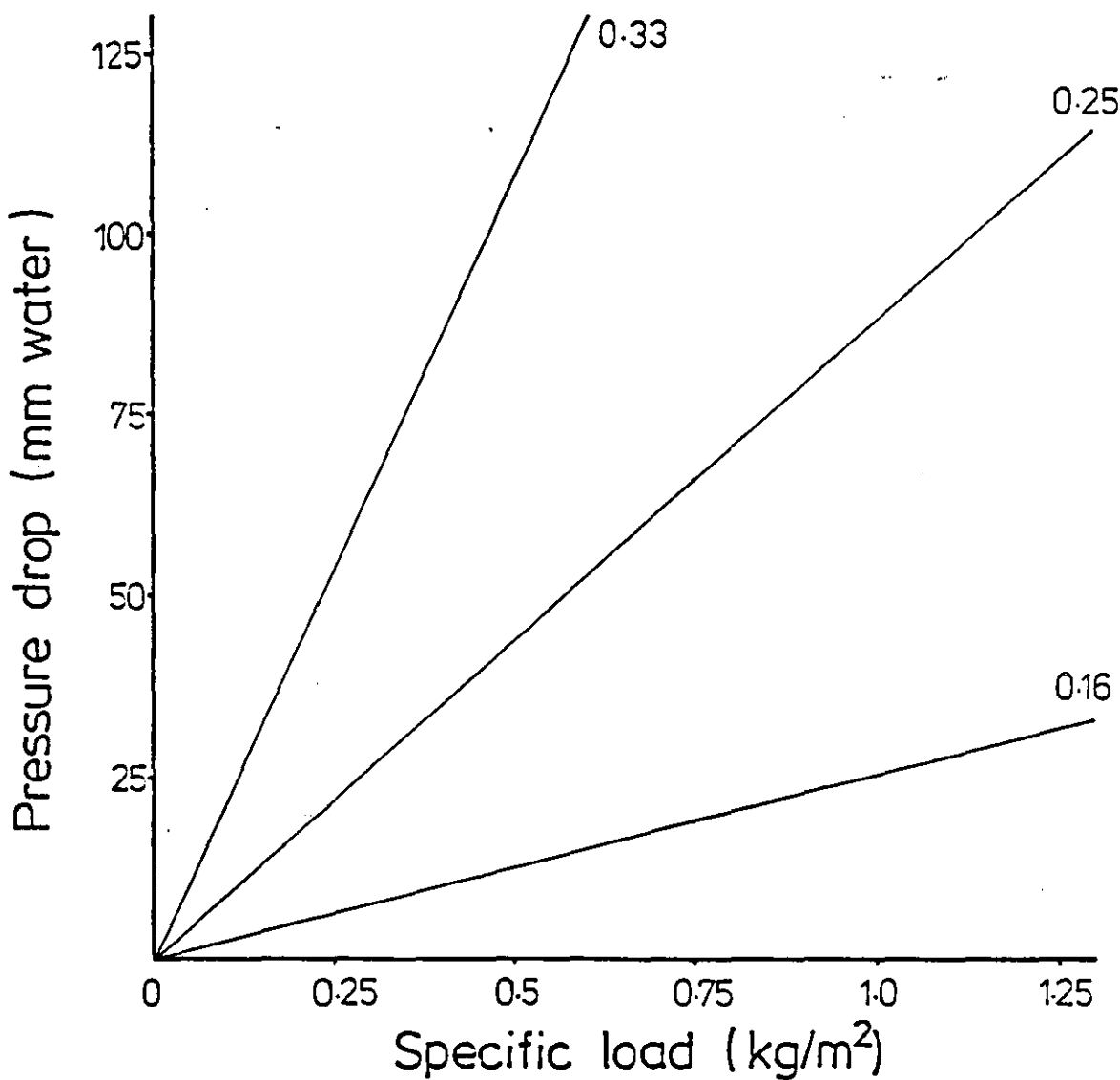
Appendix 2.2.1.

A typical Laplace transform solution as used in section 2.2 is given below:-

Differential equation is:

$$\alpha \frac{d^2 y}{dt^2} + \frac{dy}{dt} + \alpha g = 0 \qquad (A2.2-1)$$

Initial conditions

$$y(0) = y_0$$

$$\frac{dy(0)}{dt} = y'(0) = -\alpha g$$

Taking Laplace transforms of A2.2.1 gives

$$\alpha \left[s^2 Y(s) - sy(0) - y'(0) \right]$$
$$+ \left[s Y(s) - y(0) \right] + \frac{\alpha g}{s} = 0$$

which gives,

$$Y(s) = \frac{\alpha s^2 y_0 + s y_0 - \alpha^2 g s - \alpha g}{s^2 (\alpha s + 1)}$$

Separating by partial fractions

$$Y(s) = \frac{A}{s^2} + \frac{B}{s} + \frac{C}{(\alpha s + 1)}$$

$$= \frac{A(\alpha s + 1) + B s(\alpha s + 1) + C s^2}{s^2 (\alpha s + 1)}$$

So,

$$s^0 \Rightarrow A = -\alpha g$$

$$s^1 \Rightarrow B + \alpha A = y_0 - \alpha^2 g$$

$$s^2 \Rightarrow \alpha B + C = \alpha y_0$$

$$C = 0 \quad ; \quad B = y_0$$

Hence,

$$Y(s) = -\frac{\alpha g}{s^2} + \frac{y_0}{s}$$

Inversing the transform results in

$$y = y_0 - \alpha g t$$

Check,

$$t = 0 \quad \Rightarrow \quad y = y_0$$

and,

$$\frac{dy}{dt} = -\alpha g$$

so $t = 0 \Rightarrow \frac{dy}{dt} = -\alpha g$

236

Appendix 2.2.2.

Two typical print outs from the computer programme for determining particle trajectories in a triangular channel using the equations of 2.2. are given below:

A PARTICLE'S TRAJECTORY IN A TRIANGULAR CHANNEL WITH SIDE WALL FILTRATION

LENGTH OF CHANNEL IS 27 CM
HEIGHT OF CHANNEL IS 1 CM
WIDTH OF CHANNEL IS .5 CM
AVERAGE FACE VELOCITY IS 2.5 CM/S

THE PARTICLE HAS:
    DIAMETER OF 10 MICRONS
    SPECIFIC GRAVITY OF 4
    SETTLING VELOCITY OF 1.21111111 CM/S

PARTICLE'S INITIAL POSITION IS (0 , .5 , .3)

TIME	X	Y	Z
0.000	0.00	.50	.30
.010	1.66	.49	.27
.020	3.46	.48	.24
.030	5.39	.46	.20
.040	7.44	.45	.17
.050	9.60	.44	.14
.060	11.87	.43	.12
.070	14.24	.42	.09
.080	16.69	.40	.06
.090	19.23	.39	.03
.100	21.84	.38	0.00
.101	22.23	.38	0.00

PARTICLE'S FINAL POSITION IS (22.22 , .37 , 0) AT TIME .1014 SECS

A PARTICLE'S TRAJECTORY IN A TRIANGULAR CHANNEL WITH SIDE WALL FILTRATIC

LENGTH OF CHANNEL IS 27 CM
HEIGHT OF CHANNEL IS 1 CM
WIDTH OF CHANNEL IS .5 CM
AVERAGE FACE VELOCITY IS 2.5 CM/S

THE PARTICLE HAS:
     DIAMETER OF 10 MICRONS
     SPECIFIC GRAVITY OF 4
     SETTLING VELOCITY OF 1.21111111 CM/S

PARTICLE'S INITIAL POSITION IS < 0 , .25 , .24 >

TIME	X	Y	Z
0.000	0.00	.25	.24
.010	.10	.24	.22
.020	.21	.23	.21
.030	.34	.21	.20
.040	.47	.20	.18
.050	.61	.19	.17
.060	.74	.18	.16
.070	.86	.17	.15
.080	..96	.15	.14
.090	1.04	.14	.13
.100	1.09	.13	.12
.110	1.11	.12	.11
.114	1.11	.11	.11

PARTICLE'S FINAL POSITION IS < 1.1 , .11 , .11 > AT TIME .1138 SECS

<u>Appendix 2.3</u>

The following appendix gives an example print out for the
computation of the pressure drop against specific load for each of the
deep pleat and mini pleat arrangements. Graphical representations of
a full range of results at different bulk densities and velocities is
given for each type of filter.

ALL VARIABLES IN S.I. UNITS

FACE VELOCITY .0125
LOAD INCREMENTS 1
AREA OF MEDIA 18
MEDIA THICKNESS 5E-04
GAS VISCOSITY 1.85E-05
GAS DENSITY 1.1
POWDER BULK DENSITY 625

DIMENSIONS OF FILTER UNIT
        HEIGHT .58
        WIDTH   .58
        DEPTH   .25

ANGLE OF SPACER TO MEDIA (RADS) .5236

SPC LOAD KG/M^2	PRESS DROP MM WATER
.000	7.4
.059	8.2
.117	9.0
.176	10.0
.234	11.0
.293	12.1
.351	13.4
.410	14.9
.468	16.4
.527	18.2
.585	19.2
.644	21.1
.702	23.0
.761	24.9
.819	26.9
.878	28.9
.936	31.0
.995	33.1
1.053	35.4
1.112	37.8
1.170	40.7
1.229	44.4
1.287	50.2
1.346	62.7
1.404	119.0
1.463	*83.6

FIGURE A2.3 -1: Comparison of theory with experiment for a deep pleat filter at 1.25 cm/s with BS 2831 No.2 dust.
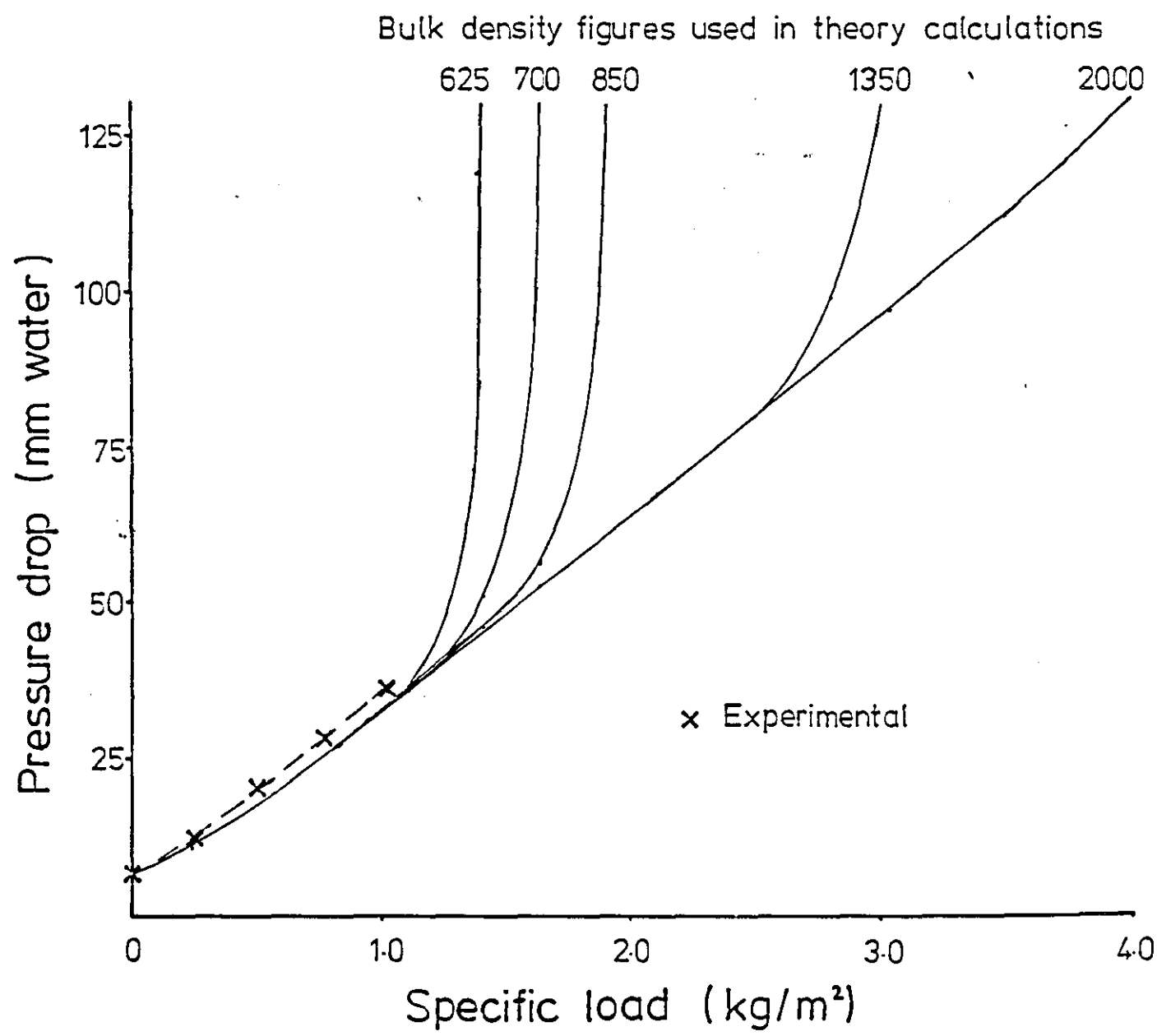
FIGURE A2.3-2 : Comparison of theory with experiment for a deep pleat filter at 2.5cm/s with BS 2831 No.2 dust.
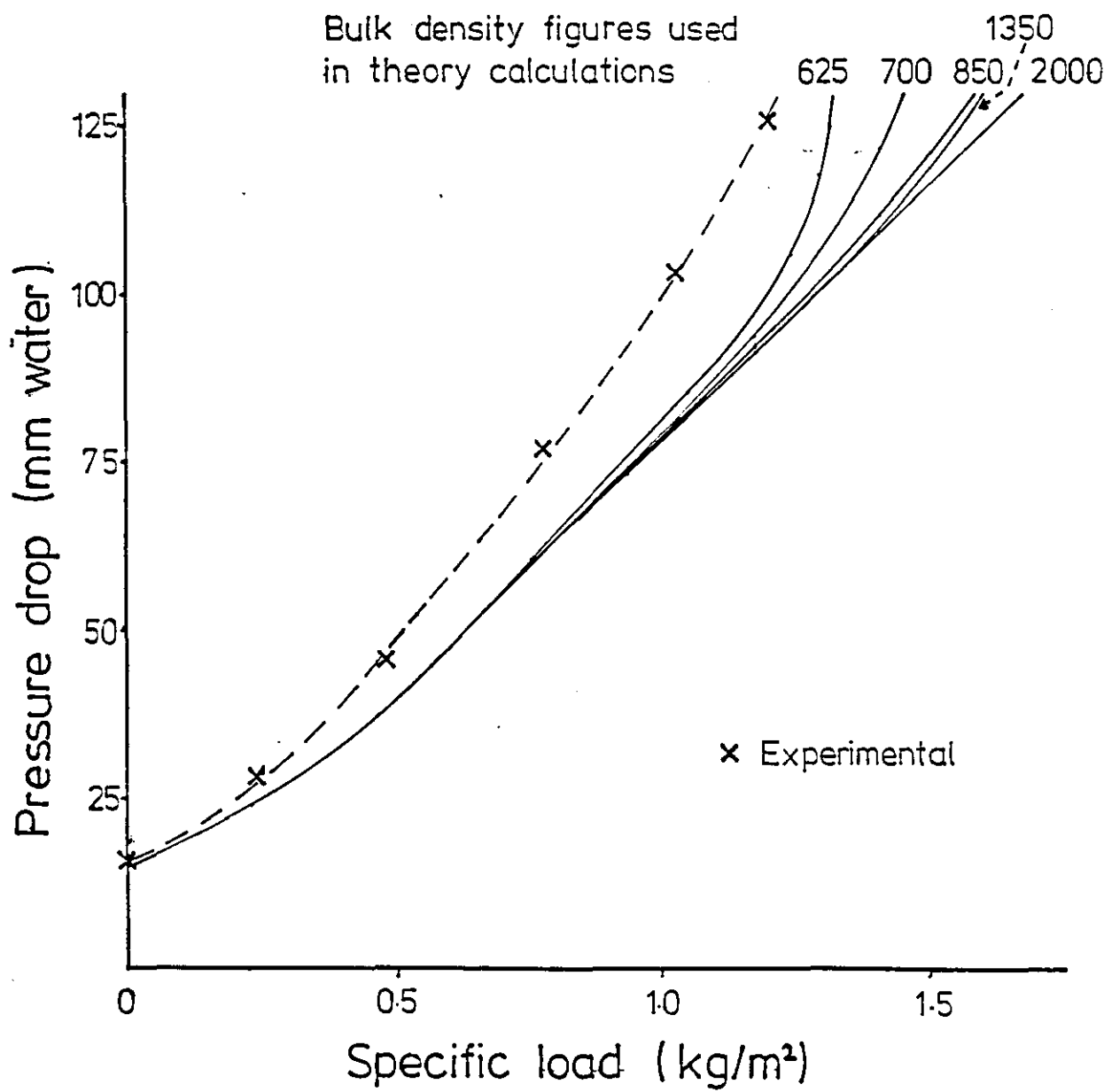
FIGURE A2.3-3 : Comparison of theory with experiment for a deep pleat filter at 3.5cm/s with BS 2831 No.2 dust.
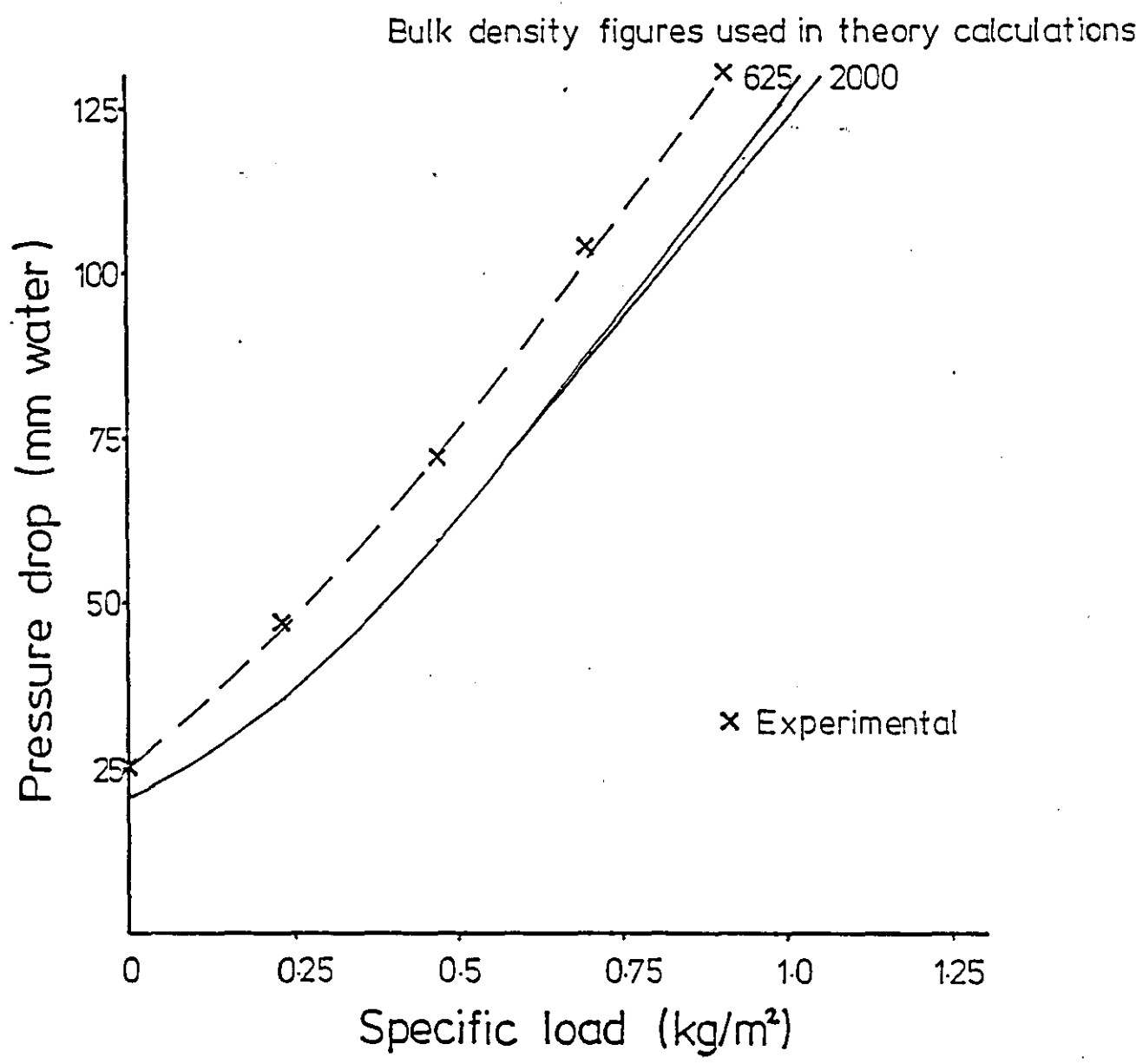
ALL VARIABLES IN S.I. UNITS

FACE VELOCITY .0125
LOAD INCREMENTS 2
AREA OF MEDIA 38
MEDIA THICKNESS 3.3E-04
GAS VISCOSITY 1.85E-05
GAS DENSITY 1.1
POWDER BULK DENSITY 700
DIMENSIONS OF FILTER UNIT

     HEIGHT .58
     WIDTH .6
     DEPTH .25
NUMBER OF PANELS 12
DISTANCE BETWEEN PANELS .05

SPC LOAD KG/M^2	PRESS DROP MM WATER
.000	7.3
.054	8.3
.108	9.7
.162	13.1
.216	31.5
.270	*83.3

FIGURE A2.3-4: Comparison of theory with experiment for a mini pleat filter at 1.25 cm/s with BS 2831 No.2 dust.

Bulk density figures used in theory calculations
700   850   1350   2000

Pressure drop (mm water)

Specific load (kg/m²)
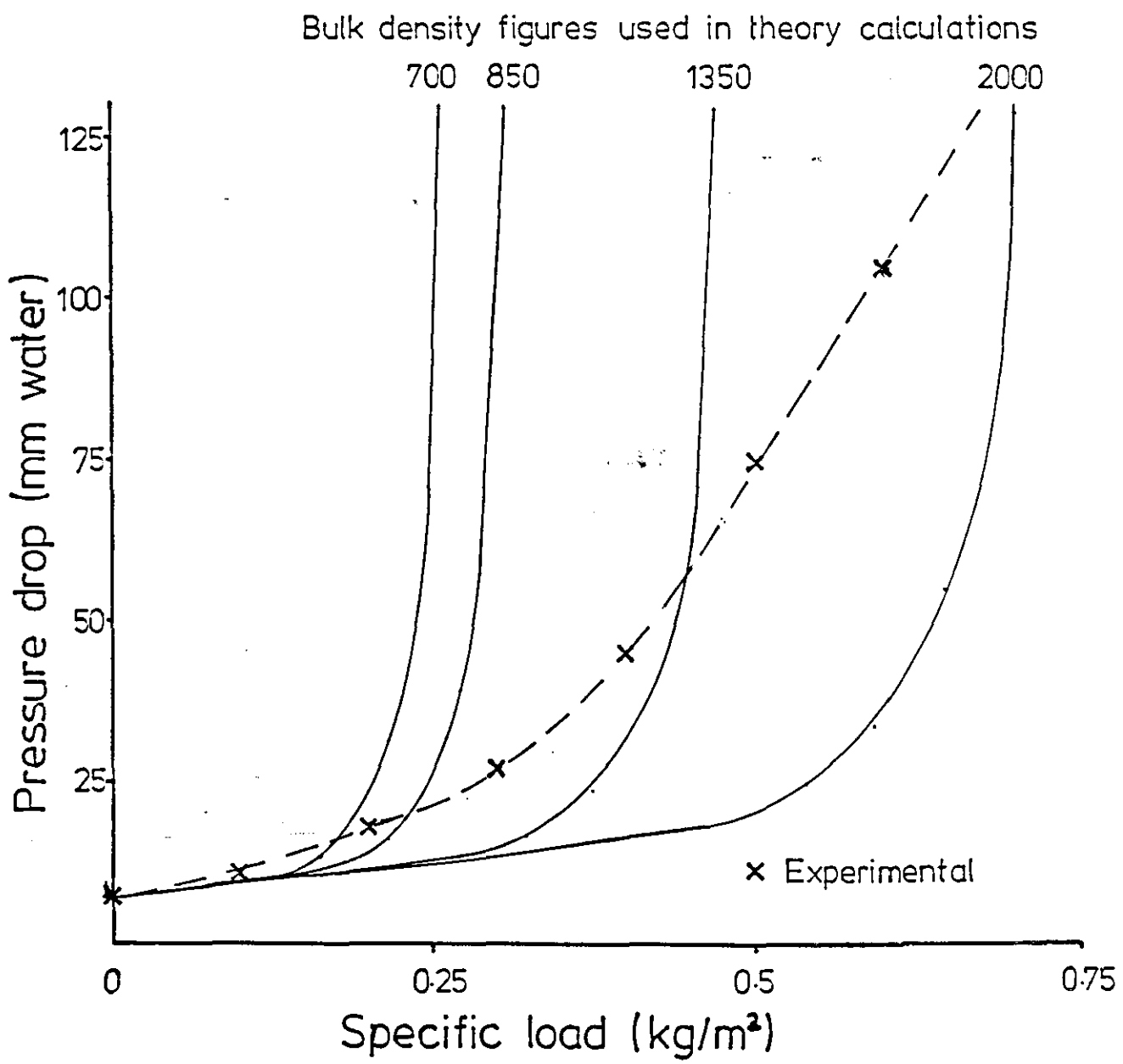
× Experimental

FIGURE A2.3-5 : Comparison of theory with experiment for a mini pleat filter at 4 cm/s with BS 2831 No. 2 dust.
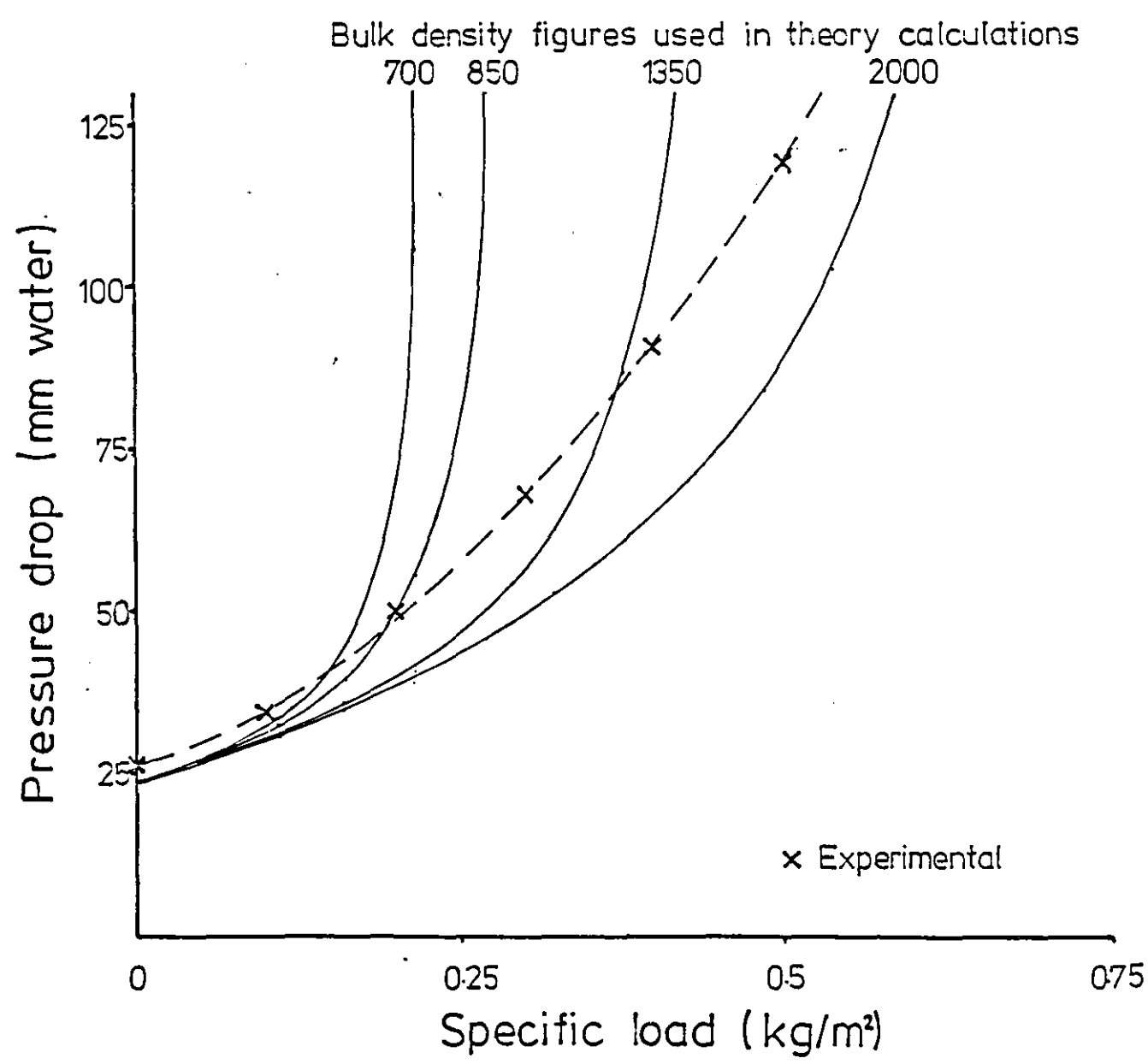
FIGURE A2.3-6 : Comparison of theory with experiment for a mini pleat filter at 2.5cm/s with BS2831 No.2 dust.
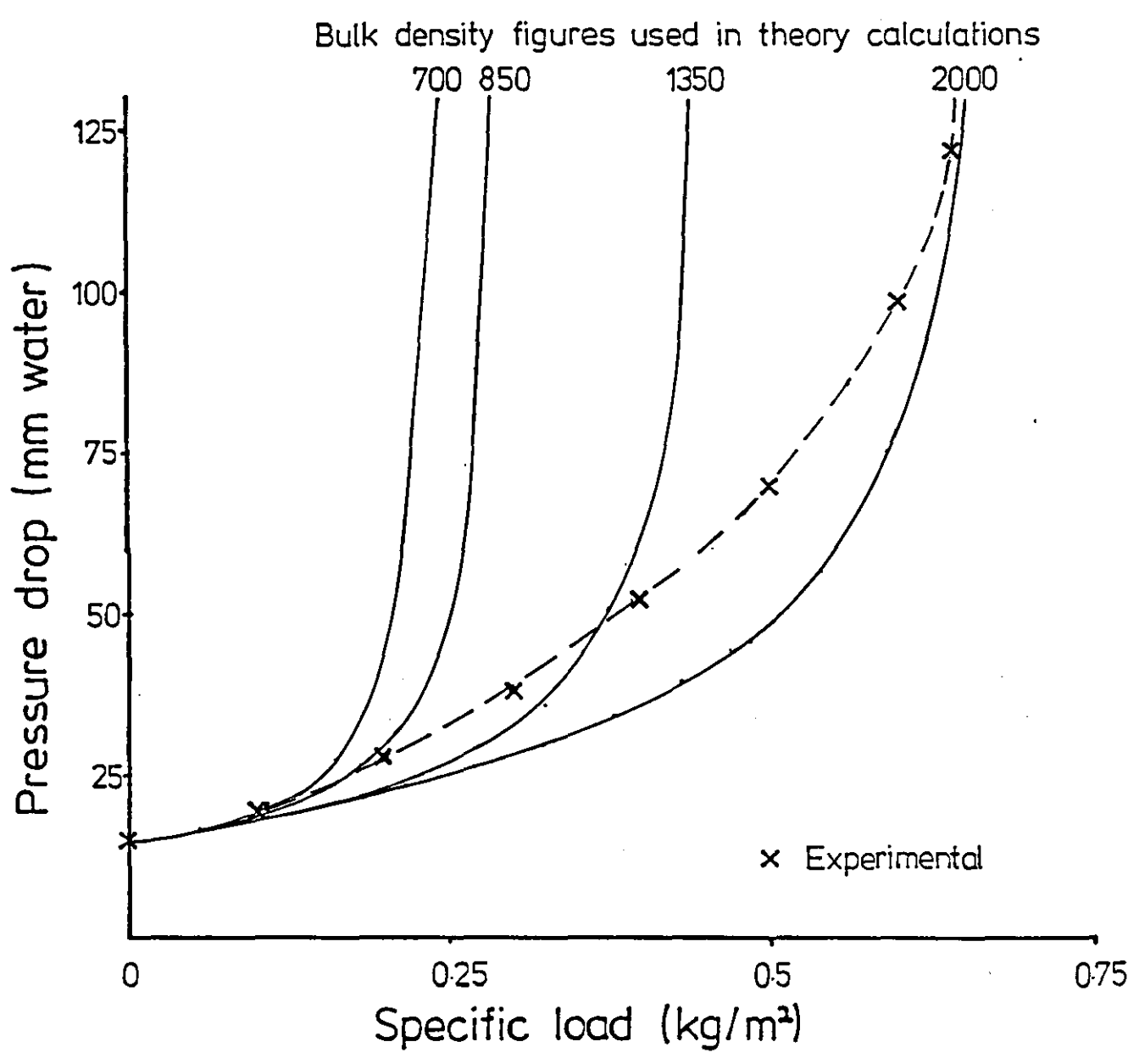
Appendix 2.4.1

The following appendix gives examples of particle trajectory end points entering a deep pleat filter panel with the channels 5 mm wide and the flow rate through the filter being that of a standard deep pleat panel filter. Position and particle size effect is illustrated.

```
OVERALL FLOWRATE .47222
FILTER FACE AREA .3364
FILTER FACE VELOCITY .025
PLEAT SPACING 5E-03

PARTICLE DENSITY 4000

GAS DENSITY 1.1
GAS VISCOSITY 1.85E-05


PARTICLE SIZE OF 1 MICRONS
```

XSTART*	YSTART*	XEND*	YEND*
-4	.10	71.0E-3	1.10
-4	.20	100.2E-3	1.13
-4	.30	50.5E-3	1.17
-4	.40	85.7E-3	1.22
-4	.50	58.8E-3	1.27
-4	.60	86.9E-3	1.33
-4	.70	.5E-3	1.38
-4	.80	71.9E-3	1.44
-4	.90	43.1E-3	1.51
-4	1.00	5.6E-3	1.57

```
PARTICLE SIZE OF 5 MICRONS
```

XSTART*	YSTART*	XEND*	YEND*
-4	.10	34.3E-3	1.45
-4	.20	55.0E-3	1.40
-4	.30	45.1E-3	1.38
-4	.40	65.5E-3	1.37
-4	.50	64.4E-3	1.36
-4	.60	58.9E-3	1.35
-4	.70	71.9E-3	1.40
-4	.80	64.9E-3	1.46
-4	.90	44.0E-3	1.52
-4	1.00	13.2E-3	1.58

```
PARTICLE SIZE OF 10 MICRONS
```

XSTART*	YSTART*	XEND*	YEND*
PARTICLE IMPACT			
-4	.10	973.5E-3	.14
PARTICLE IMPACT			
-4	.20	920.7E-3	.29
PARTICLE IMPACT			
-4	.30	983.9E-3	.43
PARTICLE IMPACT			
-4	.40	791.0E-3	.58
PARTICLE IMPACT			
-4	.50	672.5E-3	.74
-4	.60	10.5E-3	1.04
-4	.70	55.9E-3	1.16
-4	.80	41.8E-3	1.26
-4	.90	28.5E-3	1.36
-4	1.00	15.3E-3	1.45

*   Results as ratio to half pleat space

N.B.   S.I. Units used unless stated

250

Appendix 2.4.2

The following appendix gives print outs of the revised deep pleat theory model for the velocities used in figure 2.7.

FACE VELOCITY .0125
LOAD INCREMENTS .3
AREA OF MEDIA 4.15
MEDIA THICKNESS 6E-04
GAS VISCOSITY 1.85E-05
GAS DENSITY 1.1
POWDER BULK DENSITY 700

DIMENSIONS OF FILTER UNIT
         HEIGHT .54
         WIDTH .14
         DEPTH .25

ANGLE OF SPACER TO MEDIA (RADS) .5236

SPC LOAD KG/M2	PRESS DROP MM WATER
0.000	7.9
.086	9.2
.172	10.7
.258	12.5
.344	14.8
.431	17.0
.517	19.5
.603	21.9
.689	25.0
.775	28.1
.861	31.3
.947	34.5
1.033	37.8
1.119	41.6
1.206	CHANNEL BLOCKED
1.206	54.9 (ESTIMATE ONLY)
1.292	76.8 (ESTIMATE ONLY)
1.378	163.0 (ESTIMATE ONLY)

FACE VELOCITY .025
LOAD INCREMENTS .3
AREA OF MEDIA 4.15
MEDIA THICKNESS 6E-04
GAS VISCOSITY 1.85E-05
GAS DENSITY 1.1
POWDER BULK DENSITY 700

DIMENSIONS OF FILTER UNIT
         HEIGHT .54
         WIDTH .14
         DEPTH .25

ANGLE OF SPACER TO MEDIA (RADS) .5236

SPC LOAD KG/M2	PRESS DROP MM WATER
0.000	15.9
.086	19.1
.172	23.0
.258	27.6
.344	33.1
.431	39.5
.517	46.4
.603	54.1
.689	61.8
.775	69.5
.861	77.3
.947	85.1
1.033	93.2
1.119	102.3
1.206	CHANNEL BLOCKED
1.206	130.1 (ESTIMATE ONLY)

FACE VELOCITY .035
LOAD INCREMENTS .3
AREA OF MEDIA 4.15
MEDIA THICKNESS 6E-04
GAS VISCOSITY 1.85E-05
GAS DENSITY 1.1
POWDER BULK DENSITY 700

DIMENSIONS OF FILTER UNIT
         HEIGHT .54
         WIDTH .14
         DEPTH .25

ANGLE OF SPACER TO MEDIA (RADS) .5236

SPC LOAD KG/M2	PRESS DROP MM WATER
0.000	22.4
.086	27.5
.172	33.6
.258	41.2
.344	50.3
.431	61.4
.517	73.4
.603	85.6
.689	97.8
.775	110.1
.861	122.4
.947	134.8

N.B. S.I. Units used unless stated

Particle deposition on face of mini pleat filter

y, starting point, mm

dp (μm)	St	0.2	0.4	0.6	0.8	1.0	1.2
1	0.16	.066	.030	.052	.095	.184	-
2	0.63	.053	.006	.131	.250	.650	-
3	1.41	.085	.127	.262	.616	-	-
4	2.51	- .027	.154	.460	1.252	-	-
6	5.65	.074	.371	1.111	3.111	-	-
8	10.04	.109	.644	1.951	5.59	-	-
10	15.69	.169	.953	3.000	8.243	-	-

TABLE A2.5.1.

End point of particle trajectories - x coordinate with origin of point source transverse to planar field (mm). St based on velocity through 1 mm dia. holes.
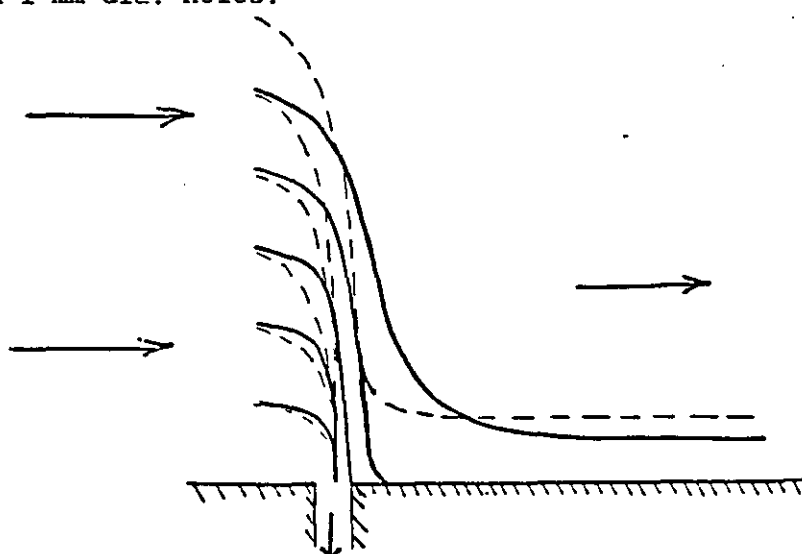
Figure A2.5-1. Trajectories of particles $(\rho_p = 4000$ kg/m$^3)$ along the filter face and into 1 mm dia holes. Illustrates build up on far side of hole

    - - - - - - - - 1 μm dia. particles

    ——————— 4 μm dia. particles

Appendix 2.5.2

The following appendix gives figures demonstrating the channel expansion and bulk density influences within the minipleat filter model. Also included are typical print outs incorporating these effects.Figure 2.8 in chapter 2 illustrates the revised model.

FIG A 2·5·2-1: Comparison of channel expansion effect for mini pleat arrangement theory at a face velocity of 2·5 cm/s, bulk density 800 kg/m³
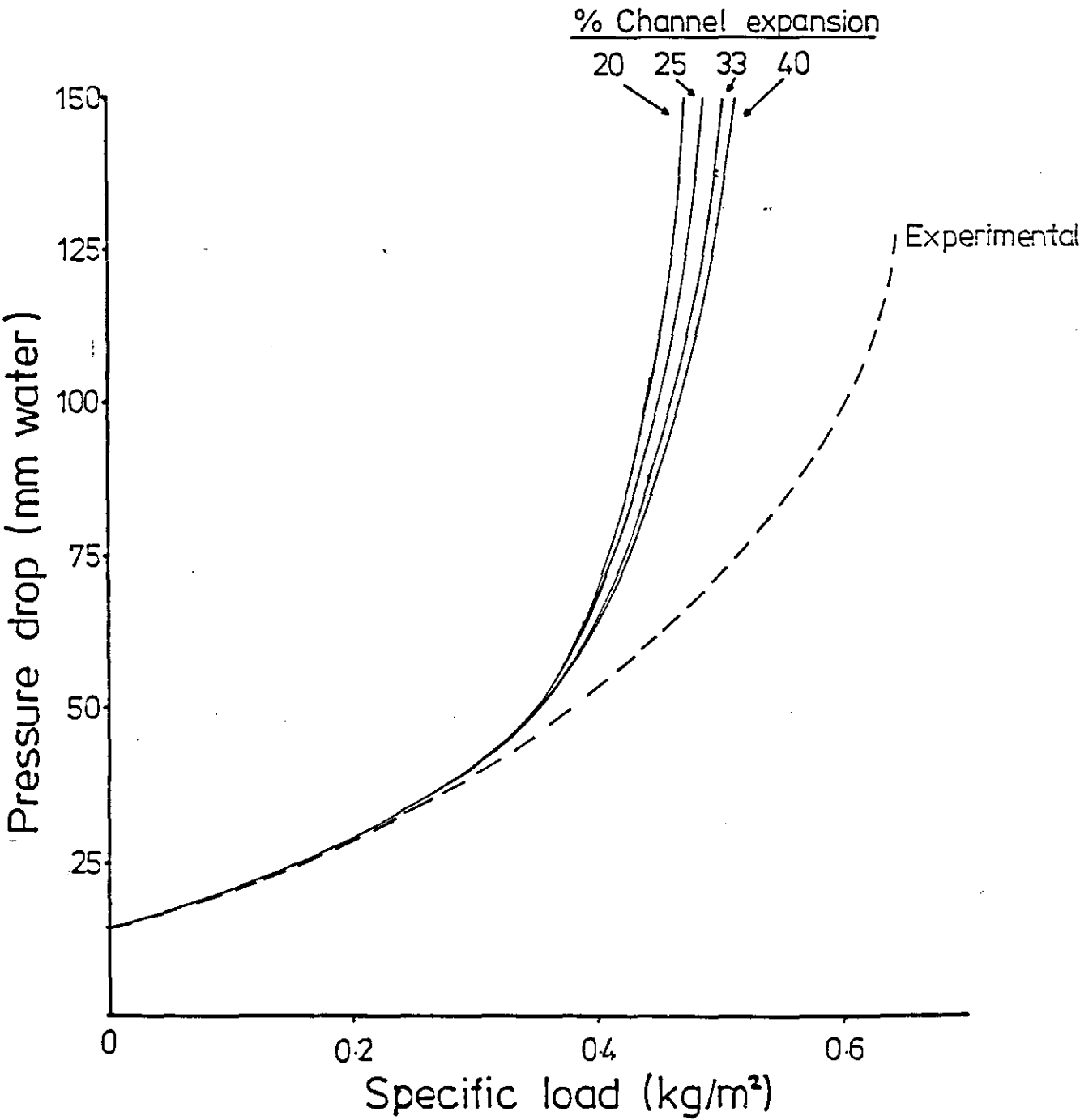
FIG.A2.5.2-2: Comparison of bulk density effect for mini pleat arrangement theory at a face velocity of 2.5 cm/s, channel expansion 33%
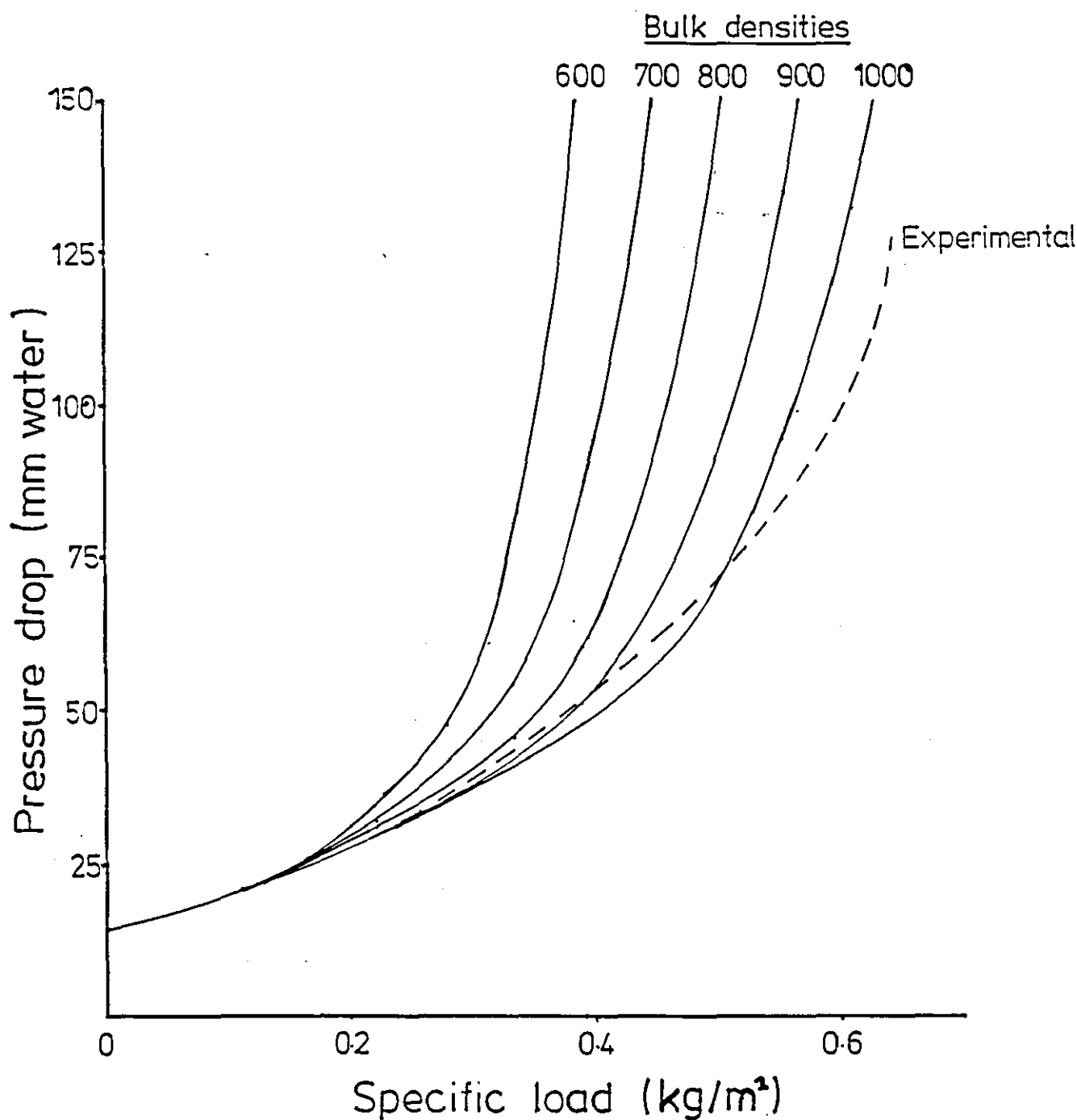
FACE VELOCITY .04
LOAD INCREMENTS .1
AREA OF MEDIA 3.7
MEDIA THICKNESS 6E-04
GAS VISCOSITY 1.85E-05
GAS DENSITY 1.1
INITIAL POWDER BULK DENSITY 850
FINAL POWDER BULK DENSITY 1000
DIMENSIONS OF FILTER UNIT
        HEIGHT .58
        WIDTH .05
        DEPTH .503

SPACER WIDTH 5.57630839E-04
CHANNEL WIDTH .02
CHANNEL EXPANSION (%) 40

NUMBER OF PANELS 1
DISTANCE BETWEEN PANELS .06

SPC LOAD KG/M2	PRESS DROP MM WATER
0.000	23.2
.028	25.9
.056	29.0
.083	32.3
.111	36.1
.139	40.2
.167	44.7
.195	49.6
.222	55.0
.250	59.4
.278	65.3
.306	71.3
.334	77.7
.361	84.4
.389	91.9
.417	100.4
.445	110.4
.473	122.4
.500	137.1

N.B. S.I. Units used unless stated

FACE VELOCITY .025
LOAD INCREMENTS .1
AREA OF MEDIA 3.7
MEDIA THICKNESS 6E-04
GAS VISCOSITY 1.85E-05
GAS DENSITY 1.1
INITIAL POWDER BULK DENSITY 700
FINAL POWDER BULK DENSITY 1000
DIMENSIONS OF FILTER UNIT
        HEIGHT .58
        WIDTH .05
        DEPTH .503

SPACER WIDTH 5.57630839E-04
CHANNEL WIDTH .02
CHANNEL EXPANSION (%) 33

NUMBER OF PANELS 1
DISTANCE BETWEEN PANELS .06

SPC LOAD KG/M2	PRESS DROP MM WATER
0.000	14.3
.028	15.7
.056	17.3
.083	19.1
.111	21.0
.139	23.1
.167	25.5
.195	28.0
.222	30.8
.250	34.0
.278	36.2
.306	39.6
.334	43.3
.361	47.5
.389	52.5
.417	58.3
.445	65.4
.473	74.1
.500	84.6
.528	97.3
.556	112.5
.584	130.3

FACE VELOCITY .0125
LOAD INCREMENTS .1
AREA OF MEDIA 3.7
MEDIA THICKNESS 6E-04
GAS VISCOSITY 1.85E-05
GAS DENSITY 1.1
INITIAL POWDER BULK DENSITY 700
FINAL POWDER BULK DENSITY 900
DIMENSIONS OF FILTER UNIT
        HEIGHT .58
        WIDTH .05
        DEPTH .503

SPACER WIDTH 5.57630839E-04
CHANNEL WIDTH .02
CHANNEL EXPANSION (%) 25

NUMBER OF PANELS 1
DISTANCE BETWEEN PANELS .06

SPC LOAD KG/M2	PRESS DROP MM WATER
0.000	7.0
.028	7.6
.056	8.3
.083	9.0
.111	9.7
.139	10.6
.167	11.5
.195	12.6
.222	13.7
.250	15.0
.278	16.5
.306	18.3
.334	20.5
.361	21.4
.389	24.6
.417	29.9
.445	34.5
.473	41.6
.500	51.0
.528	62.2
.556	76.0
.584	93.1
.612	114.1
.639	106.1

Appendix 3.2.1

Filter media characterisation

For the most part this was available from the manufacturer's data. However, insufficient information was available describing the fibre size distributions. These were measured using scanning electron microscopy and the results are presented below.

TABLE A3.2.1.-1   Fibre size distributions for various media

Size (μm) (dia.)	Cumulative Number %					
	F38Z	F41Z	F43Z	F44Z	F45Y	F47W
0	0	0	0	0	0	0
0.8	36.5	32.3	29.1	20.2	10.6	4.1
1.6	65.3	64.5	54.8	50.0	37.2	26.0
2.4	78.8	79.1	71.5	64.5	56.4	49.3
3.2	85.3	87.3	81.6	73.4	67.0	01.6
4	91.8	92.4	88.3	84.6	79.8	71.2
6	96.5	97.4	96.1	94.3	91.5	83.6
8	98.2	99.3	97.8	97.6	94.7	89.0
10	99.4	100	98.9	99.2	97.9	93.1
12	100	100	100	100	100	97.3
>12	100	100	100	100	100	100
Mean size μm 50% cut	1.18	1.24	1.34	1.60	2.13	2.45

Appendix 3.2.2

Influence of sample tube diameter and sample flowrate on sampling efficiency

A series of tests were made using a Royco 225/512 particle size analyser. ~~The purpose was to measure the significance of~~ Atmospheric aerosol was drawn through ~~sampling inefficiencies.~~ a short (20 mm) sampling tube (A), a rotameter with an integral valve and a 0.3 m long 5 mm bore tube (B) into a Royco 225/512. A range of sampling tubes of varying bore were used. The efficiency of aerosol sample delivery to the sensing instrument was measured and the results are tabulated below. Some general observations are:-

(i)   Lower flowrates reduced sampling efficiency for the same tube bore size.

(ii) For a constant flowrate increasing the tube bore size reduces sampling efficiency.

(iii) At a constant velocity of gas reducing the tube bore size reduces the sampling efficiency particularly of large particles.

(iv) The use of the rotameter for flow metering introduces very high particle losses for particles greater than 1μm. A 26% loss was observed for particles greater than 1.8μm and 50% for those greater than 2.7μm when the Royco was operating at its nominal flowrate. However, losses for particles less than 1μm were small.

These observations lead to the following conclusions which were taken into consideration when sampling during experimental work.

(i)   The smaller the tube bore diameter the less the deposition for the same flowrate.

(ii) To correct the flowrate such that the same velocity exists in any tube results in more aerosol deposition in smaller bore sampling tubes.

(iii) The introduction of a flowmeter into the sampling line adversely effects the sampling efficiency of particles greater than 1μm.

The results presented below are the sampling efficiency expressed as:-

$$\eta = \frac{\text{Atmospheric count} - \text{count}}{\text{Atmospheric count}} \times 100\%$$

where the atmospheric count is that obtained with no sample tube fitted.

1. System parameters

All figures are at 45.2 cc/s sampling rate sampling tube absent

Mean size (μm)	Tube B	Tube B + rotameter	rotameter alone
0.35	7.4	11.2	3.8
0.45	5.1	12.7	7.6
0.85	11.5	18.0	6.5
1.80	21.0	47.4	26.4
size > 2.4	29.2	87.5	58.3

Sampling tests : bore sizes refer to tube A.

2. All 5 mm bore size flow rate variation by rotameter

Mean size (μm)	40 cc/s	30 cc/s	10 cc/s
0.35	21.7	24.1	37.7
0.45	35.1	41.3	63.1
0.85	41.9	58.4	81.3
1.80	42.1	73.7	78.9
Size > 2.4	100	100	100

3. Flowrate stable at 26 cc/s (rotameter controlled), bore size variation

Mean Size (µm)	5 mm	3 mm	2 mm	1 mm
0.35	54.6	44.2	46.4	39.7
0.45	60.6	53.6	53.0	31.0
0.85	64.9	59.3	57.4	9.9
1.80	52.6	47.4	36.8	0
Size > 2.4	100	100	95.8	87.5

4. Same velocity, 230 cm/s, different bore size - velocity maintained rotameter

Mean Size (µm)	5 mm	3 mm	2 mm	1 mm
0.35	11.2	20.4	45.1	66.2
0.45	12.7	47.2	66.1	80.4
0.85	18.0	62.7	82.0	90.7
1.80	47.4	73.7	93.2	95
Size > 2.4	87.5	100	100	100

5. Same bore size, 1 mm, variation of flowrate by rotameter

Mean Size (µm)	7 cc/s	15 cc/s	20 cc/s
0.35	54.0	38.9	31.8
0.45	70.0	49.4	43.1
0.85	83.9	54.3	51.2
1.80	94.7	76.8	74.2
Size > 2.4	100	95.8	91.7

Appendix 3.4.1

Analysis of data collected from experiments of 3.4

The pressure drop response with specific load at various face velocities was measured for different dusts being collected on conventional HEPA filter media. These results are presented on the following pages and their analysis by a computer curve fitting routine is included. A number of empirical equations have been obtained for the pressure drop - loading characteristics of each dust tested. These are also presented below.

RESULT ANALYSIS FOR: ALUMINA 1200 GRID

NO. OF VELOCITIES MEASURED IN EXPERIMENTAL WORK WAS   5
MAXIMUM NUMBER OF DATA POINTS FOR ANY VELOCITY IS   6

FILTER PACKING DENSITY IS   4 %
MEAN FIBRE DIAMETER IS .5 MIC'MTRS
MEAN PORE SIZE OF FILTER IS   2 MIC'MTRS

THE MEAN PARTICLE SIZE IS 4.1 MIC'MTRS
REGIME DIVISION IS WHERE PRESSURE DROP/VELOCITY= 13.7

EXPERIMENTAL RESULTS

VELOCITY NO. 1 IS 2 CMS/S

PRESSURE DROP (MM WATER)	SPECIFIC LOAD (KG/M2)
10.2	0
13.2	.06
18	.154
27.7	.306
36.6	.426
48.5	.6

VELOCITY NO. 2 IS 3 CMS/S

PRESSURE DROP (MM WATER)	SPECIFIC LOAD (KG/M2)
15.2	0
	.114
	.214
	.337
	.449
73.7	.512

VELOCITY NO. 3 IS 4 CMS/S

PRESSURE DROP (MM WATER)	SPECIFIC LOAD (KG/M2)
21.3	0
	.104
48.3	.204
76.2	.331
104	.46
121	.516

VELOCITY NO. 4 IS 6 CMS/S

PRESSURE DROP (MM WATER)	SPECIFIC LOAD (KG/M2)
31.2	0
40.4	.051
63.5	.143
95.3	.263
150	.42
256	.651

VELOCITY NO. 5 IS 8 CMS/S

PRESSURE DROP (MM WATER)	SPECIFIC LOAD (KG/M2)
43.1	0
63.2	.083
82	.143
148.6	.297
215.1	.403
273.1	.493

263

EXPERIMENTAL ANALYSIS

BEST FIT EQUATIONS AT EACH VELOCITY ARE:

EQUATIONS FOR VELOCITY NO. 1 (I.E. 2 CM/S) ARE:

(1) FOR P.D./VEL < 13.7
P.D.= 10.0796417 *EXP(3.4939388 *L)

(2) FOR P.D./VEL >= 13.7
P.D.= 6.02023112 + 71.0189705 *L

PD=PRESSURE DROP,L=SPECIFIC LOAD

EQUATIONS FOR VELOCITY NO. 2 (I.E. 3 CM/S) ARE:

(1) FOR P.D./VEL < 13.7
P.D.= 15.1427773 *EXP(3.50534095 *L)

(2) FOR P.D./VEL >= 13.7
P.D.= .146539807 + 142.478027 *L

PD=PRESSURE DROP,L=SPECIFIC LOAD

EQUATIONS FOR VELOCITY NO. 3 (I.E. 4 CM/S) ARE:

(1) FOR P.D./VEL < 13.7
P.D.= 21.426956 *EXP(4.06500453 *L)

(2) FOR P.D./VEL >= 13.7
P.D.=-3.85281172 + 241.139888 *L

PD=PRESSURE DROP,L=SPECIFIC LOAD

EQUATIONS FOR VELOCITY NO. 4 (I.E. 6 CM/S) ARE:

(1) FOR P.D./VEL < 13.7
P.D.= 31.379275 *EXP(4.78313998 *L)

(2) FOR P.D./VEL >= 13.7
P.D.=-18.5565144 + 417.518398 *L

PD=PRESSURE DROP,L=SPECIFIC LOAD

EQUATIONS FOR VELOCITY NO. 5 (I.E. 8 CM/S) ARE:

(1) FOR P.D./VEL < 13.7
P.D.= 43.2131956 *EXP(4.50490638 *L)

(2) FOR P.D./VEL >= 13.7
P.D.=-40.0180392 + 635.250727 *L

PD=PRESSURE DROP,L=SPECIFIC LOAD

DETAIL OF LIN CONST.TERM VS VEL. FIT(PD/V< 13.7)

ORDER OF BEST POLYNOMIAL FOUND = 1

ORDER	GOODNESS OF FIT
0	9.04237934E-05
1	3.92908174E-05

COEFFICIENTS OF BEST FIT POLYNOMIAL (ORDER 1)

Y = 4.95862401
+ X * .0557635128

RESIDUALS FOR ABOVE CURVE FIT

POLYNOMIAL ORDER = 1

NO.	X	Y	WT.	YCALC	DIFF
1	2	5.04	1	5.07	-.03
2	3	5.048	1	5.126	-.078
3	4	5.357	1	5.1820	.175
4	6	5.35	1	5.408	-.063
5	8	5.402	1	5.405	-3E-03

SUM OF ERRORS SQUARED = .0417202051

264

ORDER OF BEST POLYNOMIAL FOUND = 2

ORDER   GOODNESS OF FIT

0   8.79735489E-04
1   2.7926269E-04
2   2.18595279E-04

COEFFICIENTS OF BEST FIT POLYNOMIAL (ORDER 2)

Y = 2.09762233
 + X * .703611486
 + X↑2 * -.048983296

RESIDUALS FOR ABOVE CURVE FIT

POLYNOMIAL ORDER = 2

NO.	X	Y	WT.	YCALC	DIFF
1	2	3.494	1	3.309	.185
2	3	3.505	1	3.768	-.262
3	4	4.065	1	4.128	-.063
4	6	4.783	1	4.556	.227
5	8	4.505	1	4.592	-.087

SUM OF ERRORS SQUARED = .166183494

DETAIL OF CONST.GRAD.TERM VS VEL.FIT(PD/V)= 13.7)

ORDER OF BEST POLYNOMIAL FOUND = 1

ORDER   GOODNESS OF FIT

0   .0164502874
1   1.15324952E-03

COEFFICIENTS OF BEST FIT POLYNOMIAL (ORDER 1)

Y = 4.48354026
 + X * -1.23551954

RESIDUALS FOR ABOVE CURVE FIT

POLYNOMIAL ORDER = 1

NO.	X	Y	WT.	YCALC	DIFF
1	2	3.01	1	2.013	.998
2	3	.049	1	.777	-.728
3	4	-.963	1	-.459	-.505
4	6	-3.093	1	-2.93	-.163
5	8	-5.002	1	-5.401	.398

SUM OF ERRORS SQUARED = 1.96541971

DETAIL OF LINEAR GRAD.TERM VS VEL.FIT(PD/V)= 13.7)

ORDER OF BEST POLYNOMIAL FOUND = 2

ORDER   GOODNESS OF FIT

0   .629437635
1   .0476147444
2   .0134792558

COEFFICIENTS OF BEST FIT POLYNOMIAL (ORDER 2)

Y = 7.09328045
 + X * 16.3761044
 + X↑2 * -.928968448

RESIDUALS FOR ABOVE CURVE FIT

POLYNOMIAL ORDER = 2

NO.	X	Y	WT.	YCALC	DIFF
1	2	35.509	1	36.13	-.62
2	3	47.493	1	47.861	-.368
3	4	60.285	1	57.734	2.551
4	6	69.586	1	71.907	-2.321
5	8	79.406	1	78.648	.758

SUM OF ERRORS SQUARED = 10.4368179

(1) WHEN PD/VEL < 13.7 (MM WATER/CM/S) USE RELATIONSHIP:

PD=V*(4.95862401 + .0557635128 *V)*EXP[(2.09762233 + .703611486 *V↑2)*L]

(2) WHEN PD/VEL>= 13.7 (MM WATER/CM/S) USE RELATIONSHIP:

PD=V*[(4.48354026 +-1.23551954 *V)+(7.09328045 + 16.3761044 *V↑2)*L]

(WHERE PD=PRESSURE DROP-MM WATER;V=VELOCITY-CM/S,L=SPECIFIC LOAD-

---

CALCULATIONS FROM RESULTS

RESULTS FOR VELOCITY OF 2.5 CMS/S

P.DROP	LOAD
12.74	0
26.92	.2
45.71	.4
66.82	.6
87.94	.8
109.0	1
130.1	1.2

GRAPH OF SPECIFIC LOAD AGAINST PRESSURE DROP

PRESSURE DROP

130

SPECIFIC LOAD
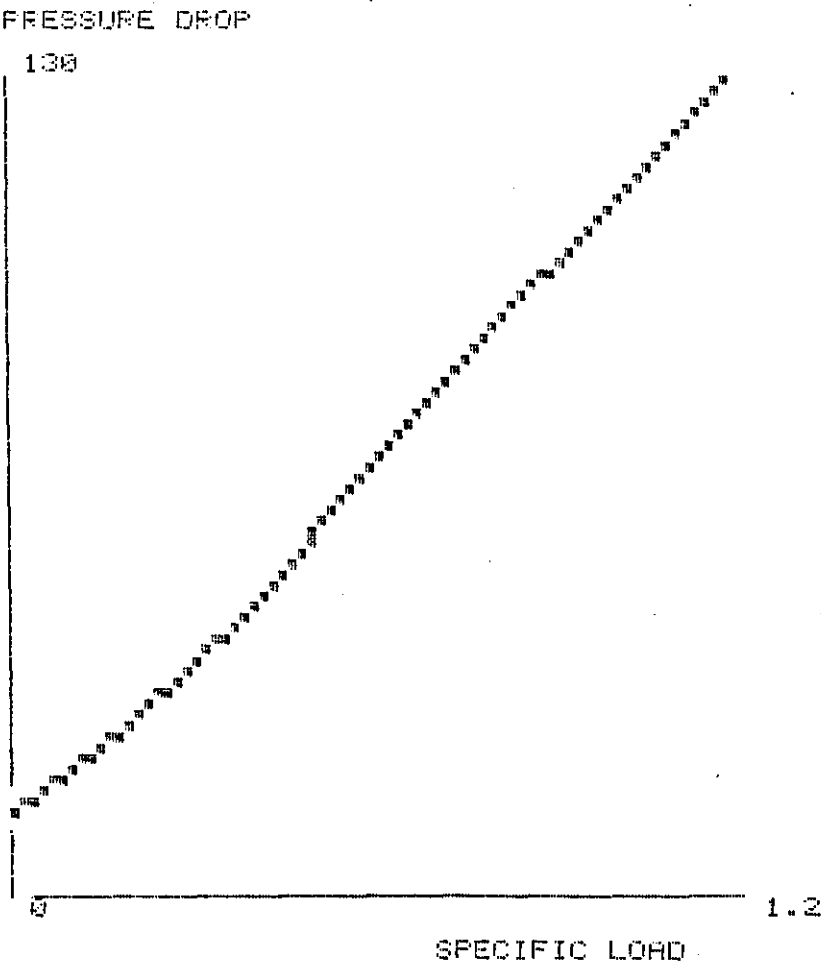
RESULT ANALYSIS FOR: ALUMINA BS NO.2 TEST DUST

NO. OF VELOCITIES MEASURED IN EXPERIMENTAL WORK WAS 5
MAXIMUM NUMBER OF DATA POINTS FOR ANY VELOCITY IS 6

FILTER PACKING DENSITY IS 4 %
MEAN FIBRE DIAMETER IS .5 MIC'MTRS
MEAN PORE SIZE OF FILTER IS 2 MIC'MTRS

THE MEAN PARTICLE SIZE IS 4.9 MIC'MTRS
REGIME DIVISION IS WHERE PRESSURE DROP/VELOCITY= 13.4

EXPERIMENTAL RESULTS

VELOCITY NO. 1 IS 2 CMS/S

PRESSURE DROP (MM WATER)	SPECIFIC LOAD (KG/M2)
10.4	0
15.2	.2
23.6	.4
30.4	.6
37.8	.7
43.1	.8

VELOCITY NO. 2 IS 3.25 CMS/S

PRESSURE DROP (MM WATER)	SPECIFIC LOAD (KG/M2)
17.1	0
27.1	.2
41.4	.4
50.1	.5
60.1	.6
80	.8

VELOCITY NO. 3 IS 5.1 CMS/S

PRESSURE DROP (MM WATER)	SPECIFIC LOAD (KG/M2)
27	0
44.9	.3
60.2	.3
77.5	.4
115.3	.6
155	.8

VELOCITY NO. 4 IS 8 CMS/S

PRESSURE DROP (MM WATER)	SPECIFIC LOAD (KG/M2)
43.2	0
74	.2
101.6	.3
134.8	.4
203.2	.6
272	.8

VELOCITY NO. 5 IS 10 CMS/S

PRESSURE DROP (MM WATER)	SPECIFIC LOAD (KG/M2)
54.5	0
93.5	.2
117	.25
186	.4
279	.5
371	.8

BEST FIT EQUATIONS AT EACH VELOCITY ARE:

EQUATIONS FOR VELOCITY NO. 1 (I.E. 2 CM/S) ARE:
        (1) FOR P.D./VEL < 13.4
            P.D.= 10.3702901 *EXP(1.94036025 *L)

        (2) FOR P.D./VEL >= 13.4
            P.D.= .316666722 + 53.4999999 *L

        PD=PRESSURE DROP,L=SPECIFIC LOAD

EQUATIONS FOR VELOCITY NO. 2 (I.E. 3.25 CM/S) ARE:
        (1) FOR P.D./VEL < 13.4
            P.D.= 17.2049388 *EXP(2.21050604 *L)

        (2) FOR P.D./VEL >= 13.4
            P.D.= .292857125 + 99.6428572 *L

        PD=PRESSURE DROP,L=SPECIFIC LOAD

EQUATIONS FOR VELOCITY NO. 3 (I.E. 5.1 CM/S) ARE:
        (1) FOR P.D./VEL < 13.4
            P.D.= 26.8502425 *EXP(2.6542449 *L)

        (2) FOR P.D./VEL >= 13.4
            P.D.= .0166666847 + 193.75 *L

        PD=PRESSURE DROP,L=SPECIFIC LOAD

EQUATIONS FOR VELOCITY NO. 4 (I.E. 8 CM/S) ARE:
        (1) FOR P.D./VEL < 13.4
            P.D.= 42.9056052 *EXP(2.8278834 *L)

        (2) FOR P.D./VEL >= 13.4
            P.D.=-2.46666658 + 343 *L

        PD=PRESSURE DROP,L=SPECIFIC LOAD

EQUATIONS FOR VELOCITY NO. 5 (I.E. 10 CM/S) ARE:
        (1) FOR P.D./VEL < 13.4
            P.D.= 54.3747763 *EXP(3.028299 *L)

        (2) FOR P.D./VEL >= 13.4
            P.D.= 1.16666682 + 462.5 *L

        PD=PRESSURE DROP,L=SPECIFIC LOAD

THE BEST FIT RELATIONSHIP PD VS L AT ANY VELOCITY

(1) WHEN PD/VEL < 13.4 (MM WATER/CM/S) USE RELATIONSHIP:
PD=V*(5.15375638 + .0273588057 *V)*EXP[(1.39043809 + .30777544 *
  *V↑2)*L]
(2) WHEN PD/VEL>= 13.4 (MM WATER/CM/S) USE RELATIONSHIP:
PD=V*[(.0120089129 + 0 *V)+(17.7584603 + 4.80976219 *V+-.1985825
(WHERE PD=PRESSURE DROP-MM WATER;V=VELOCITY-CM/S,L=SPECIFIC LOAD-K

RESULT ANALYSIS FOR: ALUMINA 20-30 MICRON CUT

NO. OF VELOCITIES MEASURED IN EXPERIMENTAL WORK WAS   3
MAXIMUM NUMBER OF DATA POINTS FOR ANY VELOCITY IS   5

FILTER PACKING DENSITY IS   4 %
MEAN FIBRE DIAMETER IS .5 MIC'MTRS
MEAN PORE SIZE OF FILTER IS   2 MIC'MTRS

THE MEAN PARTICLE SIZE IS 22.8 MIC'MTRS
REGIME DIVISION IS WHERE PRESSURE DROP/VELOCITY= 5.9

EXPERIMENTAL RESULTS

VELOCITY NO. 1 IS 2 CMS/S

PRESSURE DROP (MM WATER)	SPECIFIC LOAD (KG/M2)
10.2	0
11.4	.19
13.4	.42
16.2	.65
20.4	1.1

VELOCITY NO. 2 IS 4 CMS/S

PRESSURE DROP (MM WATER)	SPECIFIC LOAD (KG/M2)
20.6	0
23.2	.17
28.8	.45
37.6	.89
43.2	1.16

VELOCITY NO. 3 IS 10 CMS/S

PRESSURE DROP (MM WATER)	SPECIFIC LOAD (KG/M2)
53	0
58	.09
73	.33
88	.61
98	.83

MORE DATA AT SMALL LOADS FOR VEL. NO. 1 WOULD IMPROVE ACCURACY
PROGRAM WILL REPEAT FOLLOWING DATA POINT TO CONTINUE 11.4 , .19

MORE DATA AT SMALL LOADS FOR VEL. NO. 2 WOULD IMPROVE ACCURACY
PROGRAM WILL REPEAT FOLLOWING DATA POINT TO CONTINUE 23.2 , .17

MORE DATA AT SMALL LOADS FOR VEL. NO. 3 WOULD IMPROVE ACCURACY
PROGRAM WILL REPEAT FOLLOWING DATA POINT TO CONTINUE 58 , .09

BEST FIT EQUATIONS AT EACH VELOCITY ARE:

EQUATIONS FOR VELOCITY NO. 1 (I.E. 2 CM/S) ARE:
    (1) FOR P.D./VEL < 5.9
      P.D.= 10.2 *EXP(.585398075 *L)

    (2) FOR P.D./VEL >= 5.9
      P.D.= 9.08635291 + 10.2900199 *L

    PD=PRESSURE DROP.L=SPECIFIC LOAD

EQUATIONS FOR VELOCITY NO. 2 (I.E. 4 CM/S) ARE:
    (1) FOR P.D./VEL < 5.9
      P.D.= 20.6000001 *EXP(.699183508 *L)

    (2) FOR P.D./VEL >= 5.9
      P.D.= 19.8547106 + 20.2543473 *L

    PD=PRESSURE DROP.L=SPECIFIC LOAD

EQUATIONS FOR VELOCITY NO. 3 (I.E. 10 CM/S) ARE:
    (1) FOR P.D./VEL < 5.9
      P.D.= 53.0000008 *EXP(1.00167862 *L)

    (2) FOR P.D./VEL >= 5.9
      P.D.= 51.6451613 + 55.5299539 *L

    PD=PRESSURE DROP.L=SPECIFIC LOAD

THE BEST FIT RELATIONSHIP PD VS L AT ANY VELOCITY

(1) WHEN PD/VEL < 5.9 (MM WATER/CM/S) USE RELATIONSHIP:

PD=V*(5.04999999 + .0250000086 *V)*EXP[(.465135776 + .0617503665
1E-04 *V↑2)*L]

(2) WHEN PD/VEL>= 5.9 (MM WATER/CM/S) USE RELATIONSHIP:

PD=V*[(4.51019062 + .0671201324 *V)+(5.34871275 +-.132421313 *V+
V↑2)*L]

(WHERE PD=PRESSURE DROP-MM WATER:V=VELOCITY-CM/S.L=SPECIFIC LOAD-K

NO. OF VELOCITIES MEASURED IN EXPERIMENTAL WORK WAS 5
MAXIMUM NUMBER OF DATA POINTS FOR ANY VELOCITY IS 4

FILTER PACKING DENSITY IS 4 %
MEAN FIBRE DIAMETER IS .5 MIC'MTRS
MEAN PORE SIZE OF FILTER IS 2 MIC'MTRS

THE MEAN PARTICLE SIZE IS 52.3 MIC'MTRS
REGIME DIVISION IS WHERE PRESSURE DROP/VELOCITY= 0

EXPERIMENTAL RESULTS

VELOCITY NO. 1 IS 2 CMS/S

PRESSURE DROP (MM WATER)	SPECIFIC LOAD (KG/M2)
10.2	0
11.2	.291
12.4	.73
13.7	1.09

VELOCITY NO. 2 IS 4 CMS/S

PRESSURE DROP (MM WATER)	SPECIFIC LOAD (KG/M2)
21.3	0
24.4	.483
26.9	.86
30	1.33

VELOCITY NO. 3 IS 6 CMS/S

PRESSURE DROP (MM WATER)	SPECIFIC LOAD (KG/M2)
32.3	0
36.8	.483
40.6	.86
45.2	1.33

VELOCITY NO. 4 IS 8 CMS/S

PRESSURE DROP (MM WATER)	SPECIFIC LOAD (KG/M2)
43.4	0
50.3	.483
55.1	.86
60.4	1.33

VELOCITY NO. 5 IS 10 CMS/S

PRESSURE DROP (MM WATER)	SPECIFIC LOAD (KG/M2)
55.4	0
63.5	.483
69.6	.86
76.2	1.33

MORE DATA AT SMALL LOADS FOR VEL. NO. 1 WOULD IMPROVE ACCURACY
INSUFFICIENT DATA FOR CALCULATION

MORE DATA AT SMALL LOADS FOR VEL. NO. 2 WOULD IMPROVE ACCURACY
INSUFFICIENT DATA FOR CALCULATION

MORE DATA AT SMALL LOADS FOR VEL. NO. 3 WOULD IMPROVE ACCURACY
INSUFFICIENT DATA FOR CALCULATION

MORE DATA AT SMALL LOADS FOR VEL. NO. 4 WOULD IMPROVE ACCURACY
INSUFFICIENT DATA FOR CALCULATION

MORE DATA AT SMALL LOADS FOR VEL. NO. 5 WOULD IMPROVE ACCURACY
INSUFFICIENT DATA FOR CALC

BEST FIT EQUATIONS AT EACH VELOCITY ARE:

EQUATIONS FOR VELOCITY NO. 1 (I.E. 2 CM/S) ARE:

    (1) FOR P.D./VEL < 0
      NO VALID EQUATION DUE TO INSUFFICIENT DATA

    (2) FOR P.D./VEL >= 0
      P.D.= 10.2211448 + 3.13675719 *L

    PD=PRESSURE DROP,L=SPECIFIC LOAD

EQUATIONS FOR VELOCITY NO. 2 (I.E. 4 CM/S) ARE:

    (1) FOR P.D./VEL < 0
      NO VALID EQUATION DUE TO INSUFFICIENT DATA

    (2) FOR P.D./VEL >= 0
      P.D.= 21.2813798 + 6.52519817 *L

    PD=PRESSURE DROP,L=SPECIFIC LOAD

EQUATIONS FOR VELOCITY NO. 3 (I.E. 6 CM/S) ARE:

    (1) FOR P.D./VEL < 0
      NO VALID EQUATION DUE TO INSUFFICIENT DATA

    (2) FOR P.D./VEL >= 0
      P.D.= 32.2353186 + 9.69332556 *L

    PD=PRESSURE DROP,L=SPECIFIC LOAD

EQUATIONS FOR VELOCITY NO. 4 (I.E. 8 CM/S) ARE:

    (1) FOR P.D./VEL < 0
      NO VALID EQUATION DUE TO INSUFFICIENT DATA

    (2) FOR P.D./VEL >= 0
      P.D.= 43.9624292 + 12.6401356 *L

    PD=PRESSURE DROP,L=SPECIFIC LOAD

EQUATIONS FOR VELOCITY NO. 5 (I.E. 10 CM/S) ARE:

    (1) FOR P.D./VEL < 0
      NO VALID EQUATION DUE TO INSUFFICIENT DATA

    (2) FOR P.D./VEL >= 0
      P.D.= 55.5948154 + 15.4297007 *L

    PD=PRESSURE DROP,L=SPECIFIC LOAD

THE BEST FIT RELATIONSHIP PD VS L AT ANY VELOCITY

(1) WHEN PD/VEL < 0 (MM WATER/CM/S) USE RELATIONSHIP:

INSUFFICIENT DATA FOR RELATIONSHIP

(2) WHEN PD/VEL>= 0 (MM WATER/CM/S) USE RELATIONSHIP:

PD=V*[(5.04981803 + .0536288501 *V)+(1.50840993 + .0419795223 *V↑2)*L]

(WHERE PD=PRESSURE DROP-MM WATER;V=VELOCITY-CM/S,L=SPECIFIC LOAD-

The effect on the pressure drop response of uneven loading of the filter media

The pressure drop at all points across the filter is taken as P. For a filter of area A, assume a small fraction of the area, αA, covered by depth $\beta \sigma_H$ of dust. The remaining area $(1-\alpha)A$ is covered by a layer of dust depth σ_H
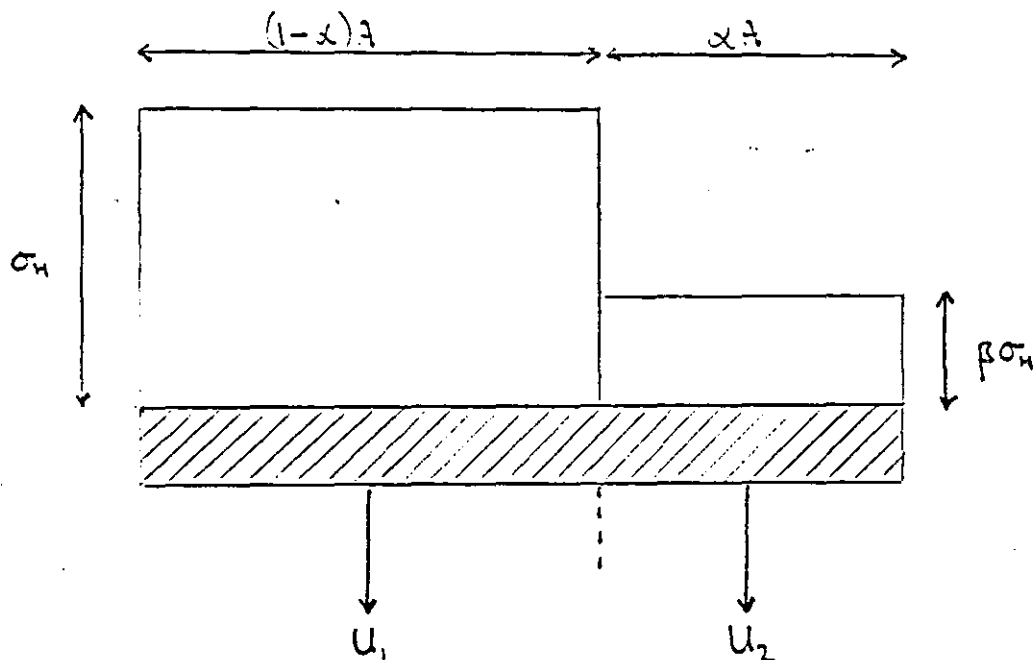
Assume Darcy's law applies and the volumetric flowrate Q is constant. Hence

$$\Delta P = \beta' u_1 \sigma_H = \beta' u_2 \beta \sigma_H \qquad (A3-1)$$

Also

$$Q = (1-\alpha) A u_1 + \alpha A u_2$$

Now average depth σ_{H_a} of the dust layer is

$$A \sigma_{H_a} = (1-\alpha) A \sigma_H + \alpha A \beta \sigma_H$$

$$\sigma_H = \sigma_{H_a} / (1 - \alpha + \alpha\beta) \qquad (A3-2)$$

Similarly average face velocity

$$u_{0a} = \frac{Q}{A} = (1-\alpha) u_1 + \alpha u_2 \qquad (A3-3)$$

Now from (A3-1)

$$u_2 = u_1 / \beta$$

So in (A3-3)

$$u_1 = \frac{u_{0a}}{(1 - \alpha + \alpha/\beta)} \qquad (A3-4)$$

Therefore overall substituting (A3-2) and (A3-4) into $\Delta P = \beta' u_1 \sigma_H$

$$\Delta P = \frac{\beta' u_{0a} \sigma_H}{\{1 - \alpha(1-1/\beta)\}\{1 - \alpha(1-\beta)\}} \qquad (A3-5)$$

Hence it can be shown that a β is always less than 1 for uneven load then the denominator will always be >1 and so the pressure drop will be lower than that predicted by Darcy's law. Furthermore ~~the greater~~ the greater the denominator so the greater the effect on reducing pressure drop.

Below are typical size analyses for each of the dusts used in the experimental programme of chapters 3 and 4. In particular cases where the dust varied significantly between batches more than one example is quoted. All dusts were analysed by Coulter Counter and this size distribution has been used for all analytical and theoretical work. The results quoted are the average of ten identical experimental analyses. Errors are therefore reduced but statistical variations for individual measurements in the order of 5-20% are common depending on particle size. Comparisons by alternative techniques were made on some dusts (Andreasen pipette and a Sedigraph have been used) but only for verification. This was acceptable and hence only the Coulter results are reported.

Abralox P3

Particle dia. (μm)	Cum. wt. %
1.0	0
1.25	2.9
1.5	6.3
1.75	10.6
2.0	15.9
2.5	28.4
3.0	42.5
3.5	55.2
4.0	67.5
4.5	77.8
5.0	84.9
6.0	94.5
8.0	99.1
10.0	99.8
15.0	100

1200 Grid Alumina Dust

Particle dia. (µm)	Cum. wt. %
2.0	0
2.51	4.3
3.17	15.7
4.0	43.0
5.03	77.8
6.34	95.3
8.0	98.9
10.07	99.5
12.69	99.6
16.0	100

Abralox P5

Particle dia (µm)	Cum. wt. %
1.0	0
1.26	1.2
1.58	3.4
2.0	8.5
2.52	17.8
3.17	31.8
4.0	48.2
5.04	68.0
6.35	84.6
8.0	95.5
10.08	99.3
12.7	99.9
16.0	100

BS 2831 No.2. Dust

Particle dia. (μm)	Cum. wt. %		
	Batch 1	Batch 2*	Batch 5
1.0	0	0	0
1.26	0	0.7	0
1.58	0	1.4	0.1
2.0	0	2.8	0.3
2.52	2.3	6.2	0.8
3.17	8.5	16.4	2.6
4.0	24.5	36.9	10.6
5.04	50.6	63.7	44.7
6.35	80.4	86.0	85.6
8.0	95.9	96.8	97.9
10.08	98.8	99.4	99.9
12.7	99.1	99.7	100
16.0	99.2	100	100
20.16	99.5	100	100
25.39	100	100	100

*Figures given are from intrepolation as orginally different channel sizes were used to measure the cumulative weight percentage.
Note
Batches 3 and 4 fell within the range of batches 2 and 5.

Abralox P15

Particle dia. (μm)	Cum. wt. %
3.17	0
4.0	0.8
5.03	2.4
6.34	6.7
8.0	17.8
10.07	41.8
12.69	73.3
16.0	94.1
20.15	99.2
25.39	99.5
32	99.8
40.31	100

15 – 40 μm Alumina dust

Particle dia. (μm)	Cum. wt. %
3.17	0
4.0	0.1
5.03	0.2
6.34	0.5
8.0	0.9
10.07	1.4
12.69	2.1
16.0	3.9
20.15	17.8
25.39	68.0
32.0	97.4
40.31	99.0
50.79	100

Alumina 20 – 30 micron dust

Particle dia. (μm)	Cum. wt. %
6.34	0
8.0	0.1
10.07	0.2
12.69	0.5
16.0	0.9
20.15	8.3
25.39	79.3
32.0	99.6
40.31	100

Alumina 28 - 53 micron dust

Particle dia. (μm)	Cum. wt. %
8.0	0
10.07	0.1
12.69	0.2
16.0	0.3
20.15	0.7
25.39	1.5
32.0	11.7
40.31	60.8
50.79	93.5
64.0	99.9
80.6	100

Alumina 28 - 50 micron dust

Particle dia. (μm)	Cum. wt. %
10.07	0
12.69	0.1
16.0	0.3
20.15	0.6
25.39	1.3
32.0	9.5
40.31	67.3
50.79	98.6
64.0	100

Dusts of greater size

For these dusts a combination of coulter counter and sieve analysis was used. Results are in table below.

Particle Size Analyis - Sieve and Coulter

Size (μm)	Cum % under size by weight sample			
	50-70 μm	53-70 μm	63-105 μm	105-150 μm
* 150				100
* 106			96.8	83.9
* 90			43.4	17.1
* 75	99.5	99.8	25.7	0.8
* 63	82.1	86.5	12.0	
* 53	49.9	43.5	6.4	
50.8	21.3	10.3	3.3	
40.8	3.1	1.1	1.7	
32.0	2.0	0.6	1.1	
25.4	1.0	0.4	0.8	
20.2	0.3	0.2	0.6	
16.0	0.1	0.1	0.4	
12.7	0	0	0.3	
10.1			0.2	
8			0.1	

(The leftmost column from 50.8 to 8 is bracketed as "Coulter counter")

* - Seive diameter

Appendix 3.5.2.

This appendix details analysis of the dust height profile across a
channel and bulk density measurements found on samples taken from
loaded deep pleat filters. The complete sample was of four complete
channels from a sheet centre. The sample was further divided into 5 at
5 cm intervals from the channel entrance. Each of these samples was
also cut in half for measurement of the dust layer height across one
of the four channels using a travelling microscope. Measurements were
taken from left to right where left is zero height at the channels
bottom edge where the spacer would meet the media. The following
tables give the results for each test made.

TABLE A3.5.2-1: BS 2821 No.2 dust at 1.25cm/s

Total wt. 12.80 g   total area 149 cm^2
Media wt. 1.79 g
Dust wt. 11.01 g   Av. specific load 0.74 kg/m^2

Section No.	1	2	3	4	5
Position (cm)	0.5	5.10	10.15	15.20	20.25
Section wt.	2.99	3.16	2.59	2.04	1.95
Medium wt.	0.36	0.36	0.36	0.34	0.37
	2.63	2.80	2.23	1.70	1.58
Section area	29	30.5	30.5	30.5	27.5
Section Spec.	0.91	0.92	0.73	0.56	0.57

Dust Layer Height across a channel (mm)

Section No.	1	2	3	4	5
Dist. from edge (cm)					
0	0	0.06	0	0.04	0
3	0.90	1.26	1.04	1.79	0.88
6	2.19	1.39	0.81	0.96	0.88
9	1.41	1.02	0.99	0.85	0.70
12	0.88	0.57	1.08	0.74	0.57
15	0.46	0.08	0	0.12	0.24

Averages

Ave. Dust layer ht. (mm)	1.35	1.06	0.98	1.09	0.76
Ave. Dust volume (mm³)	3.92	3.23	2.99	3.32	2.09
Ave. Dust bulk density (kg/m³)	671	867	746	512	756

This gives:-

    (1) Overall dust layer height   1.05 mm

    (2) Overall bulk density 710 kg/m³

TABLE A3.5.2-2: BS 2831 No.2 dust at 2.25cm/s

    Total wt. 17.04 g   total area 143 cm²

    Media wt. 1.72 g

    Dust wt. 15.32 g   Av. specific load 1.07 kg/m²

Section No.	1	2	3	4	5
Position (cm)	0.5	5.10	10.15	15.20	20.25
Section wt. (g)	3.77	3.97	3.27	2.82	3.21
Medium wt. (g)	0.35	0.36	0.34	0.35	0.32
Dust wt. (g)	3.42	3.61	2.93	2.47	2.89
Section area (cm²)	28	29.5	29	28	28.5
Section Spec. load (kg/m²)	1.22	1.22	1.01	0.88	1.01

Dust Layer Height across a channel (mm)

Section No. dist. from edge (cm)	1	2	3	4	5
0	0	0.05	0	0.07	0
3	2.35	2.57	1.95	0.90	1.19
6	2.83	1.70	1.00	1.03	0.94
9	1.85	2.27	1.09	1.22	1.08
12	0.66	0.95	0.98	1.04	0.96
15	0.12	0	0	0.07	0.04

Averages

Ave. Dust layer ht. (mm)	1.92	1.87	1.26	1.05	1.04
Ave. Dust volume (mm^3)	5.38	5.52	3.64	2.93	2.97
Ave. Dust bulk density (kg/m^3)	636	654	805	843	973

This gives:-

    (1) Overall dust layer height 1.43 mm

    (2) Overall bulk density 782 kg/m^3

TABLE A3.5.2-3: BS 2831 No.2 dust at 3.5 cm/s

    Total wt. 10.35 g   total area 138 cm^2

    Media wt. 1.66 g

    Dust wt. 8.72 g   Av. specific load 0.63 kg/m^2

Section No.	1	2	3	4	5
Position (cm)	0.5	5.10	10.15	15.20	20.25
Section wt. (g)	2.35	2.33	1.84	1.74	2.12
Medium wt. (g)	0.32	0.35	0.34	0.35	0.30
Dust wt. (g)	2.03	1.98	1.50	1.39	1.82
Section area (cm^2)	27	29	28	29	25
Section Spec. load (kg/m^2)	0.75	0.68	0.54	0.48	0.73

Dust Layer Height across a channel (mm)

Section No.	1	2	3	4	5
Dist. from edge (cm)					
0	0	0.28	0	0.07	0.28
3	1.19	1.25	1.09	1.02	1.00
6	0.92	1.16	1.09	0.64	0.89
9	1.72	0.82	0.67	0.53	0.90
12	0.50	0.42	0.75	0.61	0.59
15	0.17	0	0.21	0.03	0.27

Averages

Ave. Dust layer ht. (mm)	1.08	0.97	0.90	0.70	0.85
Ave. Dust volume (mm^3)	2.92	2.64	2.52	2.03	2.13
Ave. Dust bulk density (kg/m^2)	695	750	595	685	854

This gives:-

    (1) Overall dust layer height   0.89 mm

    (2) Overall bulk density 716 kg/m^3

TABLE A3.5.2-4: BS 2831 No.2 dust at 2.5 cm/s

    Total wt. 6.35 g   total area 137 cm^2

    Media wt. 1.60 g

    Dust wt. 4.95 g   Av. specific load 0.36 kg/m^2

Section No.	1	2	3	4	5
Position (cm)	0.5	5.10	10.15	15.20	20.25
Section wt. (g)	2.10	1.27	1.16	1.04	0.98
Medium wt. (g)	0.33	0.32	0.32	0.33	0.30
Dust wt. (g)	1.77	0.95	0.84	0.71	0.68
Section area (cm^2)	28	28	28	28	25
Section Spec. load (kg/m^2)	0.63	0.34	0.30	0.25	0.27

Dust Layer Height across a channel (mm)

Section No.	1	2	3	4	5
Dist. from edge (cm)					
0	0	0.15	0	0	0
3	1.56	1.06	1.06	0.47	0.63
6	0.87	0.48	0.57	0.52	0.57
9	1.46	0.76	0.55	0.56	0.58
12	1.29	0.26	0.61	0.57	0.65
15	0	0	0.11	0	0

Averages

Ave. Dust layer ht. (mm)	1.30	0.64	0.70	0.53	0.61
Ave. Dust volume (cm^3)	3.63	1.79	1.95	1.48	1.52
Ave. Dust bulk density (kg/m^3)	488	531	431	480	447

This gives:-

   (1) Overall dust layer height 0.76 mm

   (2) Overall bulk density 475 kg/m^3

Appendix 4.1.1

In the following appendix graphs of cumulative dust weight against position are shown for the original deep pleat dust distribution tests. A sample of the Coulter counter analysis carried out on these filter sheets is also given. Overall the results showed little variation of size distribution at any point in the filter.

FIG.A.4.1.1-1: FILTER SHEET NO.2
(15-40 µM Dust)
Plot of cumulative weight of dust vs. position

Cumulative weight of dust (%)

Distance travelled along filter pleat (cm)

□ Overall average
○ . Base section 17% total wt.
× Centre   "   74%   "   "
+ Top   "   9%   "   "
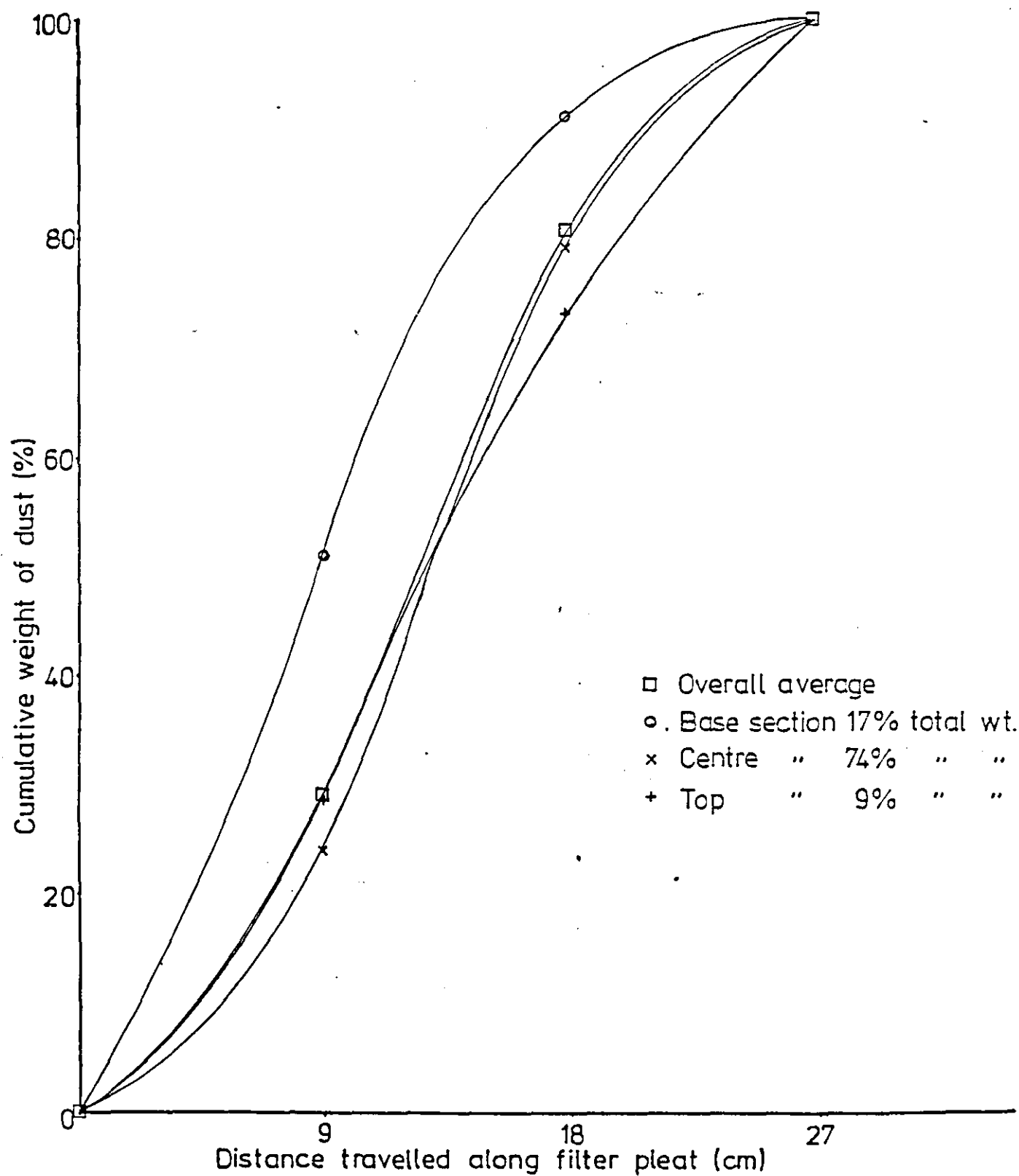
FIG A4·1·1-2: FILTER SHEET NO.4
(3·2 µM Mean dust)
Plot of cumulative weight of dust vs. position

Cumulative weight of dust (%)

□ Overall average
○ Base section 32% total wt.
× Centre   "   22%   "   "
+ Top   "   46%   "   "

Distance travelled along filter pleat (cm)

288
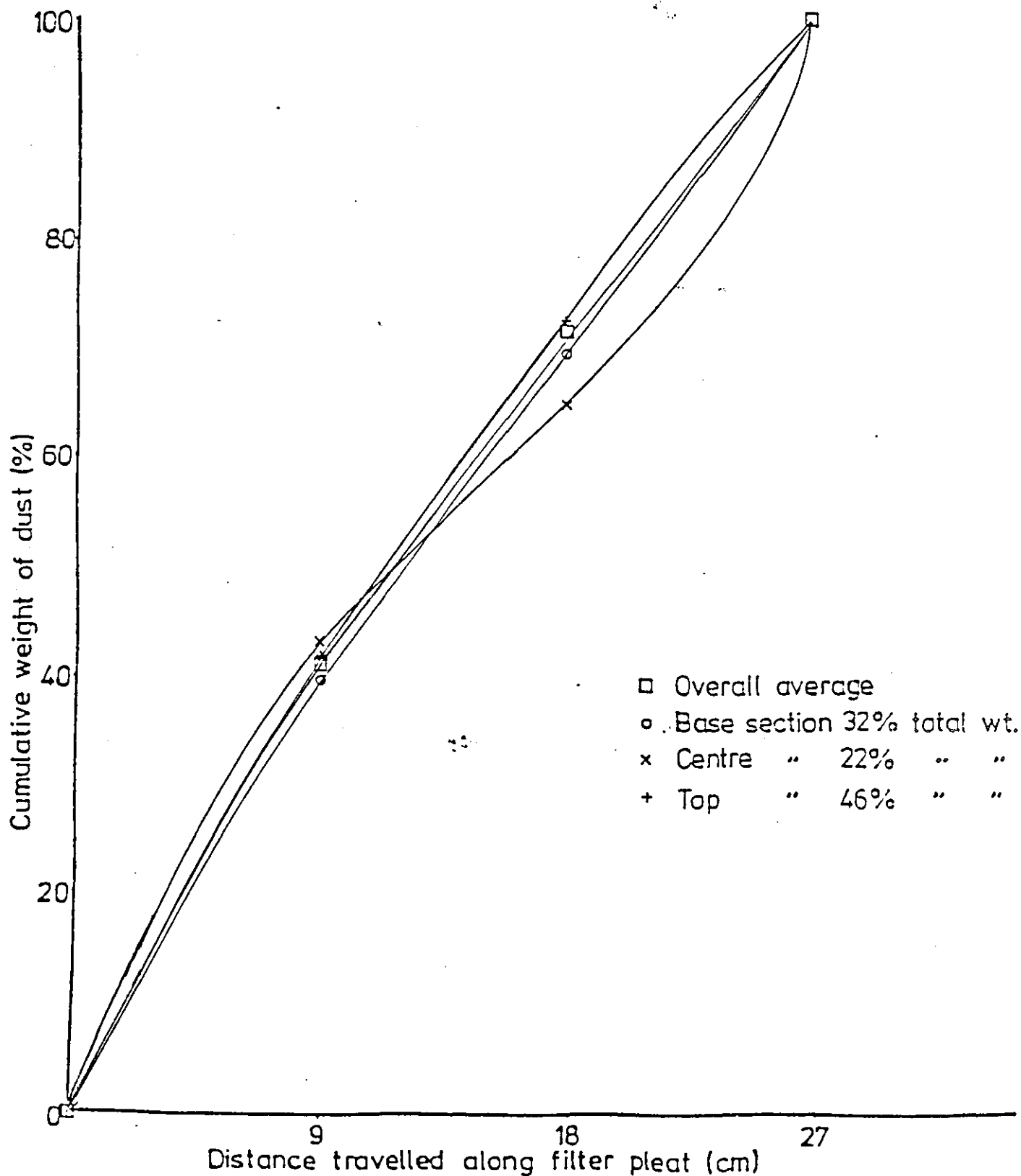
FIG A4·1·1-3: FILTER SHEET NO. 6
(B.S. NO. 2 ·05 Kg/M²)
Plot of cumulative weight of dust vs. position

□ Overall average
o Base section 21% total wt.
× Centre   "   34%   "   "
+ Top   "   45%   "   "

Cumulative weight of dust (%)

Distance travelled along filter pleat (cm)
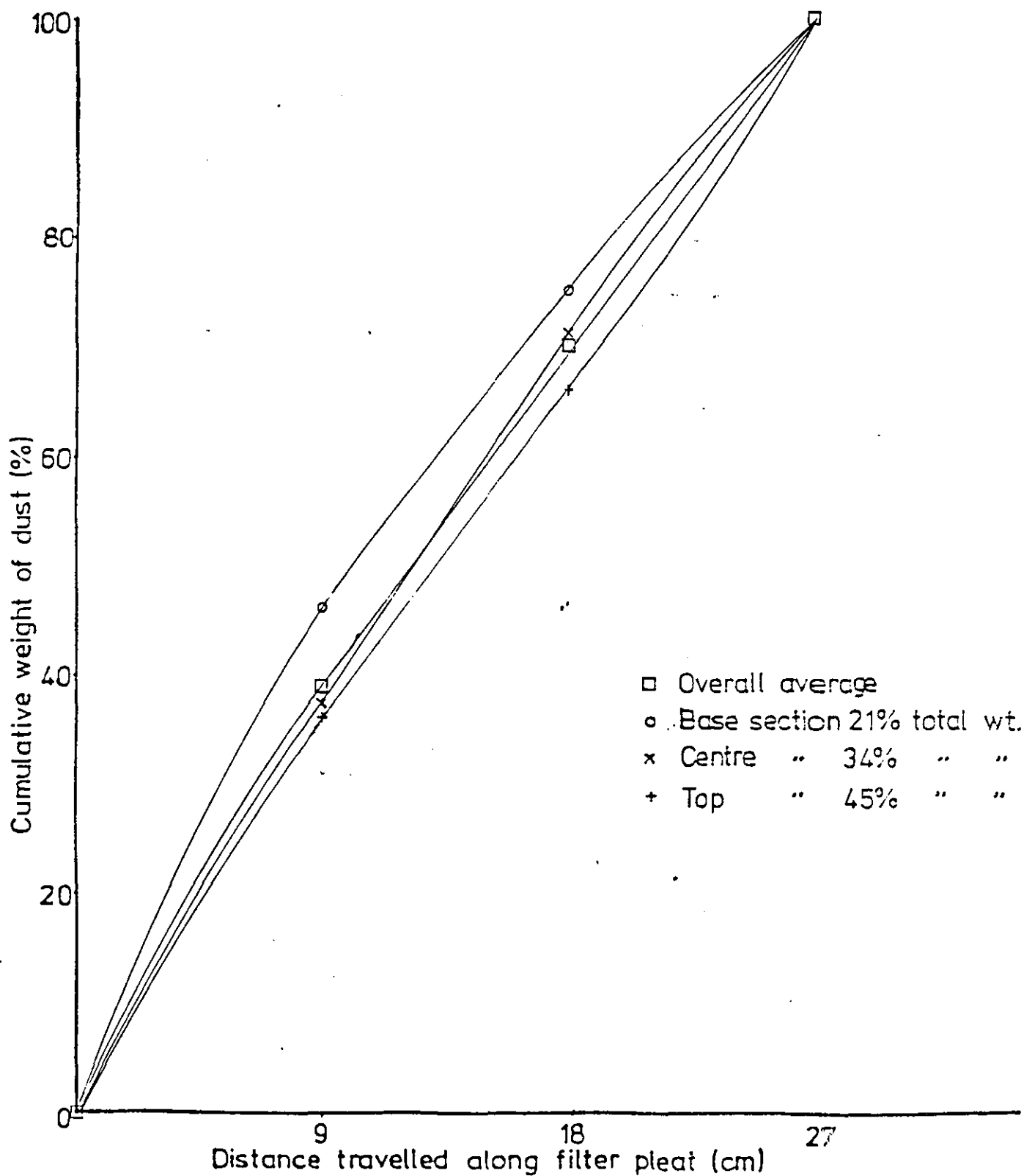
FIG A.4.1.1-4: FILTER SHEET NO.8
(B.S. NO.2 ·025 Kg/M²)
Plot of cumulative weight of dust vs. position

Legend:
- □ Overall average
- ○ Base section 18% total wt.
- × Centre "   30% "   "
- + Top   "   52% "   "

Y-axis: Cumulative weight of dust (%)

X-axis: Distance travelled along filter pleat (cm)
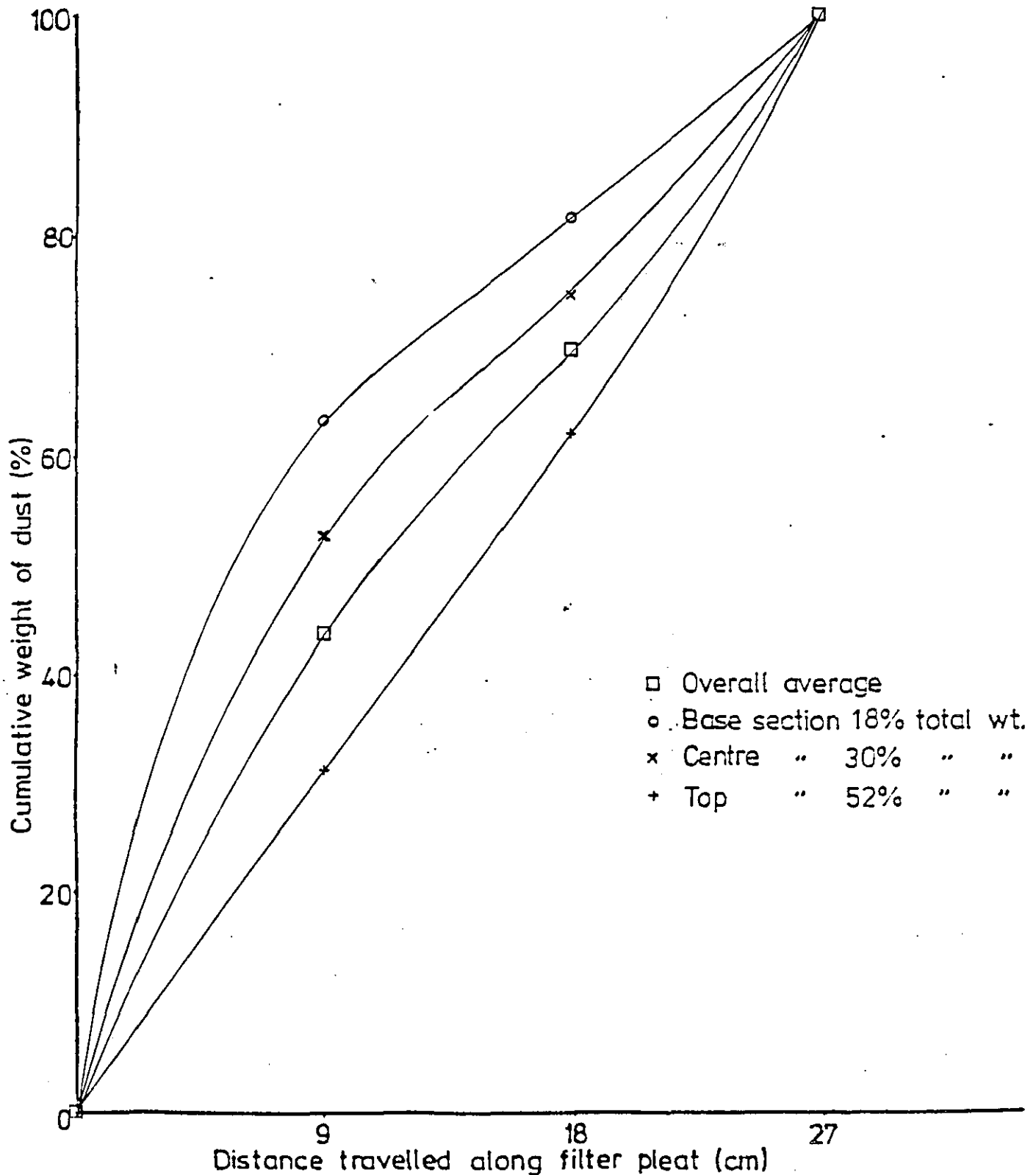
FIG A4·1·1-5: FILTER SHEET NO.10
(B.S. NO.2 ·01 Kg/M²)

Plot of cumulative weight of dust vs. position
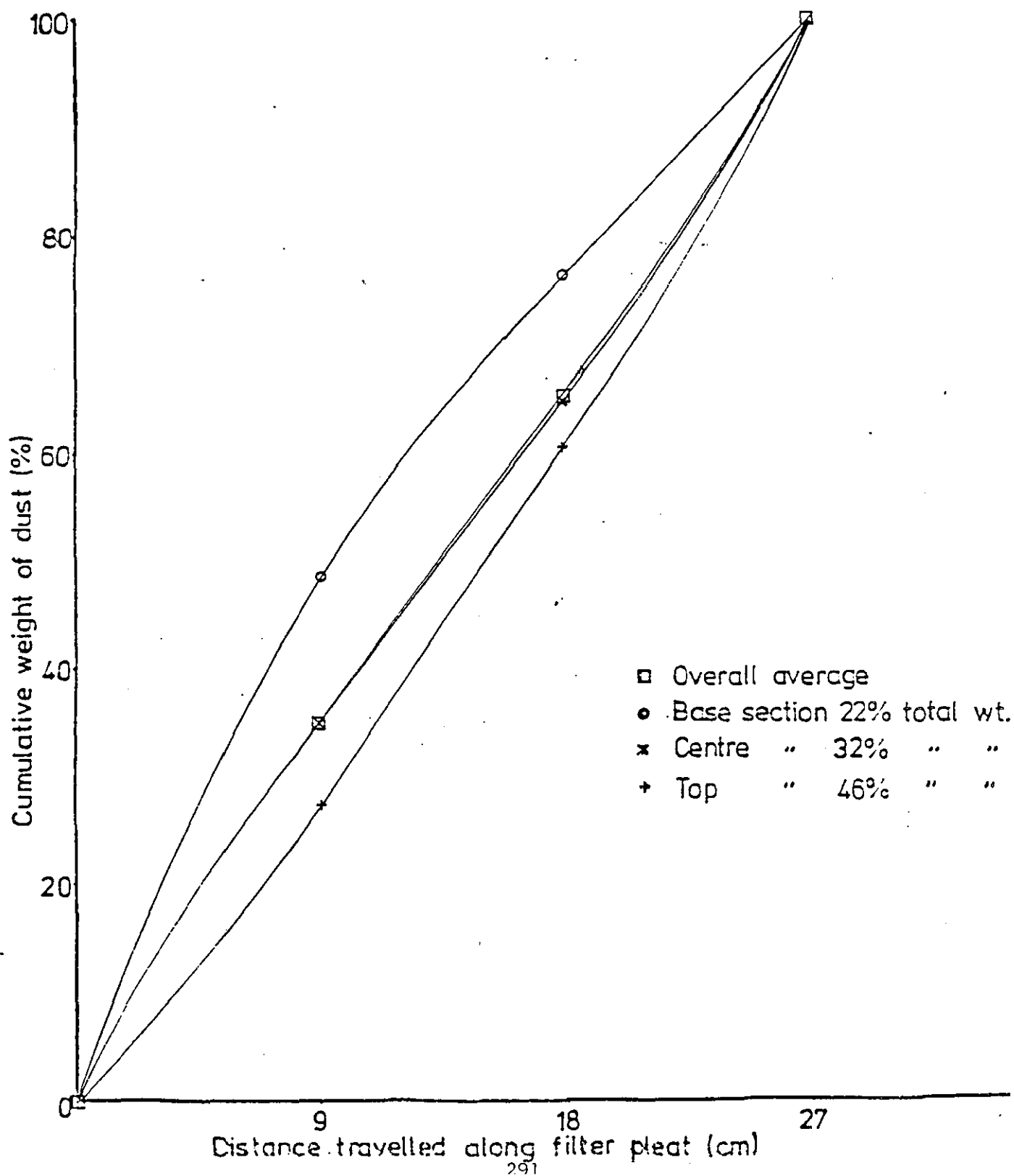
Legend:
- □ Overall average
- ○ Base section 22% total wt.
- ✕ Centre " 32% " "
- + Top " 46% " "

Cumulative weight of dust (%)

Distance travelled along filter pleat (cm)

LOUGHBOROUGH UNIVERSITY OF TECHNOLOGY

CHEMICAL ENGINEERING DEPARTMENT

PARTICLE SIZE ANALYSIS COULTER COUNTER

REFERENCE:-R OWEN. 6/N/1

SIZE MICRONS	SIGMA/N	REL..WT.	CUM%WT<
17	0	.39	99.6
15	.94	.16	99.43
13	.94	.11	99.32
12	.88	.11	99.2
11	.65	.18	99.01
10	.92	.21	98.8
9	.89	.66	98.14
8	1.01	1.97	96.17
7	.85	4.92	91.24
6	1.47	11.1	80.13
5	1.21	18.54	61.59
4	1.35	26.2	35.38
3	1.36	23.16	12.22
2	1.52	9.3	2.92
1	2.43	2.92	0

LOUGHBOROUGH UNIVERSITY OF TECHNOLOGY

CHEMICAL ENGINEERING DEPARTMENT

PARTICLE SIZE ANALYSIS COULTER COUNTER

REFERENCE:-R OWEN. 6/N/2

SIZE MICRONS	SIGMA/N	REL.WT.	CUM%WT<
17	0	.41	99.58
15	.99	.08	99.5
13	.99	.05	99.44
12	1.37	.2	99.24
11	.7	.25	98.98
10	.66	.24	98.74
9	.96	.77	97.97
8	.74	1.36	96.61
7	.63	3.33	93.28
6	1.14	8.68	84.59
5	.82	16.58	68.01
4	.8	26.79	41.21
3	1.38	25.99	15.22
2	.96	11.48	3.73
1	2.13	3.73	0

LOUGHBOROUGH UNIVERSITY OF TECHNOLOGY

CHEMICAL ENGINEERING DEPARTMENT

PARTICLE SIZE ANALYSIS COULTER COUNTER

REFERENCE:-R OWEN.   6/M/3

SIZE MICRONS	SIGMA/N	REL.WT.	CUM%WT<
17	0	1.01	98.98
15	0	0	98.98
13	1	.09	98.88
12	1.22	.2	98.68
11	.79	.21	98.47
10	.75	.28	98.19
9	.82	.83	97.36
8	.95	1.63	95.72
7	1.12	4.24	91.47
6	1.33	8.85	82.62
5	1.49	16.2	66.41
4	.98	25.34	41.07
3	1.24	25.48	15.59
2	.93	11.64	3.94
1	1.81	3.94	0

Appendix 4.1.2

This appendix gives results from the deep pleat filter test work
in section 4.1.2. which have not been presented in the main text.
The following table gives the dust load distribution found on all the
sheets examined. As dust size distribution showed little difference
with respect to position either along the channel or within the filter
just one complete example has been included to illustrate the dust
size distribution effect.

SAMPLE CODE	DUST WEIGHT (GRAMS)	DUST LOADING (KG/M2)
B/B/1	.09862	.03653
B/B/2	.09037	.03347
B/B/3	.08781	.03252
B/M/1	.12975	.04806
B/M/2	.09687	.03588
B/M/3	.09668	.03581
B/T/1	.10075	.03732
B/T/2	.08741	.03237
B/T/3	.08607	.03188
C/B/1 *	.17339	.06422
C/B/2 *	.13785	.05106
C/B/3 *	.12004	.04446
C/M/1	.18232	.06753
C/M/2 **	.16923	.06268
C/M/3	.16547	.06129
C/T/1	.15451	.05723
C/T/2	.16023	.05934
C/T/3	.14493	.05368
D/B/1	.23461	.08689
D/B/2	.18639	.06903
D/B/3	.18018	.06673
D/M/1 *	.24950	.09241
D/M/2 *	.25870	.09581
D/M/3 *	.25013	.09264
D/T/1 *	.21914	.08116
D/T/2 *	.23835	.08828
D/T/3 *	.22666	.08395
E/B/1 (?))	.20501	.07593
E/B/2 (?))	.05543	.02052
E/B/3 (?))	.05767	.02136
E/M/1)	.38494	.14257
E/M/2)(!!)	.32970	.12211
E/M/3 **)	.29852	.11056
E/T/1)	.20741	.07682
E/T/2)	.23206	.08595
E/T/3)	.26516	.09821

*   These results must be treated with suspicion as small amounts
    of dust were lost due to electrostatic charges from the filter
    membrane container. Estimates of the loss were made.
** These results are estimates only as large amounts of dust
    were lost during the weighing process.
?   These results are probably unrepresentative. A channel block-
    age is the likely explanation.
!! The results from sheet 'E' have probably been adversely affe-
    cted by the above and so cannot be regarded as typical.

FIGURE A4.1.2-1

CUMULATIVE WEIGHT VS. PARTICLE SIZE

(SHEET C BASE)
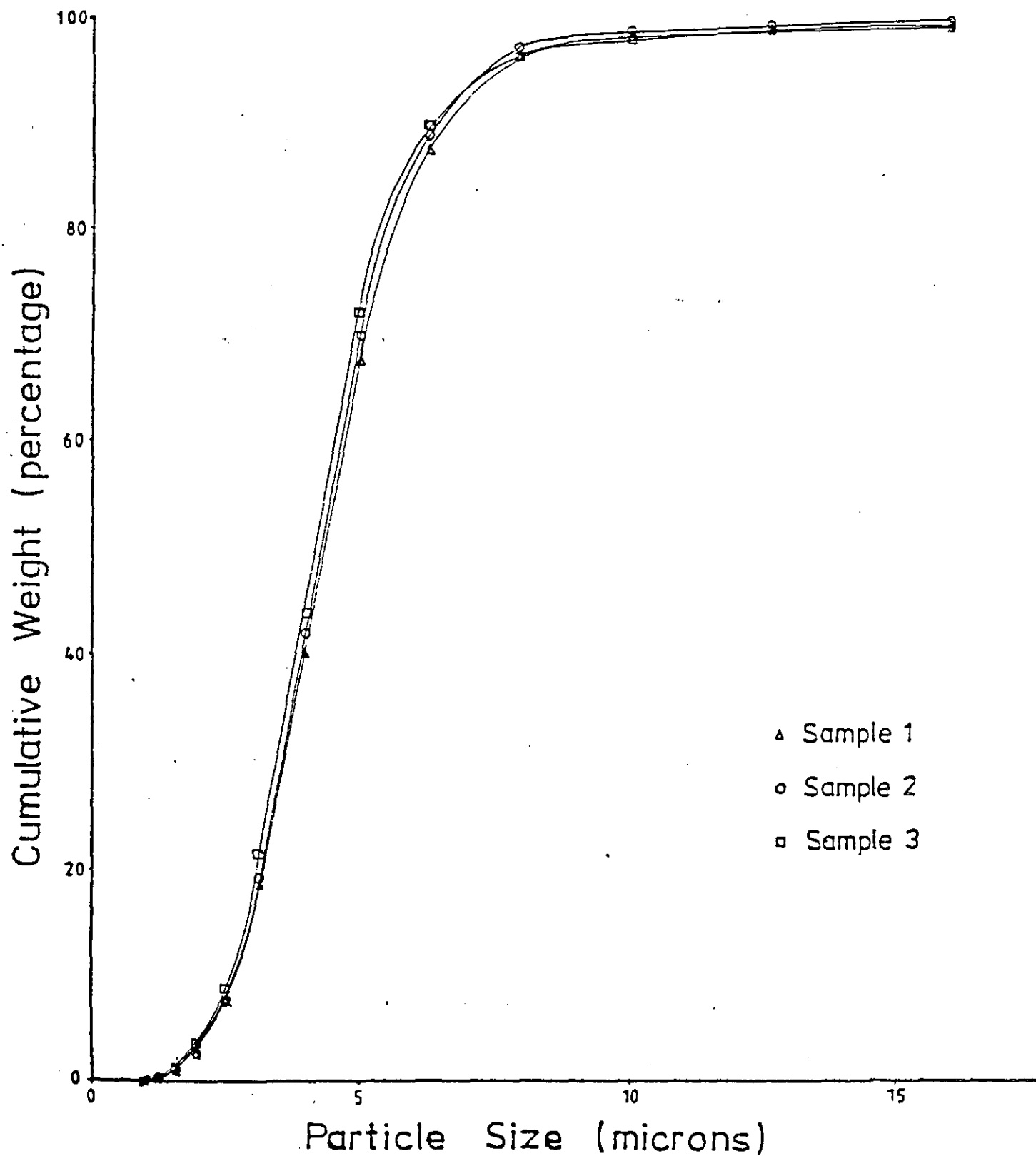
FIGURE A41.2-2

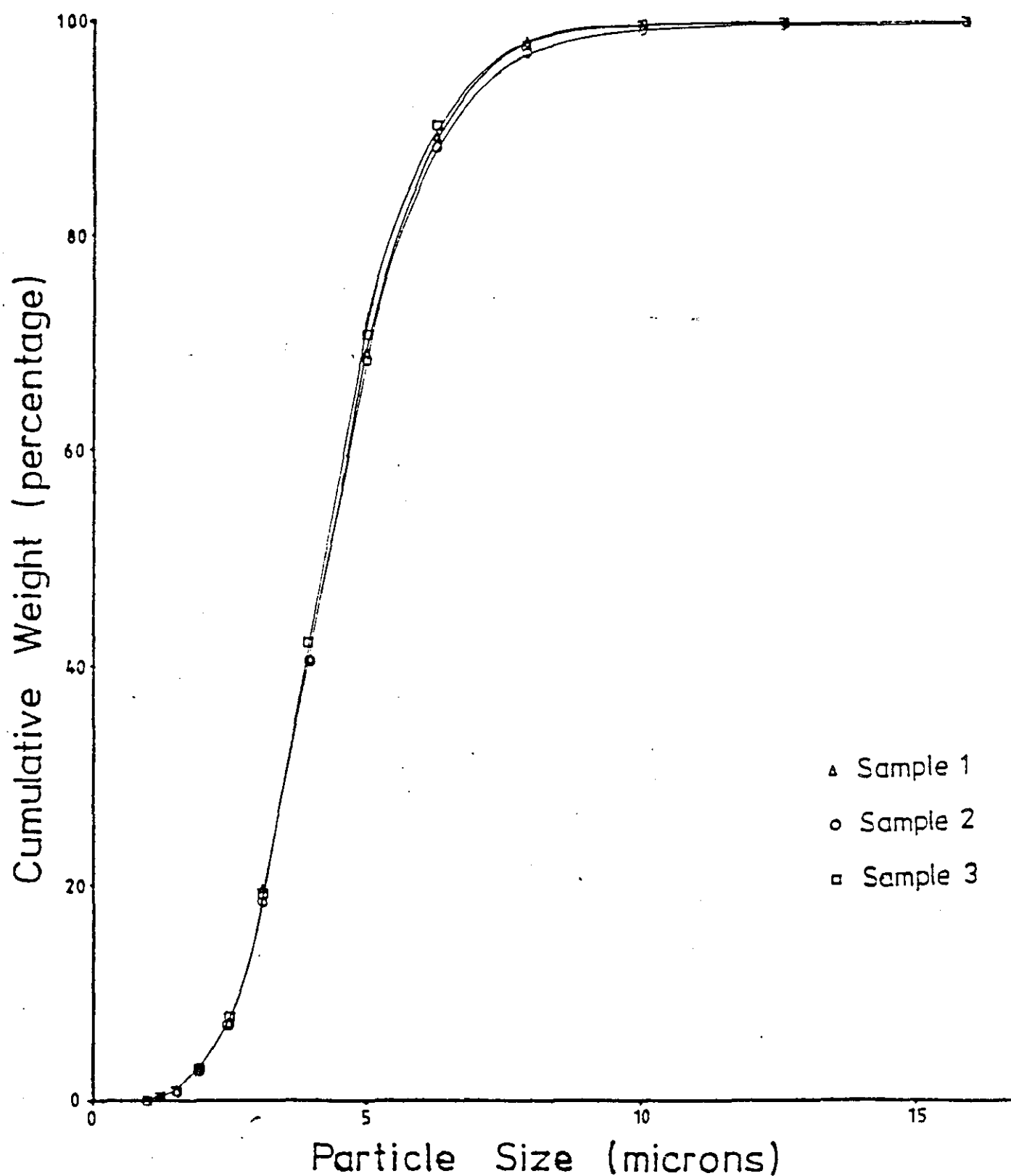CUMULATIVE WEIGHT VS. PARTICLE SIZE

(SHEET C MIDDLE)
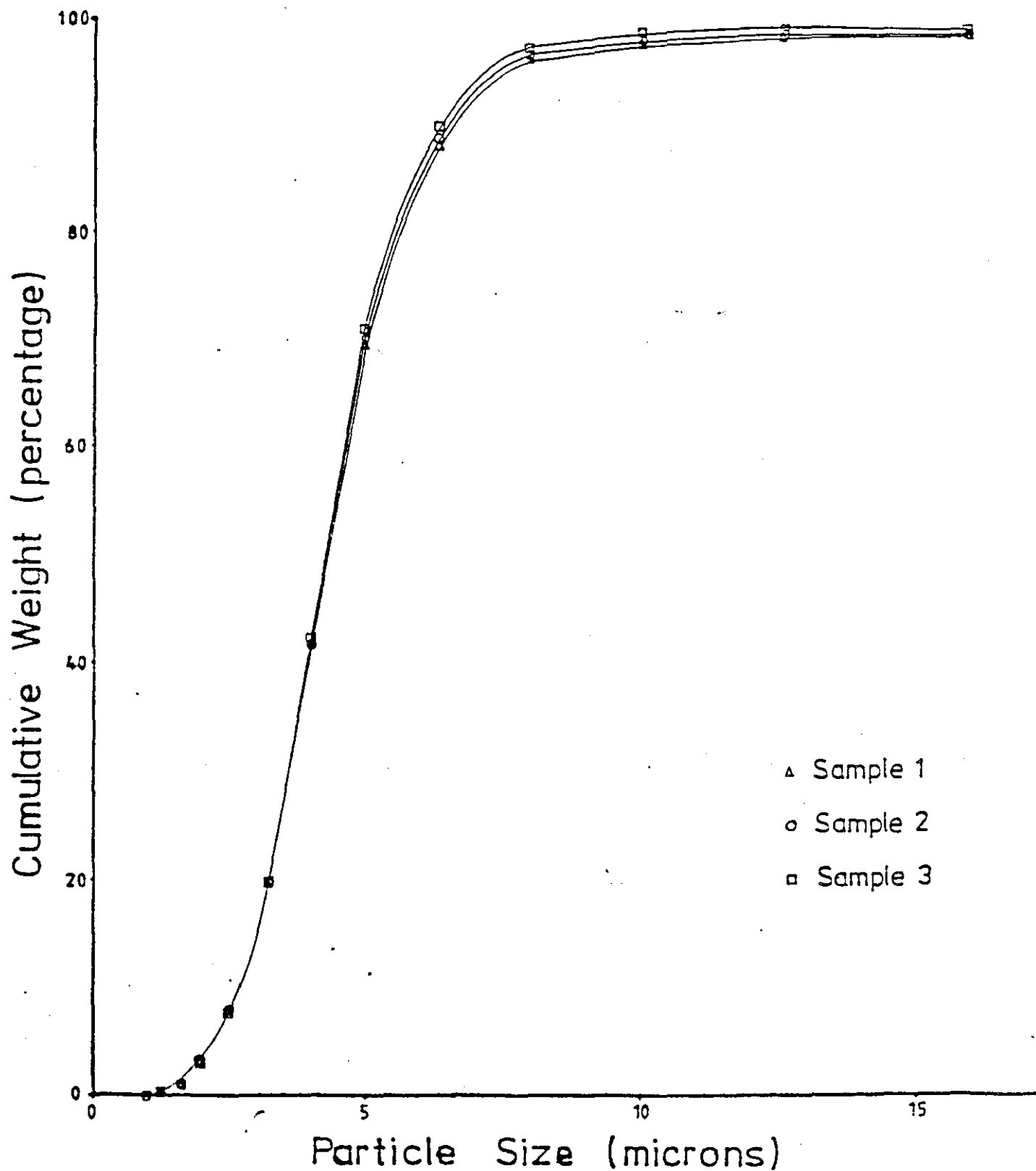
FIGURE A4.1.2-3
CUMULATIVE WEIGHT VS. PARTICLE SIZE
(SHEET C TOP)

Appendix 4.2.1

The following tables give the experimental average results found for the pressure drop response with increasing load for both the mini and deep pleat filter arrangements. Different dust and face velocities have been considered.

TABLES A4.2.1 - 1 Minipleat filter results

a) B.S. 2831 No. 2 Dust

Specific load kg/m²	Face vel. (cm/s)	Pressure drop (mm H₂O)			
		1.25	1.9	2.5	4.0
0		7.5	10.8	15.1	27.0
0.1		11.2	15.3	19.2	35.3
0.2		17.6	22.5	26.7	48.1
0.3		27.2	32.3	37.0	65.9
0.4		43.1	44.7	49.8	88.2
0.5		69.6	61.4	67.8	115.4
0.6		100.8	84.7	93.6	134.7
0.7		131.6	122.5	139.5	

b) 3 μm dust at 2.5 cm/s face velocity

Specific load kg/m²	Pressure drop mm H₂O
0	13.4
.04	20.0
.09	27.6
.14	36.0
.19	46.9
.24	59.6
.28	71.1
.33	87.6
.38	106.6
.43	128.2

c) Cycloned dust at 2.5 cm/s face velocity

Specific load kg/m^2	Pressure drop mm H$_2$O
0	15.0
.02	18.5
.04	22.5
.06	25.5
.08	28.5

TABLES A4.2 - 2 Deep pleat filter results

a) BS 2831 No.2. dust at 1.25 cm/s face velocity

Specific load kg/m^2	Pressure drop mm H$_2$O
0	7.1
0.10	10.9
0.20	14.2
0.30	17.2
0.41	17.2
0.51	20.5
0.61	24.1
0.71	26.4
0.82	30.2
0.92	33.5
1.02	36.5

b) BS 2831 No.2. dust at 2.25 cm/s face velocity

Specific load kg/m^2	Pressure drop mm H$_2$O
0	16.2
0.12	21.8
0.24	28.4
0.36	36.0
0.48	45.7
0.60	58.4
0.72	71.1
0.84	85.0
0.96	96.5
1.08	110.4
1.20	125.7

c) BS 2831 No.2. dust at 3.5 cm/s face velocity

Specific load kg/m^2	Pressure drop mm H$_2$O
0	25.4
0.07	31.7
0.15	38.6
0.23	46.9
0.31	55.3
0.39	62.2
0.47	72.3
0.55	83.8
0.63	95.2
0.70	104.1
0.78	116.8
0.86	130.8

d) BS 2831 No.2. dust at 2.5 cm/s face velocity

Specific load kg/m^2	Pressure drop mm H$_2$O
0	14.9
0.05	21.3
0.10	28.4
0.15	36.0
0.21	45.2
0.26	56.6
0.31	67.3
0.36	79.2
0.42	91.9
0.47	104.1
0.52	116.3
0.57	129.5

Appendix 4.2.2

Photographs are given of the various stages of loading of the mini pleat arrangement as well as photographs taken of completed filters for both mini and deep pleat designs. Also in this appendix are the series of random measurements of channel width taken from a fully loaded mini pleat filter. Furthermore the Coulter analyses taken to compare the dust size distribution inside and outside a minipleat filter channel are given. A sample size analysis of dust size found at the front and back of a deep pleat channel is also included. Only the result for the 3.5 cm/s face velocity test is given but all other velocities gave similar results. However, for dust weight distribution in a deep pleat filter channel results at all velocities have been described.

TABLE A4.2.2 - 1 Random measurements of channel width

The below is for a mini pleat filter which has been loaded with BS 2831 No.2 dust at a face velocity of 2.5 cm/s measurements were taken.

a) On the main face at the channel center

loaded channel (mm)	clean channel (mm)	complete channel pitch (mm)
0.86	0.46	1.32
1.11	0.39	1.50
0.87	0.41	1.28
0.97	0.56	1.53
0.97	0.58	1.55
0.90	0.47	1.37
0.92	0.49	1.41
Mean 0.94	0.48	1.42

Thus 66% of channel pitch is occupied by the loaded channel

b) Cross-section along the channel taken at the centre of the channel width

(i) At the front of the channel

loaded channel (mm)	clean channel (mm)
1.07	0.40
0.94	0.38
1.04	0.39

Mean		
	1.02	0.39

Gives 72% occupied by the loaded channel

(ii) At the centre of the channel length

loaded channel (mm)	clean channel (mm)
0.87	0.52
0.88	0.49
0.94	0.58

Mean		
	0.90	0.53

Gives 63% occupied by the loaded channel

(iii) At the end of the channel length

loaded channel (mm)	clean channel (mm)
0.50	0.97
0.57	0.82
0.52	1.06

Mean		
	0.53	0.95

Gives 35% occupied by the loaded channel

c) Cross section along the channel taken at the stitching seam

(i) At the front of the channel

loaded channel (mm)	clean channel (mm)
0.86	0.68
0.76	0.70

Mean   0.81   0.69

Gives 54% occupied by the loaded channel

(ii) At the centre of the channel length

loaded channel (mm)	clean channel (mm)
0.96	0.78
0.81	0.69

Mean   0.89   0.74

Gives 55% occupied by the loaded channel

(iii) At the end of the channel length

loaded channel (mm)	clean channel (mm)
1.02	0.62
0.84	0.83

Mean   0.93   0.73

Gives 56% occupied by the loaded channel

From these measurements an approximate overall channel expansion can be calculated. It is assumed that there is no expansion at the stitching seam but the expansion measured at the channel centre (w.r.t. width) is effective for 80% of the channel width. It is also assumed that the expansion with respect to channel length is graduated. The figures from table b are used assuming a linear relationship to find the mean channel expansion with respect to

length. By making the assumption that only 80% of the channel width is affected then overall channel expansion in the loaded channel of 1.21 times was calculated. A further 10% was allowed on this figure to account for the enhancement effect when air would actually be passing through the filter. Hence an expansion figure of 1.33 times the original channel volume for the loaded side was derived.

TABLE A4.2.2-2: Comparison of dust size distribution inside and outside a minipleat channel.

Particle dia. um	Inside channel cum. wt. %	Outside channel cum. wt. %
20.16	100	100
16	100	100
12.7	99.9	99.93
10.08	99.67	99.52
8	98.67	97.7
6.35	92.94	89.46
5.04	77.01	68.03
4	50.8	38.34
3.17	26.37	16.19
2.52	11.21	5.62
2	4.45	1.94
1.58	1.53	0.65
1.26	0.49	0.21
1	0	0

TABLE A4.2.2-3: Dust size distribution along a deep pleat filter channel where filter face velocity was 3.5 cm/s.

Particle dia. um	Inside channel cum. wt. %	Outside channel cum. wt. %
12/7	100	100
10.08	99.87	99.88
8	99	98.94
6.35	90.38	89.95
5.04	53.57	51.42
4	15.3	14.29
3.17	4.32	3.93
2.52	1.54	1.39
2	0.66	0.58
1.58	0.27	0.23
1.26	0.09	0.08
1	0	0

TABLE A4.2.2-4: Dust weight distribution along a deep pleat filter channel. Figures given as a percentage of the total dust weight along the channel. Unless otherwise state the dust is BS 2831 No.2.

Position	Face Velocity (cm/s)			
	1.25	2.5	3.5	2.5 (3 um dust)
Front	43	38	37	50
Middle	29	32	34	24
Back	28	30	29	26

FIG. A.4.2.2-1: Minipleat filter loaded at a face velocity of 1.25 cm/s
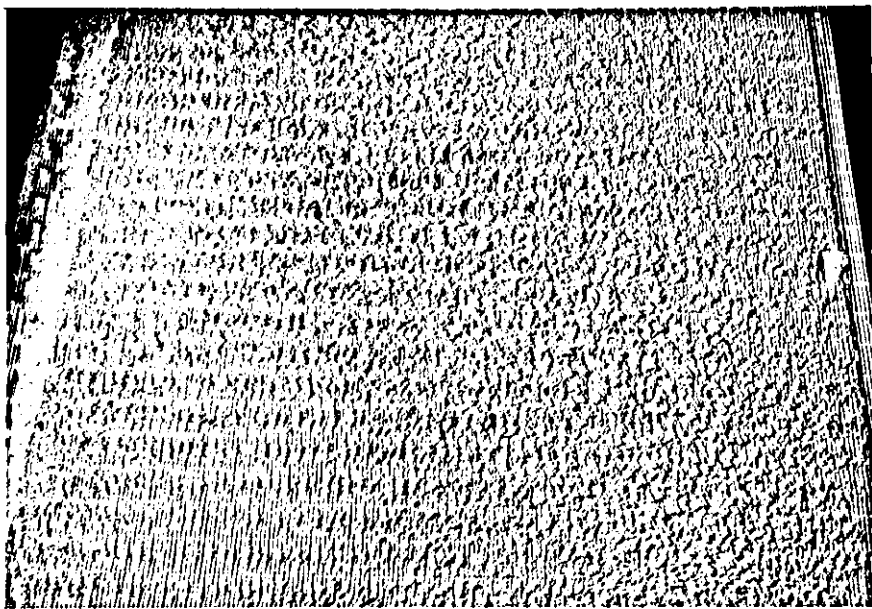
air flow

(a) Overall view
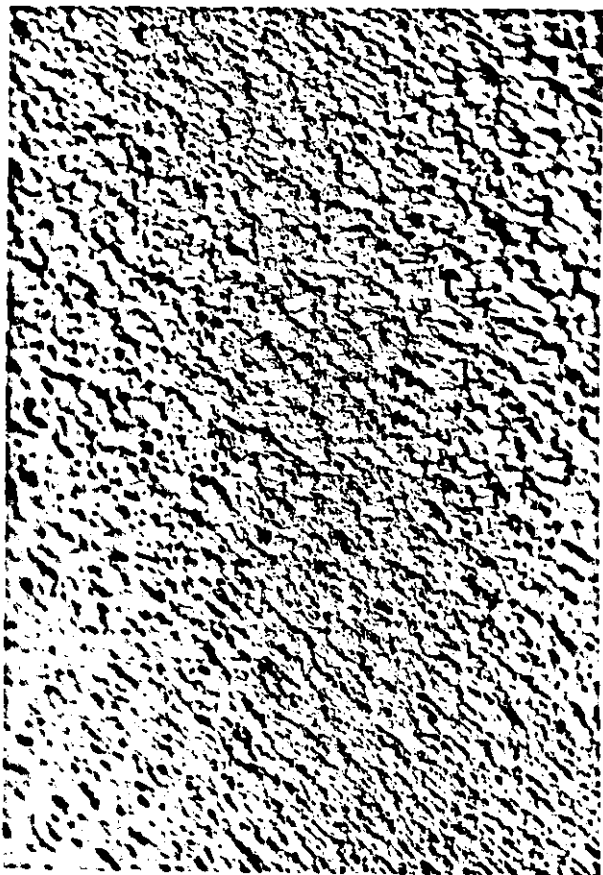
(b) Close up (top)
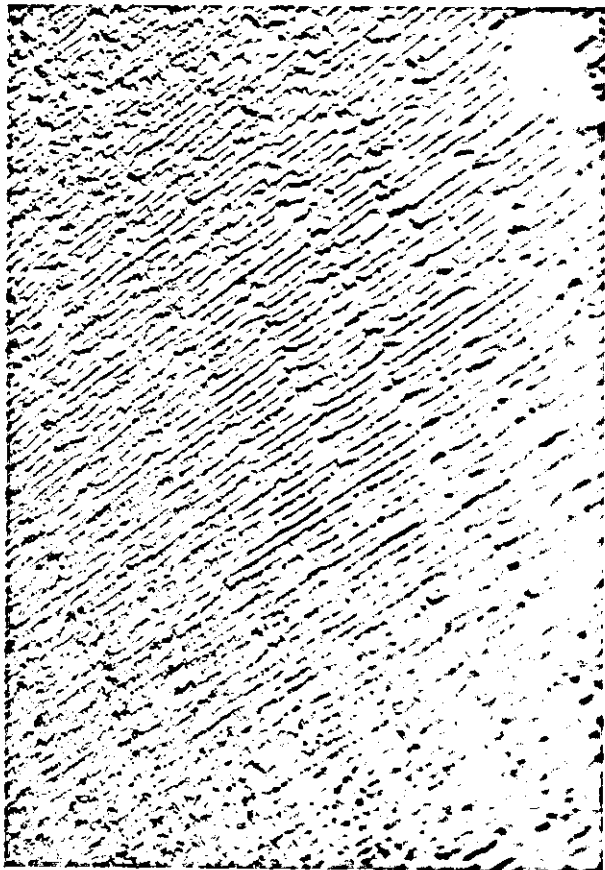
(c) Close up (bottom)

FIG. A4.2.2-2: Minipleat filter loaded at a face velocity of 1.9 cm/s
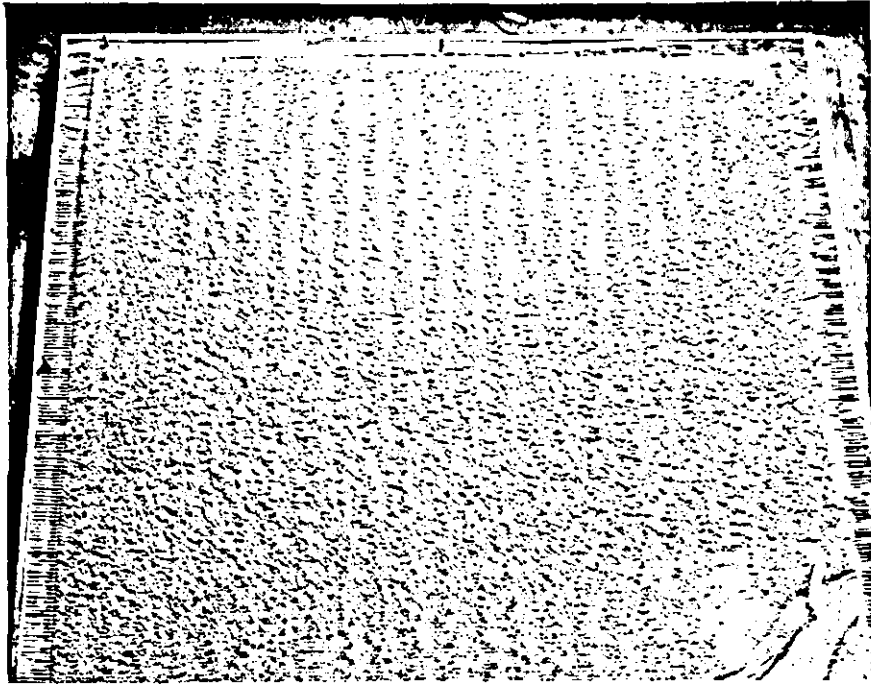
(a) Overall view
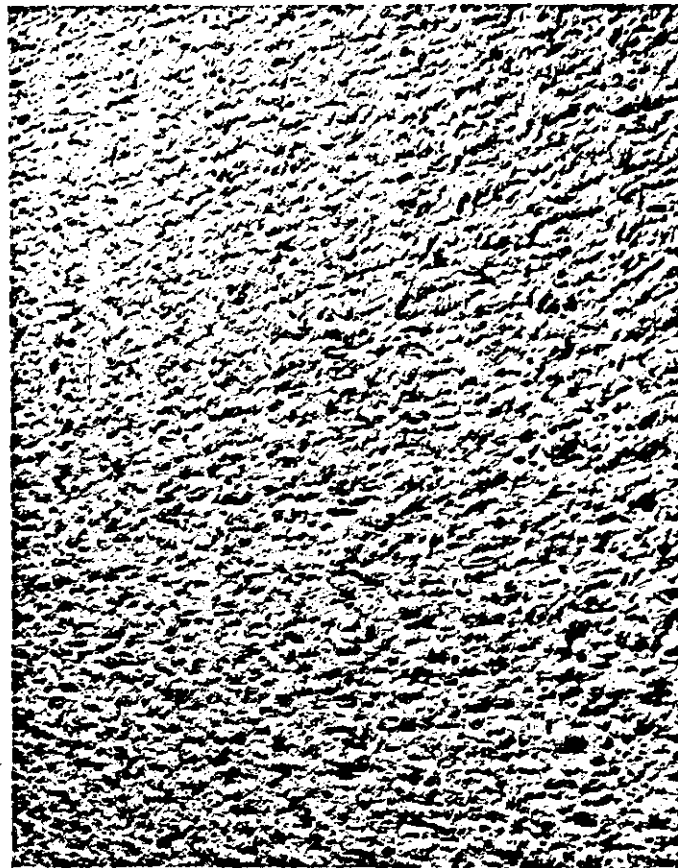
(b) Close up view

FIG. A4.2.2-6: Close up views of complete load on a mini pleat filter
- face velocity 4 cm/s
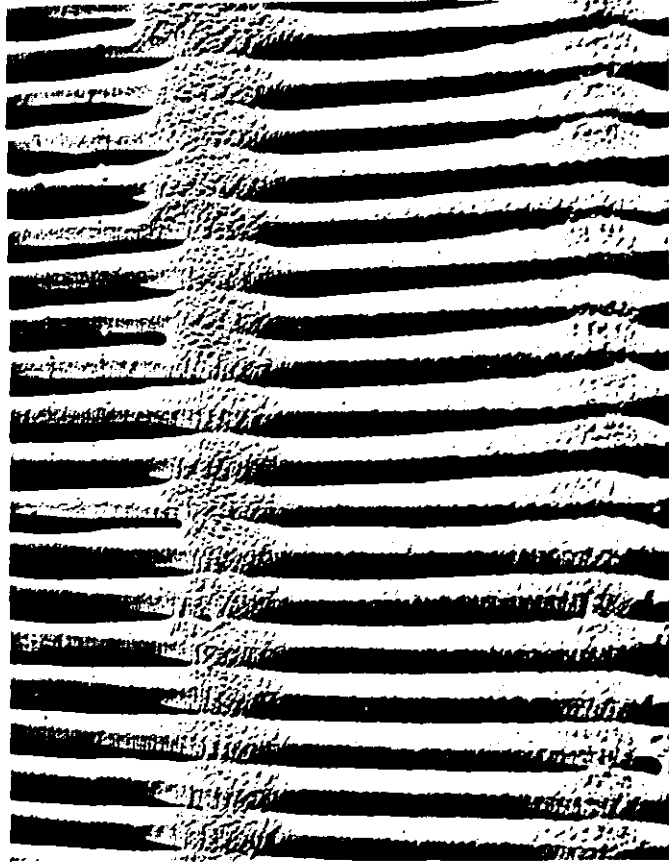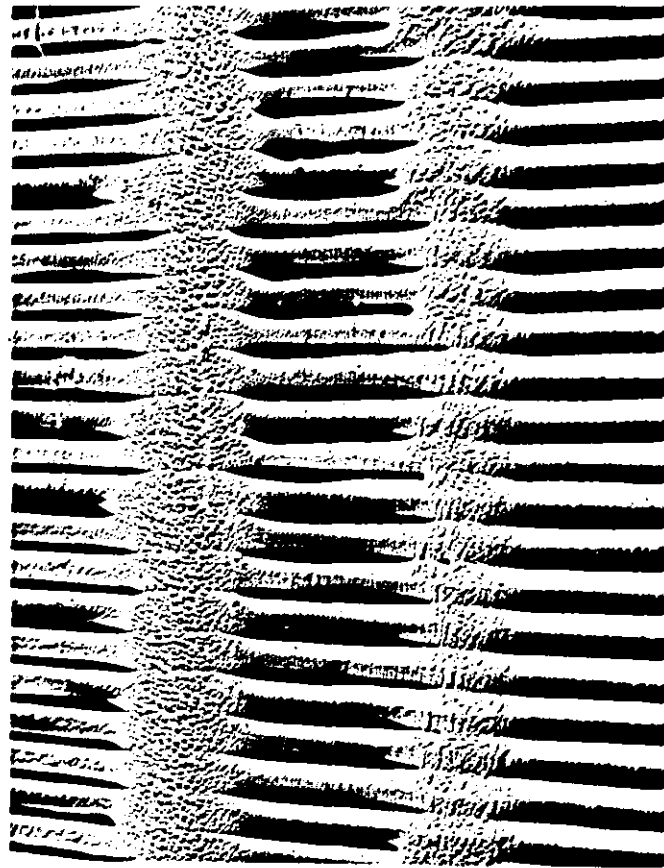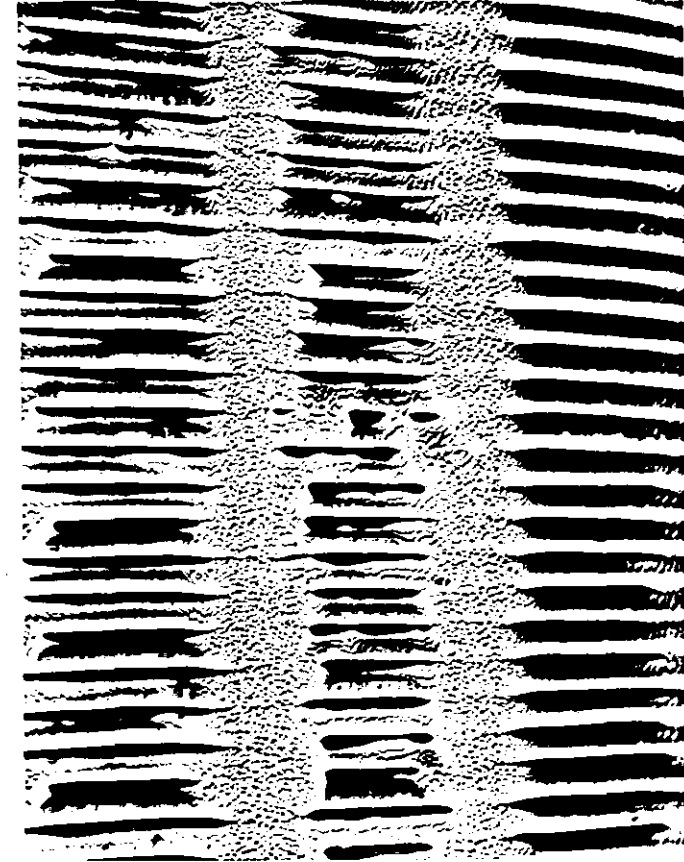
(a)   (b)   (c)

FIG. A4.2.2-7: Minipleat filters loaded with fine dust
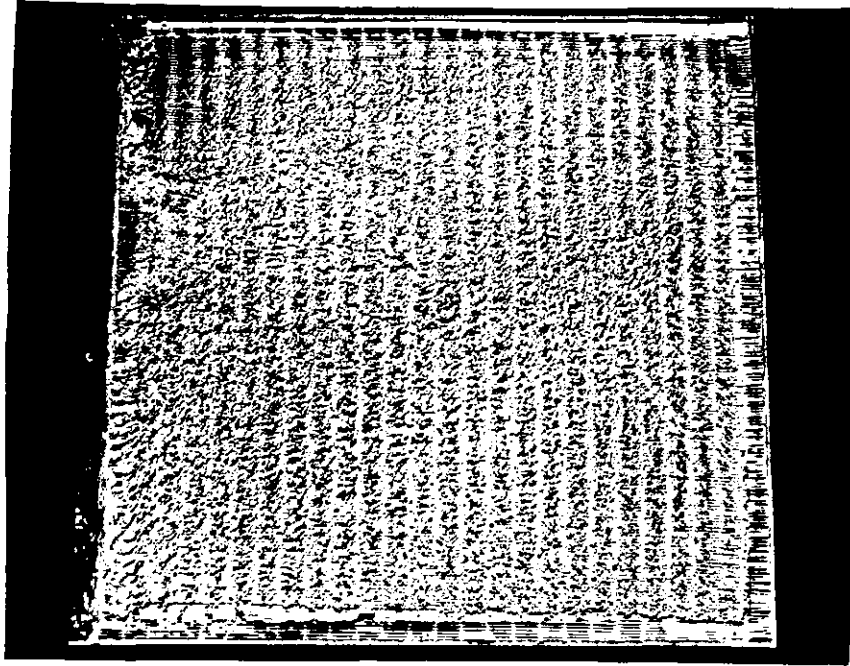
(a) Overall view, 3 um dust, full load
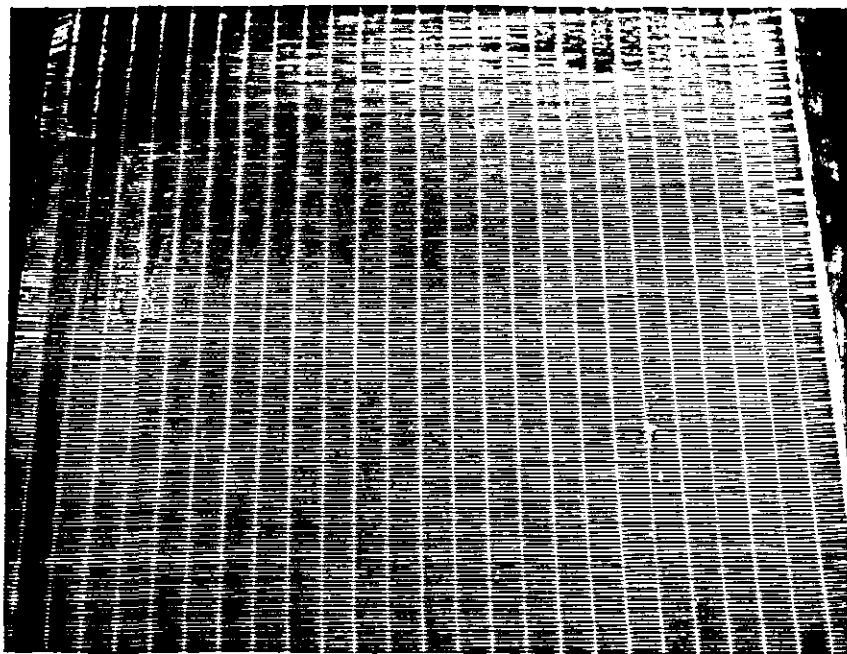
(b) Overall view, cycloned dust, partial load

FIG. A4·2·2-8: Progressive loading of a minipleat filter with pleats arranged vertically.
– Face velocity increased from 2·5-5 cm/s.
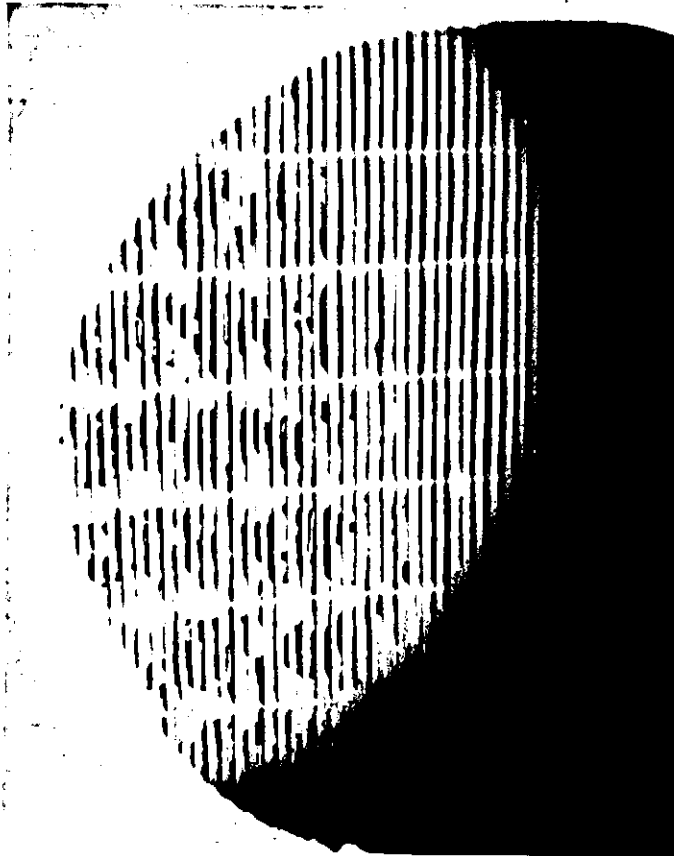
(a)
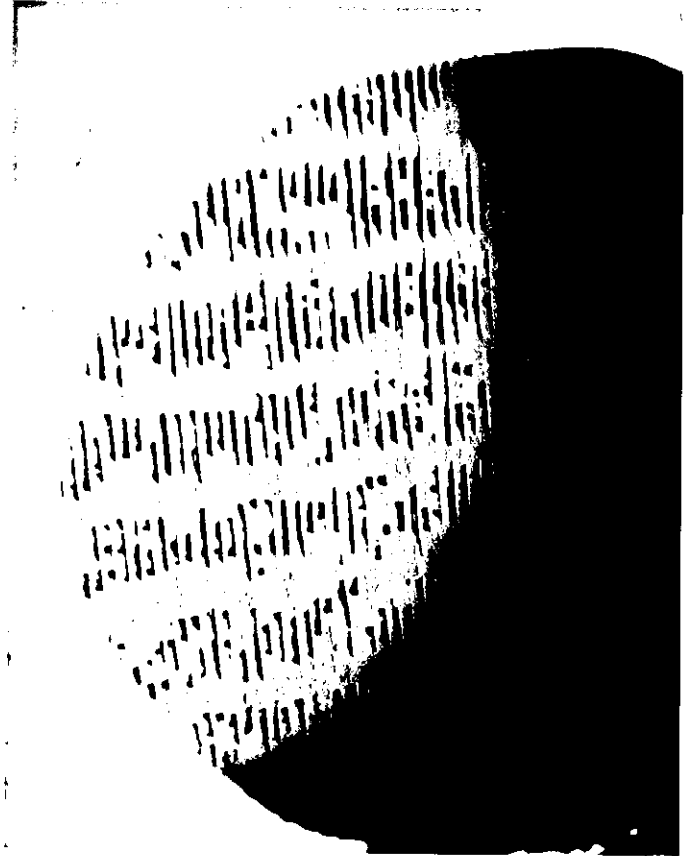
(b)

(c)
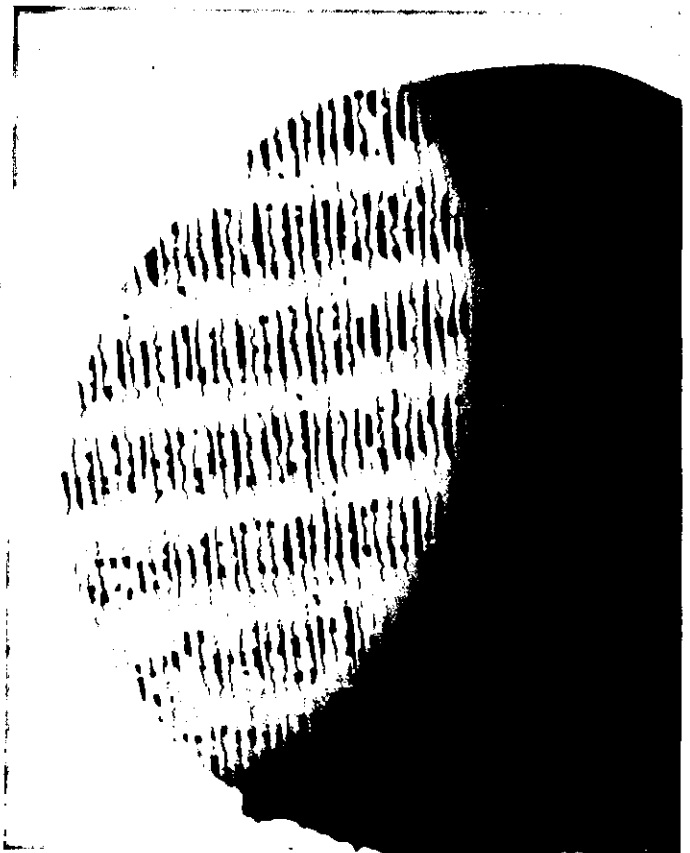
(d)

FIG. A4.2.2-12: Deep pleat filter loaded at 3.5 cm/s (BS 2831 No.2 dust)
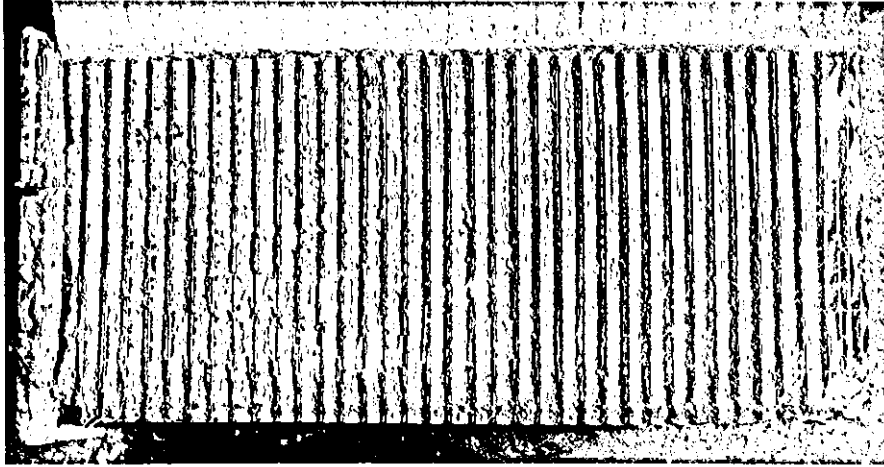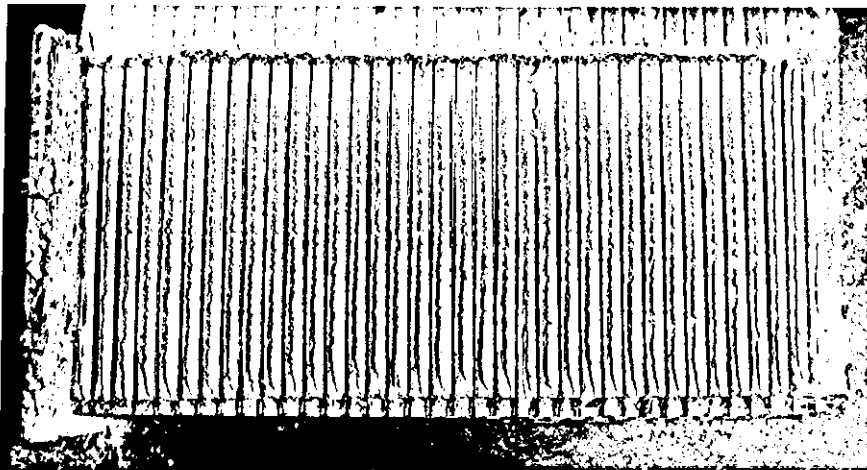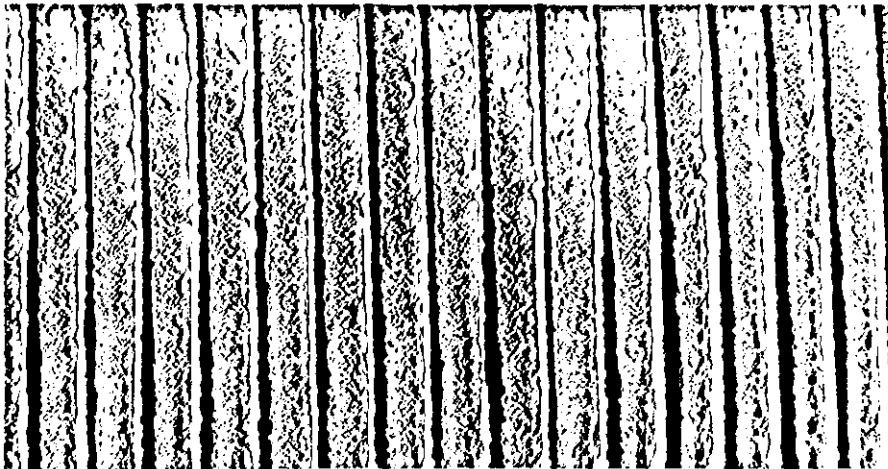

(a) Overall view - filter sheet
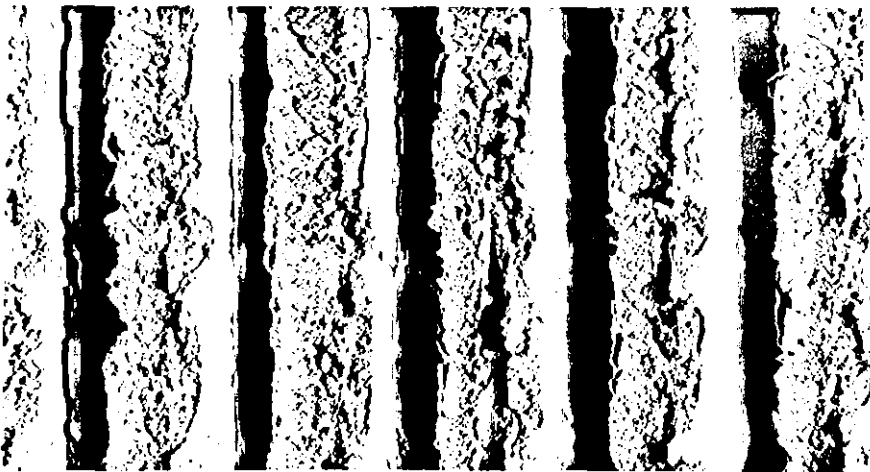

(b) Overall view - filter spacer
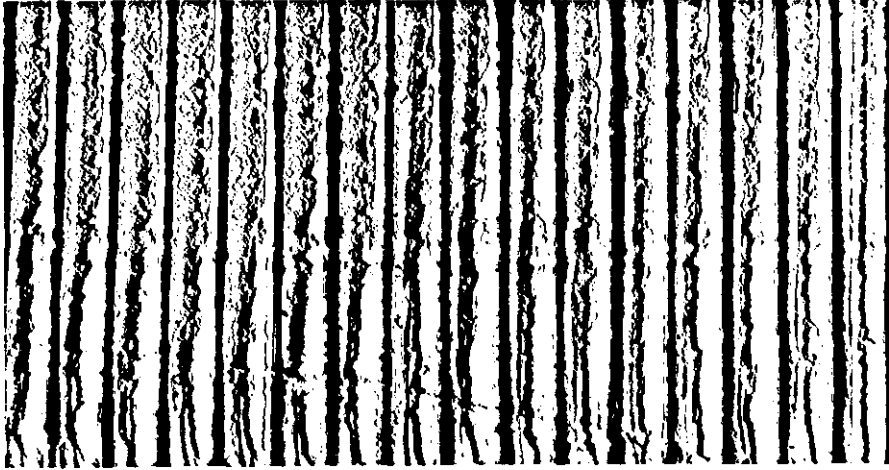
(c) Entrance

(d) End

(e) Close up-entrance

(f) Close up-centre

(g) Close up-end